

Global Carbon Budget 2024

Pierre Friedlingstein [1,2], Michael O'Sullivan [1], Matthew W. Jones [3], Robbie M. Andrew [4], Judith Hauck [5,6], Peter Landschützer [7], Corinne Le Quéré [3], Hongmei Li [8,9], Ingrid T. Lujckx [10], Are Olsen [11,12], Glen P. Peters [4], Wouter Peters [10,13], Julia Pongratz [14,9], Clemens Schwingshackl [14], Stephen Sitch [1], Josep G. Canadell [15], Philippe Ciais [16], Robert B. Jackson [17], Simone R. Alin [18], Almut Arneth [19], Vivek Arora [20], Nicholas R. Bates [21], Meike Becker [11,12], Nicolas Bellouin [22], Carla F. Berghoff [23], Henry C. Bittig [24], Laurent Bopp [2], Patricia Cadule [2], Katie Campbell [25], Matthew A. Chamberlain [26], Naveen Chandra [27], Frédéric Chevallier [16], Louise P. Chini [28], Thomas Colligan [29], Jeanne Decayeux [30], Laique M. Djeutchouang [31,32], Xinyu Dou [33], Carolina Duran Rojas [1], Kazutaka Enyo [34], Wiley Evans [25], Amanda R. Fay [35], Richard A. Feely [18], Daniel J. Ford [1], Adrianna Foster [36], Thomas Gasser [37], Marion Gehlen [16], Thanos Gkritzalis [7], Giacomo Grassi [38], Luke Gregor [39], Nicolas Gruber [39], Özgür Gürses [5], Ian Harris [40], Matthew Hefner [41,42], Jens Heinke [43], George C. Hurtt [28], Yosuke Iida [34], Tatiana Ilyina [44,8,9], Andrew R. Jacobson [45], Atul K. Jain [46], Tereza Jarníková [47], Annika Jersild [29], Fei Jiang [48], Zhe Jin [49,50], Etsushi Kato [51], Ralph F. Keeling [52], Kees Klein Goldewijk [53], Jürgen Knauer [54,15], Jan Ivar Korsbakken [4], [Xin Lan \[55,56\]](#), Siv K. Lauvset [57,12], Nathalie Lefèvre [58], Zhu Liu [33], Junjie Liu [59,60], Lei Ma [28], Shamil Maksyutov [61], Gregg Marland [41,42], Nicolas Mayot [62], Patrick C. McGuire [63], Nicolas Metz [58], Natalie M. Monacci [64], Eric J. Morgan [52], Shin-Ichiro Nakaoka [61], Craig Neill [26], Yosuke Niwa [61], Tobias Nützel [14], Lea Olivier [5,14], Tsuneo Ono [65], Paul I. Palmer [66,67], Denis Pierrot [68], Zhangcai Qin [69], Laure Resplandy [70], Alizée Roobaert [7], Thais M. Rosan [1], Christian Rödenbeck [71], Jörg Schwinger [57,12], T. Luke Smallman [66,67], Stephen M. Smith [72], Reinel Sospedra-Alfonso [73], Tobias Steinhoff [74,57], Qing Sun [75], Adrienne J. Sutton [18], Roland Séférian [30], Shintaro Takao [61], Hiroaki Tatebe [76,77], Hanqin Tian [78], Bronte Tilbrook [26,79], Olivier Torres [2], Etienne Tourigny [80], Hiroyuki Tsujino [81], Francesco Tubiello [82], Guido van der Werf [10], Rik Wanninkhof [68], Xuhui Wang [50], Dongxu Yang [83], Xiaojuan Yang [84], Zhen Yu [85], Wenping Yuan [86], Xu Yue [87], Sönke Zachle [71], Ning Zeng [88, 29], Jiye Zeng [61].

1. Faculty of Environment, Science and Economy, University of Exeter, Exeter EX4 4QF, UK
2. Laboratoire de Météorologie Dynamique, Institut Pierre-Simon Laplace, CNRS, Ecole Normale Supérieure, Université PSL, Sorbonne Université, Ecole Polytechnique, Paris, France
3. Tyndall Centre for Climate Change Research, School of Environmental Sciences, University of East Anglia, Norwich Research Park, Norwich NR4 7TJ, UK
4. CICERO Center for International Climate Research, Oslo 0349, Norway
5. Alfred-Wegener-Institut, Helmholtz-Zentrum für Polar- und Meeresforschung, Am Handelshafen 12, 27570 Bremerhaven, Germany
6. Universität Bremen, Bremen, Germany
7. Flanders Marine Institute (VLIZ), Jacobsenstraat 1, 8400, Ostend, Belgium

Style Definition: Heading 1: Outline numbered + Level: 1 + Numbering Style: 1, 2, 3, ... + Start at: 1 + Alignment: Left + Aligned at: 0.63 cm + Indent at: 1.27 cm

Style Definition: Heading 2: Outline numbered + Level: 2 + Numbering Style: a, b, c, ... + Start at: 1 + Alignment: Left + Aligned at: 1.9 cm + Indent at: 2.54 cm

Style Definition: Heading 3: Outline numbered + Level: 3 + Numbering Style: i, ii, iii, ... + Start at: 1 + Alignment: Right + Aligned at: 3.49 cm + Indent at: 3.81 cm

Style Definition: Heading 4: Outline numbered + Level: 4 + Numbering Style: 1, 2, 3, ... + Start at: 1 + Alignment: Left + Aligned at: 4.44 cm + Indent at: 5.08 cm

Style Definition: Heading 5: Outline numbered + Level: 5 + Numbering Style: a, b, c, ... + Start at: 1 + Alignment: Left + Aligned at: 5.71 cm + Indent at: 6.35 cm

Style Definition: Heading 6: Outline numbered + Level: 6 + Numbering Style: i, ii, iii, ... + Start at: 1 + Alignment: Right + Aligned at: 7.3 cm + Indent at: 7.62 cm

Style Definition: Heading 7: Outline numbered + Level: 7 + Numbering Style: 1, 2, 3, ... + Start at: 1 + Alignment: Left + Aligned at: 8.25 cm + Indent at: 8.89 cm

Style Definition: Heading 8: Outline numbered + Level: 8 + Numbering Style: a, b, c, ... + Start at: 1 + Alignment: Left + Aligned at: 9.52 cm + Indent at: 10.16 cm

Style Definition: Heading 9: Outline numbered + Level: 9 + Numbering Style: i, ii, iii, ... + Start at: 1 + Alignment: Right + Aligned at: 11.11 cm + Indent at: 11.43 cm

Deleted: 55...7,12], Nathalie Lefèvre [56...8], Zhu Liu [33], Junjie Liu [57,58...9,60], Lei Ma [28], Shamil Maksyutov [61], Gregg Marland [41,42], Nicolas Mayot [60...2], Patrick C. McGuire [61...3], Nicolas Metz [56...8], Natalie M. Monacci [62...4], Eric J. Morgan [52], Shin-Ichiro Nakaoka [59...1], Craig Neill [26], Yosuke Niwa [59...1], Tobias Nützel [14], Lea Olivier [5,14], Tsuneo Ono [63...5], Paul I. Palmer [64,65...6,67], Denis Pierrot [66...8], Zhangcai Qin [67...9], Laure Resplandy [68...0], Alizée Roobaert [7], Thais M. Rosan [1], Christian Rödenbeck [69...1], Jörg Schwinger [55...7,12], T. Luke Smallman [64,65...6,67], Stephen M. Smith [70...2], Reinel Sospedra-Alfonso [71...3], Tobias Steinhoff [72,55...4,57], Qing Sun [73...5], Adrienne J. Sutton [18], Roland Séférian [30], Shintaro Takao [59...1], Hiroaki Tatebe [74,75...6,77], Hanqin Tian [76...8], Bronte Tilbrook [26,77...9], Olivier Torres [2], Etienne Tourigny [78...0], Hiroyuki Tsujino [79...1], Francesco Tubiello [80...2], Guido van der Werf [10], Rik Wanninkhof [66...8], Xuhui Wang [50], Dongxu Yang [81...3], Xiaojuan Yang [82...4], Zhen Yu [83...5], Wenping Yuan [84...6], Xu Yue [85...7], Sönke Zachle [69...1], Ning Zeng [86...8, 29], Jiye Zeng [59] (... [1])

- 98 8. Helmholtz-Zentrum Hereon, Max-Planck-Straße 1, 21502 Geesthacht, Germany
- 99 9. Max Planck Institute for Meteorology, Bundesstraße 53, 20146 Hamburg, Germany
- 100 10. Wageningen University, Environmental Sciences Group, P.O. Box 47, 6700AA, Wageningen, The
101 Netherlands
- 102 11. Geophysical Institute, University of Bergen, Allégaten 70, 5007 Bergen, Norway
- 103 12. Bjerknes Centre for Climate Research, Bergen, Norway
- 104 13. University of Groningen, Centre for Isotope Research, Groningen, The Netherlands
- 105 14. Ludwig-Maximilians-Universität München, Luisenstr. 37, 80333 München, Germany
- 106 15. CSIRO Environment, Canberra, ACT 2101, Australia
- 107 16. Laboratoire des Sciences du Climat et de l'Environnement, LSCE/IPSL, CEA-CNRS-UVSQ, Université
108 Paris-Saclay, F-91198 Gif-sur-Yvette, France
- 109 17. Department of Earth System Science, Woods Institute for the Environment, and Precourt Institute for
110 Energy, Stanford University, Stanford, CA 94305–2210, United States of America
- 111 18. National Oceanic and Atmospheric Administration, Pacific Marine Environmental Laboratory
112 (NOAA/PMEL), 7600 Sand Point Way NE, Seattle, WA 98115, USA
- 113 19. Karlsruhe Institute of Technology, Institute of Meteorology and Climate Research/Atmospheric
114 Environmental Research, 82467 Garmisch-Partenkirchen, Germany
- 115 20. Canadian Centre for Climate Modelling and Analysis, Environment and Climate Change Canada, Victoria,
116 BC, Canada
- 117 21. ASU-BIOS, Bermuda Institute of Ocean Sciences, 31 Biological Lane, Ferry Reach, St. Georges,, GE01,
118 Bermuda
- 119 22. Department of Meteorology, University of Reading, Reading, RG6 6BB, UK
- 120 23. Instituto Nacional de Investigación y Desarrollo Pesquero, Paseo Victoria Ocampo N°1, Escollera Norte,
121 B7602HSA, Mar del Plata, Argentina
- 122 24. Leibniz Institute for Baltic Sea Research Warnemuende (IOW), Seestrasse 15, 18119 Rostock, Germany
- 123 25. Hakai Institute, British Columbia, V0P 1H0, Canada
- 124 26. CSIRO Environment, Castray Esplanade, Hobart, Tasmania 7004, Australia
- 125 27. Research Institute for Global Change, JAMSTEC, 3173-25 Showa-machi, Kanazawa, Yokohama, 236-0001,
126 Japan
- 127 28. Department of Geographical Sciences, University of Maryland, College Park, Maryland 20742, USA
- 128 29. Earth System Science Interdisciplinary Center, University of Maryland, College Park, MD 20740, USA
- 129 30. Centre National de Recherches Météorologiques, Université de Toulouse, Météo-France, CNRS UMR 3589,
130 Toulouse, France
- 131 31. School for Climate Studies, Stellenbosch University, Private Bag X1, Matieland, Stellenbosch, 7602, South
132 Africa
- 133 32. Southern Ocean Carbon – Climate Observatory, CSIR, Rosebank, Cape Town, 7700, South Africa
- 134 33. Department of Earth System Science, Tsinghua University, Beijing, China
- 135 34. Japan Meteorological Agency, 3-6-9 Toranomon, Minato City, Tokyo 105-8431, Japan
- 136 35. Columbia University and Lamont-Doherty Earth Observatory, New York, NY, USA

- 137 36. Climate and Global Dynamics Laboratory, National Center for Atmospheric Research, Boulder, CO 80305,
 138 USA
- 139 37. International Institute for Applied Systems Analysis (IIASA), Schlossplatz 1, A-2361 Laxenburg, Austria
- 140 38. European Commission, Joint Research Centre, (JRC), Ispra, Italy
- 141 39. Environmental Physics Group, ETH Zürich, Institute of Biogeochemistry and Pollutant Dynamics and
 142 Center for Climate Systems Modeling (C2SM), Zürich, Switzerland
- 143 40. NCAS-Climate, Climatic Research Unit, School of Environmental Sciences, University of East Anglia,
 144 Norwich Research Park, Norwich, NR4 7TJ, UK
- 145 41. Research Institute for Environment, Energy, and Economics, Appalachian State University, Boone, North
 146 Carolina, USA
- 147 42. Department of Geological and Environmental Sciences, Appalachian State University, Boone, North
 148 Carolina, USA
- 149 43. Potsdam Institute for Climate Impact Research (PIK), member of the Leibniz Association, P.O. Box 60 12
 150 03, 14412 Potsdam, Germany
- 151 44. Universität Hamburg, Bundesstraße 55, 20146 Hamburg, Germany
- 152 45. Cooperative Institute for Research in Environmental Sciences, CU Boulder and NOAA Global Monitoring
 153 Laboratory, Boulder, USA
- 154 46. Department of Climate, Meteorology and Atmospheric Sciences, University of Illinois, Urbana, IL 61821,
 155 USA
- 156 47. University of East Anglia, Norwich, UK
- 157 48. Jiangsu Provincial Key Laboratory of Geographic Information Science and Technology, International
 158 Institute for Earth System Science, Nanjing University, Nanjing, 210023, China
- 159 49. State Key Laboratory of Tibetan Plateau Earth System and Resource Environment, Institute of Tibetan
 160 Plateau Research, Chinese Academy of Sciences, Beijing 100101, China
- 161 50. Institute of Carbon Neutrality, Sino-French Institute for Earth System Science, College of Urban and
 162 Environmental Sciences, Peking University, Beijing 100871, China
- 163 51. Institute of Applied Energy (IAE), Minato-ku, Tokyo 105-0003, Japan
- 164 52. University of California, San Diego, Scripps Institution of Oceanography, La Jolla, CA 92093-0244, USA
- 165 53. Utrecht University, Faculty of Geosciences, Department IMEW, Copernicus Institute of Sustainable
 166 Development, Heidelberglaan 2, P.O. Box 80115, 3508 TC, Utrecht, the Netherlands
- 167 54. Hawkesbury Institute for the Environment, Western Sydney University, Penrith, New South Wales,
 168 Australia
- 169 55. [Cooperative Institute for Research in Environmental Sciences \(CIRES\), University of Colorado Boulder,](#)
 170 [Boulder, CO 80309, USA](#),
- 171 [56. National Oceanic and Atmospheric Administration Global Monitoring Laboratory \(NOAA/GML\), 325](#)
 172 [Broadway R/GML, Boulder, CO 80305, USA](#)
- 173 [57. NORCE Norwegian Research Centre, Jahnebakken 5, 5007 Bergen, Norway](#),
- 174 [58. LOCEAN/IPSL laboratory, Sorbonne Université, CNRS/IRD/MNHN, Paris, 75252, France](#)
- 175 [59. Jet Propulsion Laboratory, California Institute of Technology, Pasadena, CA, USA](#)

Deleted: , 21027

Deleted: (VA),

Moved down [1]: NORCE Norwegian Research Centre, Jahnebakken 5, 5007 Bergen, Norway

Moved (insertion) [1]

Deleted: 56.

Deleted: 57

182	60. California Institute of Technology, Pasadena, CA, USA	Deleted: 58
183	61. Earth System Division, National Institute for Environmental Studies, 16-2 Onogawa, Tsukuba, Ibaraki, 305-	Deleted: 59
184	8506 Japan	
185	62. Sorbonne Université, Laboratoire d'Océanographie de Villefranche, Villefranche-sur-Mer, France	Deleted: 60
186	63. Department of Meteorology & National Centre for Atmospheric Science (NCAS), University of Reading,	Deleted: 61
187	Reading, UK	
188	64. University of Alaska Fairbanks, College of Fisheries and Ocean Sciences, Fairbanks, AK, 99709, USA	Deleted: 62
189	65. Fisheries Research and Education Agency, 2-12-4 Fukuura, Kanazawa-Ku, Yokohama 236-8648, Japan	Deleted: 63
190	66. National Centre for Earth Observation, University of Edinburgh, EH9 3FF, UK	Deleted: 64
191	67. School of GeoSciences, University of Edinburgh, EH9 3FF, UK	Deleted: 65
192	68. NOAA Atlantic Oceanographic and Meteorological Laboratory (NOAA/AOML), 4301 Rickenbacker	Deleted: 66
193	Causeway, Miami, Florida 33149, USA	
194	69. School of Atmospheric Sciences, Sun Yat-sen University, Zhuhai 519000, China	Deleted: 67
195	70. Princeton University, Department of Geosciences and Princeton Environmental Institute, Princeton, NJ,	Deleted: 68
196	USA	
197	71. Max Planck Institute for Biogeochemistry, P.O. Box 600164, Hans-Knöll-Str. 10, 07745 Jena, Germany	Deleted: 69
198	72. Smith School of Enterprise and the Environment, University of Oxford, Oxford, UK	Deleted: 70
199	73. Canadian Centre for Climate Modelling and Analysis, Environment and Climate Change Canada, Victoria,	Deleted: 71
200	British Columbia, Canada	
201	74. GEOMAR Helmholtz Centre for Ocean Research Kiel, Wischhofstr. 1-3, 24148 Kiel, Germany	Deleted: 72
202	75. Institute for Climate and Environmental Physics, Bern, Switzerland	Deleted: 73
203	76. Research Center for Environmental Modeling and Application, Japan Agency for Marine-Earth Science and	Deleted: 74
204	Technology, Yokohama, Japan	
205	77. Advanced Institute for Marine Ecosystem Change, Japan Agency for Marine-Earth Science and Technology,	Deleted: 75
206	Yokohama, Japan	
207	78. Schiller Institute of Integrated Science and Society, Department of Earth and Environmental Sciences,	Deleted: 76
208	Boston College, Chestnut Hill, MA 02467, USA	
209	79. Australian Antarctic Partnership Program, University of Tasmania, Hobart, Australia	Deleted: 77
210	80. Barcelona Supercomputing Center, Barcelona, Spain	Deleted: 78
211	81. JMA Meteorological Research Institute, Tsukuba, Ibaraki, Japan	Deleted: 79
212	82. Statistics Division, Food and Agriculture Organization of the United Nations, Via Terme di Caracalla, Rome	Deleted: 80
213	00153, Italy	
214	83. Institute of Atmospheric Physics, Chinese Academy of Sciences, Beijing, China	Deleted: 81
215	84. Climate Change Science Institute and Environmental Sciences Division, Oak Ridge National Lab, Oak	Deleted: 82
216	Ridge, TN 37831, USA.	
217	85. School of Ecology and Applied Meteorology, Nanjing University of Information Science and Technology,	Deleted: 83
218	Nanjing 210044, PR. China	
219	86. Institute of Carbon Neutrality, College of Urban and Environmental Sciences, Peking University, Beijing	Deleted: 84
220	100091, China	

248 [87](#). School of Environmental Science and Engineering, Nanjing University of Information Science and
249 Technology (NUIST), Nanjing, 210044, China
250 [88](#). Department of Atmospheric and Oceanic Science, University of Maryland, Maryland, USA
251
252 Correspondence to: Pierre Friedlingstein (p.friedlingstein@exeter.ac.uk)

Deleted: 85

Deleted: 86

Deleted: ¶

253 Abstract

254 Accurate assessment of anthropogenic carbon dioxide (CO₂) emissions and their redistribution among the
255 atmosphere, ocean, and terrestrial biosphere in a changing climate is critical to better understand the global
256 carbon cycle, support the development of climate policies, and project future climate change. Here we describe
257 and synthesise datasets and methodologies to quantify the five major components of the global carbon budget
258 and their uncertainties. Fossil CO₂ emissions (E_{FOS}) are based on energy statistics and cement production data,
259 while emissions from land-use change (E_{LUC}) are based on land-use and land-use change data and bookkeeping
260 models. Atmospheric CO₂ concentration is measured directly, and its growth rate (G_{ATM}) is computed from the
261 annual changes in concentration. The [global net uptake of CO₂ by the ocean](#) (S_{OCEAN}, [called the ocean sink](#)) is
262 estimated with global ocean biogeochemistry models and observation-based fCO₂-products. The [global net](#)
263 [uptake of CO₂ by the land](#) (S_{LAND}, [called the land sink](#)) is estimated with dynamic global vegetation models.
264 Additional lines of evidence on land and ocean sinks are provided by atmospheric inversions, atmospheric
265 oxygen measurements and Earth System Models. The sum of all sources and sinks results in the carbon budget
266 imbalance (B_{IM}), a measure of imperfect data and incomplete understanding of the contemporary carbon cycle.
267 All uncertainties are reported as ±1σ.

Deleted: CO₂ sink

Deleted:)

Deleted: terrestrial

Deleted: sink

268 For the year 2023, E_{FOS} increased by 1.3% relative to 2022, with fossil emissions at 10.1 ± 0.5 GtC yr⁻¹ (10.3 ±
269 0.5 GtC yr⁻¹ when the cement carbonation sink is not included), E_{LUC} was 1.0 ± 0.7 GtC yr⁻¹, for a total
270 anthropogenic CO₂ emission (including the cement carbonation sink) of 11.1 ± 0.9 GtC yr⁻¹ (40.6 ± 3.2 GtCO₂
271 yr⁻¹). Also, for 2023, G_{ATM} was 5.9 ± 0.2 GtC yr⁻¹ (2.79 ± 0.1 ppm yr⁻¹), S_{OCEAN} was 2.9 ± 0.4 GtC yr⁻¹ and
272 S_{LAND} was 2.3 ± 1.0 GtC yr⁻¹, with a near zero B_{IM} (-0.02 GtC yr⁻¹). The global atmospheric CO₂ concentration
273 averaged over 2023 reached 419.31 ± 0.1 ppm. Preliminary data for 2024, suggest an increase in E_{FOS} relative
274 to 2023 of +0.8% (-0.2% to 1.7%) globally, and atmospheric CO₂ concentration increased by 2.87 ppm
275 reaching 422.45 ppm, 52% above pre-industrial level (around 278 ppm in 1750). Overall, the mean and trend
276 in the components of the global carbon budget are consistently estimated over the period 1959-2023, with a
277 near-zero overall budget imbalance, although discrepancies of up to around 1 GtC yr⁻¹ persist for the
278 representation of annual to semi-decadal variability in CO₂ fluxes. Comparison of estimates from multiple
279 approaches and observations shows: (1) a persistent large uncertainty in the estimate of land-use [change](#)
280 emissions, (2) a low agreement between the different methods on the magnitude of the land CO₂ flux in the
281 northern extra-tropics, and (3) a discrepancy between the different methods on the mean ocean sink.

Deleted: 3

Deleted: 3

Deleted: 9

Deleted: 8

Deleted: 5

Deleted: changes

296 [▲]This living data update documents changes in methods and datasets applied to this most-recent global carbon
297 budget as well as evolving community understanding of the global carbon cycle. The data presented in this
298 work are available at <https://doi.org/10.18160/GCP-2024> (Friedlingstein et al., 2024).[▲]

Formatted: Not Highlight

Formatted: Not Highlight

299

300 Executive Summary

301 **Global fossil CO₂ emissions (including cement carbonation) are expected to further increase in 2024 by**
302 **0.8%.** The 2023 emission increase was 0.14 GtC yr⁻¹ (0.5 GtCO₂ yr⁻¹) relative to 2022, bringing 2023 fossil CO₂
303 emissions to 10.1 ± 0.5 GtC yr⁻¹ (36.8 ± 1.8 GtCO₂ yr⁻¹). Preliminary estimates based on data available suggest
304 fossil CO₂ emissions to increase further in 2024, by 0.8% relative to 2023 (-0.2% to 1.7%), bringing emissions
305 to 10.2 GtC yr⁻¹ (37.4 GtCO₂ yr⁻¹).¹

Deleted: 3

Deleted: 9

306 Emissions from coal, oil and gas in 2024 are expected to be slightly above their 2023 levels (by 0.1%, 0.9% and
307 2.5% respectively). Regionally, fossil emissions in 2024 are expected to decrease by 2.8% in the European
308 Union reaching 0.7 GtC (2.4 GtCO₂), and by 0.9% in the United States (1.3 GtC, 4.9 GtCO₂). Emissions in
309 China are expected to increase in 2024 by 0.1% (3.3 GtC, 11.9 GtCO₂). Fossil emissions are also expected to
310 increase by 3.7% in India (0.9 GtC, 3.2 GtCO₂) and by 1.2% for the rest of the world (4.0 GtC, 14.5 GtCO₂) in
311 2024. Emissions from international aviation and shipping (IAS) are also expected to increase by 7.8% (0.3 GtC,
312 1.2 GtCO₂) in 2024.

Deleted: 2

Deleted: 4

Deleted: 3

Deleted: 6

Deleted: 2%, reaching

Deleted: (12.0

Deleted: 4.6

Deleted: 1

313 **Fossil CO₂ emissions decreased significantly in 23 countries with significantly growing economies during**
314 **the decade 2014-2023.** Altogether, these 23 countries contribute about 2.2 GtC yr⁻¹ (8.2 GtCO₂) fossil fuel CO₂
315 emissions over the last decade, representing about 23% of world CO₂ fossil emissions.

Deleted: 22

Deleted: 22

Deleted: 1

316 **Global CO₂ emissions from land-use, land-use change, and forestry (LULUCF) averaged 1.1 ± 0.7 GtC yr⁻¹**
317 **(4.1 ± 2.6 GtCO₂ yr⁻¹) for the 2014-2023 period with a similar preliminary projection for 2024 of 1.2 ±**
318 **0.7 GtC yr⁻¹ (4.2 ± 2.6 GtCO₂ yr⁻¹).** Since the late-1990s, emissions from LULUCF show a statistically
319 **significant decrease at a rate of around 0.2 GtC per decade.** Emissions from deforestation, the main driver of
320 global gross sources, remain high at around 1.7 GtC yr⁻¹ over the 2014-2023 period, highlighting the strong
321 potential of halting deforestation for emissions reductions. Sequestration of 1.2 GtC yr⁻¹ through re-
322 /afforestation and **forest regrowth in shifting cultivation cycles** offsets two third of the deforestation emissions.
323 Further, smaller emissions are due to other land-use transitions and peat drainage and peat fire. The highest
324 emitters during 2014-2023 in descending order were Brazil, Indonesia, and the Democratic Republic of the
325 Congo, with these 3 countries contributing more than half of global land-use CO₂ emissions.

Deleted: 1

Deleted: forestry

326 **Total anthropogenic emissions (fossil and LULUCF, including the carbonation sink) were 11.1 GtC yr⁻¹**
327 **(40.6 GtCO₂ yr⁻¹) in 2023, with a slightly higher preliminary estimate of 11.4 GtC yr⁻¹ (41.6 GtCO₂ yr⁻¹)**
328 **for 2024. Total anthropogenic emissions have been stable over the last decade (zero growth rate over the**

Deleted: marginally

Deleted: 3

Formatted: Superscript

¹ All 2024 growth rates use a leap year adjustment that corrects for the extra day in 2024.

346 2014-2023 period), much slower than over the previous decade (2004-2013) with an average growth rate
347 of 2.0% yr⁻¹.

348 The remaining carbon budget for a 50% likelihood to limit global warming to 1.5°C, 1.7°C and 2°C above
349 the 1850-1900 level has respectively been reduced to 65 GtC (235 GtCO₂), 160 GtC (585 GtCO₂) and 305
350 GtC (1110 GtCO₂) from the beginning of 2025, equivalent to around 6, 14 and 27 years, assuming 2024
351 emissions levels.

352 The concentration of CO₂ in the atmosphere is set to reach 422.45 ppm in 2024, 52% above pre-industrial
353 levels. The atmospheric CO₂ growth was 5.2 ± 0.02 GtC yr⁻¹ (2.5 ppm) during the decade 2014-2023 (48% of
354 total CO₂ emissions) with a preliminary 2024 growth rate estimate of around 6.1 GtC (2.87 ppm).

355 The ocean sink, the global net uptake of CO₂ by the ocean, has been stagnant since 2016 after rapid
356 growth during 2002-2016, largely in response to large inter-annual climate variability. The ocean CO₂ sink
357 was 2.9 ± 0.4 GtC yr⁻¹ during the decade 2014-2023 (26% of total CO₂ emissions). A slightly higher value of 3.0
358 GtC yr⁻¹ is preliminarily estimated for 2024, which marks an increase in the sink since 2023 due to the
359 prevailing El Niño and neutral conditions in 2024.

360 The land sink, the global net uptake of CO₂ by the land, continued to increase during the 2014-2023
361 period primarily in response to increased atmospheric CO₂, albeit with large interannual variability. The
362 land CO₂ sink was 3.2 ± 0.9 GtC yr⁻¹ during the 2014-2023 decade (30% of total CO₂ emissions). The land sink
363 in 2023 was 2.3 ± 1 GtC yr⁻¹, 1.6 GtC lower than in 2022, and the lowest estimate since 2015. This reduced sink
364 is primarily driven by a response of tropical land ecosystems to the onset of the 2023-2024 El Niño event,
365 combined with large wildfires in Canada in 2023. The preliminary 2024 estimate is around 3.2 GtC yr⁻¹, similar
366 to the decadal average, consistent with a land sink emerging from the El Niño state.

367 So far in 2024, global fire CO₂ emissions have been 11-32% higher than the 2014-2023 average due to
368 high fire activity in both North and South America, reaching 1.6-2.2 GtC during January-September. In
369 Canada, emissions through September were 0.2-0.3 GtC yr⁻¹, down from 0.5-0.8 GtC yr⁻¹ in 2023 but still more
370 than twice the 2014-2023 average. In Brazil, fires through September emitted 0.2-0.3 GtC yr⁻¹, 91-118% above
371 the 2014-2023 average due to intense drought. These fire emissions estimates should not be directly compared
372 with the land use emissions or the land sink, because they represent a gross carbon flux to the atmosphere and
373 do not account for post-fire recovery or distinguish between natural, climate-driven, and land-use-related fires.

374

Deleted: 5

Deleted: 5.9

Deleted: 8

Deleted: sink

Deleted: sink

Formatted: Font colour: Custom Colour (RGB(36,36,36))

Formatted: Font colour: Custom Colour (RGB(36,36,36))

380

381 1 Introduction

382 The concentration of carbon dioxide (CO₂) in the atmosphere has increased from approximately 278 parts per
383 million (ppm) in 1750 (Gulev et al., 2021), the beginning of the Industrial Era, to 419.3 ± 0.1 ppm in 2023 (Lan
384 et al., 2024a; Figure 1). The atmospheric CO₂ increase above pre-industrial levels was, initially, primarily
385 caused by the release of carbon to the atmosphere from deforestation and other land-use change activities
386 (Canadell et al., 2021). While emissions from fossil fuels started before the Industrial Era, they became the
387 dominant source of anthropogenic emissions to the atmosphere from around 1950 and their relative share has
388 continued to increase until present. Anthropogenic emissions occur on top of an active natural carbon cycle that
389 circulates carbon between the reservoirs of the atmosphere, ocean, and terrestrial biosphere on time scales from
390 sub-daily to millennial, while exchanges with geologic reservoirs occur on longer timescales (Archer et al.,
391 2009).

392 The global carbon budget (GCB) presented here refers to the mean, variations, and trends in the perturbation of
393 CO₂ in the environment, referenced to the beginning of the Industrial Era (defined here as 1750). This paper
394 describes the components of the global carbon cycle over the historical period with a stronger focus on the
395 recent period (since 1958, onset of robust atmospheric CO₂ measurements), the last decade (2014-2023), the last
396 year (2023) and the current year (2024). Finally, it provides cumulative emissions from fossil fuels and land-use
397 change since the year 1750, and since the year 1850 (the reference year for historical simulations in IPCC AR6)
398 (Eyring et al., 2016).

399 We quantify the input of CO₂ to the atmosphere by emissions from human activities, the growth rate of
400 atmospheric CO₂ concentration, and the resulting changes in the storage of carbon in the land and ocean
401 reservoirs in response to increasing atmospheric CO₂ levels, climate change and variability, and other
402 anthropogenic and natural changes (Figure 2). An understanding of this perturbation budget over time and the
403 underlying variability and trends of the natural carbon cycle is necessary to understand the response of natural
404 sinks to changes in climate, CO₂ and land-use change drivers, and to quantify emissions compatible with a given
405 climate stabilisation target.

406 The components of the CO₂ budget that are reported annually in this paper include separate and independent
407 estimates for the CO₂ emissions from (1) fossil fuel combustion and oxidation from all energy and industrial
408 processes; also including cement production and carbonation (E_{FOS} ; GtC yr⁻¹) and (2) the emissions resulting
409 from deliberate human activities on land, including those leading to land-use change (E_{LUC} ; GtC yr⁻¹); and their
410 partitioning among (3) the growth rate of atmospheric CO₂ concentration (G_{ATM} ; GtC yr⁻¹), and the uptake of
411 CO₂ (the 'CO₂ sinks') in (4) the ocean (S_{OCEAN} ; GtC yr⁻¹) and (5) on land (S_{LAND} ; GtC yr⁻¹). The CO₂ sinks as
412 defined here conceptually include the response of the land (including inland waters and estuaries) and ocean
413 (including coastal and marginal seas) to elevated CO₂ and changes in climate and other environmental
414 conditions, although in practice not all processes are fully accounted for (see Section 2.10). [Note that the term](#)

Formatted: Outline numbered + Level: 1 + Numbering
Style: 1, 2, 3, ... + Start at: 1 + Alignment: Left + Aligned at:
0 cm + Indent at: 0.76 cm

Deleted: 2024

416 [sink means that the net transfer of carbon is from the atmosphere to land or the ocean, but it does not imply any](#)
417 [permanence of that sink in the future.](#)

418 Global emissions and their partitioning among the atmosphere, ocean and land are in balance in the real world.
419 Due to the combination of imperfect spatial and/or temporal data coverage, errors in each estimate, and smaller
420 terms not included in our budget estimate (discussed in Section 2.10), the independent estimates (1) to (5) above
421 do not necessarily add up to zero. We hence estimate a budget imbalance (B_{IM}), which is a measure of the
422 mismatch between the estimated emissions and the estimated changes in the atmosphere, land and ocean, as
423 follows:

$$424 \quad B_{IM} = E_{FOS} + E_{LUC} - (G_{ATM} + S_{OCEAN} + S_{LAND}) \quad (1)$$

425 G_{ATM} is usually reported in ppm yr^{-1} , which we convert to units of carbon mass per year, GtC yr^{-1} , using 1 ppm
426 $= 2.124 \text{ GtC}$ (Ballantyne et al., 2012; Table 1). Units of gigatonnes of CO_2 (or billion tonnes of CO_2) used in
427 policy are equal to 3.664 multiplied by the value in units of GtC .

428 We also assess a set of additional lines of evidence derived from global atmospheric inversion system results
429 (Section 2.7), observed changes in oxygen concentration (Section 2.8) and Earth System Models (ESMs)
430 simulations (Section 2.9), all of these methods closing the global carbon balance (zero B_{IM}).

431 We further quantify E_{FOS} and E_{LUC} by country, including both territorial and consumption-based accounting for
432 E_{FOS} (see Section 2), and discuss missing terms from sources other than the combustion of fossil fuels (see
433 Section 2.10, Supplement S1 and S2). We also assess carbon dioxide removal (CDR) (see Sect. 2.2 and 2.3).
434 Land-based CDR is significant, but already accounted for in E_{LUC} in equation (1) (Sect 3.2.2). Other CDR
435 methods, not based on vegetation, are currently several orders of magnitude smaller than the other components
436 of the budget (Sect. 3.3), hence these are not included in equation (1), or in the global carbon budget tables or
437 figures (with the exception of Figure 2 where CDR is shown primarily for illustrative purpose).

438 The global CO_2 budget has been assessed by the Intergovernmental Panel on Climate Change (IPCC) in all
439 assessment reports (Prentice et al., 2001; Schimel et al., 1995; Watson et al., 1990; Denman et al., 2007; Ciais et
440 al., 2013; Canadell et al., 2021), and by others (e.g. Ballantyne et al., 2012). The Global Carbon Project (GCP,
441 www.globalcarbonproject.org, last access: [21 January 2025](#)) has coordinated this cooperative community effort
442 for the annual publication of global carbon budgets for the year 2005 (Raupach et al., 2007; including fossil
443 emissions only), year 2006 (Canadell et al., 2007), year 2007 (GCP, 2008), year 2008 (Le Quéré et al., 2009),
444 year 2009 (Friedlingstein et al., 2010), year 2010 (Peters et al., 2012a), year 2012 (Le Quéré et al., 2013; Peters
445 et al., 2013), year 2013 (Le Quéré et al., 2014), year 2014 (Le Quéré et al., 2015a; Friedlingstein et al., 2014),
446 year 2015 (Jackson et al., 2016; Le Quéré et al., 2015b), year 2016 (Le Quéré et al., 2016), year 2017 (Le Quéré
447 et al., 2018a; Peters et al., 2017a), year 2018 (Le Quéré et al., 2018b; Jackson et al., 2018), year 2019
448 (Friedlingstein et al., 2019; Jackson et al., 2019; Peters et al., 2020), year 2020 (Friedlingstein et al., 2020; Le
449 Quéré et al., 2021), year 2021 (Friedlingstein et al., 2022a; Jackson et al., 2022), year 2022 (Friedlingstein et al.,

Deleted: 28 October 2024

451 2022b), and most recently the year 2023 (Friedlingstein et al., 2023). Each of these papers updated previous
452 estimates with the latest available information for the entire time series.

453 We adopt a range of ± 1 standard deviation (σ) to report the uncertainties in our global estimates, representing a
454 likelihood of 68% that the true value will be within the provided range if the errors have a gaussian distribution,
455 and no bias is assumed. This choice reflects the difficulty of characterising the uncertainty in the CO₂ fluxes
456 between the atmosphere and the ocean and land reservoirs individually, particularly on an annual basis, as well
457 as the difficulty of updating the CO₂ emissions from land-use change. A likelihood of 68% provides an
458 indication of our current capability to quantify each term and its uncertainty given the available information.
459 The uncertainties reported here combine statistical analysis of the underlying data, assessments of uncertainties
460 in the generation of the datasets, and expert judgement of the likelihood of results lying outside this range. The
461 limitations of current information are discussed in the paper and have been examined in detail elsewhere
462 (Ballantyne et al., 2015; Zscheischler et al., 2017). We also use a qualitative assessment of confidence level to
463 characterise the annual estimates from each term based on the type, amount, quality, and consistency of the
464 different lines of evidence as defined by the IPCC (Stocker et al., 2013).

465 This paper provides a detailed description of the datasets and methodology used to compute the global carbon
466 budget estimates for the industrial period, from 1750 to 2024, and in more detail for the period since 1959. This
467 paper is updated every year using the format of 'living data' to keep a record of budget versions and the changes
468 in new data, revision of data, and changes in methodology that lead to changes in estimates of the carbon
469 budget. Additional materials associated with the release of each new version will be posted at the Global Carbon
470 Project (GCP) website (<http://www.globalcarbonproject.org/carbonbudget>, last access: [21 January 2025](#)), with
471 fossil fuel emissions also available through the Global Carbon Atlas (<http://www.globalcarbonatlas.org>, last
472 access: [21 January 2025](#)). All underlying data used to produce the budget can also be found at
473 <https://globalcarbonbudget.org/> (last access: [21 January 2025](#)). With this approach, we aim to provide the
474 highest transparency and traceability in the reporting of CO₂, the key driver of climate change.

475 2 Methods

476 Multiple organisations and research groups around the world generated the original measurements and data used
477 to complete the global carbon budget. The effort presented here is thus mainly one of synthesis, where results
478 from individual groups are collated, analysed, and evaluated for consistency. We facilitate access to original
479 data with the understanding that primary datasets will be referenced in future work (see Table 2 for how to cite
480 the datasets, and Section on data availability). Descriptions of the measurements, models, and methodologies
481 follow below, with more detailed descriptions of each component provided as Supplementary Information (S1 to
482 S5).

483 This is the 19th version of the global carbon budget and the 13th revised version in the format of a living data
484 update in Earth System Science Data. It builds on the latest published global carbon budget of Friedlingstein et
485 al. (2023). The main changes this year are: the inclusion of (1) data to year 2023 and a projection for the global
486 carbon budget for year 2024; and (2) an estimate of the 2024 projection of fossil emissions from Carbon

Deleted: 28 October 2024

Deleted: 28 October 2024

Deleted: 28 October 2024

Formatted: Outline numbered + Level: 1 + Numbering
Style: 1, 2, 3, ... + Start at: 1 + Alignment: Left + Aligned at:
0 cm + Indent at: 0.76 cm

490 Monitor. Other methodological differences between recent annual carbon budgets (2020 to 2024) are
491 summarised in Table 3 and previous changes since 2006 are provided in Table S9.

492 **2.1 Fossil CO₂ emissions (E_{FOS})**

493 **2.1.1 Historical period 1850-2023**

494 The estimates of global and national fossil CO₂ emissions (E_{FOS}) include the oxidation of fossil fuels through
495 both combustion (e.g., transport, heating) and chemical oxidation (e.g. carbon anode decomposition in
496 aluminium refining) activities, and the decomposition of carbonates in industrial processes (e.g. the production
497 of cement). We also include CO₂ uptake from the cement carbonation process. Several emissions sources are not
498 estimated or not fully covered: coverage of emissions from lime production are not global, and decomposition of
499 carbonates in glass and ceramic production are included only for the “Annex 1” countries of the United Nations
500 Framework Convention on Climate Change (UNFCCC) for lack of activity data. These omissions are
501 considered to be minor. Short-cycle carbon emissions - for example from combustion of biomass - are not
502 included here but are accounted for in the CO₂ emissions from land use (see Section 2.2).

503 Our estimates of fossil CO₂ emissions rely on data collection by many other parties. Our goal is to produce the
504 best estimate of this flux, and we therefore use a prioritisation framework to combine data from different
505 sources that have used different methods, while being careful to avoid double counting and undercounting of
506 emissions sources. The CDIAC-FF emissions dataset, derived largely from UN energy data, forms the
507 foundation, and we extend emissions to 2023 using energy growth rates reported by the Energy Institute (a
508 dataset formerly produced by BP). We then proceed to replace estimates using data from what we consider to be
509 superior sources, for example Annex 1 countries’ official submissions to the UNFCCC. All data points are
510 potentially subject to revision, not just the latest year. For full details see Andrew and Peters (2024).

511 Other estimates of global fossil CO₂ emissions exist, and these are compared by Andrew (2020a). The most
512 common reason for differences in estimates of global fossil CO₂ emissions is a difference in which emissions
513 sources are included in the datasets. Datasets such as those published by the Energy Institute, the US Energy
514 Information Administration, and the International Energy Agency’s ‘CO₂ emissions from fuel combustion’ are
515 all generally limited to emissions from combustion of fossil fuels. In contrast, datasets such as PRIMAP-hist,
516 CEDS, EDGAR, and GCP’s dataset aim to include all sources of fossil CO₂ emissions. See Andrew (2020a) for
517 detailed comparisons and discussion.

518 Cement absorbs CO₂ from the atmosphere over its lifetime, a process known as ‘cement carbonation’. We
519 estimate this CO₂ sink, from 1931 onwards, as the average of two studies in the literature (Cao et al., 2020; Guo
520 et al., 2021). Both studies use the same model, developed by Xi et al. (2016), with different parameterisations
521 and input data, with the estimate of Guo and colleagues being a revision of Xi et al. (2016). The trends of the
522 two studies are very similar. Since carbonation is a function of both current and previous cement production, we
523 extend these estimates to 2023 by using the growth rate derived from the smoothed cement emissions (10-year

Formatted: Outline numbered + Level: 2 + Numbering
Style: 1, 2, 3, ... + Start at: 1 + Alignment: Left + Aligned at:
0 cm + Indent at: 1.02 cm

Formatted: Outline numbered + Level: 3 + Numbering
Style: 1, 2, 3, ... + Start at: 1 + Alignment: Left + Aligned at:
0 cm + Indent at: 1.27 cm

524 smoothing) fitted to the carbonation data. In the present budget, we always include the cement carbonation
525 carbon sink in the fossil CO₂ emission component (E_{FOS}).

526 We use the Kaya Identity for a simple decomposition of CO₂ emissions into the key drivers (Raupach et al.,
527 2007). While there are variations (Peters et al., 2017a), we focus here on a decomposition of CO₂ emissions into
528 population, GDP per person, energy use per GDP, and CO₂ emissions per energy. Multiplying these individual
529 components together returns the CO₂ emissions. Using the decomposition, it is possible to attribute the change
530 in CO₂ emissions to the change in each of the drivers. This method gives a first-order understanding of what
531 causes CO₂ emissions to change each year.

532 2.1.2 2024 projection

533 We provide a projection of global fossil CO₂ emissions in 2024 by combining separate projections for China,
534 USA, EU, India, and for all other countries combined. The methods are different for each of these. For China we
535 combine monthly fossil fuel production data from the National Bureau of Statistics and trade data from the
536 Customs Administration, giving us partial data for the growth rates to date of natural gas, petroleum, and
537 cement, and of the apparent consumption itself for raw coal. We then use a regression model to project full-year
538 emissions based on historical observations. For the USA our projection is taken directly from the Energy
539 Information Administration's (EIA) Short-Term Energy Outlook (EIA, 2024), combined with the year-to-date
540 growth rate of cement clinker production. For the EU we use monthly energy data from Eurostat to derive
541 estimates of monthly CO₂ emissions, with coal emissions extended using a statistical relationship with reported
542 electricity generation from coal and other factors. For natural gas preliminary observations are available through
543 December. EU emissions from oil are derived using the EIA's projection of oil consumption for Europe. EU
544 cement emissions are based on available year-to-date data from three of the largest producers, Germany, Poland,
545 and Spain. India's projected emissions are derived from monthly estimates using the methods of Andrew
546 (2020b) and extrapolated through December assuming seasonal patterns from before 2019. Emissions from
547 international transportation (bunkers) are estimated separately for aviation and shipping. Changes in aviation
548 emissions are derived primarily from OECD monthly estimates, extrapolated using the growth rates of global
549 flight miles from Airportia, and then the final months are projected assuming normal patterns from previous
550 years. Changes in shipping emissions are derived from OECD monthly estimates for global shipping. Emissions
551 for the rest of the world are derived for coal and cement using projected growth in economic production from
552 the IMF (2024) combined with extrapolated changes in emissions intensity of economic production; for oil
553 using a global constraint from EIA; and for natural gas using a global constraint from IEA. More details on the
554 E_{FOS} methodology and its 2024 projection can be found in Supplement S.1.

555 For the first time this year, we cross check our 2024 projection with a 2024 projection from Carbon Monitor.
556 Carbon Monitor is an open access dataset (<https://carbonmonitor.org/>) of daily emissions constructed using
557 hourly to daily proxy data (e.g., electricity consumption, travel patterns, etc) instead of energy use data.

558 Available Carbon Monitor estimated emissions from January to November are combined to a new projection for,
559 December to give a full year 2024 estimate. The December projections are estimated by leveraging seasonal

Formatted: Outline numbered + Level: 3 + Numbering
Style: 1, 2, 3, ... + Start at: 1 + Alignment: Left + Aligned at:
0 cm + Indent at: 1.27 cm

Deleted: through July

Deleted: through September

Deleted: we use Holt-Winters to project the last four months
of the year.

Deleted: through August (July for coal)

Deleted: 2023

Deleted: August

Deleted: September to

Deleted: September to

569 patterns from 2019-2023 daily CO₂ emission data from Carbon Monitor. A regression model is applied
570 separately for individual countries to obtain their respective forecast. First, the seasonality component for each
571 month is assessed based on daily average emissions from 2019 to 2023, excluding 2020 due to the COVID-19
572 pandemic. Then, a linear regression model is constructed using the calculated seasonal components and the daily
573 average emissions for the months from January to November 2024. The resulting model is used to project
574 carbon emissions for the December 2024. The uncertainty range is calculated by using historical monthly
575 variance of seasonal components.

Deleted: 4-month

Deleted: August

Deleted: remaining months of

576 2.2 CO₂ emissions from land-use, land-use change and forestry (ELUC)

577 2.2.1 Historical period 1850-2023

578 The net CO₂ flux from land-use, land-use change and forestry (ELUC, called land-use change emissions in the
579 rest of the text) includes CO₂ fluxes from deforestation, afforestation, logging and forest degradation (including
580 harvest activity), shifting cultivation (cycle of cutting forest for agriculture, then abandoning), regrowth of
581 forests (following wood harvest or agriculture abandonment), peat burning, and peat drainage.

Formatted: Outline numbered + Level: 2 + Numbering Style: 1, 2, 3, ... + Start at: 1 + Alignment: Left + Aligned at: 0 cm + Indent at: 1.02 cm

Formatted: Outline numbered + Level: 3 + Numbering Style: 1, 2, 3, ... + Start at: 1 + Alignment: Left + Aligned at: 0 cm + Indent at: 1.27 cm

582 Four bookkeeping approaches were used to quantify gross emissions and gross removals and the resulting net
583 ELUC, the updated estimates each of BLUE (Hansis et al., 2015), OSCAR (Gasser et al., 2020), and H&C2023
584 (Houghton and Castanho, 2023), and the new estimates of LUCE (Qin et al. 2024). Emissions from peat burning
585 and peat drainage are added from external datasets, (see Supplement S.2.1): peat fire emissions from the Global
586 Fire Emission Database (GFED4s; van der Werf et al., 2017) and peat drainage emissions averaged from
587 estimates of the Food Agriculture Organization (Conchedda and Tubiello, 2020; FAO, 2023) and from
588 simulations with the DGVM ORCHIDEE-PEAT (Qiu et al., 2021) and the DGVM LPX-Bern (Lienert and Joos,
589 2018; Müller and Joos, 2021). Uncertainty estimates were derived from the Dynamic Global Vegetation Models
590 (DGVMs) ensemble for the time period prior to 1960, and using for the recent decades an uncertainty range of
591 $\pm 0.7 \text{ GtC yr}^{-1}$, which is a semi-quantitative measure for annual and decadal emissions and reflects our best value
592 judgement that there is at least 68% chance ($\pm 1\sigma$) that the true land-use change emission lies within the given
593 range, for the range of processes considered here.

Deleted: (

Deleted:) were used to quantify gross emissions and gross removals and the resulting net ELUC.

Deleted: , peat

Deleted: being

Deleted: three spatially explicit independent datasets (see Supplement S.2.1

594 The GCB ELUC estimates follow the CO₂ flux definition of global carbon cycle models and differ from IPCC
595 definitions adopted in National GHG Inventories (NGHGI) for reporting under the UNFCCC. The latter
596 typically include terrestrial fluxes occurring on all land that countries define as managed, following the IPCC
597 managed land proxy approach (Grassi et al., 2018). This partly includes fluxes due to environmental change
598 (e.g. atmospheric CO₂ increase), which are part of S_{LAND} in our definition. As a result, global emission estimates
599 are smaller for NGHGI than for the global carbon budget definition (Grassi et al., 2023). The same is the case
600 for the FAO estimates of carbon fluxes on forest land, which include both anthropogenic and natural fluxes on
601 managed land (Tubiello et al., 2021). We translate the GCB and NGHGI definitions to each other, to provide a
602 comparison of the anthropogenic carbon budget as reported in GCB to the official country reporting to the
603 UNFCCC convention. We further compare these estimates with the net atmosphere-to-land flux from
604 atmospheric inversion systems (see Section 2.7), averaged over managed land only.

Deleted: Food Agriculture Organization (

Deleted:)

617 ELUC contains a range of fluxes that are related to Carbon Dioxide Removal (CDR). CDR is defined as the set of
 618 anthropogenic activities that remove CO₂ from the atmosphere, ~~in addition~~ to the Earth's natural processes, ~~(such~~
 619 ~~as carbon uptake in response to atmospheric CO₂ increase)~~, and store it in durable form, such as in forest
 620 biomass, soils, long-lived products, ~~ocean or geological~~ reservoirs. Here, we quantify vegetation-based CDR
 621 that is implicitly or explicitly captured by land-use fluxes (CDR not based on vegetation is discussed in Section
 622 2.3). We quantify re/afforestation from the four bookkeeping estimates by separating forest regrowth in shifting
 623 cultivation cycles from permanent increases in forest cover (see Supplement S.2.1). The latter count as CDR,
 624 but it should be noted that the permanence of the storage under climate risks such as fire is increasingly
 625 questioned. Other CDR activities ~~related to land use but not fully accounted for in our ELUC estimate~~ include the
 626 transfer of carbon to harvested wood products (HWP), bioenergy with carbon capture and storage (BECCS), and
 627 biochar production ~~(Babiker et al., 2022; Smith et al., 2024). The different bookkeeping models all represent~~
 628 HWP ~~but~~ with varying details concerning product usage and their lifetimes. ~~BECCS and biochar are currently~~
 629 ~~only represented in bookkeeping~~ and TRENDY models with regard to the CO₂ removal through photosynthesis,
 630 ~~without accounting~~ for the durable storage. HWP, BECCS, and biochar are typically counted as CDR ~~once~~ the
 631 transfer to the durable storage site occurs and not when the CO₂ is removed from the atmosphere, which
 632 complicates a direct comparison to the GCB approach to quantify annual fluxes to and from the atmosphere. ~~We~~
 633 ~~provide estimates for CDR through HWP, BECCS, and biochar based on independent studies in Section 3.2.2,~~
 634 ~~but do not add them to our ELUC estimate to avoid potential double-counting that arises from the partial~~
 635 ~~consideration of HWP, BECCS, and biochar in the bookkeeping and TRENDY models and to avoid~~
 636 ~~inconsistencies from the temporal discrepancy between transfer to storage and removal from the atmosphere.~~

637 2.2.2 2024 Projection

638 We project the 2024 land-use emissions for BLUE, H&C2023, OSCAR, and LUCE based on their ELUC
 639 estimates for 2023 and adding the change in carbon emissions from peat fires and tropical deforestation and
 640 degradation fires (2024 emissions relative to 2023 emissions) estimated using active fire data (MCD14ML;
 641 Giglio et al., 2016). Peat drainage is assumed to be unaltered as it has low interannual variability. More details
 642 on the ELUC methodology can be found in Supplement S.2.

643 2.3 Carbon Dioxide Removal (CDR) not based on vegetation

644 While some CDR involves CO₂ fluxes via land-use and is included in ~~our estimate of ELUC, (re/afforestation) or~~
 645 ~~provided from other data sources~~ (biochar, HWP, and BECCS), other CDR occurs through fluxes of CO₂
 646 directly from the air to the geosphere. The majority of this derives from enhanced weathering through the
 647 application of crushed rock to soils, with a smaller contribution from Direct Air Carbon Capture and Storage
 648 (DACCS). We use data from the State of CDR Report (Smith et al., 2024), which compiles and harmonises
 649 reported removal rates from a combination of existing databases, surveys and novel research. Currently there are
 650 no internationally agreed methods for reporting these types of CDR, meaning estimates are based on self-
 651 disclosure by projects following their own protocols. As such, the fractional uncertainty on these numbers

Formatted: Font: Times New Roman

Deleted: additional

Deleted: ,

Formatted: Font: Times New Roman, Not Italic

Formatted: Font: Times New Roman

Formatted: Font: Times New Roman

Formatted: Font: Times New Roman

Deleted: and

Deleted: in

Deleted: or ocean

Deleted: ; IPCC, 2023

Deleted: contained

Deleted:);

Deleted: . Note that the

Deleted: Bookkeeping

Deleted: currently only represent BECCS and biochar

Deleted: but do not account

Deleted: when

Deleted: Estimates for CDR through HWP, BECCS, and biochar are thus not indicated in this budget, but can be found elsewhere (see Section 3.2.2).

Formatted: Outline numbered + Level: 3 + Numbering
 Style: 1, 2, 3, ... + Start at: 1 + Alignment: Left + Aligned at:
 0 cm + Indent at: 1.27 cm

Formatted: Outline numbered + Level: 2 + Numbering
 Style: 1, 2, 3, ... + Start at: 1 + Alignment: Left + Aligned at:
 0 cm + Indent at: 1.02 cm

Deleted: such as

Deleted: ,

Deleted:)

671 should be viewed as substantial, and they are liable to change in future years as protocols are harmonised and
672 improved.

673 2.4 Growth rate in atmospheric CO₂ concentration (G_{ATM})

674 2.4.1 Historical period 1850-2023

675 The rate of growth of the atmospheric CO₂ concentration is provided for years 1959-2023 by the US National
676 Oceanic and Atmospheric Administration Global Monitoring Laboratory (NOAA/GML; Lan et al., 2024a),
677 which includes recent revisions to the calibration scale of atmospheric CO₂ measurements (WMO-CO₂-X2019;
678 Hall et al., 2021). For the 1959-1979 period, the global growth rate is based on measurements of atmospheric
679 CO₂ concentration averaged from the Mauna Loa and South Pole stations, as observed by the CO₂ Program at
680 Scripps Institution of Oceanography (Keeling et al., 1976). For the 1980-2021 time period, the global growth
681 rate is based on the average of multiple stations selected from the marine boundary layer sites with well-mixed
682 background air (Lan et al., 2023), after fitting a smooth curve through the data for each station as a function of
683 time, and averaging by latitude band (Masarie and Tans, 1995). The annual growth rate is estimated by Lan et
684 al. (2024a) from atmospheric CO₂ concentration by taking the average of the most recent December-January
685 months corrected for the average seasonal cycle and subtracting this same average one year earlier. The growth
686 rate in units of ppm yr⁻¹ is converted to units of GtC yr⁻¹ by multiplying by a factor of 2.124 GtC per ppm,
687 assuming instantaneous mixing of CO₂ throughout the atmosphere (Ballantyne et al., 2012; Table 1).

688 The uncertainty around the atmospheric growth rate is due to three main factors. First, the network composition
689 of the marine boundary layer sites with some sites coming or going, gaps in the time series at each site, etc. This
690 uncertainty was estimated with a bootstrap method by constructing 100 "alternative" networks (Steele et al.,
691 1992; Masarie and Tans, 1995; Lan et al., 2024a). Second, the analytical uncertainty that describes the short-
692 and long-term uncertainties associated with the CO₂ analyzers. A Monte Carlo method was used to estimate the
693 total analytical uncertainty by randomly selecting errors to add to each observation from a normal distribution of
694 combined short- and long-term uncertainties. Prior to the 1980s when analyzers were less precise and CO₂
695 measurement scale was slightly less well defined, larger analytical errors were assigned to account for these
696 factors. However, the network uncertainty remains the larger term of uncertainty. The first and second
697 uncertainties are reported as 1-sigma standard deviations (i.e., 68% confidence interval), and summed in
698 quadrature to determine the global surface growth rate uncertainty, which averaged to 0.085 ppm (Lan et al.,
699 2024b). Third, the uncertainty associated with using the average CO₂ concentration from a surface network to
700 approximate the true atmospheric average CO₂ concentration (mass-weighted, in 3 dimensions) as needed to
701 assess the total atmospheric CO₂ burden. In reality, CO₂ variations measured at the stations will not exactly
702 track changes in total atmospheric burden, with offsets in magnitude and phasing due to vertical and horizontal
703 mixing. This effect must be very small on decadal and longer time scales, when the atmosphere can be
704 considered well mixed. The long-term CO₂ increase in the stratosphere lags the increase (meaning lower
705 concentrations) that we observe in the marine boundary layer, while the continental boundary layer (where most
706 of the emissions take place) leads the marine boundary layer with higher concentrations. These effects nearly

Formatted: Outline numbered + Level: 2 + Numbering
Style: 1, 2, 3, ... + Start at: 1 + Alignment: Left + Aligned at:
0 cm + Indent at: 1.02 cm

Formatted: Outline numbered + Level: 3 + Numbering
Style: 1, 2, 3, ... + Start at: 1 + Alignment: Left + Aligned at:
0 cm + Indent at: 1.27 cm

Deleted: 2024

Deleted: Ballantyne

Deleted: 2012

Deleted: 2024

Deleted: four

Deleted: long-term reproducibility of reference gas standards
(around 0.03 ppm for 1σ from the 1980s; Lan et al., 2024).
Second, small unexplained systematic analytical errors that
may have a duration of several months to two years come and
go. They have been simulated by randomising both the
duration and the magnitude (determined from the existing
evidence) in a Monte Carlo procedure. Third, the

Deleted: (Lan et al., 2024). The latter

Deleted: by NOAA/GML

Deleted: Monte Carlo

Deleted: NOAA/GML, 2019). The second and third

Deleted: ,

Deleted: , add up

Deleted: on average

Deleted: 2024). Fourth

Formatted: Subscript

727 cancel each other. In addition, the growth rate is nearly the same everywhere (Ballantyne et al., 2012). We
728 therefore maintain an uncertainty around the annual growth rate based on the multiple stations dataset ranges
729 between 0.11 and 0.72 GtC yr⁻¹, with a mean of 0.61 GtC yr⁻¹ for 1959-1979 and 0.17 GtC yr⁻¹ for 1980-2023,
730 when [when more measurement sites](#) were available (Lan et al., 2024a). We estimate the uncertainty of the
731 decadal averaged growth rate after 1980 at 0.02 GtC yr⁻¹ based on the [annual growth rate uncertainty](#) but
732 stretched over a 10-year interval. For years prior to 1980, we estimate the decadal averaged uncertainty to be
733 0.07 GtC yr⁻¹ based on a factor proportional to the annual uncertainty prior and after 1980 (0.02 * [0.61/0.17]
734 GtC yr⁻¹).

735 We assign a high confidence to the annual estimates of G_{ATM} because they are based on direct measurements
736 from [stations distributed around the world \(Lan et al., 2023\) with all CO₂ measurements consistently measured](#)
737 [against the same CO₂ standard scale \(WMO X2019\) defined by a suite of gas standards](#) (Hall et al., 2021).

738 To estimate the total carbon accumulated in the atmosphere since 1750 or 1850, we use an atmospheric CO₂
739 concentration of 278.3 ± 3 ppm or 285.1 ± 3 ppm, respectively (Gulev et al., 2021). For the construction of the
740 cumulative budget shown in Figure 3, we use the fitted estimates of CO₂ concentration from Joos and Spahni
741 (2008) to estimate the annual atmospheric growth rate using the conversion factors shown in Table 1. The
742 uncertainty of ±3 ppm (converted to ±1σ) is taken directly from the IPCC's AR5 assessment (Ciais et al., 2013).
743 Typical uncertainties in the growth rate in atmospheric CO₂ concentration from ice core data are equivalent to
744 ±0.1-0.15 GtC yr⁻¹ as evaluated from the Law Dome data (Etheridge et al., 1996) for individual 20-year intervals
745 over the period from 1850 to 1960 (Bruno and Joos, 1997).

746 2.4.2 2024 projection

747 We provide an assessment of G_{ATM} for 2024 as the average of two methods. The GCB regression method
748 models monthly global-average atmospheric CO₂ concentrations and derives the increment and annual average
749 from these. The model uses lagged observations of concentration (Lan et al., 2024a): both a 12-month lag, and
750 the lowest lag that will allow model prediction to produce an estimate for the following January, recalling that
751 the G_{ATM} increment is derived from December/January pairs. The largest driver of interannual changes is the
752 ENSO signal (Betts et al., 2016), so the monthly ENSO 3.4 index (Huang et al., 2023) is included in the model.
753 Given the natural lag between sea-surface temperatures and effects on the biosphere, and in turn effects on
754 globally mixed atmospheric CO₂ concentration, a lagged ENSO index is used, and we use both a 5-month and a
755 6-month lag. The combination of the two lagged ENSO values helps reduce possible effects of noise in a single
756 month. To help characterise the seasonal variation, we add month as a categorical variable. Finally, we flag the
757 period affected by the Pinatubo eruption (August 1991 - November 1993) as a categorical variable. Note that
758 while emissions of CO₂ are the largest driver of the trend in atmospheric CO₂ concentration, our goal here is to
759 predict divergence from that trend. Because changes in emissions from year to year are relatively minor in
760 comparison to total emissions, this has little effect on the variation of concentration from the trend line. Even the
761 relatively large drop in emissions in 2020 due to the COVID-19 pandemic does not cause any problems for the
762 model.

Deleted: a larger set of stations

Deleted: as provided by

Deleted: . (2024

Deleted: calibration and the

Deleted: multiple and consistent instruments and

Deleted: Ballantyne

Deleted: ., 2012;

Formatted: Outline numbered + Level: 3 + Numbering
Style: 1, 2, 3, ... + Start at: 1 + Alignment: Left + Aligned at:
0 cm + Indent at: 1.27 cm

Deleted: 2024

771 We also use the multi-model mean and uncertainty of the 2024 G_{ATM} estimated by the ESMs prediction system
772 (see Section 2.9). We then take the average of the GCB regression and ESMs G_{ATM} estimates, with their
773 respective uncertainty combined quadratically.

774 Similarly, the projection of the 2024 global average CO_2 concentration (in ppm), is calculated as the average of
775 the estimates from the two methods. For the GCB regression method, it is the annual average of global
776 concentration over the 12 months of 2024; for the ESMs, it is the observed global average CO_2 concentration for
777 2023 plus the annual increase in 2024 of the global average CO_2 concentration predicted by the ESMs multi-
778 model mean.

779 2.5 Ocean CO_2 sink

780 2.5.1 Historical period 1850-2023

781 The reported estimate of the global ocean anthropogenic CO_2 sink S_{OCEAN} is derived as the average of two
782 estimates. The first estimate is derived as the mean over an ensemble of ten global ocean biogeochemistry
783 models (GOBMs, Table 4 and Table S2). The second estimate is obtained as the mean over an ensemble of eight
784 surface ocean fCO_2 -observation-based data-products (Table 4 and Table S3). A ninth fCO_2 -product (UEXP-FFN-
785 U) is shown but is not included in the ensemble average as it differs from the other products by adjusting the
786 flux to a cool, salty ocean surface skin. In previous editions of the GCB, this product was following the Watson
787 et al. (2020) method but has been updated following the method of Dong et al. (2022, see Supplement S.3.1 for
788 a discussion). The GOBMs simulate both the natural and anthropogenic CO_2 cycles in the ocean. They constrain
789 the anthropogenic air-sea CO_2 flux (the dominant component of S_{OCEAN}) by the transport of carbon into the
790 ocean interior, which is also the controlling factor of present-day ocean carbon uptake in the real world. They
791 cover the full globe and all seasons and were evaluated against surface ocean carbon observations, suggesting
792 they are suitable to estimate the annual ocean carbon sink (Hauck et al., 2020). The fCO_2 -products are tightly
793 linked to observations of fCO_2 (fugacity of CO_2 , which equals pCO_2 corrected for the non-ideal behaviour of the
794 gas; Pfeil et al., 2013), which carry imprints of temporal and spatial variability, but are also sensitive to
795 uncertainties in gas-exchange parameterizations and data-sparsity (Fay et al., 2021, Gloege et al., 2021, Hauck
796 et al., 2023a). Their asset is the assessment of the mean spatial pattern of variability and its seasonality (Hauck
797 et al., 2020, Gloege et al. 2021, Hauck et al., 2023a). To benchmark trends derived from the fCO_2 -products, we
798 additionally performed a model subsampling exercise following Hauck et al. (2023a, see section S3). In
799 addition, two diagnostic ocean models are used to estimate S_{OCEAN} over the industrial era (1781-1958).

800 The global fCO_2 -based flux estimates were adjusted to remove the pre-industrial ocean source of CO_2 to the
801 atmosphere of $0.65 \pm 0.3 \text{ GtC yr}^{-1}$ from river input to the ocean (Regnier et al., 2022), to satisfy our definition of
802 S_{OCEAN} (Hauck et al., 2020). The river flux adjustment was distributed over the latitudinal bands using the
803 regional distribution of Lacroix et al. (2020; North: 0.14 GtC yr^{-1} , Tropics: 0.42 GtC yr^{-1} , South: 0.09 GtC yr^{-1}).
804 Acknowledging that this distribution is based on only one model, the advantage is that a gridded field is
805 available, and the river flux adjustment can be calculated for the three latitudinal bands and the RECCAP
806 regions (REgional Carbon Cycle Assessment and Processes (RECCAP2; Ciais et al., 2020, Poulter et al., 2022,

Formatted: Outline numbered + Level: 2 + Numbering
Style: 1, 2, 3, ... + Start at: 1 + Alignment: Left + Aligned at:
0 cm + Indent at: 1.02 cm

Formatted: Outline numbered + Level: 3 + Numbering
Style: 1, 2, 3, ... + Start at: 1 + Alignment: Left + Aligned at:
0 cm + Indent at: 1.27 cm

807 DeVries et al., 2023). This dataset suggests that more of the riverine outgassing is located in the tropics than in
808 the Southern Ocean and is thus opposed to the previously used dataset of Aumont et al. (2001). Accordingly, the
809 regional distribution is associated with a major uncertainty in addition to the large uncertainty around the global
810 estimate (Crisp et al., 2022; Gruber et al., 2023). Anthropogenic perturbations of river carbon and nutrient
811 transport to the ocean are not considered (see Section 2.10 and Supplement S.6.3).

812 We derive S_{OCEAN} from GOBMs by using a simulation (sim A) with historical forcing of climate and
813 atmospheric CO_2 from GCB (Section 2.4), accounting for model biases and drift from a control simulation (sim
814 B) with constant atmospheric CO_2 and normal year climate forcing. A third simulation (sim C) with historical
815 atmospheric CO_2 increase and normal year climate forcing is used to attribute the ocean sink to CO_2 (sim C
816 minus sim B) and climate (sim A minus sim C) effects. A fourth simulation (sim D; historical climate forcing
817 and constant atmospheric CO_2) is used to compare the change in anthropogenic carbon inventory in the interior
818 ocean (sim A minus sim D) to the observational estimate of Gruber et al. (2019) with the same flux components
819 (steady state and non-steady state anthropogenic carbon flux). The fCO_2 -products are adjusted with respect to
820 their original publications to represent the full ice-free ocean area, including coastal zones and marginal seas,
821 when the area coverage is below 99%. This is done by either area filling following Fay et al. (2021) or a simple
822 scaling approach. GOBMs and fCO_2 -products fall within the observational constraints over the 1990s (2.2 ± 0.7
823 $GtC\ yr^{-1}$, Ciais et al., 2013) before and after applying adjustments.

824 S_{OCEAN} is calculated as the average of the GOBM ensemble mean and the fCO_2 -product ensemble mean from
825 1990 onwards. Prior to 1990, it is calculated as the GOBM ensemble mean plus half of the offset between
826 GOBMs and fCO_2 -products ensemble means over 1990-2001.

827 We assign an uncertainty of $\pm 0.4\ GtC\ yr^{-1}$ to the ocean sink based on a combination of random (ensemble
828 standard deviation) and systematic uncertainties (GOBMs bias in anthropogenic carbon accumulation,
829 previously reported uncertainties in fCO_2 -products; see Supplement S.3.4). While this approach is consistent
830 within the GCB, an independent uncertainty assessment of the fCO_2 -products alone suggests a somewhat larger
831 uncertainty of up to $0.7\ GtC\ yr^{-1}$ (Ford et al. 2024, accepted). We assess a medium confidence level to the
832 annual ocean CO_2 sink and its uncertainty because it is based on multiple lines of evidence, it is consistent with
833 ocean interior carbon estimates (Gruber et al., 2019, see Section 3.6.5) and the interannual variability in the
834 GOBMs and data-based estimates is largely consistent and can be explained by climate variability. We refrain
835 from assigning a high confidence because of the deviation between the GOBM and fCO_2 -product trends
836 between around 2002 and 2020. More details on the S_{OCEAN} methodology can be found in Supplement S.3.

837 2.5.2 2024 Projection

838 The ocean CO_2 sink forecast for the year 2024 is based on (a) the historical (Lan et al., 2024a) and our 2024
839 estimate of atmospheric CO_2 concentration, (b) the historical and our 2024 estimate of global fossil fuel
840 emissions, and (c) the boreal spring (March, April, May) Oceanic Niño Index (ONI) (NCEP, 2024). Using a
841 non-linear regression approach, i.e., a feed-forward neural network, atmospheric CO_2 , ONI, and the fossil fuel
842 emissions are used as training data to best match the annual ocean CO_2 sink (i.e. combined S_{OCEAN} estimate from

Formatted: Outline numbered + Level: 3 + Numbering
Style: 1, 2, 3, ... + Start at: 1 + Alignment: Left + Aligned at:
0 cm + Indent at: 1.27 cm

Deleted: annual

Deleted: time-series

Deleted: estimated

Deleted: (Lan et al 2024),

Deleted: estimated

Deleted: annual

Deleted: from this year's carbon budget

850 GOBMs and data products) from 1959 through 2023 from this year's carbon budget. Using this relationship, the
851 2024 SOCEAN can then be estimated from the projected 2024 input data using the non-linear relationship
852 established during the network training. "To avoid overfitting, the neural network training was done using a
853 Monte Carlo approach, with a variable number of artificial neurons (varying between 2-5) and 20% of the
854 randomly selected training data were withheld for independent internal testing."

- Deleted: .
- Deleted: trained
- Deleted: hidden
- Deleted: .

855 Based on the best output performance (tested using the 20% withheld input data), the best performing number of
856 neurons was selected. In a second step, we trained the network 10 times using the best number of neurons
857 identified in step 1 and different sets of randomly selected training data. The mean of the 10 trainings is
858 considered our best forecast, whereas the standard deviation of the 10 ensembles provides a first order estimate
859 of the forecast uncertainty. This uncertainty is then combined with the SOCEAN uncertainty (0.4 GtC yr⁻¹) to
860 estimate the overall uncertainty of the 2024 projection. As an additional line of evidence, we also assess the
861 2024 atmosphere-ocean carbon flux from the ESM prediction system (see Section 2.9).

862 2.6 Land CO₂ sink

Formatted: Outline numbered + Level: 2 + Numbering
Style: 1, 2, 3, ... + Start at: 1 + Alignment: Left + Aligned at:
0 cm + Indent at: 1.02 cm

863 2.6.1 Historical Period 1850-2023

Formatted: Outline numbered + Level: 3 + Numbering
Style: 1, 2, 3, ... + Start at: 1 + Alignment: Left + Aligned at:
0 cm + Indent at: 1.27 cm

864 The terrestrial land sink (S_{LAND}) is thought to be due to the combined effects of rising atmospheric CO₂,
865 increasing N inputs, and climate change, on plant growth and terrestrial carbon storage. S_{LAND} does not include
866 land sinks directly resulting from land-use and land-use change (e.g., regrowth of vegetation) as these are part of
867 the land-use flux (E_{LUC}), although system boundaries make it difficult to attribute exactly CO₂ fluxes on land
868 between S_{LAND} and E_{LUC} (Erb et al., 2013).

869 S_{LAND} is estimated from the multi-model mean of 20 DGVMs (Table 4 and Table S1). DGVMs simulations
870 include all climate variability and CO₂ effects over land. In addition to the carbon cycle represented in all
871 DGVMs, 14 models also account for the nitrogen cycle and hence can include the effect of N inputs on S_{LAND}.
872 The DGVMs estimate of S_{LAND} does not include the export of carbon to aquatic systems or its historical
873 perturbation, which is discussed in Supplement S.6.3. DGVMs need to meet several criteria to be included in
874 this assessment. In addition, we use the International Land Model Benchmarking system (ILAMB; Collier et al.,
875 2018) for the DGVMs evaluation (see Supplement S.4.2), with an additional comparison of DGVMs with a
876 data-informed, Bayesian model-data fusion framework (CARDAMOM) (Bloom and Williams, 2015; Bloom et
877 al., 2016). The uncertainty on S_{LAND} is taken from the DGVMs standard deviation. More details on the S_{LAND}
878 methodology can be found in Supplement S.4.

Formatted: Outline numbered + Level: 3 + Numbering
Style: 1, 2, 3, ... + Start at: 1 + Alignment: Left + Aligned at:
0 cm + Indent at: 1.27 cm

879 2.6.2 2024 Projection

880 Like for the ocean forecast, the land CO₂ sink forecast for the year 2024 is based on (a) the historical (Lan et al.,
881 2024a) and our 2024 estimate of atmospheric CO₂ concentration, (b) the historical and our 2024 estimate of
882 global fossil fuel emissions, and (c) the boreal summer (June, July, August) Oceanic Niño Index (ONI) (NCEP,
883 2024). All training data are again used to best match S_{LAND} from 1959 through 2023 from this year's carbon

- Deleted: (S_{LAND})
- Deleted: annual
- Deleted: 2024
- Deleted: estimated
- Deleted: estimated
- Deleted: annual
- Deleted: from this year's carbon budget

895 budget using a feed-forward neural network. To avoid overfitting, the neural network was trained with a
896 variable number of artificial neurons (varying between 2-15), larger than for S_{OCEAN} prediction due to the
897 stronger land carbon interannual variability. As done for S_{OCEAN} , a Monte Carlo type pre-training selects the
898 optimal number of artificial neurons based on 20% withheld input data, and in a second step, an ensemble of
899 10 forecasts is produced to provide the mean forecast plus uncertainty. This uncertainty is then combined with
900 the S_{LAND} uncertainty for 2023 (1.0 GtC yr^{-1}) to estimate the overall uncertainty of the 2024 projection.

Formatted: Font: Calibri

Deleted: hidden

Formatted: Font: Calibri

Formatted: Font: Calibri

Deleted: hidden

Formatted: Font: Calibri

901 2.7 Atmospheric inversion estimate

Formatted: Outline numbered + Level: 2 + Numbering Style: 1, 2, 3, ... + Start at: 1 + Alignment: Left + Aligned at: 0 cm + Indent at: 1.02 cm

902 The world-wide network of in-situ atmospheric measurements and satellite derived atmospheric CO_2 column (X_{CO_2}) observations put a strong constraint on changes in the atmospheric abundance of CO_2 . This is true
903 globally (hence our large confidence in G_{ATM}), but also in regions with sufficient observational density found
904 mostly in the extra-tropics. This allows atmospheric inversion methods to constrain the magnitude and location
905 of the combined total surface CO_2 fluxes from all sources, including fossil and land-use change emissions and
906 land and ocean CO_2 fluxes. The inversions assume E_{FOS} to be well known, and they solve for the spatial and
907 temporal distribution of land and ocean fluxes from the residual gradients of CO_2 between stations that are not
908 explained by fossil fuel emissions. By design, such systems thus close the carbon balance ($B_{\text{IM}} = 0$) and thus
909 provide an additional perspective on the independent estimates of the ocean and land fluxes.

Deleted: $x\text{CO}_2$

911 This year's release includes fourteen inversion systems that are described in Table S4. Each system is rooted in
912 Bayesian inversion principles but uses different methodologies. These differences concern the selection of
913 atmospheric CO_2 data or X_{CO_2} , and the choice of a-priori fluxes to refine. They also differ in spatial and
914 temporal resolution, assumed correlation structures, and mathematical approach of the models (see references in
915 Table S4 for details). Importantly, the systems use a variety of transport models, which was demonstrated to be
916 a driving factor behind differences in atmospheric inversion-based flux estimates, and specifically their
917 distribution across latitudinal bands (Gaubert et al., 2019; Schuh et al., 2019). Eight inversion systems used
918 surface observations from the global measurement network (Schuldt et al., 2023, 2024). Six inversion systems
919 (CAMS-FT24r1, CMS-flux, GONGGA, COLA, GCASv2, NTFVAR) used satellite X_{CO_2} retrievals from
920 GOSAT and/or OCO-2, scaled to the WMO 2019 calibration scale, of which three inversions this year (CMS-
921 Flux, COLA, NTFVAR) used these X_{CO_2} datasets in addition to the in-situ observational CO_2 mole fraction
922 records.

Deleted: $x\text{CO}_2$

Deleted: $x\text{CO}_2$

Deleted: $x\text{CO}_2$

923 The original products delivered by the inverse modellers were modified to facilitate the comparison to the other
924 elements of the budget, specifically on two accounts: (1) global total fossil fuel emissions including cement
925 carbonation CO_2 uptake, and (2) riverine CO_2 transport. We note that with these adjustments the inverse results
926 no longer represent the net atmosphere-surface exchange over land/ocean areas as sensed by atmospheric
927 observations. Instead, for land, they become the net uptake of CO_2 by vegetation and soils that is not exported
928 by fluvial systems, similar to the DGVMs estimates. For oceans, they become the net uptake of anthropogenic
929 CO_2 , similar to the GOBMs estimates.

936 The inversion systems prescribe global fossil fuel emissions based on e.g. the GCP's Gridded Fossil Emissions
937 Dataset versions 2024.0 (GCP-GridFED; Jones et al., 2024a), which are updates to GCP-GridFEDv2021
938 presented by Jones et al. (2021b). GCP-GridFEDv2024.0 scales gridded estimates of CO₂ emissions from
939 EDGARv4.3.2 (Janssens-Maenhout et al., 2019) within national territories to match national emissions
940 estimates provided by the GCB for the years 1959-2023, which were compiled following the methodology
941 described in Section 2.1. Small differences between the systems due to for instance regridding to the transport
942 model resolution, or use of different fossil fuel emissions than GCP-GridFEDv2024.0, are adjusted in the
943 latitudinal partitioning we present, to ensure agreement with the estimate of E_{FOS} in this budget. We also note
944 that the ocean fluxes used as prior by 8 out of 14 inversions are part of the suite of the ocean process model or
945 fCO₂-products listed in Section 2.5. Although these fluxes are further adjusted by the atmospheric inversions
946 (except for Jena CarboScope), it makes the inversion estimates of the ocean fluxes not completely independent
947 of S_{OCEAN} assessed here.

948 To facilitate comparisons to the independent S_{OCEAN} and S_{LAND}, we used the same adjustments for transport and
949 outgassing of carbon transported from land to ocean, as done for the observation-based estimates of S_{OCEAN} (see
950 Supplement S.3).

951 The atmospheric inversions are evaluated using vertical profiles of atmospheric CO₂ concentrations (Figure S5).
952 More than 30 aircraft programs over the globe, either regular programs or repeated surveys over at least 9
953 months (except for SH programs), have been used to assess system performance (with space-time observational
954 coverage sparse in the SH and tropics, and denser in NH mid-latitudes; Table S8). The fourteen systems are
955 compared to the independent aircraft CO₂ measurements between 2 and 7 km above sea level between 2001 and
956 2023. Results are shown in Figure S5 and discussed in Supplement S.5.2.

957 With a relatively small ensemble of systems that cover at least one full decade (N=10), and which moreover
958 share some a-priori fluxes used with one another, or with the process-based models, it is difficult to justify using
959 their mean and standard deviation as a metric for uncertainty across the ensemble. We therefore report their full
960 range (min-max) without their mean. More details on the atmospheric inversion methodology can be found in
961 Supplement S.5.

962 2.8 Atmospheric oxygen based estimate

963 Long-term atmospheric O₂ and CO₂ observations allow estimation of the global ocean and land carbon sinks,
964 due to the coupling of O₂ and CO₂ with distinct exchange ratios for fossil fuel emissions and land uptake, and
965 uncoupled O₂ and CO₂ ocean exchange (Keeling and Manning, 2014). The global ocean and net land carbon
966 sinks were calculated following methods and constants used in Keeling and Manning (2014) but modified to
967 also include the effective O₂ source from metal refining (Battle et al., 2023). For the exchange ratio of the net
968 land sink at value of 1.05 is used, following Resplandy et al. (2019). For fossil fuels, the following values are
969 used: gas: 1.95 (+/-) 0.04, liquid: 1.44 (+/-) 0.03, solid: 1.17 (+/-) 0.03, cement: 0 (+/-) 0, gas flaring: 1.98 (+/-)
970 0.07 (Keeling, 1988). Atmospheric O₂ is observed as δ(O₂/N₂) and combined with CO₂ mole fraction observations
971 into Atmospheric Potential Oxygen (APO, Stephens et al., 1998). The APO observations from 1990 to 2024

Formatted: Outline numbered + Level: 2 + Numbering
Style: 1, 2, 3, ... + Start at: 1 + Alignment: Left + Aligned at:
0 cm + Indent at: 1.02 cm

Formatted: Font: 9 pt

972 were taken from a weighted average of flask records from three stations in the Scripps O₂ program network
973 (Alert, Canada (ALT), La Jolla, California (LJO), and Cape Grim, Australia (CGO), weighted per Keeling and
974 Manning (2014). Observed CO₂ was taken from the globally averaged marine surface annual mean growth rate
975 from the NOAA/GML Global Greenhouse Gas Reference Network (Lan et al., 2024a). The O₂ source from
976 ocean warming is based on ocean heat content from updated data from NOAA/NCEI (Levitus et al., 2012). The
977 effective O₂ source from metal refining is based on production data from Bray (2020), Flanagan (2021), and
978 Tuck (2022). Uncertainty was determined through a Monte Carlo approach with 20,000 iterations, using
979 uncertainties prescribed in Keeling and Manning (2014), including observational uncertainties from Keeling et
980 al. (2007) and autoregressive errors in fossil fuel emissions (Ballantyne et al., 2015). The reported uncertainty is
981 1 standard deviation of the ensemble. The difference between the atmospheric O₂ estimate for GCB2023 is due
982 to a revision to the Scripps O₂ program CO₂ data. As for the atmospheric inversions, the O₂ based estimates also
983 closes the carbon balance ($B_{IM} = 0$) by design and provides another independent estimate of the ocean and land
984 fluxes. Note that the O₂ method requires a correction for global air-sea O₂ flux, which has the largest uncertainty
985 at annual time scales, but which is still non negligible for decadal estimates (Nevison et al., 2008).

Deleted: 2024

986 2.9 Earth System Models estimate

987 Reconstructions and predictions from decadal prediction systems based on Earth system models (ESMs) provide
988 a novel line of evidence in assessing the atmosphere-land and atmosphere-ocean carbon fluxes in the past
989 decades and predicting their changes for the current year. The decadal prediction systems based on ESMs used
990 here consist of three sets of simulations: (i) uninitialized freely evolving historical simulations (1850-2014); (ii)
991 assimilation reconstruction incorporating observational data into the model (1960-2023); (iii) initialised
992 prediction simulations for the 1981-2024 period, starting every year from initial states obtained from the above
993 assimilation simulations. The assimilations are designed to reconstruct the actual evolution of the Earth system
994 by assimilating essential fields from data products. The assimilations' states, which are expected to be close to
995 observations, are used to start the initialised prediction simulations used for the current year (2024) global
996 carbon budget. Similar initialised prediction simulations starting every year (Nov. 1st or Jan. 1st) over the 1981-
997 2023 period (i.e., hindcasts) are also performed for predictive skill quantification and for bias correction. More
998 details on the illustration of a decadal prediction system based on an ESM can refer to Figure 1 of Li et al.
999 (2023).

Formatted: Outline numbered + Level: 2 + Numbering
Style: 1, 2, 3, ... + Start at: 1 + Alignment: Left + Aligned at:
0 cm + Indent at: 1.02 cm

1000 By assimilating physical atmospheric and oceanic data products into the ESMs, the models are able to reproduce
1001 the historical variations of the atmosphere-sea CO₂ fluxes, atmosphere-land CO₂ fluxes, and atmospheric CO₂
1002 growth rate (Li et al., 2016, 2019; Lovenduski et al., 2019a,b; Ilyina et al., 2021; Li et al., 2023). Furthermore,
1003 the ESM-based predictions have proven their skill in predicting the air-sea CO₂ fluxes for up to 6 years, the air-
1004 land CO₂ fluxes and atmospheric CO₂ growth for 2 years (Lovenduski et al., 2019a,b; Ilyina et al., 2021; Li et
1005 al., 2023). The reconstructions from the fully coupled model simulations ensure a closed budget within the Earth
1006 system, i.e., no budget imbalance term.

1008 Five ESMS, i.e., CanESM5 (Swart et al., 2019; Sospedra-Alfonso et al., 2021), EC-Earth3-CC (Döscher et al.
1009 2021; Bilbao et al., 2021; Bernardello et al., 2024), IPSL-CM6A-CO2-LR (Boucher et al., 2020), MIROC-ES2L
1010 (Watanabe et al., 2020), and MPI-ESM1-2-LR (Mauritsen et al., 2019; Li et al., 2023), have performed the set of
1011 prediction simulations. Each ESM uses a different assimilation method and combination of data products
1012 incorporated in the system, more details on the models configuration can be found in Table 4 and Supplementary
1013 Table S5. The ESMS use external forcings from the Coupled Model Intercomparison Project Phase 6 (CMIP6)
1014 historical (1960-2014) plus SSP2-4.5 baseline and CovidMIP two-year blip scenario (2015-2024) (Eyring et al.,
1015 2016; Lamboll et al., 2021). The CO₂ emissions forcing from 2015-2024 are substituted by GCB-GridFED
1016 (v2024.0, Jones et al., 2024a) to provide a consistent CO₂ forcing. Reconstructions of atmosphere-ocean CO₂
1017 fluxes (SOCEAN) and atmosphere-land CO₂ fluxes (SLAND-ELUC) for the time period from 1960-2023 are assessed
1018 here. Predictions of the atmosphere-ocean CO₂ flux, atmosphere-land CO₂ flux, and atmospheric CO₂ growth for
1019 2024 are calculated based on the predictions at a lead time of 1 year. The predictions are bias corrected using the
1020 1985-2014 climatology mean of GCB2022 (Friedlingstein et al., 2022), more details on methods can be found in
1021 Boer et al. (2016) and Li et al. (2023). The ensemble size of initialized prediction simulations is 10, and the
1022 ensemble mean for each individual model is used here. The ESMS are used here to support the assessment of
1023 SOCEAN and net atmosphere-land CO₂ flux (SLAND - ELUC) over the 1960-2023 period, and to provide an estimate
1024 of the 2024 projection of G_{ATM}.

1025 2.10 Processes not included in the global carbon budget

1026 The contribution of anthropogenic CO and CH₄ to the global carbon budget is not fully accounted for in Eq. (1)
1027 and is described in Supplement S.6.1. The contributions to CO₂ emissions of decomposition of carbonates not
1028 accounted for is described in Supplement S.6.2. The contribution of anthropogenic changes in river fluxes is
1029 conceptually included in Eq. (1) in SOCEAN and in SLAND, but it is not represented in the process models used to
1030 quantify these fluxes. This effect is discussed in Supplement S.6.3. Similarly, the loss of additional sink capacity
1031 from reduced forest cover is missing in the combination of approaches used here to estimate both land fluxes
1032 (ELUC and SLAND) and its potential effect is discussed and quantified in Supplement S.6.4.

1033 3 Results

1034 For each component of the global carbon budget, we present results for three different time periods: the full
1035 historical period, from 1850 to 2023, the decades in which we have atmospheric concentration records from
1036 Mauna Loa (1960-2023), a specific focus on last year (2023), and the projection for the current year (2024).
1037 Subsequently, we assess the estimates of the budget components of the last decades against the top-down
1038 constraints from inverse modelling of atmospheric observations, the land/ocean partitioning derived from the
1039 atmospheric O₂ measurements, and the budget components estimates from the ESMS assimilation simulations.
1040 Atmospheric inversions further allow for an assessment of the budget components with a regional breakdown of
1041 land and ocean sinks.

Formatted: Outline numbered + Level: 2 + Numbering Style: 1, 2, 3, ... + Start at: 1 + Alignment: Left + Aligned at: 0 cm + Indent at: 1.02 cm

Formatted: Indent: Left: 0 cm, First line: 0 cm, Outline numbered + Level: 1 + Numbering Style: 1, 2, 3, ... + Start at: 1 + Alignment: Left + Aligned at: 0 cm + Indent at: 0.76 cm

1042 **3.1 Fossil CO₂ Emissions**

1043 **3.1.1 Historical period 1850-2023**

1044 Cumulative fossil CO₂ emissions for 1850-2023 were 490 ± 25 GtC, including the cement carbonation sink
1045 (Figure 3, Table 8, with all cumulative numbers rounded to the nearest 5GtC). In this period, 46% of global
1046 fossil CO₂ emissions came from coal, 35% from oil, 15% from natural gas, 3% from decomposition of
1047 carbonates, and 1% from flaring. In 1850, the UK stood for 62% of global fossil CO₂ emissions. In 1893 the
1048 combined cumulative emissions of the current members of the European Union reached and subsequently
1049 surpassed the level of the UK. Since 1917 US cumulative emissions have been the largest. Over the entire
1050 period 1850-2023, US cumulative emissions amounted to 120GtC (24% of world total), the EU's to 80 GtC
1051 (16%), China's to 75 GtC (15%), and India's to 15 GtC (3%).

1052 In addition to the estimates of fossil CO₂ emissions that we provide here (see Section 2.1), there are three global
1053 datasets with long time series that include all sources of fossil CO₂ emissions: CDIAC-FF (Hefner and Marland,
1054 2024), CEDS version 2024_07_08 (Hoesly et al., 2024) and PRIMAP-hist version 2.6 (Gütschow et al., 2016;
1055 Gütschow et al., 2024), although these datasets are not entirely independent from each other (Andrew, 2020a).
1056 CEDS has cumulative emissions over 1750-2022 at 480 GtC, CDIAC-FF has 481 GtC, GCP 484 GtC,
1057 PRIMAP-hist CR 490 GtC, and PRIMAP-hist TR 492 GtC. CDIAC-FF excludes emissions from lime
1058 production. CEDS estimates higher emissions from international shipping in recent years, while PRIMAP-hist
1059 has higher fugitive emissions than the other datasets. However, in general these four datasets are in relative
1060 agreement as to total historical global emissions of fossil CO₂.

1061 **3.1.2 Recent period 1960-2023**

1062 Global fossil CO₂ emissions, E_{FOS} (including the cement carbonation sink), have increased every decade from an
1063 average of 3.0 ± 0.2 GtC yr⁻¹ for the decade of the 1960s to an average of 9.7 ± 0.5 GtC yr⁻¹ during 2014-2023
1064 (Table 7, Figure 2 and Figure 5). The growth rate in these emissions decreased between the 1960s and the
1065 1990s, from 4.3% yr⁻¹ in the 1960s (1960-1969), 3.2% yr⁻¹ in the 1970s (1970-1979), 1.6% yr⁻¹ in the 1980s
1066 (1980-1989), to 1.0% yr⁻¹ in the 1990s (1990-1999). After this period, the growth rate began increasing again in
1067 the 2000s at an average growth rate of 2.8% yr⁻¹, decreasing to 0.6% yr⁻¹ for the last decade (2014-2023).
1068 China's emissions increased by +1.9% yr⁻¹ on average over the last 10 years dominating the global trend, and
1069 India's emissions increased by +3.6% yr⁻¹, while emissions decreased in EU27 by 2.1% yr⁻¹, and in the USA by
1070 1.2% yr⁻¹. Figure 6 illustrates the spatial distribution of fossil fuel emissions for the 2014-2023 period.

1071 E_{FOS} reported here includes the uptake of CO₂ by cement via carbonation which has increased with increasing
1072 stocks of cement products, from an average of 20 MtC yr⁻¹ (0.02 GtC yr⁻¹) in the 1960s to an average of 200MtC
1073 yr⁻¹ (0.2 GtC yr⁻¹) during 2014-2023 (Figure 5).

Formatted: Outline numbered + Level: 2 + Numbering
Style: 1, 2, 3, ... + Start at: 1 + Alignment: Left + Aligned at:
0 cm + Indent at: 1.02 cm

Formatted: Outline numbered + Level: 3 + Numbering
Style: 1, 2, 3, ... + Start at: 1 + Alignment: Left + Aligned at:
0 cm + Indent at: 1.27 cm

Formatted: Outline numbered + Level: 3 + Numbering
Style: 1, 2, 3, ... + Start at: 1 + Alignment: Left + Aligned at:
0 cm + Indent at: 1.27 cm

1074 **3.1.3 Final year 2023**

1075 Global fossil CO₂ emissions were slightly higher, 1.4%, in 2023 than in 2022, with an increase of 0.14 GtC to
1076 reach 10.1 ± 0.5 GtC (including the 0.21 GtC cement carbonation sink) in 2023 (Figure 5), distributed among
1077 coal (41%), oil (32%), natural gas (21%), cement (4%), flaring (<1%), and others (<1%). Compared to 2022, the
1078 2023 emissions from coal, oil, and gas increased by 1.4%, 2.5%, and 0.1% respectively, while emissions from
1079 cement decreased by 2%. All annual growth rates presented are adjusted for the leap year, unless stated
1080 otherwise.

1081 In 2023, the largest absolute contributions to global fossil CO₂ emissions were from China (31%), the USA
1082 (13%), India (8%), and the EU27 (7%). These four regions account for 59% of global fossil CO₂ emissions,
1083 while the rest of the world contributed 41%, including international aviation and marine bunker fuels (3% of the
1084 total). Growth rates for these countries from 2022 to 2023 were 4.9% (China), -3.3% (USA), -8.4% (EU27), and
1085 8.2% (India), with +0.7% for the rest of the world, including international aviation and marine bunker fuels
1086 (+9.5%). The per-capita fossil CO₂ emissions in 2023 were 1.3 tC person⁻¹ yr⁻¹ for the globe, and were 3.9
1087 (USA), 2.3 (China), 1.5 (EU27) and 0.6 (India) tC person⁻¹ yr⁻¹ for the four highest emitters (Figure 5).

1088 **3.1.4 Year 2024 Projection**

1089 Globally, we estimate that global fossil CO₂ emissions (including cement carbonation, -0.21 GtC) will grow by
1090 0.8% in 2024 (-0.2% to +1.7%) to 10.2 GtC (37.4 GtCO₂), an historical record high². Carbon Monitor projects a
1091 comparable 2024 increase of 0.8% (0.5% to 1.1%). GCB estimates of changes in 2024 emissions per fuel types,
1092 relative to 2023, are projected to be 0.1% (range -1.0% to 1.2%) for coal, +0.9% (range 0.3% to 1.6%) for oil,
1093 +2.5% (range 1.3% to 3.8%) for natural gas, and -3.5% (range -5.3% to -1.6%) for cement.

1094 For China, projected fossil emissions in 2024 are expected to increase slightly by 0.1% (range -1.7% to 1.9%)
1095 compared with 2023 emissions, bringing 2023 emissions for China around 3.3 GtC yr⁻¹ (11.9 GtCO₂ yr⁻¹). In
1096 contrast, the Carbon Monitor estimate projects a 2024 decrease of 0.8% (range -1.3% to -1.4%). Our projected
1097 changes by fuel for China are +0.4% for coal, -1.0% for oil, +7.6% for natural gas, and -9.4% for cement.

1098 For the USA, using the Energy Information Administration (EIA) emissions projection for 2024 combined with
1099 cement clinker data from USGS, we project a decrease of 0.9% (range -2.1% to 0.3%) compared to 2023,
1100 bringing USA 2023 emissions to around 1.3 GtC yr⁻¹ (4.9 GtCO₂ yr⁻¹). Conversely, Carbon Monitor projects a
1101 2024 increase of 1.3% (1.0% to 1.6%). Our projected changes by fuel are -5.7% for coal, -0.7% for oil, +1.1%
1102 for natural gas, and -7.1% for cement.

1103 For the European Union, our projection for 2024 is for a decrease of 2.8% (range -5.2% to -0.3%) relative to
1104 2023, with 2024 emissions around 0.7 GtC yr⁻¹ (2.4 GtCO₂ yr⁻¹). The Carbon Monitor projection for the EU27 is

Formatted: Outline numbered + Level: 3 + Numbering
Style: 1, 2, 3, ... + Start at: 1 + Alignment: Left + Aligned at:
0 cm + Indent at: 1.27 cm

Formatted: Outline numbered + Level: 3 + Numbering
Style: 1, 2, 3, ... + Start at: 1 + Alignment: Left + Aligned at:
0 cm + Indent at: 1.27 cm

Deleted: 3...% to +1.9...% to 10.2 GtC (37.4 GtCO₂), an
historical record high². Carbon Monitor projects a simil... [2]

Deleted: 6% (-

Deleted: 7

Deleted: 9

Formatted: Not Highlight

Formatted: Not Highlight

Formatted: Not Highlight

Formatted: Not Highlight

Deleted: 2...% (range -1.0% to 1.4...%) for coal, +0.9%
(range 0.0...% to 1.8...%) for oil, +2.4...% (range 1.1...% to
3.8%) for natural gas, and -2.8...5% (range -4.7...3% (... [3]

Deleted: 2...% (range -1.6...% to 2.0...9%) compared with
2023 emissions, bringing 2023 emissions for China around
3.3 GtC yr⁻¹ (12.0...1.9 GtCO₂ yr⁻¹). In comparison...ontrast,
the Carbon Monitor estimate projects a 2024 decrease of
0.8% (range -1.3... to -1.9...%). Our projected changes by
fuel for China are +0.3...% for coal, -1.0.8... for oil,
+8%...6% for natural gas, and -8.1 (... [4]

Deleted: 6...% (range -2.9...% to 1.7...3%) compared to
2023, bringing USA 2023 emissions to around 1.3 GtC yr⁻¹
(4.9 GtCO₂ yr⁻¹). Conversely, Carbon Monitor projects a
2024 increase in USA emissions ...f 1.2% (-...% (1.0% to
3.5...6%). Our projected changes by fuel are -3...7% for
coal, -0.7% for oil, +1.0...% for natural gas, and -5.8 (... [5]

Deleted: 3...8% (range -6...2% to -1.4 (... [6]

² Growth rates in this section use a leap year adjustment that corrects for the extra day in 2024.

1165 slightly lower than GCB with a decrease of 4.5% (-5.4% to -3.6%). Our projected changes by fuel are -11.3%
1166 for coal, -0.6% for oil, +0.4% for natural gas, and -3.1% for cement.

1167 For India, our projection for 2024 is an increase of 3.7% (range of 3.3% to 4.0%) over 2023, with 2024
1168 emissions around 0.9 GtC yr⁻¹ (3.2 GtCO₂ yr⁻¹). The Carbon Monitor projection for India is an increase of 5.0%
1169 (4.4% to 5.5%). Our projected changes by fuel are +3.3% for coal, +3.3% for oil, +11.8% for natural gas, and
1170 +3.8% for cement.

1171 International aviation and shipping are projected to increase by 7.8% in 2024, reaching 0.3 GtC yr⁻¹ (1.2 GtCO₂
1172 yr⁻¹), with international aviation projected to be up 14% over 2023, continuing to recover from pandemic lows,
1173 and international shipping projected to rise by 3%. The Carbon Monitor projects international aviation and
1174 shipping to only increase by 2.6% in 2024.

1175 For the rest of the world, the expected change for 2024 is an increase of 1.2% (range -0.7% to 3.2%) with 2024
1176 emissions around 4.0 GtC yr⁻¹ (14.5 GtCO₂ yr⁻¹), similar to the Carbon Monitor projection of 1.5% (range -1.2%
1177 to 1.8%). The fuel-specific projected 2024 growth rates for the rest of the world are: +0.5% for coal, +0.8% for
1178 oil, +2.2% for natural gas, +2.0% for cement.

1179 For traceability, Table S6 provides a comparison of annual projections from GCB since 2015 with the actual
1180 emissions assessed in the subsequent GCB annual report.

1181 3.2 Emissions from Land Use Change

1182 3.2.1 Historical period 1850-2023

1183 Cumulative CO₂ emissions from land-use change (ELUC) for 1850-2023 were 225 ± 65 GtC (Table 8; Figure 3;
1184 Figure 16). The cumulative emissions from ELUC show a large spread among individual estimates of 150 GtC
1185 (H&C2023), 205 GtC (OSCAR), 250 GtC (LUCE) and 285 GtC (BLUE) for the four bookkeeping models and a
1186 similar wide estimate of 250 ± 85 GtC for the DGVMs (all cumulative numbers are rounded to the nearest 5
1187 GtC). Vegetation biomass observations provide independent constraints on the ELUC estimates (Li et al., 2017).
1188 Over the 1901-2012 period, the GCB bookkeeping models cumulative ELUC amounts to 165 GtC [105 to 210
1189 GtC], similar to the observation-based estimate of 155 ± 50 GtC (Li et al., 2017).

1190 3.2.2 Recent period 1960-2023

1191 In contrast to growing fossil emissions, CO₂ emissions from land-use, land-use change, and forestry remained
1192 relatively constant (around 1.5 GtC yr⁻¹) over the 1960-1999 period. Since then, they have shown a statistically
1193 significant decrease of about 0.2 GtC per decade, reaching 1.1 ± 0.7 GtC yr⁻¹ for the 2014-2023 period (Table
1194 7), but with significant spread, from 0.8 to 1.3 GtC yr⁻¹ across the four bookkeeping models (Table 5, Figure 7).
1195 Different from the bookkeeping average, the DGVMs average grows slightly larger over the 1980-2010 period
1196 and shows no sign of decreasing emissions in the recent decades, apart from in the most recent decade (Table 5,

Deleted: .

Deleted: % (-9.2

Deleted: 1.9

Deleted: 15.8

Deleted: +

Deleted: 2

Deleted: -1.3

Deleted: 5

Deleted: 4.6

Deleted: 0

Deleted: 6.1

Deleted: 5% (1.9

Deleted: 9.1

Deleted: 4.5

Deleted: 6

Deleted: 4.0

Deleted: 3.3

Deleted: 1

Deleted: 1.

Deleted: 3

Deleted: 1

Deleted: 0.

Deleted: 2.3

Deleted: 5

Formatted: Outline numbered + Level: 2 + Numbering
Style: 1, 2, 3, ... + Start at: 1 + Alignment: Left + Aligned at:
0 cm + Indent at: 1.02 cm

Formatted: Outline numbered + Level: 3 + Numbering
Style: 1, 2, 3, ... + Start at: 1 + Alignment: Left + Aligned at:
0 cm + Indent at: 1.27 cm

Formatted: Outline numbered + Level: 3 + Numbering
Style: 1, 2, 3, ... + Start at: 1 + Alignment: Left + Aligned at:
0 cm + Indent at: 1.27 cm

1221 Figure 7). This is, however, expected as DGVM-based estimates include the loss of additional sink capacity,
1222 which grows with time, while the bookkeeping estimates do not (Supplement S.6.4).

1223 We separate net $ELUC$ into five component fluxes to gain further insight into the drivers of net emissions:
1224 deforestation, forest (re-)growth, wood harvest and other forest management, peat drainage and peat fires, and
1225 all other transitions (Figure 7c; supplemental Sec. S.2.1). We further decompose the deforestation and the forest
1226 (re-)growth term into contributions from shifting cultivation vs permanent forest cover changes (Figure 7d).
1227 Averaged over the 2014–2023 period and over the four bookkeeping estimates, fluxes from deforestation amount
1228 to 1.7 [1.4 to 2.3] $GtC\ yr^{-1}$ (Table 5), of which 1.0 [0.8, 1.1] $GtC\ yr^{-1}$ are from permanent deforestation. Fluxes
1229 from forest (re-)growth amount to -1.2 [-1.5, -0.9] $GtC\ yr^{-1}$ (Table 5), of which -0.5 [-0.7, -0.3] $GtC\ yr^{-1}$ are from
1230 re/afforestation and the remainder from forest regrowth in shifting cultivation cycles. Emissions from wood
1231 harvest and other forest management (0.3 [0.0, 0.6] $GtC\ yr^{-1}$), peat drainage and peat fires (0.2 [0.2, 0.3] $GtC\ yr^{-1}$)
1232 and the net flux from other transitions (0.1 [0.0, 0.1] $GtC\ yr^{-1}$) are substantially less important globally (Table
1233 5). However, the small net flux from wood harvest and other forest management contains substantial gross
1234 fluxes that largely compensate each other (see Figure S8): 1.4 [0.9, 2.0] $GtC\ yr^{-1}$ emissions result from the
1235 decomposition of slash and the decay of wood products and -1.1 [-1.4, -0.8] $GtC\ yr^{-1}$ removals result from
1236 regrowth after wood harvesting.

1237 The split into component fluxes clarifies the potentials for emission reduction and carbon dioxide removal: the
1238 emissions from permanent deforestation - the largest of our component fluxes - could be halted (largely) without
1239 compromising carbon uptake by forests, contributing substantially to emissions reduction. By contrast, reducing
1240 wood harvesting would have limited potential to reduce emissions as it would be associated with less forest
1241 regrowth; removals and emissions cannot be decoupled here on long timescales. A similar conclusion applies to
1242 removals and emissions from shifting cultivation, which we have therefore separated out. Carbon Dioxide
1243 Removal (CDR) in forests could instead be increased by permanently increasing the forest cover through
1244 re/afforestation. Our estimate of about -0.5 $GtC\ yr^{-1}$ removed on average each year during 2014–2023 by
1245 re/afforestation is similar to independent estimates that were derived from NGHGs for CDR in managed forests
1246 (through re/afforestation plus forest management) for 2013–2022 (-0.5 $GtC\ yr^{-1}$, Pongratz et al., 2024).
1247 Re/afforestation constitutes the vast majority of all current CDR (Pongratz et al., 2024). Though they cannot be
1248 compared directly to annual fluxes from the atmosphere [and are thus not included in our estimate of \$ELUC\$](#) ,
1249 CDR through transfers between non-atmospheric reservoirs such as in durable HWPs, biochar, or BECCS
1250 comprise much smaller amounts of carbon. 218 $MtC\ yr^{-1}$ have been estimated to be transferred to HWPs,
1251 averaged over 2013–2022, (Pongratz et al., 2024). The net flux of HWPs, considering the re-release of CO_2
1252 through their decay, amounts to 91 $MtC\ yr^{-1}$ over that period (Pongratz et al., 2024). Note that some double-
1253 counting between the CDR through HWPs and the CDR through re/afforestation exists if the HWPs are derived
1254 from newly forested areas. BECCS projects have been estimated to store 0.1 $MtC\ yr^{-1}$ in geological projects
1255 worldwide in 2023, biochar projects 0.2 $MtC\ yr^{-1}$ (Pongratz et al., 2024). “Blue carbon”, i.e. coastal wetland
1256 management such as restoration of mangrove forests, saltmarshes and seagrass meadows, though at the interface
1257 of land and ocean carbon fluxes, are counted towards the land-use sector as well. Currently, bookkeeping

Deleted: .

1259 models do not include blue carbon; however, current CDR deployment in coastal wetlands is small globally, less
1260 than 0.003MtC yr⁻¹ (Powis et al., 2023).

1261 The statistically significant decrease in ELUC since the late-1990s, including the larger drop within the most
1262 recent decade, is due to the combination of decreasing emissions from deforestation (in particular permanent
1263 deforestation) and increasing removals from forest regrowth (with those from re/afforestation stagnating
1264 globally in the last decade). Emissions in 2014-2023 are 28% lower than in the late-1990s (1995-2004) and 20%
1265 lower than in 2004-2013. The steep drop in ELUC after 2015 is due to the combined effect from a peak in peat
1266 fire emissions in 2015 and a long-term decline in deforestation emissions in many countries over the 2010-2020
1267 period with largest declines in the Democratic Republic of the Congo, Brazil, China, and Indonesia. Since the
1268 processes behind gross removals, foremost forest regrowth and soil recovery, are all slow, while gross emissions
1269 include a large instantaneous component, short-term changes in land-use dynamics, such as a temporary
1270 decrease in deforestation, influences gross emissions dynamics more than gross removals dynamics, which
1271 rather are a response to longer-term dynamics. Component fluxes often differ more across the four bookkeeping
1272 estimates than the net flux, which is expected due to different process representation; in particular, the treatment
1273 of shifting cultivation, which increases both gross emissions and removals, differs across models, but also net
1274 and gross wood harvest fluxes show high uncertainty. By contrast, models agree relatively well for emissions
1275 from permanent deforestation.

1276 Overall, highest land-use emissions occur in the tropical regions of all three continents. The top three emitters
1277 (both cumulatively 1959-2023 and on average over 2014-2023) are Brazil (in particular the Amazon Arc of
1278 Deforestation), Indonesia and the Democratic Republic of the Congo, with these 3 countries contributing 0.7
1279 GtC yr⁻¹ or 60% of the global net land-use emissions (average over 2014-2023) (Figure 6b, Figure 7b). This is
1280 related to massive expansion of cropland, particularly in the last few decades in Latin America, Southeast Asia,
1281 and sub-Saharan Africa (Hong et al., 2021), to a substantial part for export of agricultural products (Pendrill et
1282 al., 2019). Emission intensity is high in many tropical countries, particularly of Southeast Asia, due to high rates
1283 of land conversion in regions of carbon-dense and often still pristine, undegraded natural forests (Hong et al.,
1284 2021). Emissions are further increased by peat fires in equatorial Asia (GFED4s, van der Werf et al., 2017). Our
1285 estimates of high ELUC in China has been revised down since the 1980s as compared to GCB2023 related to
1286 the update of the land-use forcing, which is now based on the cropland dataset by Yu et al. (2022) (see
1287 Supplement S.2.2), which suggests lower cropland expansion and thus less deforestation than the previous
1288 datasets assumed. Uptake due to land-use change occurs in several regions of the world (Figure 6b) particularly
1289 because of re/afforestation. Highest CDR in the last decade is seen in China, where our estimates show an even
1290 larger uptake since 2010 compared to GCB2023 related to the updated land-use forcing, in the EU27, partly
1291 related to expanding forest area as a consequence of the forest transition in the 19th and 20th century and
1292 subsequent regrowth of forest (Mather 2001; McGrath et al., 2015), and in the U.S. Substantial uptake through
1293 re/afforestation also exists in other regions such as Brazil, Myanmar or Russia, where, however, emissions from
1294 deforestation and other land-use changes dominate the net flux.

1295 While the mentioned patterns are robust and supported by independent literature, we acknowledge that model
1296 spread is substantially larger on regional than global levels, as has been shown for bookkeeping models (Bastos
1297 et al., 2021) as well as DGVMS (Obermeier et al., 2021). Assessments for individual regions are being
1298 performed as part of REgional Carbon Cycle Assessment and Processes (RECCAP2; Ciais et al., 2020, Poulter
1299 et al., 2022) or already exist for selected regions (e.g., for Europe by Petrescu et al., 2020, for Brazil by Rosan et
1300 al., 2021, for 8 selected countries/regions in comparison to inventory data by Schwingshackl et al., 2022). The
1301 revisions since GCB2023 reflect such uncertainties: The integration of a fourth bookkeeping model alters our
1302 estimates, though only to a limited extent given that the new model LUCE lies in between the other three
1303 models for the global ELUC estimates. Larger changes are obvious at regional level due to the revisions of the
1304 land-use forcing with a general update to more recent FAO input for agricultural areas and wood harvest, new
1305 MapBiomass input for Brazil and Indonesia and the updated cropland dataset in China.

1306 The NGHGI data under the LULUCF sector and the LULUCF estimates from FAOSTAT differ from the global
1307 models' definition of ELUC (see Section 2.2.1). In the NGHGI reporting, the natural fluxes (S_{LAND}) are counted
1308 towards ELUC when they occur on managed land (Grassi et al., 2018). To compare our results to the NGHGI
1309 approach, we perform a translation of our ELUC estimates by adding S_{LAND} in managed forest from the DGVMS
1310 simulations (following the methodology described in Grassi et al., 2023) to the bookkeeping ELUC estimate (see
1311 Supplement S.2.3). For the 2014-2023 period, we estimate that 1.8 GtC yr^{-1} of S_{LAND} occurred in managed
1312 forests. Adding this sink to ELUC changes ELUC from being a source of 1.1 GtC yr^{-1} to a sink of 0.7 GtC yr^{-1} , very
1313 similar to the NGHGI estimate that yields a sink of 0.8 GtC yr^{-1} (Figure 8, Table S10). We further apply a mask
1314 of managed land to the net atmosphere-to-land flux estimate from atmospheric inversions to obtain inverse
1315 estimates that are comparable to the NGHGI estimates and to the translated ELUC estimates from bookkeeping
1316 models (see Supplement S.2.3). The inversion-based net flux in managed land indicates a sink of 0.7 GtC yr^{-1}
1317 for 2014-2023, which agrees very well with the NGHGI and the translated ELUC estimates (Figure 8, Table S10).
1318 Additionally, the interannual variability of the inversion estimates and the translated ELUC estimates show a
1319 remarkable agreement (Pearson correlation of 0.81 in 2000-2023), which supports the suggested translation
1320 approach.

1321 The translation approach has been shown to be generally applicable also at the country-level (Grassi et al., 2023;
1322 Schwingshackl et al., 2022). Country-level analysis suggests, e.g., that the bookkeeping method estimates higher
1323 deforestation emissions than the national report in Indonesia, but less CO_2 removal by afforestation than the
1324 national report in China. The fraction of the natural CO_2 sinks that the NGHGI estimates include differs
1325 substantially across countries, related to varying proportions of managed vs total forest areas (Schwingshackl et
1326 al., 2022). By comparing ELUC and NGHGI on the basis of the component fluxes used above, we find that our
1327 estimates reproduce very closely the NGHGI estimates for emissions from permanent deforestation, peat
1328 emissions, and other transitions (Figure 8), although a difference in sign for the latter (small source in
1329 bookkeeping estimates, small sink in NGHGI) creates a notable difference between NGHGI and bookkeeping
1330 estimates. Fluxes due to forest (re-)growth & other forest management, that is, (re-)growth from re/afforestation
1331 plus the net flux from wood harvesting and other forest management and emissions and removals in shifting
1332 cultivation cycles, constitute a large sink in the NGHGI (-1.9 GtC yr^{-1} averaged over 2014-2023), since they

1333 also include S_{LAND} in managed forests. Summing up the bookkeeping estimates of (re-)growth from
1334 re/afforestation, the net flux from wood harvesting and other forest management, and the emissions and
1335 removals in shifting cultivation cycles, and adding S_{LAND} in managed forests yields a flux of -2.0 GtC yr^{-1}
1336 (averaged over 2014-2023), which compares well with the NGHGI estimate. Though estimates between
1337 NGHGI, FAOSTAT and the translated budget estimates still differ in value and need further analysis, the
1338 approach suggested by Grassi et al. (2023), which we adopt here, provides a feasible way to relate the global
1339 models' and NGHGI approach to each other and thus link the anthropogenic carbon budget estimates of land
1340 CO_2 fluxes directly to the Global Stocktake, as part of the UNFCCC Paris Agreement.

1341 3.2.3 Final year 2023

1342 The global CO_2 emissions from land-use change are estimated as $1.0 \pm 0.7 \text{ GtC}$ in 2023, similar to the 2022
1343 estimate. However, confidence in the annual change remains low. Despite El Niño conditions, which in general
1344 lead to more fires in deforestation areas, peat fire emissions in Indonesia remained below average (GFED4.1s;
1345 updated from van der Werf et al., 2017). In South America, emissions from tropical deforestation and
1346 degradation fires have been about average, as effects of the El Niño in the Amazon, such as droughts, are not
1347 expected before 2024.

1348 3.2.4 Year 2024 Projection

1349 In Southeast Asia, peat fire emissions have further dropped (from 27 Tg C in 2023 to 2 Tg C in 2024 through
1350 [December 31 2024](#); GFED4.1s, van der Werf et al., 2017), as have tropical deforestation and degradation fires
1351 (from 33 Tg C to 8 Tg C) as the El Niño conditions ceased. By contrast, emissions from tropical deforestation
1352 and degradation fires in South America have risen from 121 Tg C in 2023 to 334 Tg C in 2024 up until
1353 [December 31](#), as the impacts of the El Niño unfold, in particular drought conditions since 2023. The 2024 South
1354 American fire emissions are among the highest values in the record, which started in 1997. Part of the increase
1355 is due to elevated fire activity in the wetlands of the Pantanal. Disentangling the degree to which interannual
1356 variability in rainfall patterns and stronger environmental protection measures in both Indonesia after their 2015
1357 high fire season and in Brazil after the change in government play a role in fire trends is an important research
1358 topic. Cumulative 2024 fire emission estimates through [December 31 2024](#) are 439 Tg C for global
1359 deforestation and degradation fires and 2 Tg C for peatland fires in Southeast Asia.

1360 Based on these estimates, we expect E_{LUC} emissions of around 1.2 GtC (4.2 GtCO_2) in 2024, 0.17 GtC above the
1361 2023 level. Note that although our extrapolation includes tropical deforestation and degradation fires, the
1362 degradation attributable to selective logging, edge-effects or fragmentation is not captured. Further,
1363 deforestation and fires in deforestation zones may become more disconnected, partly due to changes in
1364 legislation in some regions. For example, Van Wees et al. (2021) found that the contribution from fires to forest
1365 loss decreased in the Amazon and in Indonesia over the period of 2003-2018.

Formatted: Outline numbered + Level: 3 + Numbering
Style: 1, 2, 3, ... + Start at: 1 + Alignment: Left + Aligned at:
0 cm + Indent at: 1.27 cm

Formatted: Outline numbered + Level: 3 + Numbering
Style: 1, 2, 3, ... + Start at: 1 + Alignment: Left + Aligned at:
0 cm + Indent at: 1.27 cm

Deleted: 1

Deleted: October 17

Deleted: 6

Deleted: 324

Deleted: October 17

Deleted: October 17

Deleted: 422

Deleted: 1

Deleted: 1

Deleted: slightly

1376 **3.3 CDR not based on vegetation**

1377 Besides the CDR through land use (Sec. 3.2), the atmosphere to geosphere flux of carbon resulting from carbon
1378 dioxide removal (CDR) activity in 2023 is estimated at 0.011 MtC/yr. This results primarily from 0.009 MtC/yr
1379 of enhanced weathering projects and 0.001 MtC/yr of DACCS. While it represents a growth of 200% in the
1380 anthropogenic sink, from the 0.0036 MtC/yr estimate in 2022, it remains about a million times smaller than
1381 current fossil CO₂ emissions. [Note that the lower estimate for DACCS is due to more accurate \(lower\) annual](#)
1382 [estimates now being available, rather than lower activity. Enhanced rock weathering has gone up relative to last](#)
1383 [year, both as a result of better coverage of projects and an actual increase in activity.](#)

Formatted: Outline numbered + Level: 2 + Numbering Style: 1, 2, 3, ... + Start at: 1 + Alignment: Left + Aligned at: 0 cm + Indent at: 1.02 cm

1384 **3.4 Total anthropogenic emissions**

1385 Cumulative anthropogenic CO₂ emissions (fossil and land use) for 1850-2023 totalled 710 ± 70 GtC (2605 ±
1386 260 GtCO₂), of which 70% (500 GtC) occurred since 1960 and 34% (240 GtC) since 2000 (Table 7 and 8).
1387 Total anthropogenic emissions more than doubled over the last 60 years, from 4.6 ± 0.7 GtC yr⁻¹ for the decade
1388 of the 1960s to an average of 10.8 ± 0.9 GtC yr⁻¹ during 2014-2023, and reaching 11.1 ± 0.9 GtC (40.6 ± 3.2
1389 GtCO₂) in 2023. However, total anthropogenic CO₂ emissions have been stable over the last decade (zero
1390 growth rate over the 2014-2023 period), much slower than the 2.0% growth rate over the previous decade
1391 (2004-2013).

Formatted: Outline numbered + Level: 2 + Numbering Style: 1, 2, 3, ... + Start at: 1 + Alignment: Left + Aligned at: 0 cm + Indent at: 1.02 cm

1392 During the historical period 1850-2023, 31% of historical emissions were from land use change and 69% from
1393 fossil emissions. However, fossil emissions have grown significantly since 1960 while land use changes have
1394 not, and consequently the contributions of land use change to total anthropogenic emissions were smaller during
1395 recent periods, 18% during the period 1960-2023 and down to 10% over the last decade (2014-2023).

1396 For 2024, we project global total anthropogenic CO₂ emissions from fossil and land use changes to be around
1397 11.4 GtC (41.6 GtCO₂), 2% above the 2023 level. All values here include the cement carbonation sink (currently
1398 about 0.2 GtC yr⁻¹).

Deleted: 3

1399 **3.5 Atmospheric CO₂**

Deleted: ¶

1400 **3.5.1 Historical period 1850-2023**

1401 Atmospheric CO₂ concentration was approximately 278 parts per million (ppm) in 1750, reaching 300 ppm in
1402 the late 1900s, 350 ppm in the late 1980s, and reaching 419.31 ± 0.1 ppm in 2023 (Lan et al., [2024a](#); Figure 1).
1403 The mass of carbon in the atmosphere increased by 51% from 590 GtC in 1750 to 890 GtC in 2023. Current
1404 CO₂ concentrations in the atmosphere are unprecedented in the last 2 million years and the current rate of
1405 atmospheric CO₂ increase is at least 10 times faster than at any other time during the last 800,000 years
1406 (Canadell et al., 2021).

Formatted: Outline numbered + Level: 3 + Numbering Style: 1, 2, 3, ... + Start at: 1 + Alignment: Left + Aligned at: 0 cm + Indent at: 1.27 cm

Deleted: 2024

1410 **3.5.2 Recent period 1960-2023**

1411 The growth rate in atmospheric CO₂ level increased from 1.7 ± 0.07 GtC yr⁻¹ in the 1960s to 5.2 ± 0.02 GtC yr⁻¹
1412 during 2014-2023 with important decadal variations (Table 7, Figure 3 and Figure 4). During the last decade
1413 (2014-2023), the growth rate in atmospheric CO₂ concentration continued to increase, albeit with large
1414 interannual variability (Figure 4).

1415 The airborne fraction (AF) is defined as the ratio of atmospheric CO₂ growth rate to total anthropogenic
1416 emissions:

1417
$$AF = G_{ATM} / (E_{FOS} + E_{LUC}) \quad (2)$$

1418 It provides a diagnostic of the relative strength of the land and ocean carbon sinks in removing part of the
1419 anthropogenic CO₂ perturbation. The evolution of AF over the last 60 years shows no significant trend,
1420 remaining at around 44%, albeit showing a large interannual and decadal variability driven by the year-to-year
1421 variability in G_{ATM} (Figure 10). The observed stability of the airborne fraction over the 1960-2023 period
1422 indicates that the ocean and land CO₂ sinks have been increasing in pace with the total anthropogenic emissions
1423 over that period, removing on average about 56% of the emissions (see Sections 3.6.2 and 3.7.2).

1424 **3.5.3 Final year 2023**

1425 The growth rate in atmospheric CO₂ concentration was 5.9 ± 0.2 GtC (2.79 ± 0.08 ppm) in 2023 (Figure 4; Lan
1426 et al., 2024a), well above the 2022 growth rate (4.6 ± 0.2 GtC) or the 2014-2023 average (5.2 ± 0.02 GtC), as to
1427 be expected during an El Niño year. The 2023 atmospheric CO₂ growth rate was the 4th largest over the 1959-
1428 2023 atmospheric observational record, closely following 2015, 2016 and 1998, all strong El Niño years.

1429 **3.5.4 Year 2024 Projection**

1430 The 2024 growth in atmospheric CO₂ concentration (G_{ATM}) is projected to be about 6.1 GtC (2.87 ppm), still
1431 high, which is common for the year after a strong El Niño year. This is the average of the GCB regression
1432 method (6.1 GtC, 2.85 ppm) and ESMS the multi-model mean (6.1 GtC, 2.88 ppm). The 2024 atmospheric CO₂
1433 concentration, averaged over the year, is expected to reach the level of 422.45 ppm, 52% over the pre-industrial
1434 level.

1435 **3.6 Ocean Sink**

1436 **3.6.1 Historical period 1850-2023**

1437 Cumulated since 1850, the ocean sink adds up to 185 ± 35 GtC, with more than two thirds of this amount (130 ±
1438 25 GtC) being taken up by the global ocean since 1960. Over the historical period, the ocean sink increased in
1439 pace with the anthropogenic emissions exponential increase (Figure 3). Since 1850, the ocean has removed 26%
1440 of total anthropogenic emissions.

Formatted: Outline numbered + Level: 3 + Numbering Style: 1, 2, 3, ... + Start at: 1 + Alignment: Left + Aligned at: 0 cm + Indent at: 1.27 cm

Formatted: Outline numbered + Level: 3 + Numbering Style: 1, 2, 3, ... + Start at: 1 + Alignment: Left + Aligned at: 0 cm + Indent at: 1.27 cm

Deleted: 2024

Formatted: Outline numbered + Level: 3 + Numbering Style: 1, 2, 3, ... + Start at: 1 + Alignment: Left + Aligned at: 0 cm + Indent at: 1.27 cm

Deleted: 5.9

Deleted: 76

Deleted: 5.

Deleted: 64

Deleted: 5

Formatted: Indent: Left: 0 cm, First line: 0 cm, Outline numbered + Level: 2 + Numbering Style: 1, 2, 3, ... + Start at: 1 + Alignment: Left + Aligned at: 0 cm + Indent at: 1.02 cm

Formatted: Outline numbered + Level: 3 + Numbering Style: 1, 2, 3, ... + Start at: 1 + Alignment: Left + Aligned at: 0 cm + Indent at: 1.27 cm

3.6.2 Recent period 1960-2023

The ocean CO₂ sink increased from 1.2 ± 0.4 GtC yr⁻¹ in the 1960s to 2.9 ± 0.4 GtC yr⁻¹ during 2014-2023 (Table 7), with interannual variations of the order of a few tenths of GtC yr⁻¹ (Figure 4, Figure 11). The ocean-borne fraction ($S_{\text{OCEAN}}/(E_{\text{FOS}}+E_{\text{LUC}})$) has been remarkably constant around 25% on average (Figure 10c), with variations around this mean illustrating the decadal variability of the ocean carbon sink. So far, there is no indication of a decrease in the ocean-borne fraction from 1960 to 2022. The increase of the ocean sink is primarily driven by the increased atmospheric CO₂ concentration, with the strongest CO₂ induced signal in the North Atlantic and the Southern Ocean (Figure 12a). The effect of climate change is much weaker, reducing the ocean sink globally by 0.17 ± 0.05 GtC yr⁻¹ (-5.9% of S_{OCEAN}) during 2014-2023 (all models simulate a weakening of the ocean sink by climate change, range -3.4 to -10.7%), and does not show clear spatial patterns across the GOBMs ensemble (Figure 12b). This is the combined effect of change and variability in all atmospheric forcing fields, previously attributed to wind and temperature changes (LeQuéré et al., 2010, Bunsen et al., 2024). The effect of warming is smaller than expected from offline calculation due to a stabilising feedback from limited exchange between surface and deep waters (Bunsen et al., 2024).

The global net air-sea CO₂ flux is a residual of large natural and anthropogenic CO₂ fluxes into and out of the ocean with distinct regional and seasonal variations (Figure 6 and S1). Natural fluxes dominate on regional scales, but largely cancel out when integrated globally (Gruber et al., 2009). Mid-latitudes in all basins and the high-latitude North Atlantic dominate the ocean CO₂ uptake where low temperatures and high wind speeds facilitate CO₂ uptake at the surface (Takahashi et al., 2009). In these regions, formation of mode, intermediate and deep-water masses transport anthropogenic carbon into the ocean interior, thus allowing for continued CO₂ uptake at the surface. Outgassing of natural CO₂ occurs mostly in the tropics, especially in the equatorial upwelling region, and to a lesser extent in the North Pacific and polar Southern Ocean, mirroring a well-established understanding of regional patterns of air-sea CO₂ exchange (e.g., Takahashi et al., 2009, Gruber et al., 2009). These patterns are also noticeable in the Surface Ocean CO₂ Atlas (SOCAT) dataset, where an ocean $f\text{CO}_2$ value above the atmospheric level indicates outgassing (Figure S1). This map further illustrates the data-sparsity in the Indian Ocean and the southern hemisphere in general.

The largest variability in the ocean sink occurs on decadal time-scales (Figure 11). The ensemble means of GOBMs and $f\text{CO}_2$ -products show the same patterns of decadal variability, although with a larger amplitude of variability in the $f\text{CO}_2$ -products than in the GOBMs. The ocean sink stagnated in the 1990s and strengthened between the early 2000s and the mid-2010s (Figure 11; Le Quéré et al., 2007; Landschützer et al., 2015, 2016; DeVries et al., 2017; Hauck et al., 2020; McKinley et al., 2020, Gruber et al., 2023). More recently, the sink seems to have entered a phase of stagnation since 2016, largely in response to large inter-annual climate variability. Different explanations have been proposed for the decadal variability in the 1990s and 2000s, ranging from the ocean's response to changes in atmospheric wind systems (e.g., Le Quéré et al., 2007, Keppler and Landschützer, 2019), including variations in upper ocean overturning circulation (DeVries et al., 2017) to the eruption of Mount Pinatubo in the 1990s (McKinley et al., 2020). The main origin of the decadal variability is a matter of debate with a number of studies initially pointing to the Southern Ocean (see review in Canadell et

Formatted: Outline numbered + Level: 3 + Numbering Style: 1, 2, 3, ... + Start at: 1 + Alignment: Left + Aligned at: 0 cm + Indent at: 1.27 cm

Deleted:)

1485 al., 2021), but also contributions from the North Atlantic and North Pacific (Landschützer et al., 2016, DeVries
1486 et al., 2019), or a global signal (McKinley et al., 2020) were proposed.

1487 On top of the decadal variability, interannual variability of the ocean carbon sink is driven by climate variability
1488 with a first-order effect from a stronger ocean sink during large El Niño events (e.g., 1997-1998) (Figure 11;
1489 Rödenbeck et al., 2014, Hauck et al., 2020; McKinley et al. 2017) leading to a reduction in CO₂ outgassing from
1490 the Tropical Pacific. During 2010-2016, the ocean CO₂ sink appears to have intensified in line with the expected
1491 increase from atmospheric CO₂ (McKinley et al., 2020). This effect is similar in the *f*CO₂-products (Figure 11,
1492 ocean sink 2016 minus 2010, GOBMs: $+0.42 \pm 0.11$ GtC yr⁻¹, *f*CO₂-products: $+0.44$ GtC yr⁻¹, range 0.18 to 0.72
1493 GtC yr⁻¹). The reduction of -0.18 GtC yr⁻¹ (range: -0.41 to -0.03 GtC yr⁻¹) in the ocean CO₂ sink in 2017 is
1494 consistent with the return to normal conditions after the El Niño in 2015/16, which caused an enhanced sink in
1495 previous years. After an increasing *SO*_{OCEAN} in 2018 and 2019, the GOBM and *f*CO₂-product ensemble means
1496 suggest a decrease of *SO*_{OCEAN}, related to the triple La Niña event 2020-2022, followed by a rebound in 2023
1497 linked to the onset of an El Niño event.

1498 Although all individual GOBMs and *f*CO₂-products fall within the observational constraint, the ensemble means
1499 of GOBMs, and *f*CO₂-products (adjusted for the riverine flux) show a mean offset increasing from 0.31 GtC yr⁻¹
1500 in the 1990s to 0.49 GtC yr⁻¹ in the decade 2014-2023 and a slightly lower offset of 0.3 GtC yr⁻¹ in 2023. In this
1501 version of the GCB, the *SO*_{OCEAN} positive trend diverges over time by a factor of 1.4 since 2002 (GOBMs: $0.25 \pm$
1502 0.04 GtC yr⁻¹ per decade, *f*CO₂-products: 0.35 GtC yr⁻¹ per decade [0.17 to 0.79 GtC yr⁻¹ per decade], *SO*_{OCEAN}:
1503 0.30 GtC yr⁻¹ per decade), but the uncertainty ranges overlap. This divergence is smaller than reported in
1504 previous GCB versions, because of the updated lower sink estimates by the *f*CO₂-products for recent years. This
1505 also leads to agreement on the trend since 2010 (GOBMs: 0.18 ± 0.06 GtC yr⁻¹ per decade, *f*CO₂-products: 0.18
1506 GtC yr⁻¹ per decade [-0.36 to 0.73 GtC yr⁻¹ per decade] *SO*_{OCEAN}: 0.18 GtC yr⁻¹ per decade). A hybrid approach
1507 recently constrained the trend 2000-2022 to 0.42 ± 0.06 GtC yr⁻¹ decade⁻¹ (Mayot et al., 2024), which aligns
1508 with the updated trends of *SO*_{OCEAN} (0.39 GtCyr⁻¹ decade⁻¹) and of the *f*CO₂-products (0.45 [$0.28, 0.84$] GtCyr⁻¹
1509 decade⁻¹), while the GOBMs result in a lower trend (0.32 ± 0.04 GtC yr⁻¹ per decade) over the same period.

1510 In the current dataset, the discrepancy between the two types of estimates stems from a persistently larger
1511 *SO*_{OCEAN} in the *f*CO₂-products in the northern extra-tropics since around 2002 and an intermittently larger *SO*_{OCEAN}
1512 in the southern extra-tropics in the period 2008-2020 (Figure 14). Note that the discrepancy in the mean flux,
1513 which was located in the Southern Ocean in GCB 2022 and earlier, was reduced due to the choice of the
1514 regional river flux adjustment (Lacroix et al., 2020 instead of Aumont et al., 2001). This comes at the expense of
1515 a discrepancy in the mean *SO*_{OCEAN} of about 0.2 GtC yr⁻¹ in the tropics. Likely explanations for the discrepancy in
1516 the trends and decadal variability in the high-latitudes are data sparsity and uneven data distribution (Bushinsky
1517 et al., 2019, Gloege et al., 2021, Hauck et al., 2023a, Mayot et al., 2024). In particular, two *f*CO₂-products were
1518 shown to overestimate the Southern Ocean CO₂ flux trend by 50 and 130% based on current sampling in a
1519 model subsampling experiment (Hauck et al., 2023a) and the largest trends in the *f*CO₂-products occurred in a
1520 data void region in the North Pacific (Mayot et al., 2024). In this respect it is highly worrisome that the coverage
1521 of *f*CO₂ observations continues to decline (Dong et al 2024) and is now down to that of the early 2000s (Fig.

Deleted:),

1523 11). Another likely contributor to the discrepancy between GOBMs and $f\text{CO}_2$ -products are model biases (as
1524 indicated by the comparison with Mayot et al., 2024, by the large model spread in the South, Figure 14, and the
1525 larger model-data $f\text{CO}_2$ mismatch, Figure S2).

1526 The reported SOCEAN estimate from GOBMs and $f\text{CO}_2$ -products is $2.2 \pm 0.4 \text{ GtC yr}^{-1}$ over the period 1994 to
1527 2007, which is in agreement with the ocean interior estimate of $2.2 \pm 0.4 \text{ GtC yr}^{-1}$, which accounts for the
1528 climate effect on the natural CO_2 flux of $-0.4 \pm 0.24 \text{ GtC yr}^{-1}$ (Gruber et al., 2019) to match the
1529 definition of SOCEAN used here (Hauck et al., 2020). This comparison depends critically on the estimate of the
1530 climate effect on the natural CO_2 flux, which is smaller from the GOBMs (-0.1 GtC yr^{-1}) than in Gruber et al.
1531 (2019). Uncertainties of these two estimates would also overlap when using the GOBM estimate of the climate
1532 effect on the natural CO_2 flux. Similarly, the SOCEAN estimates integrated over the decades 1994-2004 (21.5 GtC
1533 yr^{-1}) and 2004-2014 (25.6 GtC yr^{-1}) agree with the interior ocean-based estimates of Müller et al. (2023; $21.4 \pm$
1534 2.8 and $26.5 \pm 1.3 \text{ GtC yr}^{-1}$) but depend critically on assumptions of the climate effect on natural carbon, which
1535 in turn, are based on the $f\text{CO}_2$ -products in Müller et al. (2023).

Deleted:),

1536 3.6.3 Final year 2023

1537 The estimated ocean CO_2 sink is $2.9 \pm 0.4 \text{ GtC}$ for 2023. This is a small increase of 0.16 GtC compared to 2022,
1538 in line with the expected sink strengthening from the 2023 El Niño conditions. GOBM and $f\text{CO}_2$ -product
1539 ensemble mean estimates consistently result in an SOCEAN increase in 2023 (GOBMs: $0.17 \pm 0.15 \text{ GtC}$, $f\text{CO}_2$ -
1540 products: $0.14 [-0.04, 0.30] \text{ GtC}$). Eight GOBMs and six $f\text{CO}_2$ -products show an increase in SOCEAN , while only
1541 two GOBMs and two $f\text{CO}_2$ -products show a minor decrease in SOCEAN of less than 0.05 GtC (Figure 11). The
1542 $f\text{CO}_2$ -products have a larger uncertainty at the end of the reconstructed time series, potentially linked to
1543 uncertainties related to fewer available observations in the final year and the shift from La Niña to El Niño (see
1544 e.g. Watson et al 2020, Pérez et al 2024). Specifically, the $f\text{CO}_2$ -products' estimate of the last year is regularly
1545 adjusted in the following release owing to the tail effect and an incrementally increasing data availability. While
1546 the monthly grid cells covered may have a lag of only about a year (Figure 11 inset), the values within grid cells
1547 may change with 1-5 years lag (see absolute number of observations plotted in previous GCB releases),
1548 potentially resulting in annual changes in the flux magnitude from $f\text{CO}_2$ -products.

Formatted: Outline numbered + Level: 3 + Numbering
Style: 1, 2, 3, ... + Start at: 1 + Alignment: Left + Aligned at:
0 cm + Indent at: 1.27 cm

1549 3.6.4 Year 2024 projection

1550 Using a feed-forward neural network method (see Section 2.5.2) we project an ocean sink of 3.0 GtC for 2024,
1551 only 0.1 GtC higher than for the year 2023, consistent with El Niño to neutral conditions in 2024. The set of
1552 ESMs predictions support this estimate with a 2024 ocean sink of around $3.0 [2.9, 3.1] \text{ GtC}$.

Deleted: Projection

Formatted: Outline numbered + Level: 3 + Numbering
Style: 1, 2, 3, ... + Start at: 1 + Alignment: Left + Aligned at:
0 cm + Indent at: 1.27 cm

1553 3.6.5 Evaluation of ocean models and $f\text{CO}_2$ -products

1554 The process-based model evaluation draws a generally positive picture with GOBMs scattered around the
1555 observational values for Southern Ocean sea-surface salinity, Southern Ocean stratification index and surface

Deleted: Ocean Models

Formatted: Outline numbered + Level: 3 + Numbering
Style: 1, 2, 3, ... + Start at: 1 + Alignment: Left + Aligned at:
0 cm + Indent at: 1.27 cm

1559 ocean Revelle factor (Section S3.3 and Table S11). However, the Atlantic Meridional Overturning Circulation at
1560 26°N is underestimated by 8 out of 10 GOBMs and overestimated by one GOBM. It is planned to derive skill
1561 scores for the GOBMs in future releases based on these metrics.

1562 The model simulations allow to separate the anthropogenic carbon component (steady state and non-steady
1563 state, sim D - sim A) and to compare the model flux and DIC inventory change directly to the interior ocean
1564 estimate of Gruber et al. (2019) without further assumptions (Table S11). The GOBMs ensemble average of
1565 anthropogenic carbon inventory changes 1994-2007 amounts to 2.4 GtC yr⁻¹ and is thus lower than the 2.6 ± 0.3
1566 GtC yr⁻¹ estimated by Gruber et al. (2019) although within the uncertainty. Only three models fall within the
1567 range reported by Gruber et al. (2019). This suggests that the majority of the GOBMs [may](#) underestimate
1568 anthropogenic carbon uptake by 10-20% and some models even more. Comparison to the decadal estimates of
1569 anthropogenic carbon accumulation (Müller et al., 2023) are close to the interior ocean data based estimate for
1570 the decade 2004-2014 (GOBMs sim D minus sim A, 24.7 ± 3.6 GtC yr⁻¹, Müller et al. 27.3 ± 2.5 GtC yr⁻¹), but
1571 do not reproduce the supposedly higher anthropogenic carbon accumulation in the earlier period 1994-2004
1572 (GOBMs sim D minus sim A, 21.1 ± 3.0 GtC yr⁻¹, Müller et al. 29.3 ± 2.5 GtC yr⁻¹). Analysis of Earth System
1573 Models indicate that an underestimation by about 10% may be due to biases in ocean carbon transport and
1574 mixing from the surface mixed layer to the ocean interior (Goris et al., 2018, Terhaar et al., 2021, Bourgeois et
1575 al., 2022, Terhaar et al., 2022), biases in the chemical buffer capacity (Revelle factor) of the ocean (Vaittinada
1576 Ayar et al., 2022; Terhaar et al., 2022) and partly due to a late starting date of the simulations (mirrored in
1577 atmospheric CO₂ chosen for the preindustrial control simulation, Table S2, Bronselaer et al., 2017, Terhaar et
1578 al., 2022; 2024). Interestingly, and in contrast to the uncertainties in the surface CO₂ flux, we find the largest
1579 mismatch in interior ocean carbon accumulation in the tropics, with smaller contributions from the north and the
1580 south. The large discrepancy in accumulation in the tropics highlights the role of interior ocean carbon
1581 redistribution for those inventories (Khatiwala et al., 2009, DeVries et al., 2023).

1582 The evaluation of the ocean estimates with the *f*CO₂ observations from the SOCAT v2024 dataset for the period
1583 1990-2023 shows an RMSE from annually detrended data of 0.2 to 2.4 µatm for the eight *f*CO₂-products over
1584 the globe (Figure S2). The GOBMs RMSEs are larger and range from 2.7 to 4.9 µatm. The RMSEs are
1585 generally larger at high latitudes compared to the tropics, for both the *f*CO₂-products and the GOBMs. The
1586 *f*CO₂-products have RMSEs of 0.3 to 2.9 µatm in the Tropics, 0.6 to 2.4 µatm in the North, and 0.8 to 2.4 µatm
1587 in the South. Note that the *f*CO₂-products are based on the SOCAT v2024 database, hence SOCAT is not an
1588 independent dataset for the evaluation of the *f*CO₂-products. The GOBMs RMSEs are more spread across
1589 regions, ranging from 2.4 to 3.9 µatm in the tropics, 2.8 to 5.9 µatm in the North, and 2.7 to 6.0 µatm in the
1590 South. The higher RMSEs occur in regions with stronger climate variability, such as the northern and southern
1591 high latitudes (poleward of the subtropical gyres). Additionally, this year we evaluate the trends derived from a
1592 subset of *f*CO₂-products by subsampling four GOBMs used in Friedlingstein et al. (2023; covering the period up
1593 to the year 2022) following the approach of Hauck et al. (2023a) and evaluating the air-sea CO₂ flux trend for
1594 the 2001-2021 period, i.e. the period of strong divergence in the air-sea CO₂ exchange excluding the final year
1595 to remove the tail effect, against trend biases identified by the GOBM reconstruction. The results indicate a
1596 relationship between reconstruction bias and strength of the decadal trends (see Figure S3), indicating a

1597 tendency of the $f\text{CO}_2$ -products ensemble to overestimate the air-sea CO_2 flux trends in agreement with a recent
1598 study by Mayot et al. (2024).

599 3.7 Land Sink

600 3.7.1 Historical period 1850-2023

601 Cumulated since 1850, the terrestrial [carbon](#) sink amounts to 220 ± 60 GtC, 31% of total anthropogenic
602 emissions, [with](#) more than two thirds of this amount (150 ± 40 GtC) [being](#) taken up by [the](#) terrestrial ecosystems
603 since 1960. Over the historical period, the [land](#) sink increased in pace with the anthropogenic emissions
604 [exponential](#) increase (Figure 3).

605 3.7.2 Recent period 1960-2023

606 The terrestrial CO_2 sink S_{LAND} increased from 1.2 ± 0.5 GtC yr^{-1} in the 1960s to 3.2 ± 0.9 GtC yr^{-1} during 2014-
607 2023, with important interannual variations of up to 2 GtC yr^{-1} generally showing a decreased land sink during
608 El Niño events (Figure 9), responsible for the corresponding enhanced growth rate in atmospheric CO_2
609 concentration. The larger land CO_2 sink during 2014-2023 compared to the 1960s is reproduced by all the
610 DGVMs in response to the increase in both atmospheric CO_2 , nitrogen deposition, and the changes in climate,
611 and is consistent with the residual estimated from the other budget terms ($E_{\text{FOS}} + E_{\text{LUC}} - G_{\text{ATM}} - S_{\text{OCEAN}}$, Table 5).

612 Over the period 1960 to present the increase in the global terrestrial CO_2 sink is largely attributed to the CO_2
613 fertilisation effect (Prentice et al., 2001, Piao et al., 2009, Schimel et al., 2015) and increased nitrogen
614 deposition (Huntzinger et al., 2017, O'Sullivan et al., 2019), directly stimulating plant photosynthesis and
615 increased plant water use in water limited systems, with a small negative contribution of climate change (Figure
616 12). There is a range of evidence to support a positive terrestrial carbon sink in response to increasing
617 atmospheric CO_2 , albeit with uncertain magnitude (Walker et al., 2021). As expected from theory, the greatest
618 CO_2 effect is simulated in the tropical forest regions, associated with warm temperatures and long growing
619 seasons (Hickler et al., 2008) (Figure 12a). However, evidence from tropical intact forest plots indicate an
620 overall decline in the land sink across Amazonia (1985-2011), attributed to enhanced mortality offsetting
621 productivity gains (Brienen et al., 2015, Hubau et al., 2020). During 2014-2023 the land sink is positive in all
622 regions (Figure 6) with the exception of eastern Brazil, Bolivia, northern Venezuela, Southwest USA, central
623 Europe and Central Asia, North and South Africa, and eastern Australia, where the negative effects of climate
624 variability and change (i.e. reduced rainfall and/or increased temperature) counterbalance CO_2 effects. This is
625 clearly visible on Figure 12 where the effects of CO_2 (Figure 12a) and climate (Figure 12b) as simulated by the
626 DGVMs are isolated. The negative effect of climate can be seen across the globe, and is particularly strong in
627 most of South America, Central America, Southwest US, Central Europe, western Sahel, southern Africa,
628 Southeast Asia and southern China, and eastern Australia (Figure 12b). Globally, over the 2014-2023 period,
629 climate change reduces the land sink by 0.87 ± 0.56 GtC yr^{-1} (27% of S_{LAND}).

Formatted: Outline numbered + Level: 2 + Numbering
Style: 1, 2, 3, ... + Start at: 1 + Alignment: Left + Aligned at:
0 cm + Indent at: 1.02 cm

Formatted: Outline numbered + Level: 3 + Numbering
Style: 1, 2, 3, ... + Start at: 1 + Alignment: Left + Aligned at:
0 cm + Indent at: 1.27 cm

Deleted: CO_2

Deleted: . As for the ocean,

Deleted: have been

Formatted: Outline numbered + Level: 3 + Numbering
Style: 1, 2, 3, ... + Start at: 1 + Alignment: Left + Aligned at:
0 cm + Indent at: 1.27 cm

1633 Most DGVMs have similar S_{LAND} averaged over 2014–2023, and 14/20 models fall within the 1σ range of the
1634 residual land sink [$1.8\text{--}3.7\text{ GtC yr}^{-1}$] (see Table 5), and all models but one are within the 2σ range [$0.8\text{--}4.6\text{ GtC}$
1635 yr^{-1}]. The ED model is an outlier, with a land sink estimate of 5.1 GtC yr^{-1} for the 2014–2023 period, driven by a
1636 strong CO_2 fertilisation effect (6.3 GtC yr^{-1} in the CO_2 only (S1) simulation). There are no direct global
1637 observations of the land sink (S_{LAND}), or the CO_2 fertilisation effect, and so we are not yet in a position to rule
1638 out models based on component fluxes if their net land sink ($S_{\text{LAND-ELUC}}$) is within the observational uncertainty
1639 provided by atmospheric inversions or O_2 measurements (Table 5). Furthermore, DGVMs were compared
1640 against a model-data fusion based analysis of the land carbon cycle (CARDAMOM) (Bloom and Williams,
1641 2015; Bloom et al., 2016). Results suggest good correspondence between approaches at the interannual
1642 timescales, but divergence in the recent trend in S_{LAND} with CARDAMOM simulating a stronger trend than the
1643 DGVM multi-model mean (Figure 9).

1644 Since 2020 the globe has experienced La Niña conditions which would be expected to lead to an increased land
1645 carbon sink. This 3-year long period of La Niña conditions came to an end by the second half of 2023 and
1646 transitioned to an El Niño which lasted until mid-2024. A clear transition from maximum to a minimum in the
1647 global land sink is evident in S_{LAND} , from 2022 to 2023 and we find that a El Niño- driven decrease in tropical
1648 land sink is offset by a smaller increase in the high latitude land sink. In the past years several regions
1649 experienced record-setting fire events (see also section 3.8.3). While global burned area has declined over the
1650 past decades mostly due to declining fire activity in savannas (Andela et al., 2017), forest fire emissions are
1651 rising and have the potential to counter the negative fire trend in savannas (Zheng et al., 2021). Noteworthy
1652 extreme fire events include the 2019–2020 Black Summer event in Australia (emissions of roughly 0.2 GtC ; van
1653 der Velde et al., 2021), Siberia in 2021, where emissions approached 0.4 GtC or three times the 1997–2020
1654 average according to GFED4s, and Canada in 2023 (Byrne et al., 2024). While other regions, including Western
1655 US and Mediterranean Europe, also experienced intense fire seasons in 2021 their emissions are substantially
1656 lower.

1657 Despite these regional negative effects of climate change on S_{LAND} , the efficiency of land to remove
1658 anthropogenic CO_2 emissions has remained broadly constant over the last six decades, with a land-borne
1659 fraction ($S_{\text{LAND}}/(E_{\text{FOS}}+E_{\text{LUC}})$) of around 30% (Figure 10b).

1660 3.7.3 Final year 2023

1661 The terrestrial CO_2 sink from the DGVMs ensemble S_{LAND} was $2.3 \pm 1.0\text{ GtC}$ in 2023, 41% below the 2022 La
1662 Niña induced strong sink of $3.9 \pm 1.0\text{ GtC}$, and also below the 2014–2023 average of $3.2 \pm 0.9\text{ GtC yr}^{-1}$ (Figure
1663 4, Table 7). We estimate that the 2023 land sink was the lowest since 2015. The severe reduction in the land
1664 sink in 2023 is likely driven by the El Niño conditions, leading to a 58% reduction in S_{LAND} in the tropics (30N–
1665 30S) from 2.8 GtC in 2022 to 1.2 GtC in 2023. This is combined with intense wildfires in Canada that led to a
1666 significant CO_2 source (see also Section 3.8.3). We note that the S_{LAND} DGVMs estimate for 2023 of 2.3 ± 1.0
1667 GtC is very similar to the $2.2 \pm 1.0\text{ GtC yr}^{-1}$ estimate from the residual sink from the global budget ($E_{\text{FOS}}+E_{\text{LUC}}-$
1668 $G_{\text{ATM-SOCEAN}}$, Table 5).

Formatted: Outline numbered + Level: 3 + Numbering
Style: 1, 2, 3, ... + Start at: 1 + Alignment: Left + Aligned at:
0 cm + Indent at: 1.27 cm

1669 **3.7.4 Year 2024 projection**
1670 Using a feed-forward neural network method we project a land sink of 3.2 GtC for 2024, 0.9 GtC larger than the
1671 2023 estimate. As for the ocean sink, we attribute this to the transition from the El Niño conditions in 2023 to a
1672 neutral state. The ESMs do not provide an additional estimate of S_{LAND} as they only simulate the net
1673 atmosphere-land carbon flux ($S_{LAND-ELUC}$).

Deleted: Projection

Formatted: Outline numbered + Level: 3 + Numbering Style: 1, 2, 3, ... + Start at: 1 + Alignment: Left + Aligned at: 0 cm + Indent at: 1.27 cm

1674 **3.7.5 Evaluation of land models**
1675 The evaluation of the DGVMs shows generally higher agreement across models for runoff, and to a lesser extent
1676 for GPP, and ecosystem respiration. These conclusions are supported by a more comprehensive analysis of
1677 DGVM performance in comparison with benchmark data (Sitch et al., 2024). A relative comparison of DGVM
1678 performance (Figure S4) suggests several DGVMs (CABLE-POP, CLASSIC, OCN, ORCHIDEE) may
1679 outperform others at multiple carbon and water cycle benchmarks. However, results from Seiler et al., 2022,
1680 also show how DGVM differences are often of similar magnitude compared with the range across observational
1681 datasets. All models score high enough over the metrics tests to support their use here. There are a few
1682 anomalously low scores for individual metrics from a single model, and these can direct the effort to improve
1683 models for use in future budgets.

Deleted: Land Models

Formatted: Outline numbered + Level: 3 + Numbering Style: 1, 2, 3, ... + Start at: 1 + Alignment: Left + Aligned at: 0 cm + Indent at: 1.27 cm

1684 **3.8 Partitioning the carbon sinks**

1685 **3.8.1 Global sinks and spread of estimates**

1686 In the period 2014-2023, the bottom-up view of global net ocean and land carbon sinks provided by the GCB,
1687 SOCEAN for the ocean and $S_{LAND-ELUC}$ for the land, agrees closely with the top-down global carbon sinks
1688 delivered by the atmospheric inversions. This is shown in Figure 13, which visualises the individual decadal
1689 mean atmosphere-land and atmosphere-ocean fluxes from each, along with the constraints on their sum offered
1690 by the global fossil CO₂ emissions flux minus the atmospheric growth rate ($E_{FOS} - G_{ATM}$, $4.4 \pm 0.5 \text{ Gt C yr}^{-1}$,
1691 Table 7, shown as diagonal line on Figure 13). The GCB estimate for net atmosphere-to-surface flux ($S_{OCEAN} +$
1692 $S_{LAND-ELUC}$) during 2014-2023 is $4.9 \pm 1.2 \text{ Gt C yr}^{-1}$ (Table 7), with the difference to the diagonal representing
1693 the budget imbalance (B_M) of 0.4 GtC yr^{-1} discussed in Section 3.9. By virtue of the inversion methodology, the
1694 atmospheric inversions estimate of the net atmosphere-to-surface flux during 2014-2023 is 4.5 Gt C yr^{-1} , with a
1695 $< 0.1 \text{ GtC yr}^{-1}$ imbalance, and thus scatter across the diagonal, with inverse models trading land for ocean fluxes
1696 in their solution. The independent constraint on the net atmosphere-to-surface flux based on atmospheric O₂ by
1697 design also closes the balance and is $4.5 \pm 0.9 \text{ GtC yr}^{-1}$ over the 2014-2023 period (orange symbol on Figure
1698 13), while the ESMs estimate for the net atmosphere-to-surface flux over that period average to $4.7 [3.0, 5.8]$
1699 GtC yr^{-1} (Tables 5 and 6).

Formatted: Outline numbered + Level: 2 + Numbering Style: 1, 2, 3, ... + Start at: 1 + Alignment: Left + Aligned at: 0 cm + Indent at: 1.02 cm

Formatted: Indent: Left: 0 cm, First line: 0 cm, Outline numbered + Level: 3 + Numbering Style: 1, 2, 3, ... + Start at: 1 + Alignment: Left + Aligned at: 0 cm + Indent at: 1.27 cm

1700 The distributions based on the individual models and fCO₂-products reveal substantial spread but converge near
1701 the decadal means quoted in Tables 5 to 7. Sink estimates for SOCEAN and from inverse systems are mostly non-
1702 Gaussian, while the ensemble of DGVMs appears more normally distributed justifying the use of a multi-model

1705 mean and standard deviation for their errors in the budget. Noteworthy is that the tails of the distributions
1706 provided by the land and ocean bottom-up estimates would not agree with the global constraint provided by the
1707 fossil fuel emissions and the observed atmospheric CO₂ growth rate. This illustrates the power of the
1708 atmospheric joint constraint from G_{ATM} and the global CO₂ observation network it ~~is derived~~ from.

Deleted: derives

1709 3.8.1.1 Net atmosphere-to-land flux

Formatted: Indent: Left: 0 cm, First line: 0 cm, Outline numbered + Level: 4 + Numbering Style: 1, 2, 3, ... + Start at: 1 + Alignment: Left + Aligned at: 0 cm + Indent at: 1.52 cm

1710 The GCB estimate of the net atmosphere-to-land flux ($S_{LAND} - E_{LUC}$), calculated as the difference between
1711 S_{LAND} from the DGVMs and E_{LUC} from the bookkeeping models, amounts to a 2.1 ± 1.1 GtC yr⁻¹ sink during
1712 2014-2023 (Table 5). Estimates of net atmosphere-to-land flux ($S_{LAND} - E_{LUC}$) from the DGVMs alone ($1.7 \pm$
1713 0.6 GtC yr⁻¹, Table 5, green symbol on Figure 13) are slightly lower, although within the uncertainty of the GCB
1714 estimate and also within uncertainty of the global carbon budget constraint ($E_{FOS} - G_{ATM} - S_{OCEAN}$, 1.6 ± 0.6 GtC
1715 yr⁻¹; Table 7). Also, for 2014-2023, the inversions estimate the net atmosphere-to-land flux is a 1.4 [0.3, 2.2]
1716 GtC yr⁻¹ sink, slightly lower than the mean of the DGVMs estimates (purple versus grey symbols on Figure 13).
1717 The independent constraint based on atmospheric O₂ is even lower, 1.0 ± 0.8 GtC yr⁻¹ (orange symbol in Figure
1718 13), although its large uncertainty overlaps with the uncertainty range from other approaches. Last, the ESMs
1719 estimate for the net atmosphere-to-land flux during 2014-2023 is a 2.2 [0.3, 3.6] GtC yr⁻¹ sink, more consistent
1720 with the GCB estimates of $S_{LAND} - E_{LUC}$ (Figure 14 top row).

1721 As discussed in Section 3.5.3, the atmospheric growth rate of CO₂ was very high in 2023, 5.9 GtC (2.79 ppm)
1722 the 4th largest on record. Both DGVMs and inversions assign this large CO₂ growth rate to a severe decrease of
1723 the net atmosphere to land flux, and in particular in the tropics (Figure 14). DGVMs simulate a 2023 global the
1724 net atmosphere-to-land flux of 1.1 GtC yr⁻¹, a 55% decline relative to the 2.4 GtC yr⁻¹ sink in 2022, primarily
1725 driven by the severe reduction in S_{LAND} (-41%, see Section 3.7.3). The tropics (30N-30S) are recording a
1726 dramatic decrease in the net atmosphere-to-land flux from 1.5 GtC yr⁻¹ in 2022 to 0.1 GtC yr⁻¹ in 2023. The
1727 atmospheric inversion shows a similar story with the global net atmosphere-to-land flux declining from 2.6 GtC
1728 yr⁻¹ in 2022 to 0.9 GtC yr⁻¹ in 2023 (-64%), with the tropics turning from a 1.0 GtC yr⁻¹ sink in 2022 to a 0.4
1729 GtC yr⁻¹ source in 2023. Our results are broadly consistent with the Ke et al. (2024) study which reported a
1730 global atmosphere-to-land flux of 0.4 ± 0.2 GtC yr⁻¹ in 2023.

1731 In addition to the large decline of the tropical land uptake, the northern extra-tropics experienced warmer than
1732 average conditions, in particular in the summer over North America and North Eurasia. In Canada alone, 2023
1733 led to enhanced CO₂ release due to fires of 0.5 - 0.8 GtC yr⁻¹(see Section 3.8.3). The atmospheric inversions do
1734 simulate a slight reduction of the atmosphere-to-land flux in the northern extra-tropics (north of 30°N), from
1735 1.6 GtC yr⁻¹ in 2022 to 1.4 GtC yr⁻¹ in 2023, while the DGVM fail to capture this pattern, with a simulated
1736 northern extra-tropics net atmosphere-to-land flux larger in 2023 than in 2022 (1.0 vs 0.7 GtC yr⁻¹).

Deleted:

1737 3.8.1.2 Net atmosphere-to-ocean flux

Formatted: Indent: Left: 0 cm, First line: 0 cm, Outline numbered + Level: 4 + Numbering Style: 1, 2, 3, ... + Start at: 1 + Alignment: Left + Aligned at: 0 cm + Indent at: 1.52 cm

1738 For the 2014-2023 period, the GOBMs (2.6 ± 0.4 GtC yr⁻¹) produce a lower estimate for S_{OCEAN} than the fCO_2 -
1739 products with 3.1 [2.9, 3.7] GtC yr⁻¹, which shows up in Figure 13 as separate peaks in the distribution from the

1742 GOBMs (dark blue symbols) and from the $f\text{CO}_2$ -products (light blue symbols). Atmospheric inversions (3.1
1743 [2.4, 4.1] GtC yr^{-1}) suggest an ocean uptake more in line with the $f\text{CO}_2$ -products for the recent decade (Table 7),
1744 although the inversions range includes both the GOBMs and $f\text{CO}_2$ -products estimates (Figure 14 top row) and
1745 the inversions are not fully independent as 6 out of 10 inversions covering the last decade use $f\text{CO}_2$ -products as
1746 ocean priors and one uses a GOBM (Table S4). The independent constraint based on atmospheric O_2 (3.4 ± 0.5
1747 GtC yr^{-1}) is at the high end of the distribution of the other methods. However, as mentioned in section 2.8, the
1748 O_2 method requires a correction for global air-sea O_2 flux, which induces a non-negligible uncertainty on the
1749 decadal estimates (about 0.5 GtC yr^{-1}). The large growth in the ocean carbon sink from O_2 is compatible with
1750 the GOBMs and $f\text{CO}_2$ -products estimates when accounting for their uncertainty ranges. Lastly, the ESMs
1751 estimate, $2.5 [2.2, 2.8] \text{ GtC yr}^{-1}$, suggest a moderate ocean carbon sink, comparable to the GOBMs estimate with
1752 regard to mean and spread. We caution that the riverine transport of carbon taken up on land and outgassing
1753 from the ocean, accounted for here, is a substantial ($0.65 \pm 0.3 \text{ GtC yr}^{-1}$) and uncertain term (Crisp et al., 2022;
1754 Gruber et al., 2023; DeVries et al., 2023) that separates the GOBMs, ESMs and oxygen-based estimates on the
1755 one hand from the $f\text{CO}_2$ -products and atmospheric inversions on the other hand.

1756 3.8.2 Regional partitioning

1757 Figure 14 shows the latitudinal partitioning of the global atmosphere-to-ocean (SOCEAN), atmosphere-to-land
1758 ($\text{SLAND} - \text{ELUC}$), and their sum ($\text{SOCEAN} + \text{SLAND} - \text{ELUC}$) according to the estimates from GOBMs and ocean
1759 $f\text{CO}_2$ -products (SOCEAN), DGVMs ($\text{SLAND} - \text{ELUC}$), and from atmospheric inversions (SOCEAN and $\text{SLAND} - \text{ELUC}$).

1760 3.8.2.1 North

1761 Despite being one of the most densely observed and studied regions of our globe, annual mean carbon sink
1762 estimates in the northern extra-tropics (north of 30°N) continue to differ. The atmospheric inversions suggest an
1763 atmosphere-to-surface sink ($\text{SOCEAN} + \text{SLAND} - \text{ELUC}$) for 2014-2023 of $2.6 [2.0 \text{ to } 3.4] \text{ GtC yr}^{-1}$, which is slightly
1764 higher than the process models' estimate of $2.2 \pm 0.4 \text{ GtC yr}^{-1}$ (Figure 14). The GOBMs ($1.2 \pm 0.2 \text{ GtC yr}^{-1}$),
1765 $f\text{CO}_2$ -products ($1.4 [1.3-1.5] \text{ GtC yr}^{-1}$), and inversion systems ($1.2 [0.9 \text{ to } 1.4] \text{ GtC yr}^{-1}$) produce largely
1766 consistent estimates of the ocean sink. However, the larger flux in the $f\text{CO}_2$ -products may be related to data
1767 sparsity (Mayot et al., 2024). Thus, the difference mainly arises from the net land flux ($\text{SLAND} - \text{ELUC}$) estimate,
1768 which is $1.0 \pm 0.4 \text{ GtC yr}^{-1}$ in the DGVMs compared to $1.5 [0.6 \text{ to } 2.3] \text{ GtC yr}^{-1}$ in the atmospheric inversions
1769 (Figure 14, second row).

1770 Discrepancies in the northern land fluxes conforms with persistent issues surrounding the quantification of the
1771 drivers of the global net land CO_2 flux (Armeth et al., 2017; Huntzinger et al., 2017; O'Sullivan et al., 2022) and
1772 the distribution of atmosphere-to-land fluxes between the tropics and high northern latitudes (Baccini et al.,
1773 2017; Schimel et al., 2015; Stephens et al., 2007; Ciais et al., 2019; Gaubert et al., 2019).

1774 In the northern extra-tropics, the process models, inversions, and $f\text{CO}_2$ -products consistently suggest that most
1775 of the interannual variability stems from the land (Figure 14). Inversions generally agree on the magnitude of

Formatted: Indent: Left: 0 cm, First line: 0 cm, Outline numbered + Level: 3 + Numbering Style: 1, 2, 3, ... + Start at: 1 + Alignment: Left + Aligned at: 0 cm + Indent at: 1.27 cm

Formatted: Indent: Left: 0 cm, First line: 0 cm, Outline numbered + Level: 4 + Numbering Style: 1, 2, 3, ... + Start at: 1 + Alignment: Left + Aligned at: 0 cm + Indent at: 1.52 cm

1776 interannual variations (IAV) over land, more so than DGVMs (0.29-0.32 vs 0.14-0.63 GtC yr⁻¹, averaged over
1777 1990-2023).

1778 3.8.2.2 Tropics

1779 In the tropics (30°S-30°N), both the atmospheric inversions and process models estimate a net carbon balance
1780 ($S_{\text{OCEAN}} + S_{\text{LAND}} - E_{\text{LUC}}$) that is relatively close to neutral over the past decade (inversions: 0.3 [-0.4, 0.9] GtC yr⁻¹,
1781 process models: 0.6±0.6 GtC yr⁻¹). The GOBMs (-0.03 ± 0.3 GtC yr⁻¹), $f\text{CO}_2$ -products (0.3 [0.1, 0.6] GtC yr⁻¹),
1782 and inversion systems (0.3 [-0.1, 0.8] GtC yr⁻¹) indicate a neutral to positive tropical ocean flux (see Figure S1
1783 for spatial patterns). DGVMs indicate a net land sink ($S_{\text{LAND}} - E_{\text{LUC}}$) of 0.6 ± 0.4 GtC yr⁻¹, whereas the inversion
1784 systems indicate a neutral net land flux although with large model spread (-0.0 [-0.9, 0.8] GtC yr⁻¹, (Figure 14,
1785 third row).

1786 The tropical lands are the origin of most of the atmospheric CO₂ interannual variability (Ahlström et al., 2015),
1787 consistently among the process models and inversions (Figure 14). The interannual variability in the tropics is
1788 similar among the ocean $f\text{CO}_2$ -products (0.06-0.16 GtC yr⁻¹) and the GOBMs (0.07-0.16 GtC yr⁻¹, Figure S2).
1789 The DGVMs and inversions indicate that atmosphere-to-land CO₂ fluxes are more variable than atmosphere-to-
1790 ocean CO₂ fluxes in the tropics, with interannual variability of 0.37 to 1.33 and 0.86-0.96 GtC yr⁻¹ for DGVMs
1791 and inversions, respectively.

1792 3.8.2.3 South

1793 In the southern extra-tropics (south of 30°S), the atmospheric inversions suggest a net atmosphere-to-surface
1794 sink ($S_{\text{OCEAN}} + S_{\text{LAND}} - E_{\text{LUC}}$) for 2014-2023 of 1.5 [1.2, 1.9] GtC yr⁻¹, identical to the process models' estimate of
1795 1.5 ± 0.4 GtC yr⁻¹ (Figure 14). An approximately neutral net land flux ($S_{\text{LAND}} - E_{\text{LUC}}$) for the southern extra-
1796 tropics is estimated by both the DGVMs (0.05 ± 0.1 GtC yr⁻¹) and the inversion systems (-0.03 [-0.11, 0.08] GtC
1797 yr⁻¹). This means nearly all carbon uptake is due to oceanic sinks south of 30°S. The Southern Ocean flux in the
1798 $f\text{CO}_2$ -products (1.5[1.3, 1.7 GtC] yr⁻¹) and inversion estimates (1.6 [1.2, 1.9] GtCyr⁻¹) is marginally higher than
1799 in the GOBMs (1.4 ± 0.4 GtC yr⁻¹) (Figure 14, bottom row). This agreement is subject to the choice of the river
1800 flux adjustment (Lacroix et al., 2020, Hauck et al., 2023b). Nevertheless, the time-series of atmospheric
1801 inversions and $f\text{CO}_2$ -products diverge from the GOBMs. A substantial overestimation of the trends in the $f\text{CO}_2$ -
1802 products could be explained by sparse and unevenly distributed observations, especially in wintertime (Figure
1803 S1; Hauck et al., 2023a; Gloege et al., 2021). Model biases may contribute as well, with biases in mode water
1804 formation, stratification, and the chemical buffer capacity known to play a role in Earth System Models (Terhaar
1805 et al., 2021, Bourgeois et al., 2022, Terhaar et al., 2022).

1806 The interannual variability in the southern extra-tropics is low because of the dominance of ocean areas with
1807 low variability compared to land areas. The split between land ($S_{\text{LAND}} - E_{\text{LUC}}$) and ocean (S_{OCEAN}) shows a
1808 substantial contribution to variability in the south coming from the land, with no consistency between the
1809 DGVMs and the inversions or among inversions. This is expected due to the difficulty of separating exactly the
1810 land and oceanic fluxes when viewed from atmospheric observations alone. The S_{OCEAN} interannual variability

Formatted: Indent: Left: 0 cm, First line: 0 cm, Outline numbered + Level: 4 + Numbering Style: 1, 2, 3, ... + Start at: 1 + Alignment: Left + Aligned at: 0 cm + Indent at: 1.52 cm

Formatted: Font: Gungsuh

Formatted: Font: Gungsuh

Formatted: Indent: Left: -0.08 cm, Hanging: 0.08 cm, Outline numbered + Level: 4 + Numbering Style: 1, 2, 3, ... + Start at: 1 + Alignment: Left + Aligned at: 0 cm + Indent at: 1.52 cm

1811 was found to be higher in the $f\text{CO}_2$ -products (0.04-0.20 GtC yr⁻¹) compared to GOBMs (0.04 to 0.06 GtC yr⁻¹)
1812 in 1990-2023 (Figure S2). Inversions give an interannual variability of 0.10 to 0.13 GtC yr⁻¹. Model
1813 subsampling experiments recently illustrated that $f\text{CO}_2$ -products may overestimate decadal variability in the
1814 Southern Ocean carbon sink by 30% and the trend since 2000 by 50-130% due to data sparsity, based on one
1815 and two $f\text{CO}_2$ -products with strong variability (Gloege et al., 2021, Hauck et al., 2023a). The trend benchmark
1816 test using the method of Hauck et al., (2023a) and a subset of 6 $f\text{CO}_2$ -products confirms the sensitivity of the
1817 decadal trends in $f\text{CO}_2$ -products to reconstruction biases, particularly in the Southern Ocean, indicating an
1818 overestimation of the ensemble mean trend. However, we also find compensating positive biases in the
1819 ensemble so that the ensemble mean bias is smaller than the bias from some individual $f\text{CO}_2$ -products.

1820 3.8.2.4 RECCAP2 regions

1821 Aligning with the RECCAP-2 initiative (Ciais et al., 2022; Poulter et al., 2022; DeVries et al., 2023), we
1822 provide a breakdown of this GCB paper estimate of the E_{LUC} , S_{LAND} , Net land ($S_{\text{LAND}} - E_{\text{LUC}}$), and S_{OCEAN} fluxes
1823 over the 10 land, and 5 ocean RECCAP-2 regions, averaged over the period 2014-2023 (Figure 15). The
1824 DGVMs and inversions suggest a positive net land sink in all regions, except for South America and Africa,
1825 where the inversions indicate a small net source of respectively -0.1 [-0.8, 0.3] GtC yr⁻¹ and -0.3 [-0.7, -0.1]
1826 GtC yr⁻¹, compared to a small sink of 0.1 ± 0.3 GtC yr⁻¹ and 0.3 ± 0.1 GtC yr⁻¹ for the DGVMs. However, for
1827 South America, there is substantial uncertainty in both products (ensembles span zero). For the DGVMs, this is
1828 driven by uncertainty in both S_{LAND} (0.5 ± 0.4 GtC yr⁻¹) and E_{LUC} (0.4 ± 0.2 GtC yr⁻¹). The bookkeeping models
1829 also suggest an E_{LUC} source of around 0.4 GtC yr⁻¹ in South America and Africa, in line with the DGVMs
1830 estimates. Bookkeeping models and DGVMs similarly estimate a source of 0.3-0.4 GtC yr⁻¹ in Southeast Asia,
1831 with DGVMs suggesting a small net land sink (0.1 ± 0.1 GtC yr⁻¹). This is similar to the inversion mean estimate
1832 of a 0.1 [-0.3, 0.8] GtC yr⁻¹ sink, although the inversion spread is substantial. The inversions suggest the largest
1833 net land sinks are located in North America (0.5 [-0.1, 1.0] GtC yr⁻¹), Russia (0.6 [0.1, 0.9] GtC yr⁻¹), and East
1834 Asia (0.4 [-0.2, 1.3] GtC yr⁻¹). This agrees well with the DGVMs in North America (0.4 ± 0.1 GtC yr⁻¹), which
1835 indicate a large natural land sink (S_{LAND}) of 0.6 ± 0.2 GtC yr⁻¹, being slightly reduced by land-use related carbon
1836 losses (0.2 ± 0.1 GtC yr⁻¹). The DGVMs suggest a smaller net land sink in Russia compared to inversions
1837 (0.3 ± 0.2 GtC yr⁻¹), and a similar net sink in East Asia (0.2 ± 0.1 GtC yr⁻¹).

1838 There is generally a higher level of agreement in the estimates of regional S_{OCEAN} between the different data
1839 streams (GOBMs, $f\text{CO}_2$ -products and atmospheric inversions) on decadal scale, compared to the agreement
1840 between the different land flux estimates. All data streams agree that the largest contribution to S_{OCEAN} stems
1841 from the Southern Ocean due to a combination of high flux density and large surface area, but with important
1842 contributions also from the Atlantic (high flux density) and Pacific (large area) basins. In the Southern Ocean,
1843 GOBMs suggest a sink of 1.0 ± 0.3 GtC yr⁻¹, in line with the $f\text{CO}_2$ -products (1.0 [0.8, 1.3] GtC yr⁻¹) and
1844 atmospheric inversions (1.0 [0.7, 1.4] GtC yr⁻¹). There is similar agreement in the Pacific [Ocean](#), with GOBMs,
1845 $f\text{CO}_2$ -products, and atmospheric inversions indicating a sink of 0.6 ± 0.2 GtC yr⁻¹, 0.7 [0.6, 1.0] GtC yr⁻¹, and

Formatted: Indent: Left: 0 cm, First line: 0 cm, Outline numbered + Level: 4 + Numbering Style: 1, 2, 3, ... + Start at: 1 + Alignment: Left + Aligned at: 0 cm + Indent at: 1.52 cm

Deleted: ocean

1847 0.6 [0.1,1.0] GtC yr⁻¹, respectively. However, in the Atlantic [Ocean](#), GOBMs simulate a sink of 0.5±0.1 GtC
1848 yr⁻¹, noticeably lower than both the fCO₂-products (0.8 [0.7,1.0] GtC yr⁻¹) and atmospheric inversions (0.7
1849 [0.4,1.1] GtC yr⁻¹). It is important to note the fCO₂-products and atmospheric inversions have a substantial and
1850 uncertain river flux adjustment in the Atlantic [Ocean](#) (0.3 GtC yr⁻¹) that also leads to a mean offset between
1851 GOBMs and fCO₂-products/inversions in the latitude band of the tropics (Figure 14). The Indian Ocean due its
1852 smaller size and the Arctic Ocean due to its size and sea-ice cover that prevents air-sea gas-exchange are
1853 responsible for smaller but non negligible S_{OCEAN} fluxes (Indian Ocean: (0.3 [0.2,0.3] GtC yr⁻¹, 0.3 [0.3,0.4]
1854 GtC yr⁻¹, and 0.4 [0.3,0.6] GtC yr⁻¹ for GOBMs, fCO₂-products, and atmospheric inversions, respectively, and
1855 Arctic Ocean: (0.1 [0.1,0.1] GtC yr⁻¹, 0.2 [0.1,0.2] GtC yr⁻¹, and 0.1 [0.1,0.2] GtC yr⁻¹ for GOBMs, fCO₂-
1856 products, and atmospheric inversions, respectively). Note that the S_{OCEAN} numbers presented here deviate from
1857 numbers reported in RECCAP-2 where the net air-sea CO₂ flux is reported (i.e. without river flux adjustment for
1858 fCO₂-products and inversions, and with river flux adjustment subtracted from GOBMs in most chapters, or
1859 comparing unadjusted datasets with discussion of uncertain regional riverine fluxes as major uncertainty, e.g.
1860 Sarma et al., 2023, DeVries et al., 2023).

Deleted: ocean

Deleted: ocean

1861 3.8.2.5 Tropical vs northern land uptake

1862 A continuing conundrum is the partitioning of the global atmosphere-land flux between the northern hemisphere
1863 land and the tropical land (Stephens et al., 2017; Pan et al., 2011; Gaubert et al., 2019). It is of importance
1864 because each region has its own history of land-use change, climate drivers, and impact of increasing
1865 atmospheric CO₂ and nitrogen deposition. Quantifying the magnitude of each sink is a prerequisite to
1866 understanding how each individual driver impacts the tropical and mid/high-latitude carbon balance.

1867 We define the North-South (N-S) difference as net atmosphere-land flux north of 30°N minus the net
1868 atmosphere-land flux south of 30°N. For the inversions, the N-S difference is 1.50 [0.05,3.0] GtC yr⁻¹ across
1869 this year's inversion ensemble. An apparent clustering of six satellite-driven solutions towards a common NH
1870 land sink noted in GCB2023 is no longer clear.

1871 In the ensemble of DGVMs the N-S difference is 0.4 ± 0.5 GtC yr⁻¹, a much narrower range than the one from
1872 atmospheric inversions. Only three out of twenty DGVMs have a N-S difference larger than 1.0 GtC yr⁻¹,
1873 compared to half of the inversion systems simulating a difference at least this large. The smaller spread across
1874 DGVMs than across inversions is to be expected as there is no correlation between Northern and Tropical land
1875 sinks in the DGVMs as opposed to the inversions where the sum of the two regions being well-constrained by
1876 atmospheric observations leads to an anti-correlation between these two regions. This atmospheric N-S gradient
1877 could be used as an additional way to evaluate tropical and NH uptake in DGVMs, if their fluxes were
1878 combined with multiple transport models. Vice versa, the much smaller spread in the N-S difference between
1879 the DGVMs could help to scrutinise the inverse systems further. For example, a large northern land sink and a
1880 tropical land source in an inversion would suggest a large sensitivity to CO₂ fertilisation (the dominant factor
1881 driving the land sinks) for Northern ecosystems, which would be not mirrored by tropical ecosystems. Such a

Formatted: Indent: Left: 0 cm, First line: 0 cm, Outline numbered + Level: 4 + Numbering Style: 1, 2, 3, ... + Start at: 1 + Alignment: Left + Aligned at: 0 cm + Indent at: 1.52 cm

1884 combination could be hard to reconcile with the process understanding gained from the DGVM ensembles and
1885 independent measurements (e.g. Free Air CO₂ Enrichment experiments).

1886 3.8.3 Fire emissions in 2024

1887 Fire emissions so far in 2024 have been above the average of recent decades, chiefly due to synchronous large
1888 emissions fluxes from North and South America. Figure S9 shows global and regional emissions estimates for
1889 the period 1st Jan-30th September in each year 2003-2024. Estimates derive from two global fire emissions
1890 products: the global fire emissions database (GFED, version 4.1s; van der Werf et al., 2017), and the global fire
1891 assimilation system (GFAS, operated by the Copernicus Atmosphere Service; Kaiser et al., 2012). The two
1892 products estimate that global emissions from fires were 1.6-2.2 GtC yr⁻¹ during January-September 2024. These
1893 estimates are 11-32% above the 2014-2023 average for the same months (1.5-1.7 GtC yr⁻¹). In the GFED4.1s
1894 product, the year-to-date emissions in 2024 were highest since 2003, exceeding even the large emissions
1895 estimate of 2023, whereas the GFAS product showed lower emissions in 2024 than in 2023 and six other years
1896 since 2003.

1897 The pattern of high fire emissions from Canada in 2023, which were record-breaking (Jones et al., 2024b, Byrne
1898 et al., 2024), continued into 2024. In January-September 2024, emissions from Canada (0.2-0.3 GtC yr⁻¹) were
1899 half as great as in the same months of 2023 (0.5-0.8 GtC yr⁻¹) but still 2.1-2.3 times the average of January-
1900 September periods in 2014-2023 (and 4-6 times greater than the average of those months in 2003-2022
1901 [excluding the record-breaking year in 2023]; Figure S9). The continued anomaly in Canada propagated to the
1902 northern hemisphere, where emissions of 0.5-0.6 GtC yr⁻¹ were 26-44% above the average of 2014-2023.

1903 In January-September 2024, fire emissions from South America (0.4-0.6 GtC yr⁻¹) were 94-164% above the
1904 average of January-September periods in 2014-2023, marking 2024 out as a year with synchronous high fire
1905 emissions across the Americas. Emissions from Brazil in January-September 2024 (0.2-0.3 GtC yr⁻¹) were 91-
1906 118% above the average of January-September periods of 2014-2023 and were at a level not seen since the
1907 major drought year of 2010 (Figure S9; Aragão et al., 2018, Silva Junior et al., 2019). In 2023, deforestation fire
1908 activity in the Brazilian Amazon was below the average levels recorded in national recording systems and
1909 attributed to renewed environmental policy implementation, however the fall in Amazon deforestation fire
1910 activity was largely offset by above-average wildfires related to historic drought (Mataveli et al. 2024).
1911 According to the National Center for Monitoring and Early Warning of Natural Disasters (CEMADEN), drought
1912 conditions continued into 2024 and the current drought is the most intense and widespread Brazil has
1913 experienced since records began in 1950 (CEMADEN, 2024), prompting large wildfires anomalies across the
1914 Amazon, Cerrado and Pantanal regions (INPE, 2024).

1915 Emissions anomalies in Africa strongly influence global totals because the continent typically contributed 41-
1916 47% of global fire emissions during 2014-2023 (average of January-September periods). GFAS suggests that
1917 fire emissions in Africa through September 2024 (0.6 GtC yr⁻¹) were slightly below the average of 2014-2023,
1918 whereas GFED4.1s suggests that fire emissions through September 2024 were slightly above the average of
1919 2014-2023 (0.8 GtC yr⁻¹).

Deleted: Emissions

Formatted: Indent: Left: 0 cm, First line: 0 cm, Outline numbered + Level: 3 + Numbering Style: 1, 2, 3, ... + Start at: 1 + Alignment: Left + Aligned at: 0 cm + Indent at: 1.27 cm

1921 Tropical fire emissions through September 2024 (1.1-1.6 GtC yr⁻¹) accounted for 69-74% of the global total
1922 emissions, which is close to the average of the 2014-2023 period (1.1-1.2 GtC yr⁻¹; 72-75%). This marks a
1923 return to a more typical distribution of fire emissions between the tropics and [extra-tropics](#) after the tropical
1924 contribution fell to just 55-59% during January-September 2023 (Figure S9).

Deleted: extratropics

1925 We caution that the fire emissions fluxes presented here should not be compared directly with other fluxes of the
1926 budget (e.g. S_{LAND} or E_{LUC}) due to incompatibilities between the observable fire emission fluxes and what is
1927 quantified in the S_{LAND} and E_{LUC} components of the budget. The fire emission estimates from global fire
1928 products relate to all fire types that can be observed in Earth Observations (Giglio et al., 2018; Randerson et al.,
1929 2012; Kaiser et al., 2012), including (i) fires occurring as part of natural disturbance-recovery cycles that would
1930 also have occurred in the pre-industrial period (Yue et al., 2016; Keeley and Pausas, 2019; Zou et al., 2019), (ii)
1931 fires occurring above and beyond natural disturbance-recovery cycle due to changes in climate, CO₂ and N
1932 fertilisation and to an increased frequency of extreme drought and heatwave events (Abatzoglou et al., 2019;
1933 Jones et al., 2022; Zheng et al., 2021; Burton et al., 2024), and (iii) fires occurring in relation to land use and
1934 land use change, such as deforestation fires and agricultural fires (van der Werf et al., 2010; Magi et al., 2012).
1935 In the context of the global carbon budget, only the portion of fire emissions associated with (ii) should be
1936 included in the S_{LAND} component, and fire emissions associated with (iii) should already be accounted for in the
1937 E_{LUC} component. Emissions associated with (i) should not be included in the global carbon budget. It is not
1938 currently possible to derive specific estimates for fluxes (i), (ii), and (iii) using global fire emission products
1939 such as GFED or GFAS. In addition, the fire emissions estimates from global fire emissions products represent
1940 a gross flux of carbon to the atmosphere, whereas the S_{LAND} component of the budget is a net flux that should
1941 also include post-fire recovery fluxes. Even if emissions from fires of type (ii) could be separated from those of
1942 type (i), these fluxes may be partially or wholly offset in subsequent years by post-fire fluxes as vegetation
1943 recovers, sequestering carbon from the atmosphere to the terrestrial biosphere (Yue et al., 2016; Jones et al.,
1944 2024c). Increases in forest fire emissions and severity (emissions per unit area) from globally during the past
1945 two decades have highlighted the increasing potential for fire emissions fluxes to outweigh post-fire recovery
1946 fluxes, though long-term monitoring of vegetation recovery is required to quantify the net effect on terrestrial C
1947 storage (Jones et al., 2024c).

1948 3.9 Closing the [global carbon cycle](#)

Deleted: Global Carbon Cycle

1949 3.9.1 Partitioning of [cumulative emissions and sink fluxes](#)

Formatted: Outline numbered + Level: 2 + Numbering
Style: 1, 2, 3, ... + Start at: 1 + Alignment: Left + Aligned at:
0 cm + Indent at: 1.02 cm

1950 Emissions during the period 1850-2023 amounted to 710 ± 70 GtC and were partitioned among the atmosphere
1951 (285 ± 5 GtC; 40%), ocean (185 ± 35 GtC; 26%), and land (220 ± 60 GtC; 32%). The cumulative land sink is
1952 almost equal to the cumulative land-use emissions (225 ± 65 GtC), making the global land nearly neutral over
1953 the whole 1850-2023 period (Figure 3).

Deleted: Cumulative Emissions

Deleted: Sink Fluxes

1954 The use of nearly independent estimates for the individual terms of the global carbon budget shows a cumulative
1955 budget imbalance of 25 GtC (3% of total emissions) during 1850-2023 (Figure 3, Table 8), which, if correct,
1956 suggests that emissions could be slightly too high by the same proportion or that the combined land and ocean

Formatted: Outline numbered + Level: 3 + Numbering
Style: 1, 2, 3, ... + Start at: 1 + Alignment: Left + Aligned at:
0 cm + Indent at: 1.27 cm

1961 sinks are slightly underestimated (by about 6%), although these are well within the uncertainty range of each
1962 component of the budget. Nevertheless, part of the imbalance could originate from the estimation of significant
1963 increase in E_{FOS} and E_{LUC} between the mid 1920s and the mid 1960s which is unmatched by a similar growth in
1964 atmospheric CO_2 concentration as recorded in ice cores (Figure 3). However, the known loss of additional sink
1965 capacity of 30–40 GtC (over the 1850–2020 period) due to reduced forest cover has not been accounted for in
1966 our method and would exacerbate the budget imbalance (see Section 2.10 and Supplement S.6.4).

1967 For the more recent 1960–2023 period where direct atmospheric CO_2 measurements are available, total
1968 emissions ($E_{FOS} + E_{LUC}$) amounted to 500 ± 50 GtC, of which 410 ± 20 GtC (82%) were caused by fossil CO_2
1969 emissions, and 90 ± 45 GtC (18%) by land-use change (Table 8). The total emissions were partitioned among
1970 the atmosphere (220 ± 5 GtC; 45%), ocean (130 ± 26 GtC; 25%), and the land (150 ± 40 GtC; 30%), with a near
1971 zero (<1 GtC) unattributed budget imbalance. All components except land-use change emissions have
1972 significantly grown since 1960, with important interannual variability in the growth rate in atmospheric CO_2
1973 concentration and in the land CO_2 sink (Figure 4), and some decadal variability in all terms (Table 7).
1974 Differences with previous budget releases are documented in Figure S6.

1975 The global carbon budget averaged over the last decade (2014–2023) is shown in Figure 2, Figure 16 (right
1976 panel) and Table 7. For this period, 90% of the total emissions ($E_{FOS} + E_{LUC}$) were from fossil CO_2 emissions
1977 (E_{FOS}), and 10% from land-use change (E_{LUC}). The total emissions were partitioned among the atmosphere
1978 (48%), ocean (26%) and land (30%), with a small negative budget imbalance ($\sim 4\%$, 0.4 GtC yr^{-1}). For single
1979 years, the budget imbalance can be larger (Figure 4). For 2023, the combination of our estimated sources ($11.1 \pm$
1980 0.9 GtC yr^{-1}) and sinks (11.1 ± 0.9 GtC yr^{-1}) leads to a B_{IM} of -0.02 GtC, suggesting a near perfect closure of
1981 the global carbon budget.

1982 3.9.2 Trend and variability in the carbon budget imbalance

1983 The carbon budget imbalance (B_{IM} ; Eq. 1, Figure 4) quantifies the mismatch between the estimated total
1984 emissions and the estimated changes in the atmosphere, land, and ocean reservoirs. The budget imbalance from
1985 1960 to 2023 is very small (0.5 GtC over the period, i.e. <0.01 GtC yr^{-1} on average) and shows no trend over the
1986 full time series (Figure 4e). The process models (GOBMs and DGVMs) and fCO_2 -products have been selected
1987 to match observational constraints in the 1990s, but no further constraints have been applied to their
1988 representation of trend and variability. Therefore, the near-zero mean and trend in the budget imbalance is seen
1989 as evidence of a coherent community understanding of the emissions and their partitioning on those time scales
1990 (Figure 4). However, the budget imbalance shows substantial variability of the order of ± 1 GtC yr^{-1} , particularly
1991 over semi-decadal time scales, although most of the variability is within the uncertainty of the estimates. The
1992 positive carbon imbalance during the 1960s, and early 1990s, indicates that either the emissions were
1993 overestimated, or the sinks were underestimated during these periods. The reverse is true for the 1970s, and to a
1994 lesser extent for the 1980s and 2014–2023 period (Figure 4, Table 7).

1995 We cannot attribute the cause of the variability in the budget imbalance with our analysis, we only note that the
1996 budget imbalance is unlikely to be explained by errors or biases in the emissions alone because of its large semi-

Deleted: Variability

Deleted: Carbon Budget Imbalance

Formatted: Outline numbered + Level: 3 + Numbering
Style: 1, 2, 3, ... + Start at: 1 + Alignment: Left + Aligned at:
0 cm + Indent at: 1.27 cm

1999 decadal variability component, a variability that is atypical of emissions and has not changed in the past 60 years
2000 despite a near tripling in emissions (Figure 4). Errors in S_{LAND} and S_{OCEAN} are more likely to be the main cause
2001 for the budget imbalance, especially on interannual to semi-decadal timescales. For example, underestimation of
2002 the S_{LAND} by DGVMs has been reported following the eruption of Mount Pinatubo in 1991 possibly due to
2003 missing responses to changes in diffuse radiation (Mercado et al., 2009). Although since GCB2021 we
2004 accounted for aerosol effects on solar radiation quantity and quality (diffuse vs direct), most DGVMs only used
2005 the former as input (i.e., total solar radiation) (Table S1). Thus, the ensemble mean may not capture the full
2006 effects of volcanic eruptions, i.e. associated with high light scattering sulphate aerosols, on the land carbon sink
2007 (O’Sullivan et al., 2021). DGVMs are suspected to overestimate the land sink in response to the wet decade of
2008 the 1970s (Sitch et al., 2008). Quasi-decadal variability in the ocean sink has also been reported, with all
2009 methods agreeing on a smaller than expected ocean CO_2 sink in the 1990s and a larger than expected sink in the
2010 2000s (Figure 11; Landschützer et al., 2016, DeVries et al., 2019, Hauck et al., 2020, McKinley et al., 2020,
2011 Gruber et al., 2023) and the climate-driven variability could be substantial but is not well constrained (DeVries
2012 et al., 2023, Müller et al., 2023). Errors in sink estimates could also be driven by errors in the climatic forcing
2013 data, particularly precipitation for S_{LAND} and wind for S_{OCEAN} . Also, the BIM shows substantial departure from
2014 zero on yearly time scales (Figure 4e), highlighting unresolved variability of the carbon cycle, likely in the land
2015 sink (S_{LAND}), given its large year to year variability (Figure 4d and 9).

2016 Both the budget imbalance (BIM, Table 7) and the residual land sink from the global budget ($E_{FOS}+E_{LUC}-G_{ATM}-$
2017 S_{OCEAN} , Table 5) include an error term due to the inconsistencies that arises from combining E_{LUC} from
2018 bookkeeping models with S_{LAND} from DGVMs, most notably the loss of additional sink capacity (see Section
2019 2.10 and Supplement S.6.4). Other differences include a better accounting of land use changes practices and
2020 processes in bookkeeping models than in DGVMs, or the bookkeeping models error of having present-day
2021 observed carbon densities fixed in the past. That the budget imbalance shows no clear trend towards larger
2022 values over time is an indication that these inconsistencies probably play a minor role compared to other errors
2023 in S_{LAND} or S_{OCEAN} .

2024 Although the budget imbalance is near zero for the recent decades, it could be due to a compensation of errors.
2025 We cannot exclude an overestimation of CO_2 emissions, particularly from land-use change, given their large
2026 uncertainty, as has been suggested elsewhere (Piao et al., 2018), and/or an underestimate of the sinks. A larger
2027 DGVM estimate of the atmosphere-land CO_2 flux ($S_{LAND}-E_{LUC}$) over the extra-tropics would reconcile model
2028 results with inversion estimates for fluxes in the total land during the past decade (Figure 14; Table 5).
2029 Likewise, a larger S_{OCEAN} is also possible given the higher estimates from the fCO_2 -products, inversions and
2030 oxygen based estimates (see Section 3.6.2, Figure 11 and Figure 14), the underestimation of interior ocean
2031 anthropogenic carbon accumulation in the GOBMs (Section 3.6.5, Müller et al., 2023), known biases of ocean
2032 models (e.g., Terhaar et al., 2022; 2024), the role of potential temperature bias and skin effects in fCO_2 -products
2033 (Watson et al., 2020; Dong et al., 2022; Bellenger et al., 2023, Figure 11) and regionally larger estimates based
2034 e.g. on eddy covariance measurements and aircraft data (Dong et al., 2024a; Long et al., 2021; Jin et al., 2024).
2035 More integrated use of observations in the Global Carbon Budget, either on their own or for further constraining
2036 model results, should help resolve some of the budget imbalance (Peters et al., 2017a).

2037 **4 Tracking progress towards mitigation targets**

2038 The average growth in global fossil CO₂ emissions peaked at nearly +3% per year during the 2000s, driven by
2039 the rapid growth in emissions in China. In the last decade, however, the global growth rate has slowly declined,
2040 reaching a low +0.6% per year over 2014-2023. While this slowdown in global fossil CO₂ emissions growth is
2041 welcome, global fossil CO₂ emissions continue to grow, far from the rapid emission decreases needed to be
2042 consistent with the temperature goals of the Paris Agreement.

2043 Since the 1990s, the average growth rate of fossil CO₂ emissions has continuously declined across the group of
2044 developed countries of the Organisation for Economic Co-operation and Development (OECD), with emissions
2045 peaking in around 2005 and declining at 1.4% yr⁻¹ in the decade 2014-2023, compared to a decline of 0.9% yr⁻¹
2046 during the 2004-2013 period (Table 9). In the decade 2014-2023, territorial fossil CO₂ emissions decreased
2047 significantly (at the 95% confidence level) in 23 countries/economies whose economies grew significantly (also
2048 at the 95% confidence level): Belgium, Czechia, Denmark, Estonia, Finland, France, Gabon, Germany, Jordan,
2049 Luxembourg, Netherlands, New Zealand, Norway, Portugal, South Korea, Romania, Slovenia, Somalia, Spain,
2050 Sweden, Switzerland, United Kingdom, USA (updated from Le Quéré et al., 2019). Altogether, these 23
2051 countries emitted 2.2 GtC yr⁻¹ (8.2 GtCO₂ yr⁻¹) on average over the last decade, about 23% of world CO₂ fossil
2052 emissions. For comparison, 17 countries showed a significant decrease in territorial fossil CO₂ emissions over
2053 the previous decade (2004-2013).

2054 Decomposing emission changes into the components of growth, a Kaya decomposition, helps give an initial
2055 understanding of the drivers of the changes (Peters et al., 2017b). The reduction in growth in global fossil CO₂
2056 emissions in the last decade is due to slightly weaker economic growth, accelerating declines in CO₂ emissions
2057 per unit energy, and sustained declines in energy per unit GDP (Figure 17). These trends are a supposition of the
2058 trends at the national level. Fossil CO₂ emission declines in the USA and the EU27 are primarily driven by
2059 slightly weaker economic growth since the Global Financial Crisis (GFC) in 2008/2009, sustained declines in
2060 energy per GDP, and sustained declines in CO₂ emissions per unit energy with a slight acceleration in the USA
2061 in the last decade. In contrast, fossil CO₂ emissions continue to grow in non-OECD countries, although the
2062 growth rate has slowed from 4.9% yr⁻¹ during the 2004-2013 decade to 1.8% yr⁻¹ in the last decade (Table 9).
2063 Representing 47% of non-OECD emissions in 2023, a large part of this slowdown is due to China, which has
2064 seen emissions growth decline from 7.5% yr⁻¹ in the 2004-2013 decade to 1.9% yr⁻¹ in the last decade.
2065 Excluding China, non-OECD emissions grew at 3% yr⁻¹ in the 2004-2013 decade compared to 1.7% yr⁻¹ in the
2066 last decade. China has had weaker economic growth in the 2000s compared to the 2010s, and the rate of
2067 reduction in the energy intensity of economic production has weakened significantly since 2015 with
2068 accelerating declines in CO₂ emissions per unit energy (Figure 17). India has had strong economic growth that is
2069 not offset by declines in energy per GDP or declines in CO₂ emissions per unit energy, driving up fossil CO₂
2070 emissions. Despite the high deployment of renewables in some countries (e.g., China, India), fossil energy
2071 sources continue to grow to meet growing energy demand (Le Quéré et al., 2019). In the rest of the world,
2072 economic growth has slowed considerably in the last decade, but is only partly offset by declines in energy or
2073 carbon intensity, leading to growing emissions.

Formatted: Outline numbered + Level: 1 + Numbering
Style: 1, 2, 3, ... + Start at: 1 + Alignment: Left + Aligned at:
0 cm + Indent at: 0.76 cm

Deleted: 22

Deleted: 22

Deleted: 1

Deleted: 18

2078 Globally, fossil CO₂ emissions growth is slowing, and this is due in part to the emergence of climate policy
2079 (Eskander and Fankhauser 2020; Le Quere et al 2019) and technological change, which is leading to a shift from
2080 coal to gas and growth in renewable energies, and reduced expansion of coal capacity. At the aggregated global
2081 level, decarbonisation shows a strong and growing signal in the last decade, with smaller contributions from
2082 lower economic growth and declines in energy per GDP (Figure 17). Altogether, global fossil CO₂ emissions are
2083 still growing (average of 0.6% per year over the 2014-2023 decade), far from the reductions needed to meet the
2084 ambitious climate goals of the UNFCCC Paris agreement.

2085 Last, we update the remaining carbon budget (RCB) based on two studies, the IPCC AR6 (Canadell et al., 2021)
2086 and the revision of the IPCC AR6 estimates (Forster et al., 2024, Lamboll et al., 2023). We update the RCB
2087 assessed by the IPCC AR6 (Canadell et al., 2021), accounting for the 2020 to 2024 estimated emissions from
2088 fossil fuel combustion (E_{FOS}) and land use changes (E_{LUC}). From January 2025, the IPCC AR6 RCB (50%
2089 likelihood) for limiting global warming to 1.5°C, 1.7°C and 2°C is estimated to amount to 85, 180, and 315 GtC
2090 (305, 655, 1155 GtCO₂). The Forster et al. (2024) study proposed a significantly lower RCB than IPCC AR6,
2091 with the largest reduction being due to an update of the climate emulator (MAGICC) used to estimate the
2092 warming contribution of non-CO₂ agents, and to the warming (i.e. emissions) that occurred over the 2020-2023
2093 period. We update the Forster et al., budget accounting for the 2024 estimated emissions from fossil fuel
2094 combustion (E_{FOS}) and land use changes (E_{LUC}). From January 2025, the Forster et al., (2024) RCB (50%
2095 likelihood) for limiting global warming to 1.5°C, 1.7°C and 2°C is estimated to amount to 45, 140, and 290 GtC
2096 (160, 510, 1060 GtCO₂), significantly smaller than the updated IPCC AR6 estimate. Both the original IPCC
2097 AR6 and Forster et al. (2024) estimates include the Earth System uncertainty on the climate response to
2098 cumulative CO₂ emissions, which is reflected through the percent likelihood of exceeding the given temperature
2099 threshold, an additional uncertainty of ± 220 GtCO₂ due to alternative non-CO₂ emission scenarios, and other
2100 sources of uncertainties (see Canadell et al., 2021). The two sets of estimates overlap when considering all
2101 uncertainties.

2102 Here, we take the average of our 2024 update of both IPCC AR6 and Forster et al. (2024) estimates, giving a
2103 remaining carbon (50% likelihood) for limiting global warming to 1.5°C, 1.7°C and 2°C of respectively 65, 160,
2104 and 305 GtC (235, 585, 1110 GtCO₂) starting from January 2025. We emphasise the large uncertainties,
2105 particularly when close to the global warming limit of 1.5°C. These 1.5°C, 1.7°C and 2°C remaining carbon
2106 budgets correspond respectively to about 6, 14 and 27 years from the beginning of 2025, at the 2024 level of
2107 total anthropogenic CO₂ emissions. Reaching net-zero CO₂ emissions by 2050 entails cutting total
2108 anthropogenic CO₂ emissions by about 0.4 GtC (1.6 GtCO₂), 3.9% of 2024 emissions, each year on average,
2109 comparable to the decrease in E_{FOS} observed in 2020 during the COVID-19 pandemic. However, this would lead
2110 to cumulative emissions over 2025-2050 of 145 GtC (530 GtCO₂), well above the remaining carbon budget of
2111 65 GtC to limit global warming to 1.5°C, but still within the remaining budget of 160 GtC to limit warming to
2112 1.7°C (in phase with the “well below 2°C” ambition of the Paris Agreement). Even reaching net zero CO₂
2113 globally by 2040, which would require annual emissions cuts of 0.7 GtC (2.5 GtCO₂) on average, would still
2114 exceed the remaining carbon budget [for 1.5°C](#), with 90 GtC (325 GtCO₂) cumulative emissions over 2025-2040,

Deleted: The IPCC AR6 estimates have the advantage of a consensus building approach, while the Forster et al. (2024) estimates include significant update estimates but without the backing of the IPCC yet.

2119 unless the global emissions trajectory becomes net negative (i.e. more anthropogenic CO₂ sinks than emissions)
2120 after 2040.

2121 5 Discussion

2122 Each year when the global carbon budget is published, each flux component is updated for all previous years to
2123 consider corrections that are the result of further scrutiny and verification of the underlying data in the primary
2124 input datasets. Annual estimates may be updated with improvements in data quality and timeliness (e.g., to
2125 eliminate the need for extrapolation of forcing data such as land-use). Of all terms in the global budget, only the
2126 fossil CO₂ emissions and the growth rate in atmospheric CO₂ concentration are based primarily on empirical
2127 inputs supporting annual estimates in this carbon budget. The carbon budget imbalance, yet an imperfect
2128 measure, provides a strong indication of the limitations in observations, in understanding and representing
2129 processes in models, and/or in the integration of the carbon budget components.

2130 The persistent unexplained variability in the carbon budget imbalance limits our ability to verify reported
2131 emissions (Peters et al., 2017a) and suggests we do not yet have a complete understanding of the underlying
2132 carbon cycle dynamics on annual to decadal timescales. Resolving most of this unexplained variability should
2133 be possible through different and complementary approaches. First, as intended with our annual updates, the
2134 imbalance as an error term should be reduced by improvements of individual components of the global carbon
2135 budget that follow from improving the underlying data and statistics and by improving the models through the
2136 resolution of some of the key uncertainties detailed in Table 10. Second, additional clues to the origin and
2137 processes responsible for the variability in the budget imbalance could be obtained through a closer scrutiny of
2138 carbon variability in light of other Earth system data (e.g., heat balance, water balance), and the use of a wider
2139 range of biogeochemical observations to better understand the land-ocean partitioning of the carbon imbalance
2140 such as the constraint from atmospheric oxygen included this year. Finally, additional information could also be
2141 obtained through better inclusion of process knowledge at the regional level, and through the introduction of
2142 inferred fluxes such as those based on satellite [xCO₂](#) retrievals. The limit of the resolution of the carbon budget
2143 imbalance is yet unclear, but most certainly not yet reached given the possibilities for improvements that lie
2144 ahead.

2145 Estimates of global fossil CO₂ emissions from different datasets are in relatively good agreement when the
2146 different system boundaries of these datasets are considered (Andrew, 2020a). But while estimates of E_{FOS} are
2147 derived from reported activity data requiring much fewer complex transformations than some other components
2148 of the budget, uncertainties remain, and one reason for the apparently low variation between datasets is precisely
2149 the reliance on the same underlying reported energy data. The budget excludes some sources of fossil CO₂
2150 emissions, which available evidence suggests are relatively small (<1%). We have added emissions from lime
2151 production in China and the US, but these are still absent in most other non-Annex I countries, and before 1990
2152 in other Annex I countries.

2153 Estimates of E_{LUC} suffer from a range of intertwined issues, including the poor quality of historical land-cover
2154 and land-use change maps, the rudimentary representation of management processes in most models, and the

Formatted: Indent: Left: 0 cm, First line: 0 cm, Outline numbered + Level: 1 + Numbering Style: 1, 2, 3, ... + Start at: 1 + Alignment: Left + Aligned at: 0 cm + Indent at: 0.76 cm

Deleted: xCO₂

2156 confusion in methodologies and boundary conditions used across methods (e.g., Armeth et al., 2017; Pongratz et
2157 al., 2014, see also Supplement S.6.4 on the loss of sink capacity; Bastos et al., 2021). Uncertainties in current
2158 and historical carbon stocks in soils and vegetation also add uncertainty in the E_{LUC} estimates. Unless a major
2159 effort to resolve these issues is made, little progress is expected in the resolution of E_{LUC} . This is particularly
2160 concerning given the growing importance of E_{LUC} for climate mitigation strategies, and the large issues in the
2161 quantification of the cumulative emissions over the historical period that arise from large uncertainties in E_{LUC} .

2162 By adding the DGVMs estimates of CO_2 fluxes due to environmental change from countries' managed forest
2163 areas (part of S_{LAND} in this budget) to the budget E_{LUC} estimate, we successfully reconciled the large gap
2164 between our E_{LUC} estimate and the land use flux from NGHGs using the approach described in Grassi et al.
2165 (2021) for future scenarios and in Grassi et al. (2023) using data from the Global Carbon Budget 2021. The
2166 updated data presented here can be used as potential adjustment in the policy context, e.g., to help assess the
2167 collective countries' progress towards the goal of the Paris Agreement and avoiding double-accounting for the
2168 sink in managed forests. In the absence of this adjustment, collective progress would hence appear better than it
2169 is (Grassi et al., 2021). The application of this adjustment is also recommended in the UNFCCC Synthesis
2170 report for the first Global Stocktake (UNFCCC, 2022) whenever a comparison between LULUCF fluxes
2171 reported by countries and the global emission estimates of the IPCC is conducted. However, this adjustment
2172 should be seen as a short-term and pragmatic fix based on existing data, rather than a definitive solution to
2173 bridge the differences between global models and national inventories. Additional steps are needed to
2174 understand and reconcile the remaining differences, some of which are relevant at the country level (Grassi, et
2175 al., 2023, Schwingshackl, et al., 2022).

2176 The comparison of GOBMs, fCO_2 -products, and inversions highlights substantial discrepancy in the temporal
2177 evolution of So_{CEAN} in the Southern Ocean and northern high-latitudes (Figure 14, Hauck et al., 2023a) and in
2178 the mean So_{CEAN} in the tropics. A large part of the uncertainty in the mean fluxes stems from the regional
2179 distribution of the river flux adjustment term. The current distribution simulates the largest share of the
2180 outgassing to occur in the tropics (Lacroix et al., 2020). The long-standing sparse data coverage of fCO_2
2181 observations in the Southern compared to the Northern Hemisphere (e.g., Takahashi et al., 2009) continues to
2182 exist (Bakker et al., 2016, 2024, Figure S1) and to lead to substantially higher uncertainty in the So_{CEAN} estimate
2183 for the Southern Hemisphere (Watson et al., 2020, Gloege et al., 2021, Hauck et al., 2023a). This discrepancy,
2184 which also hampers model improvement, points to the need for increased high-quality fCO_2 observations
2185 especially in the Southern Ocean. At the same time, model uncertainty is illustrated by the large spread of
2186 individual GOBM estimates (indicated by shading in Figure 14) and highlights the need for model
2187 improvement. The issue of diverging trends in So_{CEAN} from different methods is smaller this year as the trend in
2188 the fCO_2 -products was revised downwards with the data available in this GCB release, but remains a matter of
2189 concern. Recent and on-going work suggests that the fCO_2 -products may overestimate the trend (Hauck et al.,
2190 2023a, Supplement section S3.4), though the full fCO_2 -product ensemble remains to be tested. A data-
2191 constrained model approach suggests that the GOBMs underestimate the amplitude of decadal variability, but
2192 that the fCO_2 -products overestimate the trend (Mayot et al., 2024). At the same time, evidence is accumulating
2193 that GOBMs likely underestimate the mean flux (Section 3.6.2, Terhaar et al., 2022, DeVries et al., 2023,

2194 Müller et al., 2023, Dong et al., 2024). The independent constraint from atmospheric oxygen measurements
2195 gives a larger sink for the past decade and a steeper trend. However, the estimate is consistent within
2196 uncertainties with SOCEAN, with the relatively larger ocean sink in the $f\text{CO}_2$ -products and some of the GOBMs.
2197 The assessment of the net land-atmosphere exchange from DGVMs and atmospheric inversions also shows
2198 substantial discrepancy, particularly for the estimate of the net land flux over the northern extra-tropic. This
2199 discrepancy highlights the difficulty to quantify complex processes (CO₂ fertilisation, nitrogen deposition and
2200 fertilisers, climate change and variability, land management, etc.) that collectively determine the net land CO₂
2201 flux. Resolving the differences in the Northern Hemisphere land sink will require the consideration and
2202 inclusion of larger volumes of observations.

2203 We provide metrics for the evaluation of the ocean and land models and the atmospheric inversions (Figures S2
2204 to S4, Table S11). These metrics expand the use of observations in the global carbon budget, helping 1) to
2205 support improvements in the ocean and land carbon models that produce the sink estimates, and 2) to constrain
2206 the representation of key underlying processes in the models and to allocate the regional partitioning of the CO₂
2207 fluxes. The introduction of process-based metrics targeted to evaluate the simulation of SOCEAN in the ocean
2208 biogeochemistry models is an important addition to the evaluation based on ocean carbon observations. This is
2209 an initial step towards the introduction of a broader range of observations and more stringent model evaluation
2210 that we hope will support continued improvements in the annual estimates of the global carbon budget.

2211 We assessed before that a sustained decrease of -1% in global emissions could be detected at the 66%
2212 likelihood level after a decade only (Peters et al., 2017a). Similarly, a change in behaviour of the land and/or
2213 ocean carbon sink would take as long to detect, and much longer if it emerges more slowly. To continue
2214 reducing the carbon imbalance on annual to decadal time scales, regionalising the carbon budget, and integrating
2215 multiple variables are powerful ways to shorten the detection limit and ensure the research community can
2216 rapidly identify issues of concern in the evolution of the global carbon cycle under the current rapid and
2217 unprecedented changing environmental conditions.

2218 6 Conclusions

2219 The estimation of global CO₂ emissions and sinks is a major effort by the carbon cycle research community that
2220 requires a careful compilation and synthesis of measurements, statistical estimates, and model results. The
2221 delivery of an annual carbon budget serves two purposes. First, there is a large demand for up-to-date
2222 information on the state of the anthropogenic perturbation of the climate system and its underpinning causes. A
2223 broad stakeholder community relies on the datasets associated with the annual carbon budget including
2224 scientists, policy makers, businesses, journalists, and non-governmental organisations engaged in adapting to
2225 and mitigating human-driven climate change. Second, over the last decades we have seen unprecedented
2226 changes in the human and biophysical environments (e.g., changes in the growth of fossil fuel emissions, impact
2227 of COVID-19 pandemic, Earth's warming, and strength of the carbon sinks), which call for frequent
2228 assessments of the state of the planet, a better quantification of the causes of changes in the contemporary global
2229 carbon cycle, and an improved capacity to anticipate its evolution in the future. Building this scientific

Formatted: Indent: Left: 0 cm, First line: 0 cm, Outline numbered + Level: 1 + Numbering Style: 1, 2, 3, ... + Start at: 1 + Alignment: Left + Aligned at: 0 cm + Indent at: 0.76 cm

2230 understanding to meet the extraordinary climate mitigation challenge requires frequent, robust, transparent, and
2231 traceable datasets and methods that can be scrutinised and replicated. This paper via ‘living data’ helps to keep
2232 track of new budget updates.

2233 7 Data availability

2234 The data presented here are made available in the belief that their wide dissemination will lead to greater
2235 understanding and new scientific insights of how the carbon cycle works, how humans are altering it, and how
2236 we can mitigate the resulting human-driven climate change. Full contact details and information on how to cite
2237 the data shown here are given at the top of each page in the accompanying database and summarised in Table 2.

2238 The accompanying database includes three Excel files organised in the following spreadsheets:

2239 File Global_Carbon_Budget_2024v1.0.xlsx includes the following:

- 2240 1. Summary
- 2241 2. The global carbon budget (1959-2023);
- 2242 3. The historical global carbon budget (1750-2023);
- 2243 4. Global CO₂ emissions from fossil fuels and cement production by fuel type, and the per-capita emissions
2244 (1850-2023);
- 2245 5. CO₂ emissions from land-use change from the individual bookkeeping models (1959-2023);
- 2246 6. Ocean CO₂ sink from the individual global ocean biogeochemistry models and $f\text{CO}_2$ -products (1959-
2247 2023);
- 2248 7. Terrestrial CO₂ sink from the individual DGVMs (1959-2023);
- 2249 8. Cement carbonation CO₂ sink (1959-2023).

2250 File National_Fossil_Carbon_Emissions_2024v1.0.xlsx includes the following:

- 2251 1. Summary
- 2252 2. Territorial country CO₂ emissions from fossil fuels and cement production (1850-2023);
- 2253 3. Consumption country CO₂ emissions from fossil fuels and cement production and emissions transfer from
2254 the international trade of goods and services (1990-2020) using CDIAC/UNFCCC data as reference;
- 2255 4. Emissions transfers (Consumption minus territorial emissions; 1990-2020);
- 2256 5. Country definitions.

2257 File National_LandUseChange_Carbon_Emissions_2024v1.0.xlsx includes the following:

Formatted: Indent: Left: 0 cm, First line: 0 cm, Outline numbered + Level: 1 + Numbering Style: 1, 2, 3, ... + Start at: 1 + Alignment: Left + Aligned at: 0 cm + Indent at: 0.76 cm

Formatted: Indent: Left: 0.12 cm, Outline numbered + Level: 4 + Numbering Style: 1, 2, 3, ... + Start at: 1 + Alignment: Left + Aligned at: 4.44 cm + Indent at: 5.08 cm

Formatted: Indent: Left: 0.12 cm, Outline numbered + Level: 4 + Numbering Style: 1, 2, 3, ... + Start at: 1 + Alignment: Left + Aligned at: 4.44 cm + Indent at: 5.08 cm

- 2258 1. Summary
- 2259 2. Territorial country CO₂ emissions from Land Use Change (1850-2023) from three bookkeeping models;

2260 All three spreadsheets are published by the Integrated Carbon Observation System (ICOS) Carbon Portal and
2261 are available at <https://doi.org/10.18160/GCP-2024> (Friedlingstein et al., 2024). National emissions data are also
2262 available at <https://doi.org/10.5281/zenodo.13981696> (Andrew and Peters, 2024), from the Global Carbon Atlas
2263 (<http://www.globalcarbonatlas.org/>, last access: [21 January 2025](#)) and from Our World in Data
2264 (<https://ourworldindata.org/co2-emissions>, last access: [21 January 2025](#)).

2265 Author contributions

2266 PF, MO, MWJ, RMA, JH, PL, CLQ, HL, ITL, AO, GPP, WP, JP, CS, and SSi designed the study, conducted
2267 the analysis, and wrote the paper with input from JGC, PCi and RBJ. RMA, GPP and JIK produced the fossil
2268 CO₂ emissions and their uncertainties and analysed the emissions data. MH and GMa provided fossil fuel
2269 emission data. JP, TGa, ZQ, and CS provided the bookkeeping land-use change emissions with synthesis by JP
2270 and CS. SSm provided the estimates of non-vegetation CDR fluxes. LB, MC, ÖG, NG, TI, TJ, LR, JS, RS, and
2271 HTs provided an update of the global ocean biogeochemical models; LMD, ARF, DJF, MG, LG, YI, AJ, CR,
2272 AR, JZ, and PC provided an update of the ocean fCO₂-data products, with synthesis on both streams by JH, PL
2273 and NMa. SRA, NRB, MB, CFB, HCB, KC, KE, WE, RAF, TGk, SKL, NL, NMe, NMM, SN, LO, TO, DP,
2274 AJS, ST, BT, CN, and RW provided ocean fCO₂ measurements for the year 2023, with synthesis by AO and TS.
2275 AA, VA, PCa, THC, JD, CDR, AF, JHe, AKJ, EK, JK, PCM, LM, TN, MO, QS, HTi, XYa, WY, XYu, and SZ
2276 provided an update of the Dynamic Global Vegetation Models, with synthesis by SSi and MO. HL, RSA, OT,
2277 and ET provided estimates of land and ocean sinks from Earth System Models, as well as a projection of the
2278 atmospheric growth rate for 2024. NC, FC, ARJ, FJ, ZJ, JL, SM, YN, PIP, CR, DY, and NZ provided an
2279 updated atmospheric inversion, WP, FC, and ITL developed the protocol and produced the synthesis and
2280 evaluation of the atmospheric inversions. RMA provided projections of the 2024 fossil emissions and
2281 atmospheric CO₂ growth rate. PL provided the predictions of the 2024 ocean and land sinks. LPC, GCH, KKG,
2282 TMR, GRvdW, WX, and ZY provided forcing data for land-use change. FT and GG provided data for the land-
2283 use change NGHGI harmonisation. RFK provided key atmospheric CO₂ data. EJM and RFK provided the
2284 atmospheric oxygen constraint on surface net carbon sinks. MWJ provided the historical atmospheric CO₂
2285 concentration and growth rate. MO and NB produced the aerosol diffuse radiative forcing for the DGVMs. IH
2286 provided the climate forcing data for the DGVMs. PCM provided the evaluation of the DGVMs. MWJ provided

Formatted: Indent: Left: 0.12 cm, Outline numbered +
Level: 4 + Numbering Style: 1, 2, 3, ... + Start at: 1 +
Alignment: Left + Aligned at: 4.44 cm + Indent at: 5.08 cm

Formatted: Font colour: Auto

Deleted: 28 October 2024

Deleted: 28 October 2024

2289 the emissions prior for use in the inversion systems. XD provided seasonal emissions data for most recent years
2290 for the emission prior. PF, MO and MWJ coordinated the effort, revised all figures, tables, text and numbers to
2291 ensure the update was clear from the 2023 edition and in line with the globalcarbonatlas.org.

2292 **Competing interests.**

2293 At least one of the (co-)authors is a member of the editorial board of Earth System Science Data

2294

2295 **Acknowledgements**

2296 We thank all people and institutions who provided the data used in this global carbon budget 2024 and the Global
2297 Carbon Project members for their input throughout the development of this publication. We thank Nigel Hawtin
2298 for producing Figure 2 and Figure 15. We thank Alex Vermeulen and Hannah Ritchie for respectively hosting the
2299 Global Carbon Budget datasets on the ICOS portal and the Our World in Data website. We thank [Ram Alkama](#),
2300 Ian G. C. Ashton, Dorothee Bakker, [Raffaele Bernardello](#), [Ida Bagus Mandhara Brasika](#), Sebastian Brune,
2301 Fatemeh Cheginig, Emeric Claudel, [Jason Cole](#), Lushanya Dayathilake, [Pengyue Du](#), Christian Ethé, [Stefanie](#)
2302 [Falk](#), [Kristina Frölich](#), Lonke Goddijn-Murphy, [Ian Harman](#), T. Holding, [Drew Holzworth](#), [Rajesh Janardanan](#),
2303 [Daniel Kennedy](#), [Erik Kluzek](#), Fabrice Lacroix, [Vladimir Lapin](#), [Peter Lawrence](#), [am Levis](#), Yi Liu, Damian Loher,
2304 [Zoé Lloret](#), [Adrien Martinez](#), [H. Nakano](#), [Lorna Nayagam](#), Naiqing Pan, [Shufen Pan](#), [Tristan Quaife](#), [Simone](#)
2305 [Rossi](#), Paridhi Rustogi, J. D. Shutler, Richard Sims, [Victoria Spada](#), [Sean Swenson](#), Phillip Townsend, [K. Toyama](#),
2306 [S. L. Urakawa](#), [Anthony P. Walker](#), Jing Wang, Andrew J. Watson, [S Lachlan Whyborn](#), [David K. Woolf](#), and
2307 [Yakun Zhu](#) for their involvement in the development, use and analysis of the models and data-products used here.

2308 We thank Kim Currie, Siyabulela Hamnca, [Boris Herrmann](#), [Arne Körtzinger](#), [C. Lo Monaco](#), [Team Malizia](#),
2309 Pedro Monteiro, and [Mutshutshu Tsanwani](#) who contributed to the provision of surface ocean CO₂ observations
2310 for the year 2023 (see Table S7). We also thank Stephen D. Jones of the Ocean Thematic Centre of the EU
2311 Integrated Carbon Observation System (ICOS) Research Infrastructure, Eugene Burger of NOAA's Pacific Marine
2312 Environmental Laboratory and Alex Kozyr of NOAA's National Centers for Environmental Information, for their
2313 contribution to surface ocean CO₂ data and metadata management. We thank the scientists, institutions, and
2314 funding agencies responsible for the collection and quality control of the data in SOCAT as well as the
2315 International Ocean Carbon Coordination Project (IOCCP), the Surface Ocean Lower Atmosphere Study
2316 (SOLAS) and the Integrated Marine Biosphere Research (IMBeR) program for their support. We thank Nadine

Formatted: Normal, Indent: Left: 0 cm

Moved up [2]: L. Urakawa, Anthony P.

Moved (insertion) [2]

Deleted: Kristina Frölich, Zoé Lloret, Adrien Martinez, Lorna Nayagam, Rajesh Janardanan, Yakun Zhu, Ram Alkama, Simone Rossi, Stefanie Falk, Pengyue Du, Peter Lawrence, Sean Swenson, Daniel Kennedy, Sam Levis, Erik Kluzek, ...

Deleted: Drew Holzworth, Ian Harman, Dr. Shufen Pan, Jason Cole, Victoria Spada, Vladimir Lapin, Raffaele Bernardello, K. Toyama, H. Nakano, S.

Deleted: Walker, Tristan Quaife, and

Deleted: Mutshutshu Tsanwani

Formatted: Highlight

Deleted: C. Lo Monaco,

Deleted: Arne Körtzinger

2330 Goris and Lavinia Patara for support in calculating observational ocean evaluation metrics. We thank Fortunat
2331 Joos, Samar Khatiwala and Timothy DeVries for providing historical atmospheric and ocean data. We thank data
2332 providers ObsPack GLOBALVIEWplus v9.0 and NRT v9.2 for atmospheric CO₂ observations. Ingrid T Luijkx
2333 and Wouter Peters thank the CarbonTracker Europe team at Wageningen University, including Remco de Kok,
2334 Joram Hooghiem, Linda Kooyjans and Auke van der Woude. Ian Harris thanks the Japan Meteorological Agency
2335 (JMA) for producing the Japanese 55-year Reanalysis (JRA-55). Reinel Sospedra-Alfonso thanks William J.
2336 Merryfield, Woosung Lee, Jason Cole, and Victoria Spada for their help to set up and produce CanESM5 runs.
2337 Olivier Torres thanks Patricia Cadule, Juliette Mignot, Didier Swingedouw, and Laurent Bopp for contributions
2338 to the IPSL-CM6-LR-ESMCO2 simulations. Yosuke Niwa thanks CSIRO, EC, EMPA, FMI, IPEN, JMA, LSCE,
2339 NCAR, NIES, NILU, NIWA, NOAA, SIO, and TU/NIPR for providing data for NISMON-CO2. Zhe Jin thanks
2340 Xiangjun Tian, Yilong Wang, Hongqin Zhang, Min Zhao, Tao Wang, Jinzhi Ding and Shilong Piao for their
2341 contributions to the GONGGA inversion system. Paul I. Palmer thanks Lian Fang and acknowledges ongoing
2342 support from the National Centre for Earth Observation. Ning Zeng thanks Zhiqiang Liu, Yun Liu, Eugenia
2343 Kalnay, and Gassem Asrar for their contributions to the COLA system. Fei Jiang acknowledges the High-
2344 Performance Computing Center (HPCC) of Nanjing University for doing the inversions on its blade cluster
2345 system, and thanks Weimin Ju for updating the a priori fluxes of the terrestrial ecosystems. Meike Becker and Are
2346 Olsen thank Sparebanken Vest / Agenda Vestlandet for their support for the observations on the Statsraad
2347 Lehmkuhl. Wiley Evans and Katie Campbell thank the Tula Foundation for funding support. Thanos Gkritzalis
2348 and the VLIZ ICOS team are thankful to the crew of the research vessel Simon Stevin for all the support and help
2349 they provide. Bronte Tilbrook and Craig Neill thank Australia's Integrated Marine Observing System (IMOS) for
2350 sourcing CO2 data. FAOSTAT is funded by FAO member states through their contributions to the FAO Regular
2351 Programme, data contributions by national experts are greatly acknowledged. The views expressed in this paper
2352 are the authors' only and do not necessarily reflect those of FAO. Finally, we thank all funders who have supported
2353 the individual and joint contributions to this work (see details below), as well as the two reviewers of this
2354 manuscript, and the many researchers who have provided feedback.

Deleted: anonymous

2355 **Financial and computing support**

2356 This research was supported by the following sources of funding: The Argentinian-Uruguayan Joint Technical
2357 Commission of the Maritime Front (Comisión Técnica Mixta del Frente Marítimo, CTMFM) (Argentina);
2358 Instituto Nacional de Investigación y Desarrollo Pesquero (Argentina); Australia's Integrated Marine Observing

2360 System (IMOS) which is enabled by the National Collaborative Research Infrastructure Strategy (NCRIS)
2361 (Australia); Australian Earth-System Simulator National Research Infrastructure (ACCESS-NRI) (Australia);
2362 Australian National Environmental Science Program, Climate Systems Hub (Australia); Research Foundation
2363 Flanders (ICOS Flanders, grant no. I001821N) (Belgium); Tula Foundation (Canada); National Key Research and
2364 Development Program (grant no. 2023YFF0805400) (China); National Key Research and Development Program
2365 (grant no. 2023YFB3907404) (China); Jiangsu Provincial Science Fund for Distinguished Young Scholars (Grant
2366 No: BK20231530) (China); National Natural Science Foundation (grant no. 42141020) (China); Carbon
2367 Neutrality and Energy System Transformation (CNEST) Program led by Tsinghua University, granted by National
2368 Key R&D Program of China (Grant No. 2023YFE0113000) (China); Second Tibetan Plateau Scientific
2369 Expedition and Research Program (Grant: 2022QZKK0101) (China); CAS Project for Young Scientists in Basic
2370 Research, Grant No.YSBR-037 (China); grant no. 2021YFD2200405 (China); Copernicus Atmosphere
2371 Monitoring Service, implemented by ECMWF (Grant: CAMS2 55) (European Commission); Copernicus Marine
2372 Environment Monitoring Service, implemented by MOi (Grant: CMEMS-TAC-MOB) (European Commission);
2373 H2020 4C (grant no. 821003) (European Commission); H2020 ESM2025 – Earth System Models for the Future
2374 (grant no. 101003536) (European Commission); H2020 GEORGE (grant no. 101094716) (European
2375 Commission); Horizon Europe (EYE-CLIMA: grant no. 101081395) (European Commission); ERC-2022-STG
2376 OceanPeak (Grant 101077209) (European Commission); Horizon Europe Grant 101083922 (OceanICU
2377 Improving Carbon Understanding) (European Commission); Horizon 2020 research and innovation programme
2378 under Grant Agreements N° 101056939 (RESCUE project) (European Commission); COMFORT project (grant
2379 no. 820989) (European Commission); Climate Space RECCAP-2 (European Space Agency); Ocean Carbon for
2380 Climate (European Space Agency); EO-LINCS (European Space Agency); OceanSODA project, grant no.
2381 4000112091/14/I-LG (European Space Agency); Institut National des Sciences de l’Univers (INSU) (France);
2382 Institut Polaire français, Paul-Emile Victor (IPEV) (France); Observatoire des sciences de l’univers Ecce-Terra
2383 (OSU at Sorbonne Université) (France); Institut de recherché français sur les ressources marines (IFREMER)
2384 (France); French Oceanographic Fleet (FOF) (France); ICOS-France (France); Institut de Recherche pour le
2385 Développement (IRD) (France); Agence Nationale de la Recherche - France 2030 (PEPR TRACCS programme
2386 under grant number ANR-22-EXTR-0009) (France); Institut de l’Océan and the Institut des Sciences du Calcul et
2387 des Données of Sorbonne University (IDEX SUPER 11-IDEX-0004, project-team FORMAL) (France); Federal
2388 Ministry of Education and Research, collaborative project C-SCOPE (project no. 03F0877A) (Germany);
2389 Helmholtz Association ATMO programme (Germany); Initiative and Networking Fund of the Helmholtz
2390 Association (grant no. VH-NG-19-33) (Germany); ICOS Germany (Germany); German Federal Ministry of
2391 Education and Research (BMBF), project STEPSEC (grant no. 01LS2102A) (Germany); Helmholtz Young
2392 Investigator Group Marine Carbon and Ecosystem Feedbacks in the Earth System (MarESys), grant number VH-
2393 NG-1301 (Germany); Deutsche Forschungsgemeinschaft (DFG) under Germany's Excellence Strategy – EXC
2394 2037 ‘Climate, Climatic Change, and Society’ – Project Number: 390683824 (Germany); Arctic Challenge for
2395 Sustainability phase II project (ArCS-II; grant no. JP-MXD1420318865) (Japan); Environment Research and
2396 Technology Development Fund (grant no. JPMEERF24S12206) (Japan); CREST, Japan Science and Technology
2397 Agency (grant no. JPMJCR23J4) (Japan); Global Environmental Research Coordination System, Ministry of the
2398 Environment (grant no. E2252) (Japan); Meteorological Agency (Japan); Ministry of Education, Culture, Sports,

2399 Science and Technology, MEXT program for the advanced studies of climate change projection (SENTAN) (grant
2400 numbers JPMXD0722680395 and JPMXD0722681344) (Japan); Meteorological Research Institute and the
2401 Environment Research and Technology Development Fund (JPMEERF24S12200) (Japan); NIES GOSAT project
2402 (Japan); Research Council of Norway (N-ICOS-2, grant no. 296012) (Norway); Research Council of Norway
2403 (grant no. 270061) (Norway); Swiss National Science Foundation (grant no. 200020-200511) (Switzerland);
2404 Natural Environment Research Council, National Centre for Earth Observation (NE/R016518/1) (UK); Natural
2405 Environment Research Council, UK EO Climate Information Service (NE/X019071/1) (UK); Natural
2406 Environment Research Council (NE/V01417X/1) (UK); Natural Environment Research Council, National Centre
2407 for Atmospheric Science (UK); Natural Environment Research Council (NE/Y005260/1) (UK); UK Royal Society
2408 (grant no. RP/R1\191063) (UK); Natural Environment Research Council (Grant Ref: NE/V013106/1) (UK);
2409 National Center for Atmospheric Research (NSF Cooperative Agreement No. 1852977) (USA); NOAA Ocean
2410 Acidification Program (grant no. 100018228) (USA); NOAA Global Ocean Monitoring and Observing Program
2411 (grant no. 100018302) (USA); NOAA cooperative agreement NA22OAR4320151 (USA); NOAA cooperative
2412 agreement NA20OAR4310340 (USA); NOAA (grant no. 1305M322PNRMJ0338); NASA (grant no.
2413 80NSSC22K0150); NASA (grant no. 80NM0018D0004); National Science Foundation (NSF-2019625) (USA);
2414 National Science Foundation (NSF-831361857) (USA); NASA Terrestrial Ecology Program (USA); NASA
2415 Carbon Monitoring System program (80NSSC21K1059) (USA); NASA Land Cover and Land Use Change
2416 Program (80NSSC24K0920) (USA); National Science Foundation (NSF-1903722) (USA); National Science
2417 Foundation (NSF-1852977) (USA); The U.S. Department of Energy, Office of Science, Office of Biological and
2418 Environmental Research (USA); The Department for Education SciDac (grant number: DESC0012972) (USA);
2419 IDS (grant number: 80NSSC17K0348) (USA); Schmidt Sciences, LLC (USA).

2420 We also acknowledge support from the following computing facilities: The Australian Earth-System Simulator
2421 National Research Infrastructure (ACCESS-NRI) (Australia); Deutsches Klimarechenzentrum (DKRZ) granted
2422 by its Scientific Steering Committee (WLA) under project ID bm0891 (Germany); HPC cluster Aether at the
2423 University of Bremen, financed by DFG within the scope of the Excellence Initiative (Germany); HPC resources
2424 of TGCC under the allocation A0150102201 awarded by GENCI and of CCRT under the Grant CCRT2024-
2425 p24cheva awarded by CEA/DRF (France); HPC resources of Meteo-France (France); NIES supercomputer system
2426 (Japan); UNINETT Sigma2, National Infrastructure for High Performance Computing and Data Storage in
2427 Norway (NN2980K/NS2980K) (Norway); UK CEDA JASMIN supercomputer (UK); UEA (University of East
2428 Anglia) high performance computing cluster (UK); Derecho supercomputer (doi:10.5065/D6RX99HX), provided
2429 by the Computational and Information Systems Laboratory (CISL) at NCAR (USA); Oak Ridge Leadership
2430 Computing Facility at the Oak Ridge National Laboratory (USA); ISAM simulations were performed using
2431 Cheyenne, NCAR HPC resources managed by CISL (doi:10.5065/D6RX99HX) (USA).

2432

References

- 2433 Andela, N., Morton, D. C., Giglio, L., Chen, Y., van der Werf, G. R., Kasibhatla, P. S., DeFries, R. S., Collatz, G. J.,
2434 Hantson, S., Kloster, S., Bachelet, D., Forrest, M., Lasslop, G., Li, F., Mangeon, S., Melton, J. R., Yue, C., and Randerson, J.
2435 T.: A human-driven decline in global burned area, *Science*, 356, 1356–1362, <https://doi.org/10.1126/science.aal4108>, 2017.
- 2436 Andrew, R. M.: A comparison of estimates of global carbon dioxide emissions from fossil carbon sources, *Earth Syst. Sci.*
2437 *Data*, 12, 1437–1465, <https://doi.org/10.5194/essd-12-1437-2020>, 2020a.
- 2438 Andrew, R. M.: Timely estimates of India’s annual and monthly fossil CO₂ emissions, *Earth Syst. Sci. Data*, 12, 2411–2421,
2439 <https://doi.org/10.5194/essd-12-2411-2020>, 2020b.
- 2440 Andrew, R. M. and Peters, G. P.: The Global Carbon Project’s fossil CO₂ emissions dataset (2024v17), Zenodo [dataset],
2441 <https://doi.org/10.5281/zenodo.13981696>, 2024.
- 2442 Aragão, L. E. O. C., Anderson, L. O., Fonseca, M. G., Rosan, T. M., Vedovato, L. B., Wagner, F. H., Silva, C. V. J., Silva
2443 Junior, C. H. L., Arai, E., Aguiar, A. P., Barlow, J., Berenguer, E., Deeter, M. N., Domingues, L. G., Gatti, L., Gloor, M.,
2444 Malhi, Y., Marengo, J. A., Miller, J. B., Phillips, O. L., and Saatchi, S.: 21st Century drought-related fires counteract the
2445 decline of Amazon deforestation carbon emissions, *Nat Commun*, 9, 536, <https://doi.org/10.1038/s41467-017-02771-y>,
2446 2018.
- 2447 Archer, D., Eby, M., Brovkin, V., Ridgwell, A., Cao, L., Mikolajewicz, U., Caldeira, K., Matsumoto, K., Munhoven, G.,
2448 Montenegro, A., and Tokos, K.: Atmospheric Lifetime of Fossil Fuel Carbon Dioxide, *Annu. Rev. Earth Planet. Sci.*, 37,
2449 117–134, <https://doi.org/10.1146/annurev.earth.031208.100206>, 2009.
- 2450 Armeth, A., Sitch, S., Pongratz, J., Stocker, B. D., Ciais, P., Poulter, B., Bayer, A. D., Bondeau, A., Calle, L., Chini, L. P.,
2451 Gasser, T., Fader, M., Friedlingstein, P., Kato, E., Li, W., Lindeskog, M., Nabel, J. E. M. S., Pugh, T. A. M., Robertson, E.,
2452 Viovy, N., Yue, C., and Zaehle, S.: Historical carbon dioxide emissions caused by land-use changes are possibly larger than
2453 assumed, *Nature Geosci*, 10, 79–84, <https://doi.org/10.1038/ngeo2882>, 2017.
- 2454 Asaadi, A., Arora, V. K., Melton, J. R., and Bartlett, P.: An improved parameterization of leaf area index (LAI) seasonality
2455 in the Canadian Land Surface Scheme (CLASS) and Canadian Terrestrial Ecosystem Model (CTEM) modelling framework,
2456 *15*, 6885–6907, <https://doi.org/10.5194/bg-15-6885-2018>, 2018.
- 2457 Aumont, O., Orr, J. C., Monfray, P., Ludwig, W., Amiotte-Suchet, P., and Probst, J.-L.: Riverine-driven interhemispheric
2458 transport of carbon, *Global Biogeochem. Cycles*, 15, 393–405, <https://doi.org/10.1029/1999GB001238>, 2001.
- 2459 Aumont, O., Ethé, C., Tagliabue, A., Bopp, L., and Gehlen, M.: PISCES-v2: an ocean biogeochemical model for carbon and
2460 ecosystem studies, 8, 2465–2513, <https://doi.org/10.5194/gmd-8-2465-2015>, 2015.
- 2461 [Babiker, M., G. Berndes, K. Blok, B. Cohen, A. Cowie, O. Geden, V. Ginzburg, A. Leip, P. Smith, M. Sugiyama, F. Yamba,](#)
2462 [Al Khourdajie, A., Armeth, A., Lima de Azevedo, I. M., Bataille, C., Beerling, D., Bezner Kerr, R., Bradley, J., Buck, H. J.,](#)
2463 [Cabeza, L. F., Calvin, K., Campbell, D., Carnicer Cols, J., Daioglou, V., Harmsen, M., Höglund-Isaksson, L., House, J. I.,](#)
2464 [Keller, D., de Kleijne, K., Kugelberg, S., Makarov, I., Meza, F., Minx, J. C., Morecroft, M., Nabuurs, G. J., Neufeldt, H.,](#)
2465 [Novikova, A., Nugroho, S. B., Oschlies, A., Parmesan, C., Peters, G. P., Poore, J., Portugal-Pereira, J., Postigo, J. C.,](#)
2466 [Pradhan, P., Renforth, P., Rivera-Ferre, M. G., Roe, S., Singh, P. K., Slade, R., Smith, S. M., Tirado von der Pahlen, M. C.,](#)
2467 [and Toribio Ramirez, D.: Cross sectoral perspectives. In: Climate Change 2022: Mitigation of Climate Change. Contribution](#)

2468 [of Working Group III to the Sixth Assessment Report of the Intergovernmental Panel on Climate Change \[P.R. Shukla, J.](#)
2469 [Skea, R. Slade, A. Al Khourdajie, R. van Diemen, D. McCollum, M. Pathak, S. Some, P. Vyas, R. Fradera, M. Belkacemi,](#)
2470 [A. Hasija, G. Lisboa, S. Luz, J. Malley, \(eds.\)\]. Cambridge University Press, Cambridge, UK and New York, NY, USA, doi:](#)
2471 [10.1017/9781009157926.014.2022](https://doi.org/10.1017/9781009157926.014.2022).

2472 Baccini, A., Walker, W., Carvalho, L., Farina, M., Sulla-Menashe, D., and Houghton, R. A.: Tropical forests are a net carbon
2473 source based on aboveground measurements of gain and loss, *Science*, 358, 230–234,
2474 <https://doi.org/10.1126/science.aam5962>, 2017.

2475 Bakker, D. C. E., Pfeil, B., Landa, C. S., Metz, N., O'Brien, K. M., Olsen, A., Smith, K., Cosca, C., Harasawa, S., Jones, S.
2476 D., Nakaoka, S., Nojiri, Y., Schuster, U., Steinhoff, T., Sweeney, C., Takahashi, T., Tilbrook, B., Wada, C., Wanninkhof, R.,
2477 Alin, S. R., Balestrini, C. F., Barbero, L., Bates, N. R., Bianchi, A. A., Bonou, F., Boutin, J., Bozec, Y., Burger, E. F., Cai,
2478 W.-J., Castle, R. D., Chen, L., Chierici, M., Currie, K., Evans, W., Featherstone, C., Feely, R. A., Fransson, A., Goyet, C.,
2479 Greenwood, N., Gregor, L., Hankin, S., Hardman-Mountford, N. J., Harlay, J., Hauck, J., Hoppema, M., Humphreys, M. P.,
2480 Hunt, C. W., Huss, B., Ibáñez, J. S. P., Johannessen, T., Keeling, R., Kitidis, V., Körtzinger, A., Kozyr, A., Krasakopoulou,
2481 E., Kuwata, A., Landschützer, P., Lauvset, S. K., Lefèvre, N., Lo Monaco, C., Manke, A., Mathis, J. T., Merlivat, L.,
2482 Millero, F. J., Monteiro, P. M. S., Munro, D. R., Murata, A., Newberger, T., Omar, A. M., Ono, T., Paterson, K., Pearce, D.,
2483 Pierrot, D., Robbins, L. L., Saito, S., Salisbury, J., Schlitzer, R., Schneider, B., Schweitzer, R., Sieger, R., Skjelvan, I.,
2484 Sullivan, K. F., Sutherland, S. C., Sutton, A. J., Tadokoro, K., Telszewski, M., Tuma, M., van Heuven, S. M. A. C.,
2485 Vandemark, D., Ward, B., Watson, A. J., and Xu, S.: A multi-decade record of high-quality CO₂ data in version 3 of the
2486 Surface Ocean CO₂ Atlas (SOCAT), *Earth Syst. Sci. Data*, 8, 383–413, <https://doi.org/10.5194/essd-8-383-2016>, 2016.

2487 Bakker, Dorothee C. E.; Alin, Simone R.; Bates, Nicholas; Becker, Meike; Gkritzalis, Thanos; Jones, Steve D.; Kozyr, Alex;
2488 Lauvset, Siv K.; Metz, Nicolas; Nakaoka, Shin-ichiro; O'Brien, Kevin M.; Olsen, Are; Pierrot, Denis; Steinhoff, Tobias;
2489 Sutton, Adrienne J.; Takao, Shintaro; Tilbrook, Bronte; Wada, Chisato; Wanninkhof, Rik; Akl, John; Arbilla, Lisandro A.;
2490 Arruda, Ricardo; Azetsu-Scott, Kumiko; Barbero, Leticia; Beatty, Cory M.; Berghoff, Carla F.; Bittig, Henry C.; Burger,
2491 Eugene F.; Campbell, Katie; Cardin, Vanessa; Collins, Andrew; Coppola, Laurent; Cronin, Margot; Cross, Jessica N.;
2492 Currie, Kim I.; Emerson, Steven R.; Enright, Matt P.; Enyo, Kazutaka; Evans, Wiley; Feely, Richard A.; Flohr, Anita;
2493 Gehrung, Martina; Glockzin, Michael; González-Dávila, Melchor; Hamna, Siyabulela; Hartman, Sue; Howden, Stephan D.;
2494 Kam, Kitty; Kamb, Linus; Körtzinger, Arne; Kosugi, Naohiro; Lefèvre, Nathalie; Lo Monaco, Claire; Macovei, Vlad A.;
2495 Maenner Jones, Stacy; Manalang, Dana; Martz, Todd R.; Mdokwana, Baxolele; Monacci, Natalie M.; Monteiro, Pedro M.
2496 S.; Mordy, Calvin; Morell, Julio M.; Murata, Akihiko; Neill, Craig; Noh, Jae-Hoon; Nojiri, Yukihiko; Ohman, Mark; Olivier,
2497 Léa; Ono, Tsuneo; Petersen, Wilhelm; Plueddemann, Albert J.; Prytherch, John; Rehder, Gregor; Rutgersson, Anna;
2498 Santana-Casiano, J. Magdalena; Schlitzer, Reiner; Send, Uwe; Skjelvan, Ingunn; Sullivan, Kevin F.; T'Jampens, Michiel;
2499 Tadokoro, Kazuaki; Telszewski, Maciej; Theetaert, Hannelore; Tsanwani, Mutshutshu; Vandemark, Douglas; van Ooijen,
2500 Erik; Vecchia, Martin H.; Voynova, Yoana G.; Wang, Hongjie; Weller, Robert A.; Woosley, Ryan J.: Surface Ocean CO₂
2501 Atlas Database Version 2024 (SOCATv2024) (NCEI Accession 0293257). NOAA National Centers for Environmental
2502 Information, <https://doi.org/10.25921/9wpn-th28>, last access: [21 January 2025](https://www.noaa.gov/news/21-january-2025), 2024.

Deleted: 28 October 2024

2503 Ballantyne, A. P., Alden, C. B., Miller, J. B., Tans, P. P., and White, J. W. C.: Increase in observed net carbon dioxide
2504 uptake by land and oceans during the past 50 years, *Nature*, 488, 70–72, <https://doi.org/10.1038/nature11299>, 2012.

2505 Ballantyne, A. P., Andres, R., Houghton, R., Stocker, B. D., Wanninkhof, R., Anderegg, W., Cooper, L. A., DeGrandpre,
2506 M., Tans, P. P., Miller, J. B., Alden, C., and White, J. W. C.: Audit of the global carbon budget: estimate errors and their
2507 impact on uptake uncertainty, *Biogeosciences*, 12, 2565–2584, <https://doi.org/10.5194/bg-12-2565-2015>, 2015.

2509 Bastos, A., Hartung, K., Nützel, T. B., Nabel, J. E. M. S., Houghton, R. A., and Pongratz, J.: Comparison of uncertainties in
2510 land-use change fluxes from bookkeeping model parameterisation, *12*, 745–762, <https://doi.org/10.5194/esd-12-745-2021>,
2511 2021.

2512 Battle, M. O., Raynor, R., Kesler, S., and Keeling, R.: Technical Note: The impact of industrial activity on the amount of
2513 atmospheric O₂, *Atmospheric Chem. Phys. Discuss.*, 1–17, <https://doi.org/10.5194/acp-2022-765>, 2023.
2514

2515 Bellenger, H., Bopp, L., Ethé, C., Ho, D., Duvel, J. P., Flavoni, S., Guez, L., Kataoka, T., Perrot, X., Parc, L., and Watanabe,
2516 M.: Sensitivity of the Global Ocean Carbon Sink to the Ocean Skin in a Climate Model, *J. Geophys. Res. Oceans*, *128*,
2517 e2022JC019479, <https://doi.org/10.1029/2022JC019479>, 2023.
2518

2519 Bennington, V., Gloege, L., and McKinley, G. A.: Variability in the Global Ocean Carbon Sink From 1959 to 2020 by
2520 Correcting Models with Observations, *Geophys. Res. Lett.*, *49*, e2022GL098632, <https://doi.org/10.1029/2022GL098632>,
2521 2022.

2522 Bernardello, R., Sicardi, V., Lapin, V., Ortega, P., Ruprich-Robert, Y., Tourigny, E. and Ferrer, E.: Ocean biogeochemical
2523 reconstructions to estimate historical ocean CO₂ uptake. *Earth System Dynamics*, *15*(5), pp.1255-1275,
2524 <https://doi.org/10.5194/esd-15-1255-2024>, 2024.

2525 Berthet, S., Séférian, R., Bricaud, C., Chevallier, M., Voldoire, A., and Ethé, C.: Evaluation of an Online Grid-Coarsening
2526 Algorithm in a Global Eddy-Admitting Ocean Biogeochemical Model, *J. Adv. Model Earth Sy.*, *11*, 1759–1783,
2527 <https://doi.org/10.1029/2019MS001644>, 2019.

2528 Betts, R. A., Jones, C. D., Knight, J. R., Keeling, R. F., and Kennedy, J. J.: El Niño and a record CO₂ rise, *Nat. Clim.*
2529 *Change*, *6*, 806–810, <https://doi.org/10.1038/nclimate3063>, 2016.

2530 Bilbao, R., Wild, S., Ortega, P., Acosta-Navarro, J., Arsouze, T., Bretonnière, P.A., Caron, L.P., Castrillo, M., Cruz-García,
2531 R., Cvijanovic, I. and Doblas-Reyes, F.J.: Assessment of a full-field initialised decadal climate prediction system with the
2532 CMIP6 version of EC-Earth. *Earth System Dynamics Discussions*, 2020, pp.1-30, <https://doi.org/10.5194/esd-12-173-2021>,
2533 2020.

2534 Bloom, A. A. and Williams, M.: Constraining ecosystem carbon dynamics in a data-limited world: integrating ecological
2535 “common sense” in a model–data fusion framework, *Biogeosciences*, *12*, 1299–1315, [https://doi.org/10.5194/bg-12-1299-](https://doi.org/10.5194/bg-12-1299-2015)
2536 2015, 2015.
2537

2538 Bloom, A. A., Exbrayat, J.-F., van der Velde, I. R., Feng, L., and Williams, M.: The decadal state of the terrestrial carbon
2539 cycle: Global retrievals of terrestrial carbon allocation, pools, and residence times, *Proc. Natl. Acad. Sci.*, *113*, 1285–1290,
2540 <https://doi.org/10.1073/pnas.1515160113>, 2016.
2541

2542 Boer, G. J., Smith, D. M., Cassou, C., Doblas-Reyes, F., Danabasoglu, G., Kirtman, B., Kushnir, Y., Kimoto, M., Meehl, G.
2543 A., Msadek, R., Mueller, W. A., Taylor, K. E., Zwiers, F., Rixen, M., Ruprich-Robert, Y., and Eade, R.: The Decadal
2544 Climate Prediction Project (DCPP) contribution to CMIP6, *Geosci. Model Dev.*, *9*, 3751–3777, [https://doi.org/10.5194/gmd-](https://doi.org/10.5194/gmd-9-3751-2016)
2545 9-3751-2016, 2016.
2546

2547 Boucher, O., Servonnat, J., Albright, A. L., Aumont, O., Balkanski, Y., Bastrikov, V., Bekki, S., Bonnet, R., Bony, S., Bopp,
2548 L., Braconnot, P., Brockmann, P., Cadule, P., Caubel, A., Cheruy, F., Codron, F., Cozic, A., Cugnet, D., D'Andrea, F.,
2549 Davini, P., de Lavergne, C., Denvil, S., Deshayes, J., Devilliers, M., Ducharne, A., Dufresne, J.-L., Dupont, E., Éthé, C.,
2550 Fairhead, L., Falletti, L., Flavoni, S., Foujols, M.-A., Gardoll, S., Gastineau, G., Ghattas, J., Grandpeix, J.-Y., Guenet, B.,
2551 Guez, E., Lionel, Guilyardi, E., Guimberteau, M., Hauglustaine, D., Hourdin, F., Idelkadi, A., Joussaume, S., Kageyama, M.,
2552 Khodri, M., Krinner, G., Lebas, N., Levvasseur, G., Lévy, C., Li, L., Lott, F., Lurton, T., Luysaert, S., Madec, G.,
2553 Madeleine, J.-B., Maignan, F., Marchand, M., Marti, O., Mellul, L., Meurdesoif, Y., Mignot, J., Musat, I., Ottlé, C., Peylin,
2554 P., Planton, Y., Polcher, J., Rio, C., Rochetin, N., Rousset, C., Sepulchre, P., Sima, A., Swingedouw, D., Thiéblemont, R.,
2555 Traore, A. K., Vancoppenolle, M., Vial, J., Vialard, J., Viovy, N., and Vuichard, N.: Presentation and Evaluation of the
2556 IPSL-CM6A-LR Climate Model, *J. Adv. Model. Earth Syst.*, 12, e2019MS002010, <https://doi.org/10.1029/2019MS002010>,
2557 2020.

2558 Bourgeois, T., Goris, N., Schwinger, J., and Tjiputra, J. F.: Stratification constrains future heat and carbon uptake in the
2559 Southern Ocean between 30°S and 55°S, *Nat. Commun.*, 13, 340, <https://doi.org/10.1038/s41467-022-27979-5>, 2022.

2560 Bray, E.: 2017 Minerals Yearbook: Aluminum [Advance Release], Tech. rep., U.S. Geological Survey, [https://d9-wret.s3-us-](https://d9-wret.s3-us-west-2.amazonaws.com/assets/palladium/production/atoms/files/myb1-2017-alumi.pdf)
2561 [west-2.amazonaws.com/assets/palladium/production/atoms/files/myb1-2017-alumi.pdf](https://d9-wret.s3-us-west-2.amazonaws.com/assets/palladium/production/atoms/files/myb1-2017-alumi.pdf), 2020.

2562 Brien, R. J. W., Caldwell, L., Duchesne, L., Voelker, S., Barichivich, J., Baliva, M., Ceccantini, G., Di Filippo, A.,
2563 Helama, S., Locosselli, G. M., Lopez, L., Piovesan, G., Schöngart, J., Villalba, R., and Gloor, E.: Forest carbon sink
2564 neutralized by pervasive growth-lifespan trade-offs, *Nat. Commun.*, 11, 4241, <https://doi.org/10.1038/s41467-020-17966-z>,
2565 2020.

2566 Brien, R. J. W., Phillips, O. L., Feldpausch, T. R., Gloor, E., Baker, T. R., Lloyd, J., Lopez-Gonzalez, G., Monteagudo-
2567 Mendoza, A., Malhi, Y., Lewis, S. L., Vásquez Martínez, R., Alexiades, M., Álvarez Dávila, E., Alvarez-Loayza, P.,
2568 Andrade, A., Aragão, L. E. O. C., Araujo-Murakami, A., Arets, E. J. M. M., Arroyo, L., Aymard C., G. A., Bánki, O. S.,
2569 Baraloto, C., Barroso, J., Bonal, D., Boot, R. G. A., Camargo, J. L. C., Castilho, C. V., Chama, V., Chao, K. J., Chave, J.,
2570 Comiskey, J. A., Cornejo Valverde, F., da Costa, L., de Oliveira, E. A., Di Fiore, A., Erwin, T. L., Fauset, S., Forsthofer, M.,
2571 Galbraith, D. R., Grahame, E. S., Groot, N., Hérault, B., Higuchi, N., Honorio Coronado, E. N., Keeling, H., Killeen, T. J.,
2572 Laurance, W. F., Laurance, S., Licona, J., Magnussen, W. E., Marimon, B. S., Marimon-Junior, B. H., Mendoza, C., Neill,
2573 D. A., Nogueira, E. M., Núñez, P., Pallqui Camacho, N. C., Parada, A., Pardo-Molina, G., Peacock, J., Peña-Claros, M.,
2574 Pickavance, G. C., Pitman, N. C. A., Poorter, L., Prieto, A., Quesada, C. A., Ramirez, F., Ramirez-Angulo, H., Restrepo, Z.,
2575 Roopsind, A., Rudas, A., Salomão, R. P., Schwarz, M., Silva, N., Silva-Espejo, J. E., Silveira, M., Stropp, J., Talbot, J., ter
2576 Steege, H., Teran-Aguilar, J., Terborgh, J., Thomas-Caesar, R., Toledo, M., Torello-Raventos, M., Umetsu, R. K., van der
2577 Heijden, G. M. F., van der Hout, P., Guimarães Vieira, I. C., Vieira, S. A., Vilanova, E., Vos, V. A., and Zagt, R. J.: Long-
2578 term decline of the Amazon carbon sink, 519, 344–348, <https://doi.org/10.1038/nature14283>, 2015.

2579 Bronselaer, B., Winton, M., Russell, J., Sabine, C. L., and Khatiwala, S.: Agreement of CMIP5 Simulated and Observed
2580 Ocean Anthropogenic CO₂ Uptake, *Geophys. Res. Lett.*, 44, 12,298-12,305, <https://doi.org/10.1002/2017GL074435>, 2017.

2581 Bruno, M. and Joos, F.: Terrestrial carbon storage during the past 200 years: A Monte Carlo Analysis of CO₂ data from ice
2582 core and atmospheric measurements, *Global Biogeochem. Cycles*, 11, 111–124, <https://doi.org/10.1029/96GB03611>, 1997.

2583 Burrows, S. M., Maltrud, M., Yang, X., Zhu, Q., Jeffery, N., Shi, X., Ricciuto, D., Wang, S., Bisht, G., Tang, J., Wolfe, J.,
2584 Harrop, B. E., Singh, B., Brent, L., Baldwin, S., Zhou, T., Cameron-Smith, P., Keen, N., Collier, N., Xu, M., Hunke, E. C.,

2585 Elliott, S. M., Turner, A. K., Li, H., Wang, H., Golaz, J.-C., Bond-Lamberty, B., Hoffman, F. M., Riley, W. J., Thornton, P.
2586 E., Calvin, K., and Leung, L. R.: The DOE E3SM v1.1 Biogeochemistry Configuration: Description and Simulated
2587 Ecosystem-Climate Responses to Historical Changes in Forcing, *J. Adv. Model. Earth Syst.*, 12, e2019MS001766,
2588 <https://doi.org/10.1029/2019MS001766>, 2020.

2589 Bunsen, F., Nissen, C., and Hauck, J.: The Impact of Recent Climate Change on the Global Ocean Carbon Sink. *Geophysical*
2590 *Research Letters*, 51(4), e2023GL107030, <https://doi.org/10.1029/2023GL107030>, 2024.

2591 Burton, C., Betts, R., Cardoso, M., Feldpausch, T. R., Harper, A., Jones, C. D., Kelley, D. I., Robertson, E., and Wiltshire,
2592 A.: Representation of fire, land-use change and vegetation dynamics in the Joint UK Land Environment Simulator vn4.9
2593 (JULES), *Geosci. Model Dev.*, 12, 179–193, <https://doi.org/10.5194/gmd-12-179-2019>, 2019.

2594 Burton, C., Lampe, S., Kelley, D. I., Thiery, W., Hantson, S., Christidis, N., Gudmundsson, L., Forrest, M., Burke, E.,
2595 Chang, J., Huang, H., Ito, A., Kou-Giesbrecht, S., Lasslop, G., Li, W., Nieradzik, L., Li, F., Chen, Y., Randerson, J., Reyer,
2596 C. P. O., and Mengel, M.: Global burned area increasingly explained by climate change, *Nature Climate Change*,
2597 <https://doi.org/10.1038/s41558-024-02140-w>, 2024.

2598 Bushinsky, S. M., Landschützer, P., Rödenbeck, C., Gray, A. R., Baker, D., Mazloff, M. R., Resplandy, L., Johnson, K. S.,
2599 and Sarmiento, J. L.: Reassessing Southern Ocean Air-Sea CO₂ Flux Estimates With the Addition of Biogeochemical Float
2600 Observations, *Global Biogeochem. Cycles*, 33, 1370–1388, <https://doi.org/10.1029/2019GB006176>, 2019.

2601 Byrne, B., Liu, J., Bowman, K.W., Pascolini-Campbell, M., Chatterjee, A., Pandey, S., Miyazaki, K., van der Werf, G.R.,
2602 Wunch, D., Wennberg, P.O., Roehl, C.M., and Sinha, S.: Carbon emissions from the 2023 Canadian wildfires. *Nature*, 633,
2603 835–839, <https://doi.org/10.1038/s41586-024-07878-z>, 2024.

2604 Canadell, J. G., Le Quere, C., Raupach, M. R., Field, C. B., Buitenhuis, E. T., Ciais, P., Conway, T. J., Gillett, N. P.,
2605 Houghton, R. A., and Marland, G.: Contributions to accelerating atmospheric CO₂ growth from economic activity, carbon
2606 intensity, and efficiency of natural sinks, *Proceedings of the National Academy of Sciences*, 104, 18866–18870,
2607 <https://doi.org/10.1073/pnas.0702737104>, 2007.

2608 Canadell, J. G., Monteiro, P. M. S., Costa, M. H., Cotrim da Cunha, L., Cox, P. M., Eliseev, A. V., Henson, S., Ishii, M.,
2609 Jaccard, S., Koven, C., Lohila, A., Patra, P. K., Piao, S., Rogelj, J., Syampungani, S., Zaehle, S., and Zickfeld, K.: Global
2610 Carbon and other Biogeochemical Cycles and Feedbacks. In: *Climate Change 2021: The Physical Science Basis*.
2611 Contribution of Working Group I to the Sixth Assessment Report of the Intergovernmental Panel on Climate Change
2612 [Masson-Delmotte, V., P. Zhai, A. Pirani, S. L. Connors, C. Péan, S. Berger, N. Caud, Y. Chen, L. Goldfarb, M. I. Gomis,
2613 M. Huang, K. Leitzell, E. Lonnoy, J.B.R. Matthews, T. K. Maycock, T. Waterfield, O. Yelekçi, R. Yu and B. Zhou (eds.)].
2614 Cambridge University Press, Cambridge, United Kingdom and New York, NY, USA, pp. 673–816,
2615 <https://doi.org/10.1017/9781009157896.007>, 2021.

2616 Cao, Z., Myers, R. J., Lupton, R. C., Duan, H., Sacchi, R., Zhou, N., Reed Miller, T., Cullen, J. M., Ge, Q., and Liu, G.: The
2617 sponge effect and carbon emission mitigation potentials of the global cement cycle, *Nat Commun*, 11, 3777,
2618 <https://doi.org/10.1038/s41467-020-17583-w>, 2020.

2619 Centro Nacional de Monitoramento e Alertas de Desastres Naturais (CEMADEN): Monitoramento de secas e impactos no
2620 Brasil - Agosto 2024, available at: <https://www.gov.br/cemaden/pt-br/assuntos/monitoramento/monitoramento-de-seca-para-o-brasil/monitoramento-de-secas-e-impactos-no-brasil-agosto-2024>, last access: [21 January 2025](#).

Deleted: 28 October 2024

2623 Céspedes, J., Sylvester, J. M., Pérez-Marulanda, L., Paz-Garcia, P., Reymondin, L., Khodadadi, M., Tello, J. J., and Castro-
2624 Nunez, A.: Has global deforestation accelerated due to the COVID-19 pandemic?. *J. For. Res.*, 34, 1153–1165,
2625 <https://doi.org/10.1007/s11676-022-01561-7>, 2023.

2626 Chandra, N., Patra, P. K., Niwa, Y., Ito, A., Iida, Y., Goto, D., Morimoto, S., Kondo, M., Takigawa, M., Hajima, T., and
2627 Watanabe, M.: Estimated regional CO₂ flux and uncertainty based on an ensemble of atmospheric CO₂ inversions,
2628 *Atmospheric Chem. Phys.*, 22, 9215–9243, <https://doi.org/10.5194/acp-22-9215-2022>, 2022.

2629 Chatfield, C.: The Holt-Winters Forecasting Procedure, *J. Roy. Stat. Soc. C.*, 27, 264–279, <https://doi.org/10.2307/2347162>,
2630 1978.

2631 Chau, T. T. T., Gehlen, M., and Chevallier, F.: A seamless ensemble-based reconstruction of surface ocean *p*CO₂ and air–sea
2632 CO₂ fluxes over the global coastal and open oceans, *Biogeosciences*, 19, 1087–1109, [https://doi.org/10.5194/bg-19-1087-](https://doi.org/10.5194/bg-19-1087-2022)
2633 2022, 2022.

2634 Chevallier, F., Fisher, M., Peylin, P., Serrar, S., Bousquet, P., Bréon, F.-M., Chédin, A., and Ciais, P.: Inferring CO₂
2635 sources and sinks from satellite observations: Method and application to TOVS data, *J. Geophys. Res.*, 110, D24309,
2636 <https://doi.org/10.1029/2005JD006390>, 2005.

2637 Ciais, P., Sabine, C., Bala, G., Bopp, L., Brovkin, V., Canadell, J. G., Chhabra, A., DeFries, R., Galloway, J., Heimann, M.,
2638 Jones, C., Le Quéré, C., Myneni, R., Piao, S., Thornton, P., Willem, J., Friedlingstein, P., and Munhoven, G.: Carbon and
2639 Other Biogeochemical Cycles, in *Climate Change 2013: The Physical Science Basis, Contribution of Working Group I to the*
2640 *Fifth Assessment Report of the Intergovernmental Panel on Climate Change*, edited by: Intergovernmental Panel on Climate
2641 Change, Cambridge University Press, Cambridge, United Kingdom and New York, NY, USA,
2642 <https://doi.org/10.1017/CBO9781107415324.015>, 2013.

2643 Ciais, P., Tan, J., Wang, X., Roedenbeck, C., Chevallier, F., Piao, S.-L., Moriarty, R., Broquet, G., Le Quéré, C., Canadell, J.
2644 G., Peng, S., Poulter, B., Liu, Z., and Tans, P.: Five decades of northern land carbon uptake revealed by the interhemispheric
2645 CO₂ gradient, *Nature*, 568, 221–225, <https://doi.org/10.1038/s41586-019-1078-6>, 2019.

2646 Ciais, P., Bastos, A., Chevallier, F., Lauerwald, R., Poulter, B., Canadell, P., Hugelius, G., Jackson, R. B., Jain, A., Jones,
2647 M., Kondo, M., Lujikx, I. T., Patra, P. K., Peters, W., Pongratz, J., Petrescu, A. M. R., Piao, S., Qiu, C., Von Randow, C.,
2648 Regnier, P., Saunois, M., Scholes, R., Shvidenko, A., Tian, H., Yang, H., Wang, X., and Zheng, B.: Definitions and methods
2649 to estimate regional land carbon fluxes for the second phase of the REgional Carbon Cycle Assessment and Processes
2650 Project (RECCAP-2), *Geosci. Model Dev.*, 15, 1289–1316, <https://doi.org/10.5194/gmd-15-1289-2022>, 2022.

2651 Collier, N., Hoffman, F. M., Lawrence, D. M., Keppel-Aleks, G., Koven, C. D., Riley, W. J., Mu, M., and Randerson, J. T.:
2652 The International Land Model Benchmarking (ILAMB) System: Design, Theory, and Implementation, *J. Adv. Model. Earth*
2653 *Syst.*, 10, 2731–2754, <https://doi.org/10.1029/2018MS001354>, 2018.

2654 [Conchedda, G. and Tubiello, F. N.: Drainage of organic soils and GHG emissions: Validation with country data, *Biosphere –*](#)
2655 [Biogeosciences](https://doi.org/10.5194/essd-2020-202), <https://doi.org/10.5194/essd-2020-202>, 2020.

2656 Cox, P. M., Pearson, D., Booth, B. B., Friedlingstein, P., Huntingford, C., Jones, C. D., and Luke, C. M.: Sensitivity of
2657 tropical carbon to climate change constrained by carbon dioxide variability, *Nature*, 494, 341–344,
2658 <https://doi.org/10.1038/nature11882>, 2013.

2659 De Kauwe, M. G., Medlyn, B. E., Zaehle, S., Walker, A. P., Dietze, M. C., Wang, Y.-P., Luo, Y., Jain, A. K., El-Masri, B.,
2660 Hickler, T., Wårlind, D., Weng, E., Parton, W. J., Thornton, P. E., Wang, S., Prentice, I. C., Asao, S., Smith, B., McCarthy,
2661 H. R., Iversen, C. M., Hanson, P. J., Warren, J. M., Oren, R., and Norby, R. J.: Where does the carbon go? A model–data
2662 intercomparison of vegetation carbon allocation and turnover processes at two temperate forest free-air CO₂ enrichment
2663 sites, *New Phytol.*, 203, 883–899, <https://doi.org/10.1111/nph.12847>, 2014.

2664 Delire, C., Séférian, R., Decharme, B., Alkama, R., Calvet, J.-C., Carrer, D., Gibelin, A.-L., Joetzjer, E., Morel, X., Rocher,
2665 M., and Tzanos, D.: The Global Land Carbon Cycle Simulated With ISBA-CTRIP: Improvements Over the Last Decade, *J.*
2666 *Adv. Model. Earth Syst.*, 12, e2019MS001886, <https://doi.org/10.1029/2019MS001886>, 2020.

2667 Denman, K. L., Brasseur, G., Chidthaisong, A., Ciais, P., Cox, P. M., Dickinson, R. E., Hauglustaine, D., Heinze, C.,
2668 Holland, E., Jacob, D., Lohmann, U., Ramachandran, S., Leite da Silva Dias, P., Wofsy, S. C., and Zhang, X.: Couplings
2669 Between Changes in the Climate System and Biogeochemistry, in: *Climate Change 2007: The Physical Science Basis.*
2670 *Contribution of Working Group I to the Fourth Assessment Report of the Intergovernmental Panel on Climate Change*,
2671 edited by: Solomon, S., Qin, D., Manning, M., Marquis, M., Averyt, K., Tignor, M. M. B., Miller, H. L., and Chen, Z. L.,
2672 Cambridge University Press, Cambridge, UK and New York, USA, 499–587, ISBN: 9780521705967, 2007.

2673 Denvil-Sommer, A., Gehlen, M., and Vrac, M.: Observation system simulation experiments in the Atlantic Ocean for
2674 enhanced surface ocean pCO₂ reconstructions, *Ocean Sci.*, 17, 1011–1030, <https://doi.org/10.5194/os-17-1011-2021>, 2021.

2675 DeVries, T., Holzer, M., and Primeau, F.: Recent increase in oceanic carbon uptake driven by weaker upper-ocean
2676 overturning, *Nature*, 542, 215–218, <https://doi.org/10.1038/nature21068>, 2017.

2677 DeVries, T., Quéré, C. L., Andrews, O., Berthet, S., Hauck, J., Ilyina, T., Landschützer, P., Lenton, A., Lima, I. D., Nowicki,
2678 M., Schwinger, J., and Séférian, R.: Decadal trends in the ocean carbon sink, *PNAS*, 116, 11646–11651,
2679 <https://doi.org/10.1073/pnas.1900371116>, 2019.

2680 DeVries, T., Yamamoto, K., Wanninkhof, R., Gruber, N., Hauck, J., Müller, J. D., Bopp, L., Carroll, D., Carter, B., Chau,
2681 T.-T.-T., Doney, S. C., Gehlen, M., Gloege, L., Gregor, L., Henson, S., Kim, J. H., Iida, Y., Ilyina, T., Landschützer, P., Le
2682 Quéré, C., Munro, D., Nissen, C., Patara, L., Pérez, F. F., Resplandy, L., Rodgers, K. B., Schwinger, J., Séférian, R., Sicardi,
2683 V., Terhaar, J., Triñanes, J., Tsujino, H., Watson, A., Yasunaka, S., and Zeng, J.: Magnitude, trends, and variability of the
2684 global ocean carbon sink from 1985-2018, *Glob. Biogeochem. Cycles*, n/a, e2023GB007780,
2685 <https://doi.org/10.1029/2023GB007780>, 2023.

2686

2687 Döscher, R., Acosta, M., Alessandri, A., Anthoni, P., Arneith, A., Arsouze, T., Bergmann, T., Bernadello, R., Boussetta, S.,
2688 Caron, L.P. and Carver, G.: The EC-earth3 Earth system model for the climate model intercomparison project 6.
2689 *Geoscientific Model Development Discussions*, 2021, pp.1-90, <https://doi.org/10.5194/gmd-15-2973-2022>, 2021.

2690

2691 Forster, P. M., Smith, C., Walsh, T., Lamb, W. F., Lamboll, R., Hall, B., Hauser, M., Ribes, A., Rosen, D., Gillett, N. P.,
2692 Palmer, M. D., Rogelj, J., von Schuckmann, K., Trewin, B., Allen, M., Andrew, R., Betts, R. A., Borger, A., Boyer, T.,
2693 Broersma, J. A., Buontempo, C., Burgess, S., Cagnazzo, C., Cheng, L., Friedlingstein, P., Gettelman, A., Gütschow, J., Ishii,
2694 M., Jenkins, S., Lan, X., Morice, C., Mühle, J., Kadow, C., Kennedy, J., Killeck, R. E., Krummel, P. B., Minx, J. C., Myhre,
2695 G., Naik, V., Peters, G. P., Pirani, A., Pongratz, J., Schleussner, C.-F., Seneviratne, S. I., Szopa, S., Thorne, P., Kovilakam,
2696 M. V. M., Majamäki, E., Jalkanen, J.-P., van Marle, M., Hoesly, R. M., Rohde, R., Schumacher, D., van der Werf, G., Vose,
2697 R., Zickfeld, K., Zhang, X., Masson-Delmotte, V., and Zhai, P.: Indicators of Global Climate Change 2023: annual update of

2698 key indicators of the state of the climate system and human influence, *Earth Syst. Sci. Data*, 16, 2625–2658,
2699 <https://doi.org/10.5194/essd-16-2625-2024>, 2024.

2700 Doney, S. C., Lima, I., Feely, R. A., Glover, D. M., Lindsay, K., Mahowald, N., Moore, J. K., and Wanninkhof, R.:
2701 Mechanisms governing interannual variability in upper-ocean inorganic carbon system and air–sea CO₂ fluxes: Physical
2702 climate and atmospheric dust, *Deep Sea Research Part II: Topical Studies in Oceanography*, 56, 640–655,
2703 <https://doi.org/10.1016/j.dsr2.2008.12.006>, 2009.

2704 Dong, Y., Bakker, D. C. E., Bell, T. G., Huang, B., Landschützer, P., Liss, P. S., and Yang, M.: Update on the Temperature
2705 Corrections of Global Air-Sea CO₂ Flux Estimates, *Glob. Biogeochem. Cycles*, 36, e2022GB007360,
2706 <https://doi.org/10.1029/2022GB007360>, 2022.

2707
2708 Dong, Y., Bakker, D. C. E., Bell, T. G., Yang, M., Landschützer, P., Hauck, J., Rödenbeck, C., Kitidis, V., Bushinsky, S. M.,
2709 and Liss, P. S. (2024). Direct observational evidence of strong CO₂ uptake in the Southern Ocean. *Science Advances*,
2710 10(30), eadn5781, <https://doi.org/10.1126/sciadv.adn5781>, 2024a.

2711
2712 Dong, Y., Bakker, D. C. E., and Landschützer, P.: Accuracy of ocean CO₂ uptake estimates at a risk by a reduction in the
2713 data collection. *Geophysical Research Letters*, 51, e2024GL108502, <https://doi.org/10.1029/2024GL108502>, 2024b.

2714
2715 Dorgeist, L., Schwingshackl, C., Bultan, S., and Pongratz, J.: A consistent budgeting of terrestrial carbon fluxes. *Nature*
2716 *Communications*, 15(1), 7426, <https://doi.org/10.1038/s41467-024-51126-x>, 2024.

2717
2718 Dou, X., Wang, Y., Ciais, P., Chevallier, F., Davis, S. J., Crippa, M., Janssens-Maenhout, G., Guizzardi, D., Solazzo, E.,
2719 Yan, F., Huo, D., Zheng, B., Zhu, B., Cui, D., Ke, P., Sun, T., Wang, H., Zhang, Q., Gentine, P., Deng, Z., and Liu, Z.: Near-
2720 real-time global gridded daily CO₂ emissions, *The Innovation*, 3, 100182, <https://doi.org/10.1016/j.xinn.2021.100182>, 2022.

2721 Edson, J. B., Jampana, V., Weller, R. A., Bigorre, S. P., Plueddemann, A. J., Fairall, C. W., Miller, S. D., Mahrt, L., Vickers,
2722 D., and Hershbach, H.: On the Exchange of Momentum over the Open Ocean, *J. Phys. Oceanogr.*, 43, 1589–1610,
2723 <https://doi.org/10.1175/JPO-D-12-0173.1>, 2013.

2724 EIA. Short-Term Energy Outlook: September 2023. U.S. Energy Information Administration [dataset]. Available at:
2725 <http://www.eia.gov/forecasts/steo/outlook.cfm>, last access: [21 January 2025](https://doi.org/10.1038/s41467-024-03147-w), 2023.

2726 Embury, O., Merchant, C.J., Good, S.A., Rayner, N.A., Hoyer, J.L., Atkinson, C., Block, T., Alerskans, E., Pearson, K.J.,
2727 Worsfold, M. and McCarroll, N. and Donlon, C.: Satellite-based time-series of sea-surface temperature since 1980 for
2728 climate applications. *Scientific Data*, 11(1), 326, <https://doi.org/10.1038/s41597-024-03147-w>, 2024.

2729 Erb, K.-H., Kastner, T., Luyssaert, S., Houghton, R. A., Kuemmerle, T., Olofsson, P., and Haberl, H.: Bias in the attribution
2730 of forest carbon sinks, *Nature Clim Change*, 3, 854–856, <https://doi.org/10.1038/nclimate2004>, 2013.

2731 Erb, K.-H., Kastner, T., Plutzer, C., Bais, A. L. S., Carvalhais, N., Fetzel, T., Gingrich, S., Haberl, H., Lauk, C.,
2732 Niedertscheider, M., Pongratz, J., Thurner, M., and Luyssaert, S.: Unexpectedly large impact of forest management and
2733 grazing on global vegetation biomass, *Nature*, 553, 73–76, <https://doi.org/10.1038/nature25138>, 2018.

Deleted: 28 October 2024

- 2735 Eskander, S. M. S. U. and Fankhauser, S.: Reduction in greenhouse gas emissions from national climate legislation, *Nat.*
2736 *Clim. Chang.*, 10, 750–756, <https://doi.org/10.1038/s41558-020-0831-z>, 2020.
- 2737 Etheridge, D. M., Steele, L. P., Langenfelds, R. L., Francey, R. J., Barnola, J.-M., and Morgan, V. I.: Natural and
2738 anthropogenic changes in atmospheric CO₂ over the last 1000 years from air in Antarctic ice and firn, *J. Geophys. Res.*,
2739 101, 4115–4128, <https://doi.org/10.1029/95JD03410>, 1996.
- 2740 Eyring, V., Bony, S., Meehl, G. A., Senior, C. A., Stevens, B., Stouffer, R. J., and Taylor, K. E.: Overview of the Coupled
2741 Model Intercomparison Project Phase 6 (CMIP6) experimental design and organization, *Geosci. Model Dev.*, 9, 1937–1958,
2742 <https://doi.org/10.5194/gmd-9-1937-2016>, 2016.
- 2743 FAO, Food and Agriculture Organization of the United Nations (FAO): Impact of the Ukraine-Russia conflict on global food
2744 security and related matters under the mandate of the Food and Agriculture Organization of the United Nations (FAO),
2745 Hundred and Seventieth Session of the Council, <https://www.fao.org/3/nj164en/nj164en.pdf>, last access: 21 January 2025,
2746 2023.
- 2747 [FAO: FAOSTAT Climate Change: Agrifood systems emissions. Emissions from Drained, available at](http://www.fao.org/faostat/en/#data/GV)
2748 <http://www.fao.org/faostat/en/#data/GV>, last access: 12 January 2025, 2023.
- 2749 Fay, A. R., Gregor, L., Landschützer, P., McKinley, G. A., Gruber, N., Gehlen, M., Iida, Y., Laruelle, G. G., Rödenbeck, C.,
2750 Roobaert, A., and Zeng, J.: SeaFlux: harmonization of air–sea CO₂ fluxes from surface pCO₂ data products using a
2751 standardized approach, *Earth System Science Data*, 13, 4693–4710, <https://doi.org/10.5194/essd-13-4693-2021>, 2021.
- 2752 Feng, L., Palmer, P. I., Bösch, H., and Dance, S.: Estimating surface CO₂ fluxes from space-borne CO₂ dry air mole fraction
2753 observations using an ensemble Kalman Filter, *Atmospheric Chem. Phys.*, 9, 2619–2633, [https://doi.org/10.5194/acp-9-](https://doi.org/10.5194/acp-9-2619-2009)
2754 2619-2009, 2009.
- 2755 Feng, L., Palmer, P. I., Parker, R. J., Deutscher, N. M., Feist, D. G., Kivi, R., Morino, I., and Sussmann, R.: Estimates of
2756 European uptake of CO₂ inferred from GOSAT XCO₂ retrievals: sensitivity to measurement bias inside and outside Europe,
2757 *Atmos. Chem. Phys.*, 16, 1289–1302, <https://doi.org/10.5194/acp-16-1289-2016>, 2016.
- 2758 Flanagan, D.: 2017 Minerals Yearbook: Copper [Advance Release], Tech. rep., U.S. Geological Survey,
2759 <https://pubs.usgs.gov/myb/vol1/2017/myb1-2017-copper.pdf>, 2021.
- 2760 Ford, D., Blannin, J., Watts, J., Watson, A., Landschützer, P., Jersild, A. and Shutler, J.: A comprehensive analysis of air-sea
2761 CO₂ flux uncertainties constructed from surface ocean data products, *Global Biogeochemical Cycles*, accepted, 2024.
- 2762 Friedlingstein, P., Houghton, R. A., Marland, G., Hackler, J., Boden, T. A., Conway, T. J., Canadell, J. G., Raupach, M. R.,
2763 Ciais, P., and Le Quéré, C.: Update on CO₂ emissions, *Nature Geosci*, 3, 811–812, <https://doi.org/10.1038/ngeo1022>, 2010.
- 2764 Friedlingstein, P., Andrew, R. M., Rogelj, J., Peters, G. P., Canadell, J. G., Knutti, R., Luderer, G., Raupach, M. R.,
2765 Schaeffer, M., van Vuuren, D. P., and Le Quéré, C.: Persistent growth of CO₂ emissions and implications for reaching
2766 climate targets, *Nature Geosci*, 7, 709–715, <https://doi.org/10.1038/ngeo2248>, 2014.
- 2767 Friedlingstein, P., Jones, M. W., O’Sullivan, M., Andrew, R. M., Hauck, J., Peters, G. P., Peters, W., Pongratz, J., Sitch, S.,
2768 Le Quéré, C., Bakker, D. C. E., Canadell, J. G., Ciais, P., Jackson, R. B., Anthoni, P., Barbero, L., Bastos, A., Bastrikov, V.,
2769 Becker, M., Bopp, L., Buitenhuis, E., Chandra, N., Chevallier, F., Chini, L. P., Currie, K. I., Feely, R. A., Gehlen, M.,

Deleted: 28 October 2024

Formatted: Subscript

2771 Gilfillan, D., Gkritzalis, T., Goll, D. S., Gruber, N., Gutekunst, S., Harris, I., Haverd, V., Houghton, R. A., Hurtt, G., Ilyina,
2772 T., Jain, A. K., Joetzier, E., Kaplan, J. O., Kato, E., Klein Goldewijk, K., Korsbakken, J. I., Landschützer, P., Lauvset, S. K.,
2773 Lefèvre, N., Lenton, A., Lienert, S., Lombardozi, D., Marland, G., McGuire, P. C., Melton, J. R., Metz, N., Munro, D. R.,
2774 Nabel, J. E. M. S., Nakaoka, S.-I., Neill, C., Omar, A. M., Ono, T., Pregon, A., Pierrot, D., Poulter, B., Rehder, G.,
2775 Resplandy, L., Robertson, E., Rödenbeck, C., Séférian, R., Schwinger, J., Smith, N., Tans, P. P., Tian, H., Tilbrook, B.,
2776 Tubiello, F. N., van der Werf, G. R., Wiltshire, A. J., and Zaehle, S.: Global Carbon Budget 2019, *Earth Syst. Sci. Data*, 11,
2777 1783–1838, <https://doi.org/10.5194/essd-11-1783-2019>, 2019.

2778 Friedlingstein, P., O’Sullivan, M., Jones, M. W., Andrew, R. M., Hauck, J., Olsen, A., Peters, G. P., Peters, W., Pongratz, J.,
2779 Sitch, S., Le Quéré, C., Canadell, J. G., Ciais, P., Jackson, R. B., Alin, S., Aragão, L. E. O. C., Armeth, A., Arora, V., Bates,
2780 N. R., Becker, M., Benoit-Cattin, A., Bittig, H. C., Bopp, L., Bultan, S., Chandra, N., Chevallier, F., Chini, L. P., Evans, W.,
2781 Florentie, L., Forster, P. M., Gasser, T., Gehlen, M., Gilfillan, D., Gkritzalis, T., Gregor, L., Gruber, N., Harris, I., Hartung,
2782 K., Haverd, V., Houghton, R. A., Ilyina, T., Jain, A. K., Joetzier, E., Kadono, K., Kato, E., Kitidis, V., Korsbakken, J. I.,
2783 Landschützer, P., Lefèvre, N., Lenton, A., Lienert, S., Liu, Z., Lombardozi, D., Marland, G., Metz, N., Munro, D. R.,
2784 Nabel, J. E. M. S., Nakaoka, S.-I., Niwa, Y., O’Brien, K., Ono, T., Palmer, P. I., Pierrot, D., Poulter, B., Resplandy, L.,
2785 Robertson, E., Rödenbeck, C., Schwinger, J., Séférian, R., Skjelvan, I., Smith, A. J. P., Sutton, A. J., Tanhua, T., Tans, P. P.,
2786 Tian, H., Tilbrook, B., van der Werf, G., Vuichard, N., Walker, A. P., Wanninkhof, R., Watson, A. J., Willis, D., Wiltshire,
2787 A. J., Yuan, W., Yue, X., and Zaehle, S.: Global Carbon Budget 2020, *Earth Syst. Sci. Data*, 12, 3269–3340,
2788 <https://doi.org/10.5194/essd-12-3269-2020>, 2020.

2789 Friedlingstein, P., Jones, M. W., O’Sullivan, M., Andrew, R. M., Bakker, D. C. E., Hauck, J., Le Quéré, C., Peters, G. P.,
2790 Peters, W., Pongratz, J., Sitch, S., Canadell, J. G., Ciais, P., Jackson, R. B., Alin, S. R., Anthoni, P., Bates, N. R., Becker, M.,
2791 Bellouin, N., Bopp, L., Chau, T. T. T., Chevallier, F., Chini, L. P., Cronin, M., Currie, K. I., Decharme, B., Djeutchouang, L.
2792 M., Dou, X., Evans, W., Feely, R. A., Feng, L., Gasser, T., Gilfillan, D., Gkritzalis, T., Grassi, G., Gregor, L., Gruber, N.,
2793 Gürses, Ö., Harris, I., Houghton, R. A., Hurtt, G. C., Iida, Y., Ilyina, T., Luijkx, I. T., Jain, A., Jones, S. D., Kato, E.,
2794 Kennedy, D., Klein Goldewijk, K., Knauer, J., Korsbakken, J. I., Körtzinger, A., Landschützer, P., Lauvset, S. K., Lefèvre,
2795 N., Lienert, S., Liu, J., Marland, G., McGuire, P. C., Melton, J. R., Munro, D. R., Nabel, J. E. M. S., Nakaoka, S.-I., Niwa,
2796 Y., Ono, T., Pierrot, D., Poulter, B., Rehder, G., Resplandy, L., Robertson, E., Rödenbeck, C., Rosan, T. M., Schwinger, J.,
2797 Schwingshackl, C., Séférian, R., Sutton, A. J., Sweeney, C., Tanhua, T., Tans, P. P., Tian, H., Tilbrook, B., Tubiello, F., van
2798 der Werf, G. R., Vuichard, N., Wada, C., Wanninkhof, R., Watson, A. J., Willis, D., Wiltshire, A. J., Yuan, W., Yue, C.,
2799 Yue, X., Zaehle, S., and Zeng, J.: Global Carbon Budget 2021, *Earth Syst. Sci. Data*, 14, 1917–2005,
2800 <https://doi.org/10.5194/essd-14-1917-2022>, 2022a.

2801 Friedlingstein, P., O’Sullivan, M., Jones, M. W., Andrew, R. M., Gregor, L., Hauck, J., Le Quéré, C., Luijkx, I. T., Olsen, A.,
2802 Peters, G. P., Peters, W., Pongratz, J., Schwingshackl, C., Sitch, S., Canadell, J. G., Ciais, P., Jackson, R. B., Alin, S. R.,
2803 Alkama, R., Armeth, A., Arora, V. K., Bates, N. R., Becker, M., Bellouin, N., Bittig, H. C., Bopp, L., Chevallier, F., Chini, L.
2804 P., Cronin, M., Evans, W., Falk, S., Feely, R. A., Gasser, T., Gehlen, M., Gkritzalis, T., Gloege, L., Grassi, G., Gruber, N.,
2805 Gürses, Ö., Harris, I., Hefner, M., Houghton, R. A., Hurtt, G. C., Iida, Y., Ilyina, T., Jain, A. K., Jersild, A., Kadono, K.,
2806 Kato, E., Kennedy, D., Klein Goldewijk, K., Knauer, J., Korsbakken, J. I., Landschützer, P., Lefèvre, N., Lindsay, K., Liu,
2807 J., Liu, Z., Marland, G., Mayot, N., McGrath, M. J., Metz, N., Monacci, N. M., Munro, D. R., Nakaoka, S., Niwa, Y.,
2808 O’Brien, K., Ono, T., Palmer, P. I., Pan, N., Pierrot, D., Pocock, K., Poulter, B., Resplandy, L., Robertson, E., Rödenbeck,
2809 C., Rodriguez, C., Rosan, T. M., Schwinger, J., Séférian, R., Shutler, J. D., Skjelvan, I., Steinhoff, T., Sun, Q., Sutton, A. J.,
2810 Sweeney, C., Takao, S., Tanhua, T., Tans, P. P., Tian, X., Tian, H., Tilbrook, B., Tsujino, H., Tubiello, F., van der Werf, G.
2811 R., Walker, A. P., Wanninkhof, R., Whitehead, C., Willstrand Wranne, A., Wright, R., Yuan, W., Yue, C., Yue, X., Zaehle,

2812 S., Zeng, J., and Zheng, B.: Global Carbon Budget 2022, *Earth Syst. Sci. Data*, 14, 4811–4900, [https://doi.org/10.5194/essd-](https://doi.org/10.5194/essd-14-4811-2022)
2813 14-4811-2022, 2022b.

2814

2815 Friedlingstein, P., O'Sullivan, M., Jones, M. W., Andrew, R. M., Bakker, D. C. E., Hauck, J., Landschützer, P., Le Quéré, C.,
2816 Luijkx, I. T., Peters, G. P., Peters, W., Pongratz, J., Schwingshackl, C., Sitch, S., Canadell, J. G., Ciais, P., Jackson, R. B.,
2817 Alin, S. R., Anthoni, P., Barbero, L., Bates, N. R., Becker, M., Bellouin, N., Decharme, B., Bopp, L., Brasika, I. B. M.,
2818 Cadule, P., Chamberlain, M. A., Chandra, N., Chau, T.-T.-T., Chevallier, F., Chini, L. P., Cronin, M., Dou, X., Enyo, K.,
2819 Evans, W., Falk, S., Feely, R. A., Feng, L., Ford, D. J., Gasser, T., Ghattas, J., Gkritzalis, T., Grassi, G., Gregor, L., Gruber,
2820 N., Gürses, Ö., Harris, I., Hefner, M., Heinke, J., Houghton, R. A., Hurtt, G. C., Iida, Y., Ilyina, T., Jacobson, A. R., Jain, A.
2821 K., Jarmiková, T., Jersild, A., Jiang, F., Jin, Z., Joos, F., Kato, E., Keeling, R. F., Kennedy, D., Klein Goldewijk, K., Knauer,
2822 J., Korsbakken, J. I., Körtzinger, A., Lan, X., Lefèvre, N., Li, H., Liu, J., Liu, Z., Ma, L., Marland, G., Mayot, N., McGuire,
2823 P. C., McKinley, G. A., Meyer, G., Morgan, E. J., Munro, D. R., Nakaoka, S., Niwa, Y., O'Brien, K. M., Olsen, A., Omar, A.
2824 M., Ono, T., Paulsen, M., Pierrot, D., Pocock, K., Poulter, B., Powis, C. M., Rehder, G., Resplandy, L., Robertson, E.,
2825 Rödenbeck, C., Rosan, T. M., Schwinger, J., Séférian, R., Smallman, T. L., Smith, S. M., Sospedra-Alfonso, R., Sun, Q.,
2826 Sutton, A. J., Sweeney, C., Takao, S., Tans, P. P., Tian, H., Tilbrook, B., Tsujino, H., Tubiello, F., van der Werf, G. R., van
2827 Ooijen, E., Wanninkhof, R., Watanabe, M., Wimart-Rousseau, C., Yang, D., Yang, X., Yuan, W., Yue, X., Zaehle, S., Zeng,
2828 J., and Zheng, B.: Global Carbon Budget 2023, *Earth Syst. Sci. Data*, 15, 5301–5369, [https://doi.org/10.5194/essd-15-5301-](https://doi.org/10.5194/essd-15-5301-2023)
2829 2023, 2023.

2830 Friedlingstein, P., O'Sullivan, M., Jones, M. W., Andrew, R. M., Hauck, J., Landschützer, P., Le Quéré, C., Li, H., Luijkx, I.
2831 T., Olsen, A., Peters, G. P., Peters, W., Pongratz, J., Schwingshackl, C., Sitch, S., Canadell, J. G., Ciais, P., Jackson, R. B.,
2832 Alin, S. R., Arneeth, A., Arora, V., Bates, N. R., Becker, M., Bellouin, N., Berghoff, C. F., Bittig, H. C., Bopp, L., Cadule, P.,
2833 Campbell, K., Chamberlain, M. A., Chandra, N., Chevallier, F., Chini, L. P., Colligan, T., Decayeux, J., Djeutchouang, L.
2834 M., Dou, X., Duran Rojas, C., Enyo, K., Evans, W., Fay, A. R., Feely, R. A., Ford, D. J., Foster, A., Gasser, T., Gehlen, M.,
2835 Gkritzalis, T., Grassi, G., Gregor, L., Gruber, N., Gürses, Ö., Harris, I., Hefner, M., Heinke, J., Hurtt, G. C., Iida, Y., Ilyina,
2836 T., Jacobson, A. R., Jain, A. K., Jarmiková, T., Jersild, A., Jiang, F., Jin, Z., Kato, E., Keeling, R. F., Klein Goldewijk, K.,
2837 Knauer, J., Korsbakken, J. I., Lauvset, S. K., Lefèvre, N., Liu, Z., Liu, J., Ma, L., Maksyutov, S., Marland, G., Mayot, N.,
2838 McGuire, P. C., Metzl, N., Monacci, N. M., Morgan, E. J., Nakaoka, S., Neill, C., Niwa, Y., Nützel, T., Olivier, L., Ono, T.,
2839 Palmer, P. I., Pierrot, D., Qin, Z., Resplandy, L., Roobaert, A., Rosan, T. M., Rödenbeck, C., Schwinger, J., Smallman, T. L.,
2840 Smith, S. M., Sospedra-Alfonso, R., Steinhoff, T., Sun, Q., Sutton, A. J., Séférian, R., Takao, S., Tatebe, H., Tian, H.,
2841 Tilbrook, B., Torres, O., Tourigny, E., Tsujino, H., Tubiello, F., van der Werf, G., Wanninkhof, R., Wang, X., Yang, D.,
2842 Yang, X., Yu, Z., Yuan, W., Yue, X., Zaehle, S., Zeng, N., Zeng, J.: Supplemental data of the Global Carbon Budget 2024,
2843 ICOS-ERIC Carbon Portal, <https://doi.org/10.18160/GCP-2024>, 2024.

2844 Ganzenmüller, R., Bultan, S., Winkler, K., Fuchs, R., Zabel, F., and Pongratz, J.: Land-use change emissions based on high-
2845 resolution activity data substantially lower than previously estimated, *Environ. Res. Lett.*, 17, 064050,
2846 <https://doi.org/10.1088/1748-9326/ac70d8>, 2022.

2847 Gasser, T., Crepin, L., Quilcaille, Y., Houghton, R. A., Ciais, P., and Obersteiner, M.: Historical CO₂ emissions from land
2848 use and land cover change and their uncertainty, *Biogeosciences*, 17, 4075–4101, <https://doi.org/10.5194/bg-17-4075-2020>,
2849 2020.

2850 Gaubert, B., Stephens, B. B., Basu, S., Chevallier, F., Deng, F., Kort, E. A., Patra, P. K., Peters, W., Rödenbeck, C., Saeki,
2851 T., Schimel, D., Van der Laan-Luijkx, I., Wofsy, S., and Yin, Y.: Global atmospheric CO₂ inverse models converging on

2852 neutral tropical land exchange, but disagreeing on fossil fuel and atmospheric growth rate, *Biogeosciences*, 16, 117–134,
2853 <https://doi.org/10.5194/bg-16-117-2019>, 2019.

2854 GCP: The Global Carbon Budget 2007, available at: <http://www.globalcarbonproject.org/carbonbudget/archive.htm>, last
2855 access: 21 January 2025, 2007.

2856 Giglio, L., Schroeder, W., and Justice, C. O.: The collection 6 MODIS active fire detection algorithm and fire products,
2857 *Remote Sensing of Environment*, 178, 31–41, <https://doi.org/10.1016/j.rse.2016.02.054>, 2016.

2858 Gloege, L., McKinley, G. A., Landschützer, P., Fay, A. R., Frölicher, T. L., Fyfe, J. C., Ilyina, T., Jones, S., Lovenduski, N.
2859 S., Rodgers, K. B., Schlunegger, S., and Takano, Y.: Quantifying Errors in Observationally Based Estimates of Ocean
2860 Carbon Sink Variability, *Global Biogeochem. Cy.*, 35, e2020GB006788, <https://doi.org/10.1029/2020GB006788>, 2021.

2861 Gloege, L., Yan, M., Zheng, T., and McKinley, G. A.: Improved Quantification of Ocean Carbon Uptake by Using Machine
2862 Learning to Merge Global Models and pCO₂ Data, *J. Adv. Model. Earth Syst.*, 14, e2021MS002620,
2863 <https://doi.org/10.1029/2021MS002620>, 2022.

2864 Golar, G., Malik, A., Muis, H., Herman, A., Nurudin, N., and Lukman, L.: The social-economic impact of COVID-19
2865 pandemic: implications for potential forest degradation, *Heliyon*, 6, e05354, <https://doi.org/10.1016/j.heliyon.2020.e05354>,
2866 2020.

2867 Goris, N., Tjiputra, J. F., Olsen, A., Schwinger, J., Lauvset, S. K., and Jeansson, E.: Constraining Projection-Based Estimates
2868 of the Future North Atlantic Carbon Uptake, *J. Clim.*, 31, 3959–3978, <https://doi.org/10.1175/JCLI-D-17-0564.1>, 2018.

2869 Grassi, G., House, J., Kurz, W. A., Cescatti, A., Houghton, R. A., Peters, G. P., Sanz, M. J., Viñas, R. A., Alkama, R.,
2870 Arneith, A., Bondeau, A., Dentener, F., Fader, M., Federici, S., Friedlingstein, P., Jain, A. K., Kato, E., Koven, C. D., Lee,
2871 D., Nabel, J. E. M. S., Nassikas, A. A., Perugini, L., Rossi, S., Sitch, S., Viovy, N., Wiltshire, A., and Zaehle, S.:
2872 Reconciling global-model estimates and country reporting of anthropogenic forest CO₂ sinks, *Nature Clim Change*, 8, 914–
2873 920, <https://doi.org/10.1038/s41558-018-0283-x>, 2018.

2874 Grassi, G., Stehfest, E., Rogelj, J., van Vuuren, D., Cescatti, A., House, J., Nabuurs, G.-J., Rossi, S., Alkama, R., Viñas, R.
2875 A., Calvin, K., Ceccherini, G., Federici, S., Fujimori, S., Gusti, M., Hasegawa, T., Havlik, P., Humpenöder, F., Korosuo, A.,
2876 Perugini, L., Tubiello, F. N., and Popp, A.: Critical adjustment of land mitigation pathways for assessing countries' climate
2877 progress, *Nat. Clim. Chang.*, 11, 425–434, <https://doi.org/10.1038/s41558-021-01033-6>, 2021.

2878 Grassi, G., Schwingshackl, C., Gasser, T., Houghton, R. A., Sitch, S., Canadell, J. G., Cescatti, A., Ciais, P., Federici, S.,
2879 Friedlingstein, P., Kurz, W. A., Sanz Sanchez, M. J., Abad Viñas, R., Alkama, R., Bultan, S., Ceccherini, G., Falk, S., Kato,
2880 E., Kennedy, D., Knauer, J., Korosuo, A., Melo, J., McGrath, M. J., Nabel, J. E. M. S., Poulter, B., Romanovskaya, A. A.,
2881 Rossi, S., Tian, H., Walker, A. P., Yuan, W., Yue, X., and Pongratz, J.: Harmonising the land-use flux estimates of global
2882 models and national inventories for 2000–2020, *Earth Syst. Sci. Data*, 15, 1093–1114, [https://doi.org/10.5194/essd-15-1093-](https://doi.org/10.5194/essd-15-1093-2023)
2883 2023, 2023.

2884 Gregor, L., Lebehot, A. D., Kok, S., and Scheel Monteiro, P. M.: A comparative assessment of the uncertainties of global
2885 surface ocean CO₂ estimates using a machine-learning ensemble (CSIR-ML6 version 2019a)–have we hit the
2886 wall?. *Geoscientific Model Development*, 12(12), 5113–5136, <https://doi.org/10.5194/gmd-12-5113-2019>, 2019.

Deleted: 28 October 2024

- 2888 Gregor, L., Shutler, J., and Gruber, N.: High-resolution variability of the ocean carbon sink. *Global Biogeochemical Cycles*,
2889 38(8), e2024GB008127, <https://doi.org/10.1029/2024GB008127>, 2024.
- 2890 Gruber, N., Bakker, D. C. E., DeVries, T., Gregor, L., Hauck, J., Landschützer, P., McKinley, G. A., and Müller, J. D.:
2891 Trends and variability in the ocean carbon sink. *Nat. Rev. Earth Environ.*, 4, 119–134, <https://doi.org/10.1038/s43017-022->
2892 00381-x, 2023.
- 2893 Gruber, N., Clement, D., Carter, B. R., Feely, R. A., van Heuven, S., Hoppema, M., Ishii, M., Key, R. M., Kozyr, A.,
2894 Lauvset, S. K., Lo Monaco, C., Mathis, J. T., Murata, A., Olsen, A., Perez, F. F., Sabine, C. L., Tanhua, T., and Wanninkhof,
2895 R.: The oceanic sink for anthropogenic CO₂ from 1994 to 2007, 363, 1193–1199, <https://doi.org/10.1126/science.aau5153>,
2896 2019.
- 2897 Guan, D., Liu, Z., Geng, Y., Lindner, S., and Hubacek, K.: The gigatonne gap in China’s carbon dioxide inventories, *Nature*
2898 *Clim Change*, 2, 672–675, <https://doi.org/10.1038/nclimate1560>, 2012.
- 2899 Gulev, S. K., Thorne, P. W., Ahn, J., Dentener, F. J., Domingues, C. M., Gerland, S., Gong, D. S., Kaufman, S., Nnamchi,
2900 H. C., Quaas, J., Rivera, J. A., Sathyendranath, S., Smith, S. L., Trewin, B., von Shuckmann, K., and Vose, R. S.: Changing
2901 State of the Climate System. In: *Climate Change 2021: The Physical Science Basis. Contribution of Working Group I to the*
2902 *Sixth Assessment Report of the Intergovernmental Panel on Climate Change* [Masson-Delmotte, V., Zhai, P., Pirani, A.,
2903 Connors, S. L., Péan, C., Berger, S., Caud, N., Chen, Y., Goldfarb, L., Gomis, M. I., Huang, M., Leitzell, K., Lonnoy, E.,
2904 Matthews, J.B.R., Maycock, T.K., Waterfield, T., Yelekçi, O., Yu, R. and Zhou, B. (eds.)]. Cambridge University Press,
2905 Cambridge, United Kingdom and New York, NY, USA, pp. 287–422, <https://doi.org/10.1017/9781009157896.004>, 2021.
- 2906 Guo, R., Wang, J., Bing, L., Tong, D., Ciais, P., Davis, S. J., Andrew, R. M., Xi, F., and Liu, Z.: Global CO₂ uptake by
2907 cement from 1930 to 2019, 13, 1791–1805, <https://doi.org/10.5194/essd-13-1791-2021>, 2021.
- 2908 Gürses, Ö., Oziel, L., Karakuş, O., Sidorenko, D., Völker, C., Ye, Y., Zeising, M., Butzin, M., and Hauck, J.: Ocean
2909 biogeochemistry in the coupled ocean–sea ice–biogeochemistry model FESOM2.1–REcoM3, *Geosci. Model Dev.*, 16,
2910 4883–4936, <https://doi.org/10.5194/gmd-16-4883-2023>, 2023.
- 2911 Gütschow, J., Jeffery, M. L., Gieseke, R., Gebel, R., Stevens, D., Krapp, M., and Rocha, M.: The PRIMAP-hist national
2912 historical emissions time series, 8, 571–603, <https://doi.org/10.5194/essd-8-571-2016>, 2016.
- 2913 Gütschow, J., Busch, D. and Pflüger, M.: The PRIMAP-hist national historical emissions time series (1750-2023) v2.6,
2914 Zenodo [dataset], <https://doi.org/10.5281/zenodo.13752654>, 2023.
- 2915 Hall, B. D., Crotwell, A. M., Kitzis, D. R., Mefford, T., Miller, B. R., Schibig, M. F., and Tans, P. P.: Revision of the World
2916 Meteorological Organization Global Atmosphere Watch (WMO/GAW) CO₂ calibration scale, 14, 3015–3032,
2917 <https://doi.org/10.5194/amt-14-3015-2021>, 2021.
- 2918 Hansis, E., Davis, S. J., and Pongratz, J.: Relevance of methodological choices for accounting of land use change carbon
2919 fluxes, *Global Biogeochem. Cycles*, 29, 1230–1246, <https://doi.org/10.1002/2014GB004997>, 2015.
- 2920 Hauck, J., Nissen, C., Landschützer, P., Rödenbeck, C., Bushinsky, S., and Olsen, A.: Sparse observations induce large
2921 biases in estimates of the global ocean CO₂ sink: an ocean model subsampling experiment, *Philos. Trans. R. Soc. Math.*
2922 *Phys. Eng. Sci.*, 381, 20220063, <https://doi.org/10.1098/rsta.2022.0063>, 2023a.

2923

2924 Hauck, J., Gregor, L., Nissen, C., Patara, L., Hague, M., Mongwe, P., Bushinsky, S., Doney, S. C., Gruber, N., Le Quéré, C.,
 2925 Manizza, M., Mazloff, M., Monteiro, P. M. S., and Terhaar, J.: The Southern Ocean Carbon Cycle 1985–2018: Mean,
 2926 Seasonal Cycle, Trends, and Storage. *Global Biogeochemical Cycles*, 37(11), e2023GB007848,
 2927 <https://doi.org/10.1029/2023GB007848>, 2023b.

2928 Hauck, J., Zeising, M., Le Quéré, C., Gruber, N., Bakker, D. C. E., Bopp, L., Chau, T. T. T., Gürses, Ö., Ilyina, T.,
 2929 Landschützer, P., Lenton, A., Resplandy, L., Rödenbeck, C., Schwinger, J., and Séférian, R.: Consistency and Challenges in
 2930 the Ocean Carbon Sink Estimate for the Global Carbon Budget, *Front. Mar. Sci.*, 7, 571720,
 2931 <https://doi.org/10.3389/fmars.2020.571720>, 2020.

2932 Haverd, V., Smith, B., Nieradzki, L., Briggs, P. R., Woodgate, W., Trudinger, C. M., Canadell, J. G., and Cuntz, M.: A new
 2933 version of the CABLE land surface model (Subversion revision r4601) incorporating land use and land cover change, woody
 2934 vegetation demography, and a novel optimisation-based approach to plant coordination of photosynthesis, *Geosci. Model
 2935 Dev.*, 11, 2995–3026, <https://doi.org/10.5194/gmd-11-2995-2018>, 2018.

2936 Heinke, J., Rolinski, S., and Müller, C.: Modelling the role of livestock grazing in C and N cycling in grasslands with
 2937 LPJmL5.0-grazing, *Geosci. Model Dev.*, 16, 2455–2475, <https://doi.org/10.5194/gmd-16-2455-2023>, 2023.

2938 Hefner, M., Marland, G., Boden, T., Andres, R.: Global, Regional, and National Fossil-Fuel CO₂ Emissions: 1751-2020
 2939 CDIAC-FF [dataset], available at: <https://energy.appstate.edu/cdiac-appstate/data-products>, last access: [21 January 2025](#),
 2940 2023.

2941 Hefner, M.; Marland G; (2023): Global, Regional, and National Fossil-Fuel CO₂ Emissions: 1751-2020 CDIAC-FF,
 2942 Research Institute for Environment, Energy, and Economics, Appalachian State University,
 2943 <https://rieec.appstate.edu/projects-programs/cdiac>

2944 Hickler, T., Smith, B., Prentice, I. C., Mjöfors, K., Miller, P., Arneth, A., and Sykes, M. T.: CO₂ fertilization in temperate
 2945 FACE experiments not representative of boreal and tropical forests, *Glob. Change Biol.*, 14, 1531–1542,
 2946 <https://doi.org/10.1111/j.1365-2486.2008.01598.x>, 2008.

2947 Hoesly, R. M., Smith, S. J., Feng, L., Klimont, Z., Janssens-Maenhout, G., Pitkanen, T., Seibert, J. J., Vu, L., Andres, R. J.,
 2948 Bolt, R. M., Bond, T. C., Dawidowski, L., Kholod, N., Kurokawa, J., Li, M., Liu, L., Lu, Z., Moura, M. C. P., O'Rourke, P.
 2949 R., and Zhang, Q.: Historical (1750–2014) anthropogenic emissions of reactive gases and aerosols from the Community
 2950 Emissions Data System (CEDS), *Geosci. Model Dev.*, 11, 369–408, <https://doi.org/10.5194/gmd-11-369-2018>, 2018.

2951 Hoesly, R., Smith, S. J., Prime, N., Ahsan, H., Suchyta, H., O'Rourke, P., Crippa, M., Klimont, Z., Guizzardi, D., Behrendt,
 2952 J., Feng, L., Harkins, C., McDonald, B., Mott, A., McDuffie, A., Nicholson, M. and Wang, S.: CEDS v_2024_07_08
 2953 Release Emission Data, Zenodo [dataset], <https://doi.org/10.5281/zenodo.12803196>, 2024.

2954 Hong, C., Burney, J. A., Pongratz, J., Nabel, J. E. M. S., Mueller, N. D., Jackson, R. B., and Davis, S. J.: Global and regional
 2955 drivers of land-use emissions in 1961–2017, *Nature*, 589, 554–561, <https://doi.org/10.1038/s41586-020-03138-y>, 2021.

2956 Holding, T., Ashton, I. G., Shutler, J. D., Land, P. E., Nightingale, P. D., Rees, A. P., Brown, I., Piolle, J.-F., Kock, A.,
 2957 Bange, H. W., Woolf, D. K., Goddijn-Murphy, L., Pereira, R., Paul, F., Girard-Ardhuin, F., Chapron, B., Rehder, G.,

Deleted: 28 October 2024

- 2959 Ardhuin, F., and Donlon, C. J.: The FluxEngine air–sea gas flux toolbox: simplified interface and extensions for in situ
2960 analyses and multiple sparingly soluble gases, *Ocean Sci.*, 15, 1707–1728, <https://doi.org/10.5194/os-15-1707-2019>, 2019.
- 2961 Houghton, R. A. and Castanho, A.: Annual emissions of carbon from land use, land-use change, and forestry from 1850 to
2962 2020, *Earth Syst. Sci. Data*, 15, 2025–2054, <https://doi.org/10.5194/essd-15-2025-2023>, 2023.
- 2963 Houghton, R. A., House, J. I., Pongratz, J., van der Werf, G. R., DeFries, R. S., Hansen, M. C., Le Quéré, C., and
2964 Ramankutty, N.: Carbon emissions from land use and land-cover change, *Biogeosciences*, 9, 5125–5142,
2965 <https://doi.org/10.5194/bg-9-5125-2012>, 2012.
- 2966 Huang, B., Thorne, P. W., Banzon, V. F., Boyer, T., Chepurin, G., Lawrimore, J. H., Menne, M. J., Smith, T. M., Vose, R.
2967 S., and Zhang, H.-M.: NOAA Extended Reconstructed Sea Surface Temperature (ERSST), Version 5,
2968 <https://doi.org/10.7289/V5T72FNM>, 2017.
- 2969 Hubau, W., Lewis, S.L., Phillips, O.L., Affum-Baffoe, K., Beekman, H., Cuní-Sanchez, A., Daniels, A.K., Ewango, C.E.N.,
2970 Fauset, S., Mukinzi, J.M., Sheil, D., Sonké, B., Sullivan, M.J.P., Sunderland, T.C.H., Taedoumg, H., Thomas, S.C., White,
2971 L.J.T., Abernethy, K.A., Adu-Bredu, S., Amani, C.A., Baker, T.R., Banin, L.F., Baya, F., Begne, S.K., Bennett, A.C.,
2972 Benedet, F., Bitariho, R., Bocko, Y.E., Boeckx, P., Boundja, P., Brienen, R.J.W., Brncic, T., Chezeaux, E., Chuyong, G.B.,
2973 Clark, C.J., Collins, M., Comiskey, J.A., Coomes, D.A., Dargie, G.C., de Haulleville, T., Kamdem, M.N.D., Doucet, J.-L.,
2974 Esquivel-Muelbert, A., Feldpausch, T.R., Fofanah, A., Folli, E.G., Gilpin, M., Gloor, E., Gonmadje, C., Gourlet-Fleury, S.,
2975 Hall, J.S., Hamilton, A.C., Harris, D.J., Hart, T.B., Hockemba, M.B.N., Hladik, A., Ifo, S.A., Jeffery, K.J., Jucker, T.,
2976 Yakusu, E.K., Kearsley, E., Kenfack, D., Koch, A., Leal, M.E., Levesley, A., Lindsell, J.A., Lisingo, J., Lopez-Gonzalez, G.,
2977 Lovett, J.C., Makana, J.-R., Malhi, Y., Marshall, A.R., Martin, J., Martin, E.H., Mbayu, F.M., Medjibe, V.P., Mihindou, V.,
2978 Mitchard, E.T.A., Moore, S., Munishi, P.K.T., Bengone, N.N., Ojo, L., Ondo, F.E., Peh, K.S.-H., Pickavance, G.C., Poulsen,
2979 A.D., Poulsen, J.R., Qie, L., Reitsma, J., Rovero, F., Swaine, M.D., Talbot, J., Taplin, J., Taylor, D.M., Thomas, D.W.,
2980 Toirambe, B., Mukendi, J.T., Tuagben, D., Umunay, P.M., van der Heijden, G.M.F., Verbeeck, H., Vleminckx, J., Willcock,
2981 S., Wöll, H., Woods, J.T., Zemagho, L.: Asynchronous carbon sink saturation in African and Amazonian tropical forests,
2982 *Nature*, 579, 80–87, <https://doi.org/10.1038/s41586-020-2035-0>, 2020.
- 2983 Humphrey, V., Zscheischler, J., Ciais, P., Gudmundsson, L., Sitch, S., and Seneviratne, S. I.: Sensitivity of atmospheric CO₂
2984 growth rate to observed changes in terrestrial water storage, *Nature*, 560, 628–631, [https://doi.org/10.1038/s41586-018-](https://doi.org/10.1038/s41586-018-0424-4)
2985 0424-4, 2018.
- 2986 Humphrey, V., Berg, A., Ciais, P., Gentile, P., Jung, M., Reichstein, M., Seneviratne, S. I., and Frankenberg, C.: Soil
2987 moisture–atmosphere feedback dominates land carbon uptake variability, *Nature*, 592, 65–69,
2988 <https://doi.org/10.1038/s41586-021-03325-5>, 2021.
- 2989 Huntzinger, D. N., Michalak, A. M., Schwalm, C., Ciais, P., King, A. W., Fang, Y., Schaefer, K., Wei, Y., Cook, R. B.,
2990 Fisher, J. B., Hayes, D., Huang, M., Ito, A., Jain, A. K., Lei, H., Lu, C., Maignan, F., Mao, J., Parazoo, N., Peng, S., Poulter,
2991 B., Ricciuto, D., Shi, X., Tian, H., Wang, W., Zeng, N., and Zhao, F.: Uncertainty in the response of terrestrial carbon sink to
2992 environmental drivers undermines carbon-climate feedback predictions, *Sci Rep*, 7, 4765, [https://doi.org/10.1038/s41598-](https://doi.org/10.1038/s41598-017-03818-2)
2993 017-03818-2, 2017.

2994 Iida, Y., Takatani, Y., Kojima, A., and Ishii, M.: Global trends of ocean CO₂ sink and ocean acidification: an observation-
2995 based reconstruction of surface ocean inorganic carbon variables, *J Oceanogr*, 77, 323–358, [https://doi.org/10.1007/s10872-](https://doi.org/10.1007/s10872-2996)
3000 020-00571-5, 2021.

2997 Ilyina, T., Li, H., Spring, A., Müller, W. A., Bopp, L., Chikamoto, M. O., Danabasoglu, G., Dobrynin, M., Dunne, J.,
2998 Fransner, F., Friedlingstein, P., Lee, W., Lovenduski, N. S., Merryfield, W. J., Mignot, J., Park, J. Y., Séférian, R., Sospedra-
2999 Alfonso, R., Watanabe, M., and Yeager, S.: Predictable Variations of the Carbon Sinks and Atmospheric CO₂ Growth in a
3000 Multi-Model Framework, *Geophys. Res. Lett.*, 48, e2020GL090695, <https://doi.org/10.1029/2020GL090695>, 2021.

3001 IMF: International Monetary Fund: World Economic Outlook, available at: <http://www.imf.org>, last access: [21 January](#)
3002 [2025](#), 2024.

3003 Instituto Nacional de Pesquisas Espaciais (INPE): Portal TerraBrasilis, available at: [http://terrabrasilis.dpi.inpe.br/en/home-](http://terrabrasilis.dpi.inpe.br/en/home-3004)
3004 [page/](#), last access: [21 January 2025](#).

3005 Jto, A. and Inatomi, M.: Use of a process-based model for assessing the methane budgets of global terrestrial ecosystems and
3006 evaluation of uncertainty, 9, 759–773, <https://doi.org/10.5194/bg-9-759-2012>, 2012.

3007 Jackson, R. B., Canadell, J. G., Le Quéré, C., Andrew, R. M., Korsbakken, J. I., Peters, G. P., and Nakićenovic, N.:
3008 Reaching peak emissions, *Nature Clim Change*, 6, 7–10, <https://doi.org/10.1038/nclimate2892>, 2016.

3009 Jackson, R. B., Le Quéré, C., Andrew, R. M., Canadell, J. G., Korsbakken, J. I., Liu, Z., Peters, G. P., and Zheng, B.: Global
3010 energy growth is outpacing decarbonization, *Environ. Res. Lett.*, 13, 120401, <https://doi.org/10.1088/1748-9326/aaf303>,
3011 2018.

3012 Jackson, R. B., Friedlingstein, P., Andrew, R. M., Canadell, J. G., Le Quéré, C., and Peters, G. P.: Persistent fossil fuel
3013 growth threatens the Paris Agreement and planetary health, *Environ. Res. Lett.*, 14, 121001, [https://doi.org/10.1088/1748-](https://doi.org/10.1088/1748-3014)
3014 9326/ab57b3, 2019.

3015 Jackson, R. B., Friedlingstein, P., Quéré, C. L., Abernethy, S., Andrew, R. M., Canadell, J. G., Ciais, P., Davis, S. J., Deng,
3016 Z., Liu, Z., Korsbakken, J. I., and Peters, G. P.: Global fossil carbon emissions rebound near pre-COVID-19 levels, *Environ.*
3017 *Res. Lett.*, 17, 031001, <https://doi.org/10.1088/1748-9326/ac55b6>, 2022.

3018 Jacobson, A. R., Schuldt, K. N., Tans, P., Andrews, A., Miller, J. B., Oda, T., Basu, S., Mund, J., Weir, B., Ott, L., Aalto, T.,
3019 Abshire, J. B., Aikin, K., Aoki, S., Apadula, F., Arnold, S., Baier, B., Bartyzel, J., Beyersdorf, A., Biermann, T., Biraud, S.
3020 C., Boenisch, H., Brailsford, G., Brand, W. A., Chen, G., Chen, H., Chmura, L., Clark, S., Colomb, A., Commane, R., Conil,
3021 S., Couret, C., Cox, A., Cristofanelli, P., Cuevas, E., Curcoll, R., Daube, B., Davis, K. J., De Wekker, S., Della Coletta, J.,
3022 Delmotte, M., DiGangi, E., DiGangi, J. P., di Sarra, A. G., Dlugokencky, E., Elkins, J. W., Emmenegger, L., Fang, S.,
3023 Fischer, M. L., Forster, G., Frumau, A., Galkowski, M., Gatti, L. V., Gehrlein, T., Gerbig, C., Gheusi, F., Gloor, E., Gomez-
3024 Trueba, V., Goto, D., Griffis, T., Hammer, S., Hanson, C., Haszpra, L., Hatakka, J., Heimann, M., Heliasz, M., Hensen, A.,
3025 Hermansen, O., Hintsa, E., Holst, J., Ivakhov, V., Jaffe, D. A., Jordan, A., Joubert, W., Karion, A., Kawa, S. R., Kazan, V.,
3026 Keeling, R. F., Keronen, P., Kneuer, T., Kolari, P., Kominková, K., Kort, E., Kozlova, E., Krummel, P., Kubistin, D.,
3027 Labuschagne, C., Lam, D. H. Y., Lan, X., Langenfelds, R. L., Laurent, O., Laurila, T., Lauvaux, T., Lavric, J., Law, B. E.,
3028 Lee, J., Lee, O. S. M., Lehner, I., Lehtinen, K., Leppert, R., Leskinen, A., Leuenberger, M., Levin, I., Levula, J., Lin, J.,
3029 Lindauer, M., Loh, Z., Lopez, M., Luijkx, I. T., Lunder, C. R., Machida, T., Mammarella, I., Manca, G., Manning, A.,

Deleted: 28 October

Deleted: , 2023

Deleted: 28 October 2024

Deleted: IPCC: Annex II: Glossary [Möller, V, J.B.R. Matthews, R. van Diemen, C. Méndez, S. Semenov, J.S. Fuglestedt, A. Reisinger (eds.)]. In: *Climate Change 2022: Impacts, Adaptation, and Vulnerability. Contribution of Working Group II to the Sixth Assessment Report of the Intergovernmental Panel on Climate Change* [H.-O. Pörtner, D.C. Roberts, M. Tignor, E.S. Poloczanska, K. Mintenbeck, A. Alegria, M. Craig, S. Langsdorf, S. Löschke, V. Möller, A. Okem, B. Rama (eds.)], in: *Climate Change 2022 – Impacts, Adaptation and Vulnerability: Working Group II Contribution to the Sixth Assessment Report of the Intergovernmental Panel on Climate Change* [Möller, V, J.B.R. Matthews, R. van Diemen, C. Méndez, S. Semenov, J.S. Fuglestedt, A. Reisinger (eds.)], Cambridge University Press, Cambridge, UK and New York, NY, 2897–2930, <https://doi.org/10.1017/9781009325844.029>, 2023.

3049 Manning, A., Marek, M. V., Martin, M. Y., Matsueda, H., McKain, K., Meijer, H., Meinhardt, F., Merchant, L.,
3050 Mihalopoulos, N., Miles, N. L., Miller, C. E., Mitchell, L., Mölder, M., Montzka, S., Moore, F., Moossen, H., Morgan, E.,
3051 Morgui, J.-A., Morimoto, S., Müller-Williams, J., Munger, J. W., Munro, D., Myhre, C. L., Nakaoka, S.-I., Necki, J.,
3052 Newman, S., Nichol, S., Niwa, Y., Obersteiner, F., O'Doherty, S., Paplawsky, B., Peischl, J., Peltola, O., Piacentino, S.,
3053 Pichon, J.-M., Pickers, P., Piper, S., Pitt, J., Plass-Dülmer, C., Platt, S. M., Prinzivalli, S., Ramonet, M., Ramos, R., Reyes-
3054 Sanchez, E., Richardson, S. J., Riris, H., Rivas, P. P., Ryerson, T., Saito, K., Sargent, M., Sasakawa, M., Scheeren, B.,
3055 Schuck, T., Schumacher, M., Seifert, T., Sha, M. K., Shepson, P., Shook, M., Sloop, C. D., Smith, P., Stanley, K.,
3056 Steinbacher, M., Stephens, B., Sweeney, C., Thoning, K., Timas, H., Torn, M., Tørseth, K., Trisolino, P., Turnbull, J., van
3057 den Bulk, P., van Dinter, D., Vermeulen, A., Viner, B., Vitkova, G., Walker, S., Watson, A., Wofsy, S. C., Worsley, J.,
3058 Worthy, D., Young, D., Zaehle, S., Zahn, A., and Zimnoch, M.: CarbonTracker CT2022, NOAA GML [dataset],
3059 <https://doi.org/10.25925/Z1GJ-3254>, 2023a.

3060 Jacobson, A. R., Schuldt, K. N., Tans, P., Andrews, A., Miller, J. B., Oda, T., Basu, S., Mund, J., Weir, B., Ott, L., Aalto, T.,
3061 Abshire, J. B., Aikin, K., Aoki, S., Apadula, F., Arnold, S., Baier, B., Bartyzel, J., Beyersdorf, A., Biermann, T., Biraud, S.
3062 C., Boenisch, H., Brailsford, G., Brand, W. A., Chen, G., Chen, H., Chmura, L., Clark, S., Colomb, A., Commane, R., Conil,
3063 S., Couret, C., Cox, A., Cristofanelli, P., Cuevas, E., Curcoll, R., Daube, B., Davis, K. J., De Wekker, S., Della Coletta, J.,
3064 Delmotte, M., DiGangi, E., DiGangi, J. P., di Sarra, A. G., Dlugokencky, E., Elkins, J. W., Emmenegger, L., Fang, S.,
3065 Fischer, M. L., Forster, G., Frumau, A., Galkowski, M., Gatti, L. V., Gehrlein, T., Gerbig, C., Gheusi, F., Gloor, E., Gomez-
3066 Trueba, V., Goto, D., Griffiths, T., Hammer, S., Hanson, C., Haszpra, L., Hatakka, J., Heimann, M., Heliasz, M., Hensen, A.,
3067 Hermansen, O., Hints, E., Holst, J., Ivakhov, V., Jaffé, D. A., Jordan, A., Joubert, W., Karion, A., Kawa, S. R., Kazan, V.,
3068 Keeling, R. F., Keronen, P., Kneuer, T., Kolari, P., Komínková, K., Kort, E., Kozlova, E., Krummel, P., Kubistin, D.,
3069 Labuschagne, C., Lam, D. H. Y., Lan, X., Langenfelds, R. L., Laurent, O., Laurila, T., Lauvaux, T., Lavric, J., Law, B. E.,
3070 Lee, J., Lee, O. S. M., Lehner, I., Lehtinen, K., Leppert, R., Leskinen, A., Leuenberger, M., Levin, I., Levula, J., Lin, J.,
3071 Lindauer, M., Loh, Z., Lopez, M., Luijkx, I. T., Lunder, C. R., Machida, T., Mammarella, I., Manca, G., Manning, A.,
3072 Manning, A., Marek, M. V., Martin, M. Y., Matsueda, H., McKain, K., Meijer, H., Meinhardt, F., Merchant, L.,
3073 Mihalopoulos, N., Miles, N. L., Miller, C. E., Mitchell, L., Mölder, M., Montzka, S., Moore, F., Moossen, H., Morgan, E.,
3074 Morgui, J.-A., Morimoto, S., Müller-Williams, J., Munger, J. W., Munro, D., Myhre, C. L., Nakaoka, S.-I., Necki, J.,
3075 Newman, S., Nichol, S., Niwa, Y., Obersteiner, F., O'Doherty, S., Paplawsky, B., Peischl, J., Peltola, O., Piacentino, S.,
3076 Pichon, J.-M., Pickers, P., Piper, S., Pitt, J., Plass-Dülmer, C., Platt, S. M., Prinzivalli, S., Ramonet, M., Ramos, R., Reyes-
3077 Sanchez, E., Richardson, S. J., Riris, H., Rivas, P. P., Ryerson, T., Saito, K., Sargent, M., Sasakawa, M., Scheeren, B.,
3078 Schuck, T., Schumacher, M., Seifert, T., Sha, M. K., Shepson, P., Shook, M., Sloop, C. D., Smith, P., Stanley, K.,
3079 Steinbacher, M., Stephens, B., Sweeney, C., Thoning, K., Timas, H., Torn, M., Tørseth, K., Trisolino, P., Turnbull, J., van
3080 den Bulk, P., van Dinter, D., Vermeulen, A., Viner, B., Vitkova, G., Walker, S., Watson, A., Wofsy, S. C., Worsley, J.,
3081 Worthy, D., Young, D., Zaehle, S., Zahn, A., and Zimnoch, M.: CarbonTracker CT-NRT.v2023-3, NOAA GML [dataset],
3082 <https://doi.org/10.25925/7TAF-J322>, 2023b.

3083 Jain, P., Barber, Q. E., Taylor, S. W., Whitman, E., Castellanos Acuna, D., Boulanger, Y., Chavardès, R. D., Chen, J.,
3084 Englefield, P., Flannigan, M., Girardin, M. P., Hanes, C. C., Little, J., Morrison, K., Skakun, R. S., Thompson, D. K., Wang,
3085 X., Parisien, M.-A.: Drivers and Impacts of the Record-Breaking 2023 Wildfire Season in Canada. *Nature Communications*,
3086 15(1), p.6764, <https://doi.org/10.1038/s41467-024-51154-7>, 2024.

3087 Janssens-Maenhout, G., Crippa, M., Guizzardi, D., Muntean, M., Schaaf, E., Dentener, F., Bergamaschi, P., Pagliari, V.,
3088 Olivier, J. G. J., Peters, J. A. H. W., van Aardenne, J. A., Monni, S., Doering, U., Petrescu, A. M. R., Solazzo, E., and

3089 Oreggioni, G. D.: EDGAR v4.3.2 Global Atlas of the three major greenhouse gas emissions for the period 1970–2012, *Earth*
3090 *Syst. Sci. Data*, 11, 959–1002, <https://doi.org/10.5194/essd-11-959-2019>, 2019.

3091 Jean-Michel, L., Eric, G., Romain, B.-B., Gilles, G., Angélique, M., Marie, D., Clément, B., Mathieu, H., Olivier, L. G.,
3092 Charly, R., Tony, C., Charles-Emmanuel, T., Florent, G., Giovanni, R., Mounir, B., Yann, D., and Pierre-Yves, L. T.: The
3093 Copernicus Global 1/12° Oceanic and Sea Ice GLORYS12 Reanalysis, *Front. Earth Sci.*, 9, 2021.

3094 Jiang, F., Ju, W., He, W., Wu, M., Wang, H., Wang, J., Jia, M., Feng, S., Zhang, L., and Chen, J. M.: A 10-year global
3095 monthly averaged terrestrial net ecosystem exchange dataset inferred from the ACOS GOSAT v9 XCO₂ retrievals
3096 (GCAS2021), *Earth Syst. Sci. Data*, 14, 3013–3037, <https://doi.org/10.5194/essd-14-3013-2022>, 2022.

3097 Jiang, F., Wang, H., Chen, J. M., Ju, W., Tian, X., Feng, S., Li, G., Chen, Z., Zhang, S., Lu, X., Liu, J., Wang, H., Wang, J.,
3098 He, W., and Wu, M.: Regional CO₂ fluxes from 2010 to 2015 inferred from GOSAT XCO₂ retrievals using a new version of
3099 the Global Carbon Assimilation System, *Atmospheric Chem. Phys.*, 21, 1963–1985, [https://doi.org/10.5194/acp-21-1963-](https://doi.org/10.5194/acp-21-1963-2021)
3100 2021, 2021.

3101
3102 Jin, Y., Keeling, R. F., Stephens, B. B., Long, M. C., Patra, P. K., Rödenbeck, C., Morgan, E. J., Kort, E. A., and Sweeney,
3103 C.: Improved atmospheric constraints on Southern Ocean CO₂ exchange. *Proceedings of the National Academy of*
3104 *Sciences*, 121(6), e2309333121, <https://doi.org/10.1073/pnas.2309333121>, 2024.

3105
3106 Jin, Z., Wang, T., Zhang, H., Wang, Y., Ding, J., and Tian, X.: Constraint of satellite CO₂ retrieval on the global carbon
3107 cycle from a Chinese atmospheric inversion system, *Sci. China Earth Sci.*, 66, 609–618, [https://doi.org/10.1007/s11430-022-](https://doi.org/10.1007/s11430-022-1036-7)
3108 1036-7, 2023.

3109
3110 Joos, F. and Spahni, R.: Rates of change in natural and anthropogenic radiative forcing over the past 20,000 years,
Proceedings of the National Academy of Sciences, 105, 1425–1430, <https://doi.org/10.1073/pnas.0707386105>, 2008.

3111 Jones, C. D., Hickman, J. E., Rumbold, S. T., Walton, J., Lamboll, R. D., Skeie, R. B., Fiedler, S., Forster, P. M., Rogelj, J.,
3112 Abe, M., Botzet, M., Calvin, K., Cassou, C., Cole, J. N. S., Davini, P., Deushi, M., Dix, M., Fyfe, J. C., Gillett, N. P., Ilyina,
3113 T., Kawamiya, M., Kelley, M., Kharin, S., Koshiro, T., Li, H., Mackallah, C., Müller, W. A., Nabat, P., van Noije, T., Nolan,
3114 P., Ohgaito, R., Olivié, D., Oshima, N., Parodi, J., Reerink, T. J., Ren, L., Romanou, A., Séférian, R., Tang, Y., Timmreck,
3115 C., Tjiputra, J., Tourigny, E., Tsigaridis, K., Wang, H., Wu, M., Wyser, K., Yang, S., Yang, Y., and Ziehn, T.: The Climate
3116 Response to Emissions Reductions Due to COVID-19: Initial Results From CovidMIP, *Geophys. Res. Lett.*, 48,
3117 e2020GL091883, <https://doi.org/10.1029/2020GL091883>, 2021a.

3118
3119 Jones, M. W., Abatzoglou, J. T., Veraverbeke, S., Andela, N., Lasslop, G., Forkel, M., Smith, A. J. P., Burton, C., Betts, R.
3120 A., van der Werf, G. R., Sitch, S., Canadell, J. G., Santin, C., Kolden, C., Doerr, S. H., and Le Quéré, C.: Global and
3121 Regional Trends and Drivers of Fire Under Climate Change, *Rev. Geophys.*, 60, e2020RG000726,
3122 <https://doi.org/10.1029/2020RG000726>, 2022.

3123
3124 Jones, M. W., Andrew, R. M., Peters, G. P., Janssens-Maenhout, G., De-Gol, A. J., Ciais, P., Patra, P. K., Chevallier, F., and
3125 Le Quéré, C.: Gridded fossil CO₂ emissions and related O₂ combustion consistent with national inventories 1959–2018, *Sci*
Data, 8, 2, <https://doi.org/10.1038/s41597-020-00779-6>, 2021b.

Formatted: Subscript

Formatted: Subscript

3126 Jones, M. W., Andrew, R. M., Peters, G. P., Janssens-Maenhout, G., De-Gol, A. J., Dou, X., Liu, Z., Pickers, P., Ciais, P.,
3127 Patra, P. K., Chevallier, F., and Le Quéré, C.: Gridded fossil CO₂ emissions and related O₂ combustion consistent with
3128 national inventories, Zenodo [dataset], <https://doi.org/10.5281/zenodo.13909046>, 2024a.

3129 Jones, M. W., Kelley, D. I., Burton, C. A., Di Giuseppe, F., Barbosa, M. L. F., Brambleby, E., Hartley, A. J., Lombardi, A.,
3130 Mataveli, G., McNorton, J. R., Spuler, F. R., Wessel, J. B., Abatzoglou, J. T., Anderson, L. O., Andela, N., Archibald, S.,
3131 Armenteras, D., Burke, E., Carmenta, R., Chuvieco, E., Clarke, H., Doerr, S. H., Fernandes, P. M., Giglio, L., Hamilton, D.
3132 S., Hantson, S., Harris, S., Jain, P., Kolden, C. A., Kurvits, T., Lampe, S., Meier, S., New, S., Parrington, M., Perron, M. M.
3133 G., Qu, Y., Ribeiro, N. S., Saharjo, B. H., San-Miguel-Ayanz, J., Shuman, J. K., Tanpipat, V., van der Werf, G. R.,
3134 Veraverbeke, S., and Xanthopoulos, G.: State of Wildfires 2023–2024, *Earth System Science Data*, 16, 3601–3685,
3135 <https://doi.org/10.5194/essd-16-3601-2024>, 2024b.

3136 Jones, M.W., Veraverbeke, S., Andela, N., Doerr, S.H., Kolden, C., Mataveli, G., Pettinari, M.L., Le Quéré, C., Rosan, T.M.,
3137 van der Werf, G.R. and van Wees, D.: Global rise in forest fire emissions linked to climate change in the extratropics.
3138 *Science*, 386(6719), p.ead15889, 2024c.

3139 Jung, M., Reichstein, M., Schwalm, C. R., Huntingford, C., Sitch, S., Ahlström, A., Arneth, A., Camps-Valls, G., Ciais, P.,
3140 Friedlingstein, P., Gans, F., Ichii, K., Jain, A. K., Kato, E., Papale, D., Poulter, B., Raduly, B., Rödenbeck, C., Tramontana,
3141 G., Viovy, N., Wang, Y.-P., Weber, U., Zaehle, S., and Zeng, N.: Compensatory water effects link yearly global land CO₂
3142 sink changes to temperature, *Nature*, 541, 516–520, <https://doi.org/10.1038/nature20780>, 2017.

3143 Kaiser, J. W., Heil, A., Andreae, M. O., Benedetti, A., Chubarova, N., Jones, L., Morcrette, J.-J., Razinger, M., Schultz, M.
3144 G., Suttie, M., and van der Werf, G. R.: Biomass burning emissions estimated with a global fire assimilation system based
3145 on observed fire radiative power, *Biogeosciences*, 9, 527–554, <https://doi.org/10.5194/bg-9-527-2012>, 2012.

3146 Kato, E., Kinoshita, T., Ito, A., Kawamiya, M., and Yamagata, Y.: Evaluation of spatially explicit emission scenario of land-
3147 use change and biomass burning using a process-based biogeochemical model, *J. Land Use Sci.*, 8, 104–122,
3148 <https://doi.org/10.1080/1747423X.2011.628705>, 2013.

3149 Kawasaki, T., Hasumi, H., and Tanaka, Y.: Role of tide-induced vertical mixing in the deep Pacific Ocean circulation, *J.*
3150 *Oceanogr.*, 77, 173–184, <https://doi.org/10.1007/s10872-020-00584-0>, 2021.

3151 Ke, P., Ciais, P., Sitch, S., Li, W., Bastos, A., Liu, Z., Xu, Y., Gui, X., Bian, J., Goll, D. S., Xi, Y., Li, W., O'Sullivan, M.,
3152 Goncalves de Souza, J., Friedlingstein, P., Chevallier, F.: Low latency carbon budget analysis reveals a large decline of the
3153 land carbon sink in 2023. *National Science Review*, p.nwae367, <https://doi.org/10.1093/nsr/nwae367>, 2024.
3154

3155 Keeley, J. E. and Pausas, J. G.: Distinguishing disturbance from perturbations in fire-prone ecosystems, *Int. J. Wildland Fire*,
3156 28, 282–287, <https://doi.org/10.1071/WF18203>, 2019.

3157 Keeling, C. D., Bacastow, R. B., Bainbridge, A. E., Ekdahl, C. A., Guenther, P. R., Waterman, L. S., and Chin, J. F. S.:
3158 Atmospheric carbon dioxide variations at Mauna Loa Observatory, Hawaii, *Tellus A.*, 28, 538–551,
3159 <https://doi.org/10.1111/j.2153-3490.1976.tb00701.x>, 1976.

- 3160 Keeling R.F.: Development of an Interferometric Oxygen Analyzer for Precise Measurement of the Atmospheric O₂ Mole
3161 Fraction, PhD thesis, Harvard University, Cambridge, Massachusetts, available at:
3162 https://bluemoon.ucsd.edu/publications/ralph/34_PhDthesis.pdf, last access: 21 January 2025, 1988.
- 3163 Keeling, R. F., Manning, A. C., Paplawsky, W. J., and Cox, A. C.: On the long-term stability of reference gases for
3164 atmospheric O₂/N₂ and CO₂ measurements, *Tellus B Chem. Phys. Meteorol.*, 59, 3–14, <https://doi.org/10.1111/j.1600-0889.2006.00196.x>, 2007.
- 3166 Keeling, R. F. and Manning, A. C.: 5.15 - Studies of Recent Changes in Atmospheric O₂ Content, in: *Treatise on
3167 Geochemistry (Second Edition)*, edited by: Holland, H. D. and Turekian, K. K., Elsevier, Oxford, 385–404,
3168 <https://doi.org/10.1016/B978-0-08-095975-7.00420-4>, 2014.
- 3170 Keppler, L. and Landschützer, P.: Regional Wind Variability Modulates the Southern Ocean Carbon Sink, *Sci Rep*, 9, 7384,
3171 <https://doi.org/10.1038/s41598-019-43826-y>, 2019.
- 3172 Khatiwala, S., Primeau, F., and Hall, T.: Reconstruction of the history of anthropogenic CO₂ concentrations in the ocean,
3173 *Nature*, 462, 346–349, <https://doi.org/10.1038/nature08526>, 2009.
- 3174 Khatiwala, S., Tanhua, T., Mikaloff Fletcher, S., Gerber, M., Doney, S. C., Graven, H. D., Gruber, N., McKinley, G. A.,
3175 Murata, A., Rios, A. F., and Sabine, C. L.: Global ocean storage of anthropogenic carbon, *Biogeosciences*, 10, 2169–2191,
3176 <https://doi.org/10.5194/bg-10-2169-2013>, 2013.
- 3177 Kong, Y., Zheng, B., Zhang, Q., and He, K.: Global and regional carbon budget for 2015–2020 inferred from OCO-2 based
3178 on an ensemble Kalman filter coupled with GEOS-Chem, *Atmospheric Chem. Phys.*, 22, 10769–10788,
3179 <https://doi.org/10.5194/acp-22-10769-2022>, 2022.
- 3180 Korsbakken, J. I., Peters, G. P., and Andrew, R. M.: Uncertainties around reductions in China’s coal use and CO₂ emissions,
3181 *Nature Clim Change*, 6, 687–690, <https://doi.org/10.1038/nclimate2963>, 2016.
- 3182 Krinner, G., Viovy, N., de Noblet-Ducoudré, N., Ogée, J., Polcher, J., Friedlingstein, P., Ciais, P., Sitch, S., and Prentice, I.
3183 C.: A dynamic global vegetation model for studies of the coupled atmosphere-biosphere system: DVGM for coupled climate
3184 studies, *Global Biogeochem. Cycles*, 19, GB1015, <https://doi.org/10.1029/2003GB002199>, 2005.
- 3185 Lacroix, F., Ilyina, T., and Hartmann, J.: Oceanic CO₂ outgassing and biological production hotspots induced by pre-
3186 industrial river loads of nutrients and carbon in a global modeling approach, *Biogeosciences*, 17, 55–88,
3187 <https://doi.org/10.5194/bg-17-55-2020>, 2020.
- 3188 Lacroix, F., Ilyina, T., Mathis, M., Laruelle, G. G., and Regnier, P.: Historical increases in land-derived nutrient inputs may
3189 alleviate effects of a changing physical climate on the oceanic carbon cycle, *Glob Change Biol*, 27, 5491–5513,
3190 <https://doi.org/10.1111/gcb.15822>, 2021.
- 3191 Lamboll, R. D., Nicholls, Z. R. J., Smith, C. J., Kikstra, J. S., Byers, E., and Rogelj, J.: Assessing the size and uncertainty of
3192 remaining carbon budgets, *Nat. Clim. Change*, <https://doi.org/10.1038/s41558-023-01848-5>, 2023.
- 3193

Deleted: 28 October 2024

3195 Lamboll, R. D., Jones, C. D., Skeie, R. B., Fiedler, S., Samset, B. H., Gillett, N. P., Rogelj, J., Forster, P. M., 2021:
3196 Modifying emissions scenario projections to account for the effects of COVID-19: protocol for CovidMIP, *Geosci. Model*
3197 *Dev.*, 14, 3683–3695, <https://doi.org/10.5194/gmd-14-3683-2021>, 2021.

3198 Lan, X., Tans, P. and Thoning, K.: NOAA Greenhouse Gas Marine Boundary Layer Reference - CO2 [Data set]. NOAA
3199 Global Monitoring Laboratory, https://doi.org/10.15138/DVNP-F961_2023.

3200 Lan, X., Tans, P. and K.W. Thoning: Trends in globally-averaged CO2 determined from NOAA Global Monitoring
3201 Laboratory measurements, Version 2024-09. National Oceanic and Atmospheric Administration, Global Monitoring
3202 Laboratory (NOAA/GML) [dataset], available at: <https://gml.noaa.gov/ccgg/trends/global.html>, last access: 21 January 2025,
3203 https://doi.org/10.15138/9N0H-ZH07_2024a.

3204 Lan, X., Tans, P. and Thoning, K. W.: Trends in globally-averaged CO2 determined from NOAA Global Monitoring
3205 Laboratory measurements, https://doi.org/10.15138/9N0H-ZH07_2024b.

3206 Landschützer, P., Gruber, N., Haumann, F. A., Rödenbeck, C., Bakker, D. C. E., van Heuven, S., Hoppema, M., Metzl, N.,
3207 Sweeney, C., Takahashi, T., Tilbrook, B., and Wanninkhof, R.: The reinvigoration of the Southern Ocean carbon sink,
3208 *Science*, 349, 1221–1224, <https://doi.org/10.1126/science.aab2620>, 2015.

3209 Landschützer, P., Gruber, N., and Bakker, D. C. E.: Decadal variations and trends of the global ocean carbon sink: decadal
3210 air-sea CO2 flux variability, *Global Biogeochem. Cycles*, 30, 1396–1417, <https://doi.org/10.1002/2015GB005359>, 2016.

3211 Lapola, D. M., Pinho, P., Barlow, J., Aragão, L. E. O. C., Berenguer, E., Carmenta, R., Liddy, H. M., Seixas, H., Silva, C. V.
3212 J., Silva-Junior, C. H. L., Alencar, A. A. C., Anderson, L. O., Armenteras, D., Brovkin, V., Calders, K., Chambers, J., Chini,
3213 L., Costa, M. H., Faria, B. L., Fearnside, P. M., Ferreira, J., Gatti, L., Gutierrez-Velez, V. H., Han, Z., Hibbard, K., Koven,
3214 C., Lawrence, P., Pongratz, J., Portela, B. T. T., Rounsevell, M., Ruane, A. C., Schaldach, R., da Silva, S. S., von Randow,
3215 C., Walker, W. S.: The drivers and impacts of Amazon forest degradation. *Science*, 379(6630), p.eabp8622,
3216 <https://doi.org/10.1126/science.abp8622>, 2023.

3217 Law, R. M., Ziehn, T., Matear, R. J., Lenton, A., Chamberlain, M. A., Stevens, L. E., Wang, Y.-P., Srbinovsky, J., Bi, D.,
3218 Yan, H., and Vohralik, P. F.: The carbon cycle in the Australian Community Climate and Earth System Simulator
3219 (ACCESS-ESM1) – Part 1: Model description and pre-industrial simulation, *Geosci. Model Dev.*, 10, 2567–2590,
3220 <https://doi.org/10.5194/gmd-10-2567-2017>, 2017.

3221 Lawrence, D. M., Fisher, R. A., Koven, C. D., Oleson, K. W., Swenson, S. C., Bonan, G., Collier, N., Ghimire, B., van
3222 Kampenhout, L., Kennedy, D., Kluzek, E., Lawrence, P. J., Li, F., Li, H., Lombardozzi, D., Riley, W. J., Sacks, W. J., Shi,
3223 M., Vertenstein, M., Wieder, W. R., Xu, C., Ali, A. A., Badger, A. M., Bisht, G., van den Broeke, M., Brunke, M. A., Burns,
3224 S. P., Buzan, J., Clark, M., Craig, A., Dahlin, K., Drewniak, B., Fisher, J. B., Flanner, M., Fox, A. M., Gentine, P., Hoffman,
3225 F., Keppel-Aleks, G., Knox, R., Kumar, S., Lenaerts, J., Leung, L. R., Lipscomb, W. H., Lu, Y., Pandey, A., Pelletier, J. D.,
3226 Perket, J., Randerson, J. T., Ricciuto, D. M., Sanderson, B. M., Slater, A., Subin, Z. M., Tang, J., Thomas, R. Q., Val Martin,
3227 M., and Zeng, X.: The Community Land Model Version 5: Description of New Features, Benchmarking, and Impact of
3228 Forcing Uncertainty, *J. Adv. Model Earth, Sy.*, 11, 4245–4287, <https://doi.org/10.1029/2018MS001583>, 2019.

3229 Le Quéré, C., Rödenbeck, C., Buitenhuis, E. T., Conway, T. J., Langenfelds, R., Gomez, A., Labuschagne, C., Ramonet, M.,
3230 Nakazawa, T., Metzl, N., Gillett, N., and Heimann, M.: Saturation of the Southern Ocean CO2 Sink Due to Recent Climate
3231 Change, *Science*, 316, 1735–1738, <https://doi.org/10.1126/science.1136188>, 2007.

Deleted: 28 October 2024, 2024

- 3233 Le Quéré, C., Raupach, M. R., Canadell, J. G., Marland, G., Bopp, L., Ciais, P., Conway, T. J., Doney, S. C., Feely, R. A.,
 3234 Foster, P., Friedlingstein, P., Gurney, K., Houghton, R. A., House, J. I., Huntingford, C., Levy, P. E., Lomas, M. R., Majkut,
 3235 J., Metzl, N., Ometto, J. P., Peters, G. P., Prentice, I. C., Randerson, J. T., Running, S. W., Sarmiento, J. L., Schuster, U.,
 3236 Sitch, S., Takahashi, T., Viovy, N., van der Werf, G. R., and Woodward, F. I.: Trends in the sources and sinks of carbon
 3237 dioxide, *Nature Geosci.*, 2, 831–836, <https://doi.org/10.1038/ngeo689>, 2009.
- 3238 Le Quéré, C., Andres, R. J., Boden, T., Conway, T., Houghton, R. A., House, J. I., Marland, G., Peters, G. P., van der Werf,
 3239 G. R., Ahlström, A., Andrew, R. M., Bopp, L., Canadell, J. G., Ciais, P., Doney, S. C., Enright, C., Friedlingstein, P.,
 3240 Huntingford, C., Jain, A. K., Jourdain, C., Kato, E., Keeling, R. F., Klein Goldewijk, K., Levis, S., Levy, P., Lomas, M.,
 3241 Poulter, B., Raupach, M. R., Schwinger, J., Sitch, S., Stocker, B. D., Viovy, N., Zaehle, S., and Zeng, N.: The global carbon
 3242 budget 1959–2011, *Earth Syst. Sci. Data*, 5, 165–185, <https://doi.org/10.5194/essd-5-165-2013>, 2013.
- 3243 Le Quéré, C., Peters, G. P., Andres, R. J., Andrew, R. M., Boden, T. A., Ciais, P., Friedlingstein, P., Houghton, R. A.,
 3244 Marland, G., Moriarty, R., Sitch, S., Tans, P., Armeth, A., Arvanitis, A., Bakker, D. C. E., Bopp, L., Canadell, J. G., Chini, L.,
 3245 P., Doney, S. C., Harper, A., Harris, I., House, J. I., Jain, A. K., Jones, S. D., Kato, E., Keeling, R. F., Klein Goldewijk, K.,
 3246 Körtzinger, A., Koven, C., Lefèvre, N., Maignan, F., Omar, A., Ono, T., Park, G.-H., Pfeil, B., Poulter, B., Raupach, M. R.,
 3247 Regnier, P., Rödenbeck, C., Saito, S., Schwinger, J., Segsneider, J., Stocker, B. D., Takahashi, T., Tilbrook, B., van
 3248 Heuven, S., Viovy, N., Wanninkhof, R., Wiltshire, A., and Zaehle, S.: Global carbon budget 2013, *Earth Syst. Sci. Data*, 6,
 3249 235–263, <https://doi.org/10.5194/essd-6-235-2014>, 2014.
- 3250 Le Quéré, C., Moriarty, R., Andrew, R. M., Peters, G. P., Ciais, P., Friedlingstein, P., Jones, S. D., Sitch, S., Tans, P.,
 3251 Armeth, A., Boden, T. A., Bopp, L., Bozec, Y., Canadell, J. G., Chini, L. P., Chevallier, F., Cosca, C. E., Harris, I.,
 3252 Hoppema, M., Houghton, R. A., House, J. I., Jain, A. K., Johannessen, T., Kato, E., Keeling, R. F., Kitidis, V., Klein
 3253 Goldewijk, K., Koven, C., Landa, C. S., Landschützer, P., Lenton, A., Lima, I. D., Marland, G., Mathis, J. T., Metzl, N.,
 3254 Nojiri, Y., Olsen, A., Ono, T., Peng, S., Peters, W., Pfeil, B., Poulter, B., Raupach, M. R., Regnier, P., Rödenbeck, C., Saito,
 3255 S., Salisbury, J. E., Schuster, U., Schwinger, J., Séférian, R., Segsneider, J., Steinhoff, T., Stocker, B. D., Sutton, A. J.,
 3256 Takahashi, T., Tilbrook, B., van der Werf, G. R., Viovy, N., Wang, Y.-P., Wanninkhof, R., Wiltshire, A., and Zeng, N.:
 3257 Global carbon budget 2014, *Earth Syst. Sci. Data*, 7, 47–85, <https://doi.org/10.5194/essd-7-47-2015>, 2015a.
- 3258 Le Quéré, C., Moriarty, R., Andrew, R. M., Canadell, J. G., Sitch, S., Korsbakken, J. I., Friedlingstein, P., Peters, G. P.,
 3259 Andres, R. J., Boden, T. A., Houghton, R. A., House, J. I., Keeling, R. F., Tans, P., Armeth, A., Bakker, D. C. E., Barbero,
 3260 L., Bopp, L., Chang, J., Chevallier, F., Chini, L. P., Ciais, P., Fader, M., Feely, R. A., Gkritzalis, T., Harris, I., Hauck, J.,
 3261 Ilyina, T., Jain, A. K., Kato, E., Kitidis, V., Klein Goldewijk, K., Koven, C., Landschützer, P., Lauvset, S. K., Lefèvre, N.,
 3262 Lenton, A., Lima, I. D., Metzl, N., Millero, F., Munro, D. R., Murata, A., Nabel, J. E. M. S., Nakaoka, S., Nojiri, Y.,
 3263 O'Brien, K., Olsen, A., Ono, T., Pérez, F. F., Pfeil, B., Pierrot, D., Poulter, B., Rehder, G., Rödenbeck, C., Saito, S.,
 3264 Schuster, U., Schwinger, J., Séférian, R., Steinhoff, T., Stocker, B. D., Sutton, A. J., Takahashi, T., Tilbrook, B., van der
 3265 Laan-Luijkx, I. T., van der Werf, G. R., van Heuven, S., Vandemark, D., Viovy, N., Wiltshire, A., Zaehle, S., and Zeng, N.:
 3266 Global Carbon Budget 2015, *Earth Syst. Sci. Data*, 7, 349–396, <https://doi.org/10.5194/essd-7-349-2015>, 2015b.
- 3267 Le Quéré, C., Andrew, R. M., Canadell, J. G., Sitch, S., Korsbakken, J. I., Peters, G. P., Manning, A. C., Boden, T. A., Tans,
 3268 P. P., Houghton, R. A., Keeling, R. F., Alin, S., Andrews, O. D., Anthoni, P., Barbero, L., Bopp, L., Chevallier, F., Chini, L.,
 3269 P., Ciais, P., Currie, K., Delire, C., Doney, S. C., Friedlingstein, P., Gkritzalis, T., Harris, I., Hauck, J., Haverd, V.,
 3270 Hoppema, M., Klein Goldewijk, K., Jain, A. K., Kato, E., Körtzinger, A., Landschützer, P., Lefèvre, N., Lenton, A., Lienert,
 3271 S., Lombardozzi, D., Melton, J. R., Metzl, N., Millero, F., Monteiro, P. M. S., Munro, D. R., Nabel, J. E. M. S., Nakaoka, S.,

3272 O'Brien, K., Olsen, A., Omar, A. M., Ono, T., Pierrot, D., Poulter, B., Rödenbeck, C., Salisbury, J., Schuster, U., Schwinger,
3273 J., Séférian, R., Skjelvan, I., Stocker, B. D., Sutton, A. J., Takahashi, T., Tian, H., Tilbrook, B., van der Laan-Luijkx, I. T.,
3274 van der Werf, G. R., Viovy, N., Walker, A. P., Wiltshire, A. J., and Zaehle, S.: Global Carbon Budget 2016, *Earth Syst. Sci.*
3275 *Data*, 8, 605–649, <https://doi.org/10.5194/essd-8-605-2016>, 2016.

3276 Le Quéré, C., Andrew, R. M., Friedlingstein, P., Sitch, S., Pongratz, J., Manning, A. C., Korsbakken, J. I., Peters, G. P.,
3277 Canadell, J. G., Jackson, R. B., Boden, T. A., Tans, P. P., Andrews, O. D., Arora, V. K., Bakker, D. C. E., Barbero, L.,
3278 Becker, M., Betts, R. A., Bopp, L., Chevallier, F., Chini, L. P., Ciais, P., Cosca, C. E., Cross, J., Currie, K., Gasser, T.,
3279 Harris, I., Hauck, J., Haverd, V., Houghton, R. A., Hunt, C. W., Hurtt, G., Ilyina, T., Jain, A. K., Kato, E., Kautz, M.,
3280 Keeling, R. F., Klein Goldewijk, K., Körtzinger, A., Landschützer, P., Lefèvre, N., Lenton, A., Lienert, S., Lima, I.,
3281 Lombardozi, D., Metzl, N., Millero, F., Monteiro, P. M. S., Munro, D. R., Nabel, J. E. M. S., Nakaoka, S., Nojiri, Y., Padin,
3282 X. A., Peregon, A., Pfeil, B., Pierrot, D., Poulter, B., Rehder, G., Reimer, J., Rödenbeck, C., Schwinger, J., Séférian, R.,
3283 Skjelvan, I., Stocker, B. D., Tian, H., Tilbrook, B., Tubiello, F. N., van der Laan-Luijkx, I. T., van der Werf, G. R., van
3284 Heuven, S., Viovy, N., Vuichard, N., Walker, A. P., Watson, A. J., Wiltshire, A. J., Zaehle, S., and Zhu, D.: Global Carbon
3285 Budget 2017, *Earth Syst. Sci. Data*, 10, 405–448, <https://doi.org/10.5194/essd-10-405-2018>, 2018a.

3286 Le Quéré, C., Andrew, R. M., Friedlingstein, P., Sitch, S., Hauck, J., Pongratz, J., Pickers, P. A., Korsbakken, J. I., Peters, G.
3287 P., Canadell, J. G., Armeth, A., Arora, V. K., Barbero, L., Bastos, A., Bopp, L., Chevallier, F., Chini, L. P., Ciais, P., Doney,
3288 S. C., Gkritzalis, T., Goll, D. S., Harris, I., Haverd, V., Hoffman, F. M., Hoppema, M., Houghton, R. A., Hurtt, G., Ilyina, T.,
3289 Jain, A. K., Johannessen, T., Jones, C. D., Kato, E., Keeling, R. F., Klein Goldewijk, K., Landschützer, P., Lefèvre, N.,
3290 Lienert, S., Liu, Z., Lombardozi, D., Metzl, N., Munro, D. R., Nabel, J. E. M. S., Nakaoka, S., Neill, C., Olsen, A., Ono, T.,
3291 Patra, P., Peregon, A., Peters, W., Peylin, P., Pfeil, B., Pierrot, D., Poulter, B., Rehder, G., Resplandy, L., Robertson, E.,
3292 Rocher, M., Rödenbeck, C., Schuster, U., Schwinger, J., Séférian, R., Skjelvan, I., Steinhoff, T., Sutton, A., Tans, P. P.,
3293 Tian, H., Tilbrook, B., Tubiello, F. N., van der Laan-Luijkx, I. T., van der Werf, G. R., Viovy, N., Walker, A. P., Wiltshire,
3294 A. J., Wright, R., Zaehle, S., and Zheng, B.: Global Carbon Budget 2018, *Earth Syst. Sci. Data*, 10, 2141–2194,
3295 <https://doi.org/10.5194/essd-10-2141-2018>, 2018b.

3296 Le Quéré, C., Korsbakken, J. I., Wilson, C., Tosun, J., Andrew, R., Andres, R. J., Canadell, J. G., Jordan, A., Peters, G. P.,
3297 and van Vuuren, D. P.: Drivers of declining CO₂ emissions in 18 developed economies, *Nat. Clim. Chang.*, 9, 213–217,
3298 <https://doi.org/10.1038/s41558-019-0419-7>, 2019.

3299 Le Quéré, C., Peters, G. P., Friedlingstein, P., Andrew, R. M., Canadell, J. G., Davis, S. J., Jackson, R. B., and Jones, M. W.:
3300 Fossil CO₂ emissions in the post-COVID-19 era, *Nat. Clim. Chang.*, 11, 197–199, [https://doi.org/10.1038/s41558-021-](https://doi.org/10.1038/s41558-021-01001-0)
3301 [01001-0](https://doi.org/10.1038/s41558-021-01001-0), 2021.

3302 Levitus, S., Antonov, J. I., Boyer, T. P., Baranova, O. K., Garcia, H. E., Locarnini, R. A., Mishonov, A. V., Reagan, J. R.,
3303 Seidov, D., Yarosh, E. S., and Zweng, M. M.: World ocean heat content and thermosteric sea level change (0–2000 m),
3304 1955–2010, *Geophys. Res. Lett.*, 39, <https://doi.org/10.1029/2012GL051106>, 2012.
3305

3306 Li, H., Ilyina, T., Müller, W. A., and Sienz, F.: Decadal predictions of the North Atlantic CO₂ uptake, *Nat. Commun.*, 7,
3307 11076, <https://doi.org/10.1038/ncomms11076>, 2016.
3308

3309 Li, H., Ilyina, T., Müller, W. A., and Landschützer, P.: Predicting the variable ocean carbon sink, *Sci. Adv.*, 5, eaav6471,
3310 <https://doi.org/10.1126/sciadv.aav6471>, 2019.

3311
3312 Li, H., Ilyina, T., Loughran, T., Spring, A., and Pongratz, J.: Reconstructions and predictions of the global carbon budget
3313 with an emission-driven Earth system model, *Earth Syst. Dyn.*, 14, 101–119, <https://doi.org/10.5194/esd-14-101-2023>, 2023.

3314 Li, W., Ciais, P., Peng, S., Yue, C., Wang, Y., Thurner, M., Saatchi, S. S., Armeth, A., Avitabile, V., Carvalhais, N., Harper,
3315 A. B., Kato, E., Koven, C., Liu, Y. Y., Nabel, J. E. M. S., Pan, Y., Pongratz, J., Poulter, B., Pugh, T. A. M., Santoro, M.,
3316 Sitch, S., Stocker, B. D., Viovy, N., Wiltshire, A., Yousefpour, R., and Zaehle, S.: Land-use and land-cover change carbon
3317 emissions between 1901 and 2012 constrained by biomass observations, *Biogeosciences*, 14, 5053–5067,
3318 <https://doi.org/10.5194/bg-14-5053-2017>, 2017.

3319 Liao, E., Resplandy, L., Liu, J., and Bowman, K. W.: Amplification of the Ocean Carbon Sink During El Niños: Role of
3320 Poleward Ekman Transport and Influence on Atmospheric CO₂, *Global Biogeochem. Cy.*, 34, e2020GB006574,
3321 <https://doi.org/10.1029/2020GB006574>, 2020.

3322 Lienert, S. and Joos, F.: A Bayesian ensemble data assimilation to constrain model parameters and land-use carbon
3323 emissions, *Biogeosciences*, 15, 2909–2930, <https://doi.org/10.5194/bg-15-2909-2018>, 2018.

3324 Liu, J., Baskaran, L., Bowman, K., Schimel, D., Bloom, A. A., Parazoo, N. C., Oda, T., Carroll, D., Menemenlis, D., Joiner,
3325 J., Commane, R., Daube, B., Gatti, L. V., McKain, K., Miller, J., Stephens, B. B., Sweeney, C., and Wofsy, S.: Carbon
3326 Monitoring System Flux Net Biosphere Exchange 2020 (CMS-Flux NBE 2020), 13, 299–330, <https://doi.org/10.5194/essd-13-299-2021>, 2021.

3328 Liu, Z., Guan, D., Wei, W., Davis, S. J., Ciais, P., Bai, J., Peng, S., Zhang, Q., Hubacek, K., Marland, G., Andres, R. J.,
3329 Crawford-Brown, D., Lin, J., Zhao, H., Hong, C., Boden, T. A., Feng, K., Peters, G. P., Xi, F., Liu, J., Li, Y., Zhao, Y.,
3330 Zeng, N., and He, K.: Reduced carbon emission estimates from fossil fuel combustion and cement production in China,
3331 *Nature*, 524, 335–338, <https://doi.org/10.1038/nature14677>, 2015.

3332 Liu, Z., Zeng, N., Liu, Y., Kalnay, E., Asrar, G., Wu, B., Cai, Q., Liu, D., and Han, P.: Improving the joint estimation of
3333 CO₂ and surface carbon fluxes using a constrained ensemble Kalman filter in COLA (v1.0), *Geosci. Model Dev.*, 15, 5511–
3334 5528, <https://doi.org/10.5194/gmd-15-5511-2022>, 2022.

3335
3336 Long, M. C., Stephens, B. B., McKain, K., Sweeney, C., Keeling, R. F., Kort, E. A., Morgan, E. J., Bent, J. D., Chandra, N.,
3337 Chevallier, F., Commane, R., Daube, B. C., Krummel, P. B., Loh, Z., Luijkx, I. T., Munro, D., Patra, P., Peters, W.,
3338 Ramonet, M., Rödenbeck, C., Stavert, A., Tans, P., Wofsy, S. C.: Strong Southern Ocean carbon uptake evident in airborne
3339 observations. *Science*, 374(6572), 1275–1280, <https://doi.org/10.1126/science.abi4355>, 2021.

3340
3341 Lovenduski, N. S., Bonan, G. B., Yeager, S. G., Lindsay, K., and Lombardozzi, D. L.: High predictability of terrestrial
3342 carbon fluxes from an initialized decadal prediction system, *Environ. Res. Lett.*, 14, 124074, <https://doi.org/10.1088/1748-9326/ab5c55>, 2019a.

3343
3344
3345 Lovenduski, N. S., Yeager, S. G., Lindsay, K., and Long, M. C.: Predicting near-term variability in ocean carbon uptake,
3346 *Earth Syst. Dyn.*, 10, 45–57, <https://doi.org/10.5194/esd-10-45-2019>, 2019b.

3347 Lutz, F., Herzfeld, T., Heinke, J., Rolinski, S., Schaphoff, S., von Bloh, W., Stoorvogel, J. J., and Müller, C.: Simulating the
3348 effect of tillage practices with the global ecosystem model LPJmL (version 5.0-tillage), *Geosci. Model Dev.*, 12, 2419–2440,
3349 <https://doi.org/10.5194/gmd-12-2419-2019>, 2019.

3350 Ma, L., Hurtt, G., Ott, L., Sahajpal, R., Fisk, J., Lamb, R., Tang, H., Flanagan, S., Chini, L., Chatterjee, A., and Sullivan, J.:
3351 Global evaluation of the Ecosystem Demography model (ED v3.0), *Geosci. Model Dev.*, 15, 1971–1994,
3352 <https://doi.org/10.5194/gmd-15-1971-2022>, 2022.

3353

3354 Magi, B. I., Rabin, S., Shevliakova, E., and Pacala, S.: Separating agricultural and non-agricultural fire seasonality at
3355 regional scales, *Biogeosciences*, 9, 3003–3012, <https://doi.org/10.5194/bg-9-3003-2012>, 2012.

3356

3357 Maksyutov, S., Oda, T., Saito, M., Janardanan, R., Belikov, D., Kaiser, J. W., Zhuravlev, R., Ganshin, A., Valsala, V. K.,
3358 Andrews, A., Chmura, L., Dlugokencky, E., Haszpra, L., Langenfelds, R. L., Machida, T., Nakazawa, T., Ramonet, M.,
3359 Sweeney, C., and Worthy, D.: Technical note: A high-resolution inverse modelling technique for estimating surface CO₂
3360 fluxes based on the NIES-TM–FLEXPART coupled transport model and its adjoint, *Atmos. Chem. Phys.*, 21, 1245–1266,
3361 <https://doi.org/10.5194/acp-21-1245-2021>, 2021.

3362 Masarie, K. A. and Tans, P. P.: Extension and integration of atmospheric carbon dioxide data into a globally consistent
3363 measurement record, *J. Geophys. Res.*, 100, 11593, <https://doi.org/10.1029/95JD00859>, 1995.

3364 Mataveli, G., Jones, M.W., Carmenta, R., Sanchez, A., Dutra, D.J., Chaves, M., de Oliveira, G., Anderson, L.O. and Aragão,
3365 L.E.: Deforestation falls but rise of wildfires continues degrading Brazilian Amazon forests. *Global Change Biology*, 30(2),
3366 p.e17202, <https://doi.org/10.1111/gcb.17202>, 2024.

3367 Mather, A. S.: The transition from deforestation to reforestation in Europe, in: *Agricultural technologies and tropical*
3368 *deforestation* (eds. Angelsen, A.; Kaimowitz, D.), CABI in association with centre for international Forestry Research, 35–
3369 52, 2001.

3370 Mauritsen, T., Bader, J., Becker, T., Behrens, J., Bittner, M., Brokopf, R., Brovkin, V., Claussen, M., Crueger, T., Esch, M.,
3371 Fast, I., Fiedler, S., Fläschner, D., Gayler, V., Giorgetta, M., Goll, D. S., Haak, H., Hagemann, S., Hedemann, C.,
3372 Hohenegger, C., Ilyina, T., Jahns, T., Jimenez-de-la-Cuesta, D., Jungclaus, J., Kleinen, T., Kloster, S., Kracher, D., Kinne,
3373 S., Kleberg, D., Lasslop, G., Kornbluh, L., Marotzke, J., Matei, D., Meraner, K., Mikolajewicz, U., Modali, K., Möbis, B.,
3374 Müller, W. A., Nabel, J. E. M. S., Nam, C. C. W., Notz, D., Nyawira, S.-S., Paulsen, H., Peters, K., Pincus, R., Pohlmann,
3375 H., Pongratz, J., Popp, M., Raddatz, T. J., Rast, S., Redler, R., Reick, C. H., Rohrschneider, T., Schemann, V., Schmidt, H.,
3376 Schnur, R., Schulzweida, U., Six, K. D., Stein, L., Stemmler, I., Stevens, B., von Storch, J.-S., Tian, F., Voigt, A., Vrese, P.,
3377 Wieners, K.-H., Wilkenskjaeld, S., Winkler, A., and Roeckner, E.: Developments in the MPI-M Earth System Model version
3378 1.2 (MPI-ESM1.2) and Its Response to Increasing CO₂, *J. Adv. Model Earth Sy.*, 11, 998–1038,
3379 <https://doi.org/10.1029/2018MS001400>, 2019.

3380 Mayot, N., Buitenhuis, E. T., Wright, R. M., Hauck, J., Bakker, D. C. E., and Le Quéré, C.: Constraining the trend in the
3381 ocean CO₂ sink during 2000–2022. *Nat Commun* 15, 8429, <https://doi.org/10.1038/s41467-024-52641-7>, 2024.

3382 McGrath, M. J., Luyssaert, S., Meyfroidt, P., Kaplan, J. O., Bürgi, M., Chen, Y., Erb, K., Gimmi, U., McInerney, D., Naudts,
3383 K., Otto, J., Pasztor, F., Ryder, J., Schelhaas, M.-J., and Valade, A.: Reconstructing European forest management from 1600
3384 to 2010, 12, 4291–4316, <https://doi.org/10.5194/bg-12-4291-2015>, 2015.

3385 McKinley, G. A., Fay, A. R., Eddebar, Y. A., Gloege, L., and Lovenduski, N. S.: External Forcing Explains Recent
3386 Decadal Variability of the Ocean Carbon Sink, *AGU Advances*, 1, e2019AV000149,
3387 <https://doi.org/10.1029/2019AV000149>, 2020.

3388 McKinley, G. A., Fay, A. R., Lovenduski, N. S., and Pilcher, D. J.: Natural Variability and Anthropogenic Trends in the
3389 Ocean Carbon Sink, *Annu. Rev. Mar. Sci.*, 9, 125–150, <https://doi.org/10.1146/annurev-marine-010816-060529>, 2017.

3390 Meiyappan, P., Jain, A. K., and House, J. I.: Increased influence of nitrogen limitation on CO₂ emissions from future land
3391 use and land use change, *Global Biogeochem. Cycles*, 29, 1524–1548, <https://doi.org/10.1002/2015GB005086>, 2015.

3392 Melton, J. R., Arora, V. K., Wisernig-Cojoc, E., Seiler, C., Fortier, M., Chan, E., and Teckentrup, L.: CLASSIC v1.0: the
3393 open-source community successor to the Canadian Land Surface Scheme (CLASS) and the Canadian Terrestrial Ecosystem
3394 Model (CTEM) – Part 1: Model framework and site-level performance, *Geosci. Model Dev.*, 13, 2825–2850,
3395 <https://doi.org/10.5194/gmd-13-2825-2020>, 2020.

3396 Mercado, L. M., Bellouin, N., Sitch, S., Boucher, O., Huntingford, C., Wild, M., and Cox, P. M.: Impact of changes in
3397 diffuse radiation on the global land carbon sink, *Nature*, 458, 1014–1017, <https://doi.org/10.1038/nature07949>, 2009.

3398 Merchant, C. J., Embury, O., Bulgin, C. E., Block, T., Corlett, G. K., Fiedler, E., Good, S. A., Mittaz, J., Rayner, N. A.,
3399 Berry, D., Eastwood, S., Taylor, M., Tsushima, Y., Waterfall, A., Wilson, R., and Donlon, C.: Satellite-based time-series of
3400 sea-surface temperature since 1981 for climate applications, *Sci. Data*, 6, 223, <https://doi.org/10.1038/s41597-019-0236-x>,
3401 2019.

3402 Moorcroft, P. R., Hurtt, G. C., and Pacala, S. W.: A Method for Scaling Vegetation Dynamics: The Ecosystem Demography
3403 Model (ed), *Ecol. Monogr.*, 71, 557–586, [https://doi.org/10.1890/0012-9615\(2001\)071\[0557:AMFSVD\]2.0.CO;2](https://doi.org/10.1890/0012-9615(2001)071[0557:AMFSVD]2.0.CO;2), 2001.

3404 Müller, J. D., Gruber, N., Carter, B., Feely, R., Ishii, M., Lange, N., Lauvset, S. K., Murata, A., Olsen, A., Pérez, F. F.,
3405 Sabine, C., Tanhua, T., Wanninkhof, R., and Zhu, D.: Decadal Trends in the Oceanic Storage of Anthropogenic Carbon
3406 From 1994 to 2014, *AGU Adv.*, 4, e2023AV000875, <https://doi.org/10.1029/2023AV000875>, 2023.

3407 [Müller, J. and Joos, F.: Committed and projected future changes in global peatlands – continued transient model simulations](#)
3408 [since the Last Glacial Maximum, *Biogeosciences*, 18, 3657–3687, <https://doi.org/10.5194/bg-18-3657-2021>, 2021.](#)

3410 Nayagam, L., Maksyutov, S., Oda, T., Janardanan, R., Trisolino, P., Zeng J., Kaiser, J.W. and Matsunaga, T.: A top-down
3411 estimation of subnational CO₂ budget using a global high-resolution inverse model with data from regional surface
3412 networks, *Environ. Res. Lett.*, 19, 0140312024, <https://doi.org/10.1088/1748-9326/ad0f74>, 2024.

3413 NCEP: National Centers for Environmental Prediction. ONI Index. Cold & Warm Episodes by Season [dataset], available at:
3414 https://origin.cpc.ncep.noaa.gov/products/analysis_monitoring/ensostuff/ONI_v5.php, last access: [21 January 2025](#), 2023.

3415 Nevison, C.D., Mahowald, N.M., Doney, S.C., Lima, I.D. and Cassar, N.: Impact of variable air-sea O₂ and CO₂ fluxes on
3416 atmospheric potential oxygen (APO) and land-ocean carbon sink partitioning, *Biogeosciences*, 5(3), pp.875-889,
3417 <https://doi.org/10.5194/bg-5-875-2008>, 2008.

3418 Niu, G.-Y., Yang, Z.-L., Mitchell, K. E., Chen, F., Ek, M. B., Barlage, M., Kumar, A., Manning, K., Niyogi, D., Rosero, E.,
3419 Tewari, M., and Xia, Y.: The community Noah land surface model with multiparameterization options (Noah-MP): 1. Model

Deleted: 28 October 2024

3421 description and evaluation with local-scale measurements, *J. Geophys. Res. Atmospheres*, 116,
3422 <https://doi.org/10.1029/2010JD015139>, 2011.

3423 Niwa, Y., Ishijima, K., Ito, A., and Iida, Y.: Toward a long-term atmospheric CO₂ inversion for elucidating natural carbon
3424 fluxes: technical notes of NISMON-CO₂ v2021.1, *Prog. Earth Planet Sci.*, 9, 42, [https://doi.org/10.1186/s40645-022-00502-](https://doi.org/10.1186/s40645-022-00502-6)
3425 6, 2022.

3426 Niwa, Y., Langenfelds, R., Krummel, P., Loh, Zoe, Worthy, Doug, Hatakka, Juha, Aalto, Tuula, Ramonet, Michel,
3427 Delmotte, Marc, Schmidt, Martina, Gheusi, Francois, Mihalopoulos, N., Morgui, J.A., Andrews, Arlyn, Dlugokencky, Ed,
3428 Lee, John, Sweeney, Colm, Thoning, Kirk, Tans, Pieter, De Wekker, Stephan, Fischer, Marc L., Jaffe, Dan, McKain,
3429 Kathryn, Viner, Brian, Miller, John B., Karion, Anna, Miller, Charles, Sloop, Christopher D., Saito, Kazuyuki, Aoki, Shuji,
3430 Morimoto, Shinji, Goto, Daisuke, Steinbacher, Martin, Myhre, Cathrine Lund, Hermanssen, Ove, Stephens, Britton, Keeling,
3431 Ralph, Afshar, Sara, Paplawsky, Bill, Cox, Adam, Walker, Stephen, Schuldt, Kenneth, Mukai, Hitoshi, Machida, Toshinobu,
3432 Sasakawa, Motoki, Nomura, Shohei, Ito, Akihiko, Iida, Yosuke, and Jones, Matthew W.: Long-term global CO₂ fluxes
3433 estimated by NICAM-based Inverse Simulation for Monitoring CO₂ (NISMON-CO₂) (ver.2022.1), National Institute for
3434 Environmental Studies Japan [dataset], <https://doi.org/10.17595/20201127.001>, 2020.

3435 Obermeier, W. A., Nabel, J. E. M. S., Loughran, T., Hartung, K., Bastos, A., Havermann, F., Anthoni, P., Arneth, A., Goll,
3436 D. S., Lienert, S., Lombardozi, D., Luyssaert, S., McGuire, P. C., Melton, J. R., Poulter, B., Sitch, S., Sullivan, M. O., Tian,
3437 H., Walker, A. P., Wiltshire, A. J., Zaehle, S., and Pongratz, J.: Modelled land use and land cover change emissions – a
3438 spatio-temporal comparison of different approaches, 12, 635–670, <https://doi.org/10.5194/esd-12-635-2021>, 2021.

3439 O'Rourke, P. R., Smith, S. J., Mott, A., Ahsan, H., McDuffie, E. E., Crippa, M., Klimont, Z., McDonald, B., Wang, S.,
3440 Nicholson, M. B., Feng, L., and Hoesly, R. M.: CEDS v_2021_04_21 Release Emission Data, Zenodo [dataset],
3441 <https://doi.org/10.5281/zenodo.4741285>, 2021.

3442 O'Sullivan, M., Zhang, Y., Bellouin, N., Harris, I., Mercado, L. M., Sitch, S., Ciais, P., and Friedlingstein, P.: Aerosol–light
3443 interactions reduce the carbon budget imbalance, *Environ. Res. Lett.*, 16, 124072, <https://doi.org/10.1088/1748-9326/ac3b77>,
3444 2021.

3445 O'Sullivan, M., Friedlingstein, P., Sitch, S., Anthoni, P., Arneth, A., Arora, V. K., Bastrikov, V., Delire, C., Goll, D. S., Jain,
3446 A., Kato, E., Kennedy, D., Knauer, J., Lienert, S., Lombardozi, D., McGuire, P. C., Melton, J. R., Nabel, J. E. M. S.,
3447 Pongratz, J., Poulter, B., Séférian, R., Tian, H., Vuichard, N., Walker, A. P., Yuan, W., Yue, X., and Zaehle, S.: Process-
3448 oriented analysis of dominant sources of uncertainty in the land carbon sink, *Nat. Commun.*, 13, 4781,
3449 <https://doi.org/10.1038/s41467-022-32416-8>, 2022.

3450 O'Sullivan, M., Spracklen, D. V., Batterman, S. A., Arnold, S. R., Gloor, M., and Buermann, W.: Have Synergies Between
3451 Nitrogen Deposition and Atmospheric CO₂ Driven the Recent Enhancement of the Terrestrial Carbon Sink?, *Glob.*
3452 *Biogeochem. Cycles*, 33, 163–180, <https://doi.org/10.1029/2018GB005922>, 2019.

3453 Palmer, P. I., Feng, L., Baker, D., Chevallier, F., Bösch, H., and Somkuti, P.: Net carbon emissions from African biosphere
3454 dominate pan-tropical atmospheric CO₂ signal, *Nat Commun*, 10, 3344, <https://doi.org/10.1038/s41467-019-11097-w>, 2019.

3455 Pan, Y., Birdsey, R. A., Fang, J., Houghton, R., Kauppi, P. E., Kurz, W. A., Phillips, O. L., Shvidenko, A., Lewis, S. L.,
3456 Canadell, J. G., Ciais, P., Jackson, R. B., Pacala, S. W., McGuire, A. D., Piao, S., Rautiainen, A., Sitch, S., and Hayes, D.: A

3457 Large and Persistent Carbon Sink in the World's Forests, *Science*, 333, 988–993, <https://doi.org/10.1126/science.1201609>,
3458 2011.

3459 Pendrill, F., Persson, U. M., Godar, J., Kastner, T., Moran, D., Schmidt, S., and Wood, R.: Agricultural and forestry trade
3460 drives large share of tropical deforestation emissions, *Global Environmental Change*, 56, 1–10,
3461 <https://doi.org/10.1016/j.gloenvcha.2019.03.002>, 2019.

3462 Pérez, F. F., Becker, M., Goris, N., Gehlen, M., López-Mozos, M., Tjiputra, J., Olsen, A., Müller, J. D., Huertas, I. E., Chau,
3463 T. T. T., Cainzos, V., Velo, A., Benard, G., Hauck, J., Gruber, N., and Wanninkhof, R.: An Assessment of CO₂ Storage and
3464 Sea-Air Fluxes for the Atlantic Ocean and Mediterranean Sea Between 1985 and 2018. *Global Biogeochemical Cycles*,
3465 38(4), e2023GB007862, <https://doi.org/10.1029/2023GB007862>, 2024.

3466 Peters, G. P., Minx, J. C., Weber, C. L., and Edenhofer, O.: Growth in emission transfers via international trade from 1990 to
3467 2008, *Proceedings of the National Academy of Sciences*, 108, 8903–8908, <https://doi.org/10.1073/pnas.1006388108>, 2011a.

3468 Peters, G. P., Marland, G., Le Quéré, C., Boden, T., Canadell, J. G., and Raupach, M. R.: Rapid growth in CO₂ emissions
3469 after the 2008–2009 global financial crisis, *Nature Clim Change*, 2, 2–4, <https://doi.org/10.1038/nclimate1332>, 2012a.

3470 Peters, G. P., Andrew, R. M., Boden, T., Canadell, J. G., Ciais, P., Le Quéré, C., Marland, G., Raupach, M. R., and Wilson,
3471 C.: The challenge to keep global warming below 2 °C, *Nature Clim Change*, 3, 4–6, <https://doi.org/10.1038/nclimate1783>,
3472 2013.

3473 Peters, G. P., Le Quéré, C., Andrew, R. M., Canadell, J. G., Friedlingstein, P., Ilyina, T., Jackson, R. B., Joos, F.,
3474 Korsbakken, J. I., McKinley, G. A., Sitch, S., and Tans, P.: Towards real-time verification of CO₂ emissions, *Nature Clim*
3475 *Change*, 7, 848–850, <https://doi.org/10.1038/s41558-017-0013-9>, 2017a.

3476 Peters, G. P., Andrew, R. M., Canadell, J. G., Fuss, S., Jackson, R. B., Korsbakken, J. I., Le Quéré, C. and Nakicenovic, N.:
3477 Key indicators to track current progress and future ambition of the Paris Agreement, 7, 118–122,
3478 <https://doi.org/10.1038/nclimate3202>, 2017b.

3479 Peters, G. P., Andrew, R. M., Canadell, J. G., Friedlingstein, P., Jackson, R. B., Korsbakken, J. I., Le Quéré, C., and
3480 Peregón, A.: Carbon dioxide emissions continue to grow amidst slowly emerging climate policies, *Nat. Clim. Chang.*, 10, 3–
3481 6, <https://doi.org/10.1038/s41558-019-0659-6>, 2020.

3482 Peters, W., Miller, J. B., Whitaker, J., Denning, A. S., Hirsch, A., Krol, M. C., Zupanski, D., Bruhwiler, L., and Tans, P. P.:
3483 An ensemble data assimilation system to estimate CO₂ surface fluxes from atmospheric trace gas observations, *J. Geophys.*
3484 *Res. Atmospheres*, 110, <https://doi.org/10.1029/2005JD006157>, 2005.

3485 Petrescu, A. M. R., Peters, G. P., Janssens-Maenhout, G., Ciais, P., Tubiello, F. N., Grassi, G., Nabuurs, G.-J., Leip, A.,
3486 Carmona-Garcia, G., Winiwarter, W., Höglund-Isaksson, L., Günther, D., Solazzo, E., Kiesow, A., Bastos, A., Pongratz, J.,
3487 Nabel, J. E. M. S., Conchedda, G., Pilli, R., Andrew, R. M., Schelhaas, M.-J., and Dolman, A. J.: European anthropogenic
3488 AFOLU greenhouse gas emissions: a review and benchmark data, *Earth Syst. Sci. Data*, 12, 961–1001,
3489 <https://doi.org/10.5194/essd-12-961-2020>, 2020.

3490 Pfeil, B., Olsen, A., Bakker, D. C. E., Hankin, S., Koyuk, H., Kozyr, A., Malczyk, J., Manke, A., Metzl, N., Sabine, C. L.,
3491 Akl, J., Alin, S. R., Bates, N., Bellerby, R. G. J., Borges, A., Boutin, J., Brown, P. J., Cai, W.-J., Chavez, F. P., Chen, A.,

3492 Cosca, C., Fassbender, A. J., Feely, R. A., González-Dávila, M., Goyet, C., Hales, B., Hardman-Mountford, N., Heinze, C.,
3493 Hood, M., Hoppema, M., Hunt, C. W., Hydes, D., Ishii, M., Johannessen, T., Jones, S. D., Key, R. M., Körtzinger, A.,
3494 Landschützer, P., Lauvset, S. K., Lefèvre, N., Lenton, A., Lourantou, A., Merlivat, L., Midorikawa, T., Mintrop, L.,
3495 Miyazaki, C., Murata, A., Nakadate, A., Nakano, Y., Nakaoka, S., Nojiri, Y., Omar, A. M., Padin, X. A., Park, G.-H.,
3496 Paterson, K., Perez, F. F., Pierrot, D., Poisson, A., Ríos, A. F., Santana-Casiano, J. M., Salisburly, J., Sarma, V. V. S. S.,
3497 Schlitzer, R., Schneider, B., Schuster, U., Sieger, R., Skjelvan, I., Steinhoff, T., Suzuki, T., Takahashi, T., Tedesco, K.,
3498 Telszewski, M., Thomas, H., Tilbrook, B., Tjiputra, J., Vandemark, D., Veness, T., Wanninkhof, R., Watson, A. J., Weiss,
3499 R., Wong, C. S., and Yoshikawa-Inoue, H.: A uniform, quality controlled Surface Ocean CO₂ Atlas (SOCAT), *Earth Syst.*
3500 *Sci. Data*, 5, 125–143, <https://doi.org/10.5194/essd-5-125-2013>, 2013.

3501 Piao, S., Ciais, P., Friedlingstein, P., de Noblet-Ducoudré, N., Cadule, P., Viovy, N., and Wang, T.: Spatiotemporal patterns
3502 of terrestrial carbon cycle during the 20th century, *Global Biogeochem. Cy.*, 23, GB4026,
3503 <https://doi.org/10.1029/2008GB003339>, 2009.

3504 Piao, S., Huang, M., Liu, Z., Wang, X., Ciais, P., Canadell, J. G., Wang, K., Bastos, A., Friedlingstein, P., Houghton, R. A.,
3505 Le Quéré, C., Liu, Y., Myneni, R. B., Peng, S., Pongratz, J., Sitch, S., Yan, T., Wang, Y., Zhu, Z., Wu, D., and Wang, T.:
3506 Lower land-use emissions responsible for increased net land carbon sink during the slow warming period, *Nature Geosci.*, 11,
3507 739–743, <https://doi.org/10.1038/s41561-018-0204-7>, 2018.

3508 Pongratz, J., Reick, C. H., Houghton, R. A., and House, J. I.: Terminology as a key uncertainty in net land use and land
3509 cover change carbon flux estimates, *Earth Syst. Dynam.*, 5, 177–195, <https://doi.org/10.5194/esd-5-177-2014>, 2014.

3510 Pongratz, J., Smith, S. M., Schwingshackl, C., Dayathilake, L., Gasser, T., Grassi, G. and Pilli, R.: Chapter 7: Current levels
3511 of CDR. in *The State of Carbon Dioxide Removal 2024 – 2nd Edition*, <https://doi.org/10.17605/OSF.IOZXSKB>, 2024.

3512 Poulter, B., Bastos, A., Canadell, J., Ciais, P., Gruber, N., Hauck, J., Jackson, R., Ishii, M., Müller, J., Patra, P., and Tian, H.:
3513 Inventorying Earth's Land and Ocean Greenhouse Gases, *Eos*, 103, <https://doi.org/10.1029/2022EO179084>, 2022.

3514 Poulter, B., Frank, D. C., Hodson, E. L., and Zimmermann, N. E.: Impacts of land cover and climate data selection on
3515 understanding terrestrial carbon dynamics and the CO₂ airborne fraction, *Biogeosciences*, 8, 2027–2036,
3516 <https://doi.org/10.5194/bg-8-2027-2011>, 2011.

3517 Poulter, B., Freeborn, P. H., Jolly, W. M., and Varner, J. M.: COVID-19 lockdowns drive decline in active fires in
3518 southeastern United States, *PNAS*, 118, e2105666118, <https://doi.org/10.1073/pnas.2105666118>, 2021.

3519 Powis, C. M., Smith, S. M., Minx, J. C., and Gasser, T.: Quantifying global carbon dioxide removal deployment, *Environ.*
3520 *Res. Lett.*, 18, 024022, <https://doi.org/10.1088/1748-9326/acb450>, 2023.

3521 Prentice, I. C., Farquhar, G. D., Fasham, M. J. R., Goulden, M. L., Heimann, M., Jaramillo, V. J., Khesghi, H. S., Le Quéré,
3522 C., Scholes, R. J., and Wallace, D. W. R.: The Carbon Cycle and Atmospheric Carbon Dioxide, in *Climate Change 2001:
3523 The Scientific Basis. Contribution of Working Group I to the Third Assessment Report of the Intergovernmental Panel on
3524 Climate Change*, edited by: Houghton, J. T., Ding, Y., Griggs, D. J., Noguer, M., van der Linden, P. J., Dai, X., Maskell, K.,
3525 and Johnson, C. A., Cambridge University Press, Cambridge, United Kingdom and New York, NY, USA, 183–237, ISBN:
3526 978-0521014953, 2001.

3527 Price, J. T. and Warren, R.: Literature Review of the Potential of “Blue Carbon” Activities to Reduce Emissions, available
3528 at: [https://avoid-net-uk.cc.ic.ac.uk/wp-content/uploads/delightful-downloads/2016/03/Literature-review-of-the-potential-of-](https://avoid-net-uk.cc.ic.ac.uk/wp-content/uploads/delightful-downloads/2016/03/Literature-review-of-the-potential-of-blue-carbon-activities-to-reduce-emissions-AVOID2-WPE2.pdf)
3529 [blue-carbon-activities-to-reduce-emissions-AVOID2-WPE2.pdf](https://avoid-net-uk.cc.ic.ac.uk/wp-content/uploads/delightful-downloads/2016/03/Literature-review-of-the-potential-of-blue-carbon-activities-to-reduce-emissions-AVOID2-WPE2.pdf), last access: [21 January 2025](#), 2016.

3530 Qin, Y., Xiao, X., Wigneron, J.-P., Ciais, P., Brandt, M., Fan, L., Li, X., Crowell, S., Wu, X., Doughty, R., Zhang, Y., Liu,
3531 F., Sitch, S., and Moore, B.: Carbon loss from forest degradation exceeds that from deforestation in the Brazilian Amazon,
3532 *Nat. Clim. Chang.*, 11, 442–448, <https://doi.org/10.1038/s41558-021-01026-5>, 2021.

3533 Qin, Z., Zhu, Y., Canadell, J.G., Chen, M., Li, T., Mishra, U. and Yuan, W.: Global spatially explicit carbon emissions from
3534 land-use change over the past six decades (1961–2020). *One Earth*, 7(5), pp.835–847,
3535 <https://doi.org/10.1016/j.oneear.2024.04.002>, 2024.

3536 [Qiu, C., Ciais, P., Zhu, D., Guenet, B., Peng, S., Petrescu, A. M. R., Lauerwald, R., Makowski, D., Gallego-Sala, A. V.,](#)
3537 [Charman, D. J., and Brewer, S. C.: Large historical carbon emissions from cultivated northern peatlands, *Sci. Adv.*, 7,](#)
3538 [eabf1332, <https://doi.org/10.1126/sciadv.abf1332>, 2021.](#)

3539 Randerson, J. T., Chen, Y., van der Werf, G. R., Rogers, B. M., and Morton, D. C.: Global burned area and biomass burning
3540 emissions from small fires: BURNED AREA FROM SMALL FIRES, *J. Geophys. Res. Biogeosciences*, 117, n/a-n/a,
3541 <https://doi.org/10.1029/2012JG002128>, 2012.

3542 Raupach, M. R., Marland, G., Ciais, P., Le Quere, C., Canadell, J. G., Klepper, G., and Field, C. B.: Global and regional
3543 drivers of accelerating CO₂ emissions, *Proceedings of the National Academy of Sciences*, 104, 10288–10293,
3544 <https://doi.org/10.1073/pnas.0700609104>, 2007.

3545 Regnier, P., Resplandy, L., Najjar, R. G., and Ciais, P.: The land-to-ocean loops of the global carbon cycle, *Nature*, 603,
3546 401–410, <https://doi.org/10.1038/s41586-021-04339-9>, 2022.

3547 Reick, C. H., Gayler, V., Goll, D., Hagemann, S., Heidkamp, M., Nabel, J. E. M. S., Raddatz, T., Roeckner, E., Schnur, R.,
3548 110 and Wilkenskjaeld, S.: JSBACH 3 – The land component of the MPI Earth System Model: documentation of version 3.2,
3549 available at: <https://doi.org/10.17617/2.3279802>, 2021.

3550 Remaud, M., Chevallier, F., Cozic, A., Lin, X., and Bousquet, P.: On the impact of recent developments of the LMDz
3551 atmospheric general circulation model on the simulation of CO₂ transport, 11, 4489, [https://doi.org/10.5194/gmd-11-4489-](https://doi.org/10.5194/gmd-11-4489-2018)
3552 2018, 2018.

3553 Resplandy, L., Keeling, R. F., Rödenbeck, C., Stephens, B. B., Khatiwala, S., Rodgers, K. B., Long, M. C., Bopp, L., and
3554 Tans, P. P.: Revision of global carbon fluxes based on a reassessment of oceanic and riverine carbon transport, *Nature*
3555 *Geosci.*, 11, 504–509, <https://doi.org/10.1038/s41561-018-0151-3>, 2018.

3556 Resplandy, L., Keeling, R. F., Eddebar, Y., Brooks, M., Wang, R., Bopp, L., Long, M. C., Dunne, J. P., Koeve, W., and
3557 Oschlies, A.: Quantification of ocean heat uptake from changes in atmospheric O₂ and CO₂ composition, *Scientific Reports*,
3558 9, 20244, <https://doi.org/10.1038/s41598-019-56490-z>, 2019.

3559 Rodenbeck, C., Houweling, S., Gloor, M., and Heimann, M.: CO₂ flux history 1982–2001 inferred from atmospheric data
3560 using a global inversion of atmospheric transport, *Atmos Chem Phys*, 3, 1919–1964, 2003.

Deleted: 28 October 2024

3562 Rödenbeck, C., Bakker, D. C. E., Metzl, N., Olsen, A., Sabine, C., Cassar, N., Reum, F., Keeling, R. F., and Heimann, M.:
3563 Interannual sea–air CO₂ flux variability from an observation-driven ocean mixed-layer scheme, 11, 4599–4613,
3564 <https://doi.org/10.5194/bg-11-4599-2014>, 2014.

3565 Rödenbeck, C., Zaehle, S., Keeling, R., and Heimann, M.: History of El Niño impacts on the global carbon cycle 1957–
3566 2017: a quantification from atmospheric CO₂ data, 373, 20170303, <https://doi.org/10.1098/rstb.2017.0303>, 2018.

3567 Rödenbeck, C., DeVries, T., Hauck, J., Le Quéré, C., and Keeling, R. F.: Data-based estimates of interannual sea–air CO₂
3568 flux variations 1957–2020 and their relation to environmental drivers, *Biogeosciences*, 19, 2627–2652,
3569 <https://doi.org/10.5194/bg-19-2627-2022>, 2022.

3570 Rosan, T. M., Klein Goldewijk, K., Ganzenmüller, R., O’Sullivan, M., Pongratz, J., Mercado, L. M., Aragao, L. E. O. C.,
3571 Heinrich, V., Randow, C. V., Wiltshire, A., Tubiello, F. N., Bastos, A., Friedlingstein, P., and Sitch, S.: A multi-data
3572 assessment of land use and land cover emissions from Brazil during 2000–2019, *Environ. Res. Lett.*, 16, 074004,
3573 <https://doi.org/10.1088/1748-9326/ac08c3>, 2021.

3574 Sakamoto, K., H. Nakano, S. Urakawa, T. Toyoda, Y. Kawakami, H. Tsujino, G. Yamanaka, 2023: Reference manual for the
3575 Meteorological Research Institute Community Ocean Model version 5 (MRI.COMv5), Technical Reports of the
3576 Meteorological Research Institute, No.87, <https://doi.org/10.11483/mritechrepo.87>.

3577 Sarma, V. V. S. S., Sridevi, B., Metzl, N., Patra, P. K., Lachkar, Z., Chakraborty, K., Goyet, C., Levy, M., Mehari, M., and
3578 Chandra, N.: Air–Sea Fluxes of CO₂ in the Indian Ocean Between 1985 and 2018: A Synthesis Based on Observation-Based
3579 Surface CO₂, Hindcast and Atmospheric Inversion Models, *Glob. Biogeochem. Cycles*, 37, e2023GB007694,
3580 <https://doi.org/10.1029/2023GB007694>, 2023.

3581 Schaphoff, S., von Bloh, W., Rammig, A., Thonicke, K., Biemans, H., Forkel, M., Gerten, D., Heinke, J., Jägermeyr, J.,
3582 Knauer, J., Langerwisch, F., Lucht, W., Müller, C., Rolinski, S., and Waha, K.: LPJmL4 – a dynamic global vegetation
3583 model with managed land – Part 1: Model description, *Geosci. Model Dev.*, 11, 1343–1375, [https://doi.org/10.5194/gmd-11-](https://doi.org/10.5194/gmd-11-1343-2018)
3584 1343-2018, 2018.

3585 Schimel, D., Alves, D., Enting, I. G., Heimann, M., Joos, F., Raynaud, D., Wigley, T., Prater, M., Derwent, R., Ehhalt, D.,
3586 Fraser, P., Sanhueza, E., Zhou, X., Jonas, P., Charlson, R., Rodhe, H., Sadasivan, S., Shine, K. P., Fouquart, Y.,
3587 Ramaswamy, V., Solomon, S., Srinivasan, J., Albritton, D., Derwent, R., Isaksen, I., Lal, M., and Wuebbles, D.: Radiative
3588 Forcing of Climate Change, in: *Climate Change 1995: The Science of Climate Change*, Contribution of Working Group I to
3589 the Second Assessment Report of the Intergovernmental Panel on Climate Change [Houghton, J. T., Meira Filho, L. G.,
3590 Callander, B. A., Harris, N., Kattenberg, A., and Maskell, K. (eds.)], Cambridge University Press, Cambridge, United
3591 Kingdom and New York, NY, USA, ISBN: 978-0521559621, 1995.

3592 Schimel, D., Stephens, B. B., and Fisher, J. B.: Effect of increasing CO₂ on the terrestrial carbon cycle, *Proc Natl Acad Sci*
3593 *USA*, 112, 436–441, <https://doi.org/10.1073/pnas.1407302112>, 2015.

3594 Schuh, A. E., Jacobson, A. R., Basu, S., Weir, B., Baker, D., Bowman, K., Chevallier, F., Crowell, S., Davis, K. J., Deng, F.,
3595 Denning, S., Feng, L., Jones, D., Liu, J., and Palmer, P. I.: Quantifying the Impact of Atmospheric Transport Uncertainty on
3596 CO₂ Surface Flux Estimates, *Global Biogeochem. Cycles*, 33, 484–500, <https://doi.org/10.1029/2018GB006086>, 2019.

3597 Schuldt, K. N., Mund, J., Aalto, T., Abshire, J. B., Aikin, K., Allen, G., Andrews, A., Apadula, F., Arnold, S., Baier, B.,
3598 Bakwin, P., Bartyzel, J., Bentz, G., Bergamaschi, P., Beyersdorf, A., Biermann, T., Biraud, S. C., Blanc, P.-E., Boenisch, H.,
3599 Bowling, D., Brailsford, G., Brand, W. A., Brunner, D., Bui, T. P., Băni, L., Calzolari, F., Chang, C. S., Chen, H., Chen, G.,
3600 Chmura, L., Clark, S., Climadat, S., Colomb, A., Commane, R., Conen, F., Conil, S., Couret, C., Cristofanelli, P., Cuevas,
3601 E., Curcoll, R., Daube, B., Davis, K. J., De Mazière, M., De Wekker, S., Dean-Day, J. M., Della Coletta, J., Delmotte, M.,
3602 Di Iorio, T., DiGangi, E., DiGangi, J. P., Elkins, J. W., Elsasser, M., Emmenegger, L., Fang, S., Fischer, M. L., Forster, G.,
3603 France, J., Frumau, A., Fuente-Lastra, M., Galkowski, M., Gatti, L. V., Gehrlein, T., Gerbig, C., Gheusi, F., Gloor, E., Goto,
3604 D., Griffis, T., Hammer, S., Hanisco, T. F., Hanson, C., Haszpra, L., Hatakka, J., Heimann, M., Heliasz, M., Heltai, D.,
3605 Henne, S., Hensen, A., Hermans, C., Hermansen, O., Hints, E., Hoheisel, A., Holst, J., Iraci, L. T., Ivakhov, V., Jaffé, D.,
3606 A., Jordan, A., Joubert, W., Karion, A., Kawa, S. R., Kazan, V., Keeling, R. F., Keronen, P., Kim, J., Klausen, J., Kneuer, T.,
3607 Kolari, P., Kominkova, K., Kort, E., Kozlova, E., Krümmel, P. B., Kubistin, D., Kulawik, S. S., Kumps, N., Labuschagne,
3608 C., Lam, D. H., Lan, X., Langenfelds, R. L., Lanza, A., Laurent, O., Laurila, T., Lauvaux, T., Lavric, J., Law, B. E., Lee, J.,
3609 Lehner, I., Lehtinen, K., Leppert, R., Leskinen, A., Leuenberger, M., Leung, W. H., Levin, I., Levula, J., Lin, J., Lindauer,
3610 M., Lindroth, A., Loh, Z. M., Lopez, M., Lunder, C. R., Löfvenius, M. O., Machida, T., Mammarella, I., Manca, G.,
3611 Manning, A., Manning, A., Marek, M. V., Marklund, P., Marrero, J. E., Martin, D., Martin, M. Y., Martins, G. A., Matsueda,
3612 H., McKain, K., Meijer, H., Meinhardt, F., Merchant, L., Metzger, J.-M., Mihalopoulos, N., Miles, N. L., Miller, J. B.,
3613 Miller, C. E., Mitchell, L., Monteiro, V., Montzka, S., Moore, F., Moossen, H., Morgan, E., Morgui, J.-A., Morimoto, S.,
3614 Munger, J. W., Munro, D., Mutuku, M., Myhre, C. L., Mölder, M., Müller-Williams, J., Necki, J., Newman, S., Nichol, S.,
3615 Nisbet, E., Niwa, Y., Njiru, D. M., Noe, S. M., Nojiri, Y., O'Doherty, S., Obersteiner, F., Paplawsky, B., Parworth, C. L.,
3616 Peischl, J., Peltola, O., Peters, W., Philippon, C., Piacentino, S., Pichon, J. M., Pickers, P., Piper, S., Pitt, J., Plass-Dülmer,
3617 C., Platt, S. M., Prinziavalli, S., Ramonet, M., Ramos, R., Reyes-Sanchez, E., Richardson, S. J., Rigouleau, L.-J., Riris, H.,
3618 Rivas, P. P., Rothe, M., Roulet, Y.-A., Ryerson, T., Ryoo, J.-M., Sargent, M., Sasakawa, M., Scheeren, B., Schmidt, M.,
3619 Schuck, T., Schumacher, M., Seibel, J., Seifert, T., Sha, M. K., Shepson, P., Shook, M., Sloop, C. D., Smith, P. D., Spain,
3620 G., St. Clair, J. M., Steger, D., Steinbacher, M., Stephens, B., Sweeney, C., Sørensen, L. L., Taipale, R., Takatsuji, S., Tans,
3621 P., Thoning, K., Timas, H., Tom, M., Trisolino, P., Turnbull, J., Vermeulen, A., Viner, B., Vitkova, G., Walker, S., Watson,
3622 A., Weiss, R., Weyrauch, D., Wofsy, S. C., Worsley, J., Worthy, D., Xueref-Remy, I., Yates, E. L., Young, D., Yver-Kwok,
3623 C., Zaehle, S., Zahn, A., Zellweger, C., Zimnoch, M., de Souza, R. A., di Sarra, A. G., van Dinter, D., and van den Bulk, P.
3624 (2023) Multi-laboratory compilation of atmospheric carbon dioxide data for the period 1957-2022;
3625 obspack_co2_1_GLOBALVIEWplus_v9.0_2023-09-09; NOAA Earth System Research Laboratory, Global Monitoring
3626 Laboratory, <http://doi.org/10.25925/20230801>.

3627 Schuldt, K. N., Jacobson, A. R., Aalto, T., Andrews, A., Apadula, F., Arnold, S., Bakwin, P., Bartyzel, J., Bergamaschi, P.,
3628 Biermann, T., Biraud, S. C., Blanc, P.-E., Băni, L., Calzolari, F., Chen, H., Chmura, L., Colomb, A., Condori, L., Conen, F.,
3629 Conil, S., Couret, C., Cristofanelli, P., Cuevas, E., De Mazière, M., De Wekker, S., Della Coletta, J., Delmotte, M., Di Iorio,
3630 T., Elsasser, M., Emmenegger, L., Fischer, M. L., Forster, G., Frumau, A., Fuente-Lastra, M., Galkowski, M., Gheusi, F.,
3631 Hammer, S., Hatakka, J., Heliasz, M., Heltai, D., Hensen, A., Hermans, C., Hermansen, O., Hoheisel, A., Holst, J., Jaffé, D.,
3632 A., Karion, A., Kazan, V., Keronen, P., Kneuer, T., Kolari, P., Kominkova, K., Krümmel, P. B., Kubistin, D., Kumps, N.,
3633 Lan, X., Langenfelds, R. L., Lanza, A., Laurent, O., Laurila, T., Lee, J., Lehner, I., Lehtinen, K., Leskinen, A., Leuenberger,
3634 M., Levin, I., Levula, J., Lindauer, M., Lindroth, A., Loh, Z. M., Lopez, M., Lunder, C. R., Löfvenius, M. O., Mammarella,
3635 I., Manca, G., Manning, A., Manning, A., Marek, M. V., Marklund, P., McKain, K., Meijer, H., Meinhardt, F., Metzger, J.-
3636 M., Miller, C. E., Miller, J. B., Myhre, C. L., Mölder, M., Müller-Williams, J., Necki, J., O'Doherty, S., Peltola, O.,
3637 Philippon, C., Piacentino, S., Pichon, J. M., Pickers, P., Pitt, J., Plass-Dülmer, C., Platt, S. M., Ramonet, M., Ramos, R.,
3638 Reyes-Sanchez, E., Rigouleau, L.-J., Rivas, P. P., Roulet, Y.-A., Scheeren, B., Schmidt, M., Schumacher, M., Sha, M. K.,

3639 Sloop, C. D., Smith, P. D., Steger, D., Steinbacher, M., Sweeney, C., Sorensen, L. L., Taipale, R., Tans, P., Thoning, K.,
3640 Trisolino, P., Turnbull, J., Vermeulen, A., Viner, B., Vitkova, G., Weyrauch, D., Worthy, D., Xueref-Remy, I., Young, D.,
3641 Yver-Kwok, C., Zimnoch, M., di Sarra, A. G., van Dinter, D., and van den Bulk, P. (2024) Multi-laboratory compilation of
3642 atmospheric carbon dioxide data for the period 2023-2024; obspack_co2_1_NRT_v9.2_2024-03-25; NOAA Earth System
3643 Research Laboratory, Global Monitoring Laboratory, <http://doi.org/10.25925/20240215>.

3644 Schwinger, J., Goris, N., Tjiputra, J. F., Kriest, I., Bentsen, M., Bethke, I., Ilicak, M., Assmann, K. M., and Heinze, C.:
3645 Evaluation of NorESM-OC (versions 1 and 1.2), the ocean carbon-cycle stand-alone configuration of the Norwegian Earth
3646 System Model (NorESM1), *Geosci. Model Dev.*, 9, 2589–2622, <https://doi.org/10.5194/gmd-9-2589-2016>, 2016.

3647 Schwingshackl, C., Obermeier, W. A., Bultan, S., Grassi, G., Canadell, J. G., Friedlingstein, P., Gasser, T., Houghton, R. A.,
3648 Kurz, W. A., Sitch, S., and Pongratz, J.: Differences in land-based mitigation estimates reconciled by separating natural and
3649 land-use CO₂ fluxes at the country level, *One Earth*, 5, 1367–1376, <https://doi.org/10.1016/j.oneear.2022.11.009>, 2022.

3650 Séférian, R., Nabat, P., Michou, M., Saint-Martin, D., Voldoire, A., Colin, J., Decharme, B., Delire, C., Berthet, S.,
3651 Chevallier, M., Sénési, S., Franchisteguy, L., Vial, J., Mallet, M., Joetzjer, E., Geoffroy, O., Guérémy, J.-F., Moine, M.-P.,
3652 Msadek, R., Ribes, A., Rocher, M., Roehrig, R., Salas-y-Méla, D., Sanchez, E., Terray, L., Valcke, S., Waldman, R.,
3653 Aumont, O., Bopp, L., Deshayes, J., Éthé, C., and Madec, G.: Evaluation of CNRM Earth System Model, CNRM-ESM2-1:
3654 Role of Earth System Processes in Present-Day and Future Climate, *Journal of Advances in Modeling Earth Systems*, 11,
3655 4182–4227, <https://doi.org/10.1029/2019MS001791>, 2019.

3656 Seiler, C., Melton, J. R., Arora, V. K., Sitch, S., Friedlingstein, P., Anthoni, P., Goll, D., Jain, A. K., Joetzjer, E., Lienert, S.,
3657 Lombardozi, D., Luyssaert, S., Nabel, J. E. M. S., Tian, H., Vuichard, N., Walker, A. P., Yuan, W., and Zaehe, S.: Are
3658 Terrestrial Biosphere Models Fit for Simulating the Global Land Carbon Sink?, *J. Adv. Model. Earth Syst.*, 14,
3659 e2021MS002946, <https://doi.org/10.1029/2021MS002946>, 2022.

3660 Sellar, A. A., Jones, C. G., Mulcahy, J. P., Tang, Y., Yool, A., Wiltshire, A., O'Connor, F. M., Stringer, M., Hill, R.,
3661 Palmieri, J., Woodward, S., Mora, L., Kuhlbrodt, T., Rumbold, S. T., Kelley, D. I., Ellis, R., Johnson, C. E., Walton, J.,
3662 Abraham, N. L., Andrews, M. B., Andrews, T., Archibald, A. T., Berthou, S., Burke, E., Blockley, E., Carslaw, K., Dalvi,
3663 M., Edwards, J., Folberth, G. A., Gedney, N., Griffiths, P. T., Harper, A. B., Hendry, M. A., Hewitt, A. J., Johnson, B.,
3664 Jones, A., Jones, C. D., Keeble, J., Liddicoat, S., Morgenstern, O., Parker, R. J., Predoi, V., Robertson, E., Siahann, A.,
3665 Smith, R. S., Swaminathan, R., Woodhouse, M. T., Zeng, G., and Zerroukat, M.: UKESM1: Description and Evaluation of
3666 the U.K. Earth System Model, *J. Adv. Model. Earth Syst.*, 11, 4513–4558, <https://doi.org/10.1029/2019MS001739>, 2019.

3667 Shu, S., Jain, A. K., Koven, C. D., and Mishra, U.: Estimation of Permafrost SOC Stock and Turnover Time Using a Land
3668 Surface Model With Vertical Heterogeneity of Permafrost Soils, *Global Biogeochem. Cy.*, 34, e2020GB006585,
3669 <https://doi.org/10.1029/2020GB006585>, 2020.

3670 Shutler, J. D., Land, P. E., Piolle, J.-F., Woolf, D. K., Goddijn-Murphy, L., Paul, F., Girard-Ardhuin, F., Chapron, B., and
3671 Donlon, C. J.: FluxEngine: A Flexible Processing System for Calculating Atmosphere–Ocean Carbon Dioxide Gas Fluxes
3672 and Climatologies, *J. Atmospheric Ocean. Technol.*, 33, 741–756, <https://doi.org/10.1175/JTECH-D-14-00204.1>, 2016.

3673 Silva Junior, C.H., Anderson, L.O., Silva, A.L., Almeida, C.T., Dalagnol, R., Pletsch, M.A., Penha, T.V., Paloschi, R.A. and
3674 Aragão, L.E.: Fire responses to the 2010 and 2015/2016 Amazonian droughts. *Frontiers in Earth Science*, 7, p.97,
3675 <https://doi.org/10.3389/feart.2019.00097>, 2019.

3676 Sitch, S., Huntingford, C., Gedney, N., Levy, P. E., Lomas, M., Piao, S. L., Betts, R., Ciais, P., Cox, P., Friedlingstein, P.,
3677 Jones, C. D., Prentice, I. C., and Woodward, F. I.: Evaluation of the terrestrial carbon cycle, future plant geography and
3678 climate-carbon cycle feedbacks using five Dynamic Global Vegetation Models (DGVMs): Uncertainty In Land Carbon
3679 Cycle Feedbacks, *Glob. Change Biol.*, 14, 2015–2039, <https://doi.org/10.1111/j.1365-2486.2008.01626.x>, 2008.

3680 Sitch, S., O'Sullivan, M., Robertson, E., Friedlingstein, P., Albergel, C., Anthoni, P., Armeth, A., Arora, V. K., Bastos, A.,
3681 Bastrikov, V., Bellouin, N., Canadell, J. G., Chini, L., Ciais, P., Falk, S., Harris, I., Hurtt, G., Ito, A., Jain, A. K., Jones, M.
3682 W., Joos, F., Kato, E., Kennedy, D., Klein Goldewijk, K., Kluzek, E., Knauer, J., Lawrence, P. J., Lombardozzi, D., Melton,
3683 J. R., Nabel, J. E. M. S., Pan, N., Peylin, P., Pongratz, J., Poulter, B., Rosan, T. M., Sun, Q., Tian, H., Walker, A. P., Weber,
3684 U., Yuan, W., Yue, X., Zaehle, S.: Trends and Drivers of Terrestrial Sources and Sinks of Carbon Dioxide: An Overview of
3685 the TRENDY Project, *Global Biogeochemical Cycles*, 38(7), e2024GB008102, <https://doi.org/10.1029/2024GB008102>,
3686 2024.

3687 Smallman, T. L., Milodowski, D. T., Neto, E. S., Koren, G., Ometto, J., and Williams, M.: Parameter uncertainty dominates
3688 C-cycle forecast errors over most of Brazil for the 21st century, *Earth Syst. Dyn.*, 12, 1191–1237,
3689 <https://doi.org/10.5194/esd-12-1191-2021>, 2021.

3690 Smith, B., Wårlind, D., Armeth, A., Hickler, T., Leadley, P., Siltberg, J., and Zaehle, S.: Implications of incorporating N
3691 cycling and N limitations on primary production in an individual-based dynamic vegetation model, *Biogeosciences*, 11,
3692 2027–2054, <https://doi.org/10.5194/bg-11-2027-2014>, 2014.

3693 Smith, S. M., Geden, O., Gidden, M. J., Lamb, W. F., Nemet, G. F., Minx, J. C., Buck, H., Burke, J., Cox, E., Edwards, M.
3694 R., Fuss, S., Johnstone, I., Müller-Hansen, F., Pongratz, J., Probst, B. S., Roe, S., Schenuit, F., Schulte, I., and Vaughan, N.
3695 E. The State of Carbon Dioxide Removal 2024 - 2nd Edition, <http://dx.doi.org/10.17605/OSF.IO/F85QJ>, 2024.

3696 Sospedra-Alfonso, R., Merryfield, W. J., Boer, G. J., Kharin, V. V., Lee, W.-S., Seiler, C., and Christian, J. R.: Decadal
3697 climate predictions with the Canadian Earth System Model version 5 (CanESM5), *Geosci. Model Dev.*, 14, 6863–6891,
3698 <https://doi.org/10.5194/gmd-14-6863-2021>, 2021.

3699 [Steele, L. P., Dlugokencky, E. J., Lang, P. M., Tans, P. P., Martin, R. C., and Masarie, K. A.: Slowing down of the global](https://doi.org/10.1038/358313a0)
3700 [accumulation of atmospheric methane during the 1980s. *Nature* 358, 313–316, <https://doi.org/10.1038/358313a0>, 1992.](https://doi.org/10.1038/358313a0)

3701 Stephens, B. B., Gurney, K. R., Tans, P. P., Sweeney, C., Peters, W., Bruhwiler, L., Ciais, P., Ramonet, M., Bousquet, P.,
3702 Nakazawa, T., Aoki, S., Machida, T., Inoue, G., Vinnichenko, N., Lloyd, J., Jordan, A., Heimann, M., Shibistova, O.,
3703 Langenfelds, R. L., Steele, L. P., Francey, R. J., and Denning, A. S.: Weak Northern and Strong Tropical Land Carbon
3704 Uptake from Vertical Profiles of Atmospheric CO₂, *Science*, 316, 1732–1735, <https://doi.org/10.1126/science.1137004>,
3705 2007.

3706 Stephens, B. B., Keeling, R. F., Heimann, M., Six, K. D., Mumane, R., and Caldeira, K.: Testing global ocean carbon cycle
3707 models using measurements of atmospheric O₂ and CO₂ concentration, *Glob. Biogeochem. Cycles*, 12, 213–230,
3708 <https://doi.org/10.1029/97GB03500>, 1998.

3709 Stocker, T., Qin, D., and Platner, G.-K.: Climate Change 2013: The Physical Science Basis. Contribution of Working Group
3710 I to the Fifth Assessment Report of the Intergovernmental Panel on Climate Change [Intergovernmental Panel on Climate
3711 Change (eds.)], Cambridge University Press, Cambridge, ISBN: 9789291691388, 2013.

3712 Swart, N. C., Cole, J. N. S., Kharin, V. V., Lazare, M., Scinocca, J. F., Gillett, N. P., Anstey, J., Arora, V., Christian, J. R.,
3713 Hanna, S., Jiao, Y., Lee, W. G., Majaess, F., Saenko, O. A., Seiler, C., Seinen, C., Shao, A., Sigmund, M., Solheim, L., von
3714 Salzen, K., Yang, D., and Winter, B.: The Canadian Earth System Model version 5 (CanESM5.0.3), *Geosci. Model Dev.*, 12,
3715 4823–4873, <https://doi.org/10.5194/gmd-12-4823-2019>, 2019.

3716 SX Coal: Monthly coal consumption estimates, <http://www.sxcoal.com/>, last access: [21 January 2025](#), 2022.

Deleted: 28 October 2024

3717 Takahashi, T., Sutherland, S. C., Wanninkhof, R., Sweeney, C., Feely, R. A., Chipman, D. W., Hales, B., Friederich, G.,
3718 Chavez, F., Sabine, C., Watson, A., Bakker, D. C. E., Schuster, U., Metz, N., Yoshikawa-Inoue, H., Ishii, M., Midorikawa,
3719 T., Nojiri, Y., Körtzinger, A., Steinhoff, T., Hoppema, M., Olafsson, J., Arnarson, T. S., Tilbrook, B., Johannessen, T.,
3720 Olsen, A., Bellerby, R., Wong, C. S., Delille, B., Bates, N. R., and de Baar, H. J. W.: Climatological mean and decadal
3721 change in surface ocean pCO₂, and net sea–air CO₂ flux over the global oceans, *Deep Sea Research Part II: Topical Studies*
3722 *in Oceanography*, 56, 554–577, <https://doi.org/10.1016/j.dsr2.2008.12.009>, 2009.

3723 Terhaar, J., Frölicher, T. L., and Joos, F.: Southern Ocean anthropogenic carbon sink constrained by sea surface salinity, *Sci.*
3724 *Adv.*, 7, eabd5964, <https://doi.org/10.1126/sciadv.abd5964>, 2021.

3725 Terhaar, J., Frölicher, T. L., and Joos, F.: Observation-constrained estimates of the global ocean carbon sink from Earth
3726 system models, *Biogeosciences*, 19, 4431–4457, <https://doi.org/10.5194/bg-19-4431-2022>, 2022.

3727 Terhaar, J., Goris, N., Müller, J. D., DeVries, T., Gruber, N., Hauck, J., Perez, F. F., and Séférian, R.: Assessment of Global
3728 Ocean Biogeochemistry Models for Ocean Carbon Sink Estimates in RECCAP2 and Recommendations for Future Studies.
3729 *Journal of Advances in Modeling Earth Systems*, 16(3), e2023MS003840, <https://doi.org/10.1029/2023MS003840>, 2024.

3730 Tian, H., Xu, X., Lu, C., Liu, M., Ren, W., Chen, G., Melillo, J., and Liu, J.: Net exchanges of CO₂, CH₄, and N₂O between
3731 China's terrestrial ecosystems and the atmosphere and their contributions to global climate warming, *J. Geophys. Res.*
3732 *Biogeosciences*, 116, G02011, <https://doi.org/10.1029/2010JG001393>, 2011.

3733 Tian, H., Chen, G., Lu, C., Xu, X., Hayes, D. J., Ren, W., Pan, S., Huntzinger, D. N., and Wofsy, S. C.: North American
3734 terrestrial CO₂ uptake largely offset by CH₄ and N₂O emissions: toward a full accounting of the greenhouse gas budget,
3735 *Climatic Change*, 129, 413–426, <https://doi.org/10.1007/s10584-014-1072-9>, 2015.

3736 Tsujino, H., Nakano, H., Sakamoto, K., Urakawa, L.S., Toyama, K., Kosugi, N., Kitamura, Y., Ishii, M., Nishikawa, S.,
3737 Nishikawa, H., Sugiyama, T., and Ishikawa, Y.: Impact of increased horizontal resolution of an ocean model on carbon
3738 circulation in the North Pacific Ocean. *Journal of Advances in Modeling Earth Systems*, 16, e2023MS003720,
3739 <https://doi.org/10.1029/2023MS003720>, 2024.

3740 Tubiello, F. N., Conchedda, G., Wanner, N., Federici, S., Rossi, S., and Grassi, G.: Carbon emissions and removals from
3741 forests: new estimates, 1990–2020, *Earth Syst. Sci. Data*, 13, 1681–1691, <https://doi.org/10.5194/essd-13-1681-2021>, 2021.

3742 Tuck, C.: 2022 Mineral Commodity Summary: Iron Ore, Tech. rep., U.S. Geological Survey,
3743 <https://pubs.usgs.gov/periodicals/mcs2022/mcs2022-iron-ore.pdf>, 2022.

3744 UNFCCC: Synthesis report for the technical assessment component of the first global stocktake, available at:

3745 <https://unfccc.int/documents/461466>, last access: [21 January 2025](#), 2022.

Deleted: 28 October 2024

3748 Vale, M. M., Berenguer, E., Argollo de Menezes, M., Viveiros de Castro, E. B., Pugliese de Siqueira, L., and Portela, R. de
3749 C. Q.: The COVID-19 pandemic as an opportunity to weaken environmental protection in Brazil, *Biological Conservation*,
3750 255, 108994, <https://doi.org/10.1016/j.biocon.2021.108994>, 2021.

3751 van der Laan-Luijckx, I. T., van der Velde, I. R., van der Veen, E., Tsuruta, A., Stanislawski, K., Babenhauserheide, A.,
3752 Zhang, H. F., Liu, Y., He, W., Chen, H., Masarie, K. A., Krol, M. C., and Peters, W.: The CarbonTracker Data Assimilation
3753 Shell (CTDAS) v1.0: implementation and global carbon balance 2001–2015, *Geosci. Model Dev.*, 10, 2785–2800,
3754 <https://doi.org/10.5194/gmd-10-2785-2017>, 2017.

3755 van der Velde, I. R., van der Werf, G. R., Houweling, S., Maasakkers, J. D., Borsdorff, T., Landgraf, J., Tol, P., van
3756 Kempen, T. A., van Hees, R., Hoogeveen, R., Veeffkind, J. P., and Aben, I.: Vast CO₂ release from Australian fires in 2019–
3757 2020 constrained by satellite, *Nature*, 597, 366–369, <https://doi.org/10.1038/s41586-021-03712-y>, 2021.

3758 van der Werf, G. R., Randerson, J. T., Giglio, L., Collatz, G. J., Mu, M., Kasibhatla, P. S., Morton, D. C., DeFries, R. S., Jin,
3759 Y., and van Leeuwen, T. T.: Global fire emissions and the contribution of deforestation, savanna, forest, agricultural, and
3760 peat fires (1997–2009), *Atmospheric Chem. Phys.*, 10, 11707–11735, <https://doi.org/10.5194/acp-10-11707-2010>, 2010.

3761 van der Werf, G. R., Randerson, J. T., Giglio, L., van Leeuwen, T. T., Chen, Y., Rogers, B. M., Mu, M., van Marle, M. J. E.,
3762 Morton, D. C., Collatz, G. J., Yokelson, R. J., and Kasibhatla, P. S.: Global fire emissions estimates during 1997–2016,
3763 *Earth Syst. Sci. Data*, 9, 697–720, <https://doi.org/10.5194/essd-9-697-2017>, 2017.

3764 van Wees, D., van der Werf, G. R., Randerson, J. T., Andela, N., Chen, Y., and Morton, D. C.: The role of fire in global
3765 forest loss dynamics, *Glob. Change Biol.*, 27, 2377–2391, <https://doi.org/10.1111/gcb.15591>, 2021.

3766 von Bloh, W., Schaphoff, S., Müller, C., Rolinski, S., Waha, K., and Zaehle, S.: Implementing the nitrogen cycle into the
3767 dynamic global vegetation, hydrology, and crop growth model LPJmL (version 5.0), *Geosci. Model Dev.*, 11, 2789–2812,
3768 <https://doi.org/10.5194/gmd-11-2789-2018>, 2018.

3769 Vaittinada Ayar, P., Bopp, L., Christian, J. R., Ilyina, T., Krasting, J. P., Séférian, R., Tsujino, H., Watanabe, M., Yool, A.,
3770 and Tjiputra, J.: Contrasting projections of the ENSO-driven CO₂ flux variability in the equatorial Pacific under high-
3771 warming scenario, *Earth Syst. Dynam.*, 13, 1097–1118, <https://doi.org/10.5194/esd-13-1097-2022>, 2022.

3772 Vuichard, N., Messina, P., Luyssaert, S., Guenet, B., Zaehle, S., Ghattas, J., Bastrikov, V., and Peylin, P.: Accounting for
3773 carbon and nitrogen interactions in the global terrestrial ecosystem model ORCHIDEE (trunk version, rev 4999): multi-scale
3774 evaluation of gross primary production, *Geosci. Model Dev.*, 12, 4751–4779, <https://doi.org/10.5194/gmd-12-4751-2019>,
3775 2019.

3776 Walker, A. P., Quaipe, T., Bodegom, P. M., De Kauwe, M. G., Keenan, T. F., Joiner, J., Lomas, M. R., MacBean, N., Xu, C.,
3777 Yang, X., and Woodward, F. I.: The impact of alternative trait-scaling hypotheses for the maximum photosynthetic
3778 carboxylation rate (V_{cmax}) on global gross primary production, *New Phytol.*, 215, 1370–1386,
3779 <https://doi.org/10.1111/nph.14623>, 2017.

3780 Walker, A. P., De Kauwe, M. G., Bastos, A., Belmecheri, S., Georgiou, K., Keeling, R. F., McMahon, S. M., Medlyn, B. E.,
3781 Moore, D. J. P., Norby, R. J., Zaehle, S., Anderson-Teixeira, K. J., Battipaglia, G., Brieney, R. J. W., Cabugao, K. G.,
3782 Cailleret, M., Campbell, E., Canadell, J. G., Ciais, P., Craig, M. E., Ellsworth, D. S., Farquhar, G. D., Fatichi, S., Fisher, J.
3783 B., Frank, D. C., Graven, H., Gu, L., Haverd, V., Heilmann, K., Heimann, M., Hungate, B. A., Iversen, C. M., Joos, F., Jiang,

3784 M., Keenan, T. F., Knauer, J., Körner, C., Leshyk, V. O., Leuzinger, S., Liu, Y., MacBean, N., Malhi, Y., McVicar, T. R.,
3785 Penuelas, J., Pongratz, J., Powell, A. S., Riutta, T., Sabot, M. E. B., Schleucher, J., Sitch, S., Smith, W. K., Sulman, B.,
3786 Taylor, B., Terrer, C., Torn, M. S., Treseder, K. K., Trugman, A. T., Trumbore, S. E., van Mantgem, P. J., Voelker, S. L.,
3787 Whelan, M. E., and Zuidema, P. A.: Integrating the evidence for a terrestrial carbon sink caused by increasing atmospheric
3788 CO₂, *New Phytol.*, 229, 2413–2445, <https://doi.org/10.1111/nph.16866>, 2021.

3789 Watanabe, M., Tatebe, H., Koyama, H., Hajima, T., Watanabe, M., and Kawamiya, M.: Importance of El Niño
3790 reproducibility for reconstructing historical CO₂ flux variations in the equatorial Pacific, *Ocean Sci.*, 16, 1431–1442,
3791 <https://doi.org/10.5194/os-16-1431-2020>, 2020.

3792 Watson, A. J., Schuster, U., Shutler, J. D., Holding, T., Ashton, I. G. C., Landschützer, P., Woolf, D. K., and Goddijn-
3793 Murphy, L.: Revised estimates of ocean-atmosphere CO₂ flux are consistent with ocean carbon inventory, *Nat Commun*, 11,
3794 4422, <https://doi.org/10.1038/s41467-020-18203-3>, 2020.

3795 Watson, R. T., Rohde, H., Oeschger, H., and Siegenthaler, U.: Greenhouse Gases and Aerosols, in: *Climate Change: The*
3796 *IPCC Scientific Assessment. Intergovernmental Panel on Climate Change (IPCC)*, edited by: Houghton, J. T., Jenkins, G. J.,
3797 and Ephraums, J. J., Cambridge University Press, Cambridge, ISBN: 978-0521403603, 1990.

3798 Wenzel, S., Cox, P. M., Eyring, V., and Friedlingstein, P.: Projected land photosynthesis constrained by changes in the
3799 seasonal cycle of atmospheric CO₂, *Nature*, 538, 499–501, <https://doi.org/10.1038/nature19772>, 2016.

3800 Wilkenskjeld, S., Kloster, S., Pongratz, J., Raddatz, T., and Reick, C. H.: Comparing the influence of net and gross
3801 anthropogenic land-use and land-cover changes on the carbon cycle in the MPI-ESM, *Biogeosciences*, 11, 4817–4828,
3802 <https://doi.org/10.5194/bg-11-4817-2014>, 2014.

3803 Wiltshire, A. J., Burke, E. J., Chadburn, S. E., Jones, C. D., Cox, P. M., Davies-Barnard, T., Friedlingstein, P., Harper, A. B.,
3804 Liddicoat, S., Sitch, S., and Zaehle, S.: JULES-CN: a coupled terrestrial carbon–nitrogen scheme (JULES vn5.1), 14, 2161–
3805 2186, <https://doi.org/10.5194/gmd-14-2161-2021>, 2021.

3806 Winkler, K., Yang, H., Ganzenmüller, R., Fuchs, R., Ceccherini, G., Duveiller, G., Grassi, G., Pongratz, J., Bastos, A.,
3807 Shvidenko, A., Araza, A., Herold, M., Wigneron, J.-P., and Ciais, P.: Changes in land use and management led to a decline
3808 in Eastern Europe’s terrestrial carbon sink, *Commun. Earth Environ.*, 4, 1–14, <https://doi.org/10.1038/s43247-023-00893-4>,
3809 2023.

3810 Woodward, F. I. and Lomas, M. R.: Vegetation dynamics – simulating responses to climatic change, *Biol. Rev.*, 79, 643–
3811 670, <https://doi.org/10.1017/S1464793103006419>, 2004.

3812 Wright, R. M., Le Quéré, C., Buitenhuis, E., Pitois, S., and Gibbons, M. J.: Role of jellyfish in the plankton ecosystem
3813 revealed using a global ocean biogeochemical model, 18, 1291–1320, <https://doi.org/10.5194/bg-18-1291-2021>, 2021.

3814 Wunder, S., Kaimowitz, D., Jensen, S., and Feder, S.: Coronavirus, macroeconomy, and forests: What likely impacts?, *For.*
3815 *Policy Econ.*, 131, 102536, <https://doi.org/10.1016/j.forpol.2021.102536>, 2021.

3816 Xi, F., Davis, S. J., Ciais, P., Crawford-Brown, D., Guan, D., Pade, C., Shi, T., Syddall, M., Lv, J., Ji, L., Bing, L., Wang, J.,
3817 Wei, W., Yang, K.-H., Lagerblad, B., Galan, I., Andrade, C., Zhang, Y., and Liu, Z.: Substantial global carbon uptake by
3818 cement carbonation, *Nature Geosci*, 9, 880–883, <https://doi.org/10.1038/ngeo2840>, 2016.

3819 Xia, J., Chen, Y., Liang, S., Liu, D., and Yuan, W.: Global simulations of carbon allocation coefficients for deciduous
3820 vegetation types, *Tellus B*, 67, 28016, <https://doi.org/10.3402/tellusb.v67.28016>, 2015.

3821 Yang, D., Liu, Y., Feng, L., Wang, J., Yao, L., Cai, Z., Zhu, S., Lu, N., and Lyu, D.: The First Global Carbon Dioxide Flux
3822 Map Derived from TanSat Measurements, *Adv. Atmospheric Sci.*, 38, 1433–1443, <https://doi.org/10.1007/s00376-021-1179-7>, 2021.

3824 Yang, X., Thornton, P., Ricciuto, D., Wang, Y., and Hoffman, F.: Global evaluation of terrestrial biogeochemistry in the
3825 Energy Exascale Earth System Model (E3SM) and the role of the phosphorus cycle in the historical terrestrial carbon
3826 balance, *Biogeosciences*, 20, 2813–2836, <https://doi.org/10.5194/bg-20-2813-2023>, 2023.

3827 Yu, Z., Ciais, P., Piao, S., Houghton, R. A., Lu, C., Tian, H., Agathokleous, E., Kattel, G. R., Sitch, S., Goll, D., Yue, X.,
3828 Walker, A., Friedlingstein, P., Jain, A. K., Liu, S., and Zhou, G.: Forest expansion dominates China’s land carbon sink since
3829 1980, *Nat. Commun.*, 13, 5374, <https://doi.org/10.1038/s41467-022-32961-2>, 2022.

3830 Yue, X. and Unger, N.: The Yale Interactive terrestrial Biosphere model version 1.0: description, evaluation and
3831 implementation into NASA GISS ModelE2, *Geosci. Model Dev.*, 8, 2399–2417, <https://doi.org/10.5194/gmd-8-2399-2015>,
3832 2015.

3833 Yuan, W., Liu, D., Dong, W., Liu, S., Zhou, G., Yu, G., Zhao, T., Feng, J., Ma, Z., Chen, J., Chen, Y., Chen, S., Han, S.,
3834 Huang, J., Li, L., Liu, H., Liu, S., Ma, M., Wang, Y., Xia, J., Xu, W., Zhang, Q., Zhao, X., and Zhao, L.: Multiyear
3835 precipitation reduction strongly decreases carbon uptake over northern China, *J. Geophys. Res.-Biogeo.*, 119, 881–896,
3836 <https://doi.org/10.1002/2014JG002608>, 2014.

3837 Yue, C., Ciais, P., Zhu, D., Wang, T., Peng, S. S., and Piao, S. L.: How have past fire disturbances contributed to the current
3838 carbon balance of boreal ecosystems?, *Biogeosciences*, 13, 675–690, <https://doi.org/10.5194/bg-13-675-2016>, 2016.

3839 Zaehle, S. and Friend, A. D.: Carbon and nitrogen cycle dynamics in the O-CN land surface model: 1. Model description,
3840 site-scale evaluation, and sensitivity to parameter estimates: Site-scale evaluation of a C-N model, *Global Biogeochem.*
3841 *Cycles*, 24, GB1005, <https://doi.org/10.1029/2009GB003521>, 2010.

3842 Zaehle, S., Ciais, P., Friend, A. D., and Prieur, V.: Carbon benefits of anthropogenic reactive nitrogen offset by nitrous oxide
3843 emissions, *Nature Geosci*, 4, 601–605, <https://doi.org/10.1038/ngeo1207>, 2011.

3844 Zaehle, S., Medlyn, B. E., De Kauwe, M. G., Walker, A. P., Dietze, M. C., Hickler, T., Luo, Y., Wang, Y.-P., El-Masri, B.,
3845 Thornton, P., Jain, A., Wang, S., Warlind, D., Weng, E., Parton, W., Iversen, C. M., Gallet-Budynek, A., McCarthy, H.,
3846 Finzi, A., Hanson, P. J., Prentice, I. C., Oren, R., and Norby, R. J.: Evaluation of 11 terrestrial carbon–nitrogen cycle models
3847 against observations from two temperate Free-Air CO₂ Enrichment studies, *New Phytol.*, 202, 803–822,
3848 <https://doi.org/10.1111/nph.12697>, 2014.

3849 Zeng, J., Iida, Y., Matsunaga, T., and Shirai, T.: Surface ocean CO₂ concentration and air-sea flux estimate by machine
3850 learning with modelled variable trends, *Front. Mar. Sci.*, 9, <https://doi.org/10.3389/fmars.2022.989233>, 2022.

3851 Zheng, B., Ciais, P., Chevallier, F., Chuvieco, E., Chen, Y., and Yang, H.: Increasing forest fire emissions despite the
3852 decline in global burned area, *Sci. Adv.*, 7, eabh2646, <https://doi.org/10.1126/sciadv.abh2646>, 2021.

3853 Zou, Y., Wang, Y., Ke, Z., Tian, H., Yang, J., and Liu, Y.: Development of a REgion-Specific Ecosystem Feedback Fire
3854 (RESFire) Model in the Community Earth System Model, *J. Adv. Model. Earth Syst.*, 11, 417–445,
3855 <https://doi.org/10.1029/2018MS001368>, 2019.

3856 Zscheischler, J., Mahecha, M. D., Avitabile, V., Calle, L., Carvalhais, N., Ciais, P., Gans, F., Gruber, N., Hartmann, J.,
3857 Herold, M., Ichii, K., Jung, M., Landschützer, P., Laruelle, G. G., Lauerwald, R., Papale, D., Peylin, P., Poulter, B., Ray, D.,
3858 Regnier, P., Rödenbeck, C., Roman-Cuesta, R. M., Schwalm, C., Tramontana, G., Tyukavina, A., Valentini, R., van der
3859 Werf, G., West, T. O., Wolf, J. E., and Reichstein, M.: Reviews and syntheses: An empirical spatiotemporal description of
3860 the global surface–atmosphere carbon fluxes: opportunities and data limitations, *Biogeosciences*, 14, 3685–3703,
3861 <https://doi.org/10.5194/bg-14-3685-2017>, 2017.

3862

Tables

3863

Table 1. Factors used to convert carbon in various units (by convention, Unit 1 = Unit 2 × conversion).

Unit 1	Unit 2	Conversion	Source
GtC (gigatonnes of carbon)	ppm (parts per million) (a)	2.124 (b)	Ballantyne et al. (2012)
GtC (gigatonnes of carbon)	PgC (petagrams of carbon)		1 SI unit conversion
GtCO ₂ (gigatonnes of carbon dioxide)	GtC (gigatonnes of carbon)	3.664	44.01/12.011 in mass equivalent
(a) Measurements of atmospheric CO ₂ concentration have units of dry-air mole fraction. 'ppm' is an abbreviation for micromole/mol, dry air.			
(b) The use of a factor of 2.124 assumes that all the atmosphere is well mixed within one year. In reality, only the troposphere is well mixed and the growth rate of CO ₂ concentration in the less well-mixed stratosphere is not measured by sites from the NOAA network. Using a factor of 2.124 makes the approximation that the growth rate of CO ₂ concentration in the stratosphere equals that of the troposphere on a yearly basis.			

Formatted Table

3864

3865

3866

3867

Table 2. How to cite the individual components of the global carbon budget presented here.

Component	Primary reference
Global fossil CO ₂ emissions (EFOS), total and by fuel type	Andrew and Peters (2024)
National territorial fossil CO ₂ emissions (EFOS)	Hefner and Marland (2023), UNFCCC (2024)
National consumption-based fossil CO ₂ emissions (EFOS) by country (consumption)	Peters et al. (2011a) updated as described in this paper
Net land-use change flux (ELUC)	This paper (see Table 4 for individual model references)
Growth rate in atmospheric CO ₂ concentration (GATM)	Lan et al. (2024a)
Ocean and land CO ₂ sinks (SOCEAN and SLAND)	This paper (see Table 4 for individual model and data products references)

- Formatted Table
- Formatted: Subscript
- Formatted: Subscript
- Formatted: Subscript
- Deleted: .)
- Formatted: Subscript
- Deleted: 2024)
- Formatted: Subscript
- Deleted: .)

3868
3869

Table 3. Main methodological changes in the global carbon budget since 2020. Methodological changes introduced in one year are kept for the following years unless noted. Empty cells mean there were no methodological changes introduced that year. Table S9 lists methodological changes from the first global carbon budget publication up to 2019.

Publication year	Fossil fuel emissions		LUC emissions	Reservoirs			Other changes
	Global	Country (territorial)		Atmosphere	Ocean	Land	
2020	Cement carbonation now included in the EFOS estimate, reducing EFOS by about 0.2GtC yr ⁻¹ for the last decade	India's emissions from Andrew (2020: India);	Average of three bookkeeping models; use of 17 DGVMs. Estimate of gross land use sources and sinks provided	Use of six atmospheric inversions	Based on nine models. River flux revised and partitioned NH, Tropics, SH	Based on 17 models	
Friedlingstein et al. (2020) GCB2020		Corrections to Netherland Antilles and Aruba and Soviet emissions before 1950 as per Andrew (2020: CO ₂); China's coal emissions in 2019 derived from official statistics, emissions now shown for EU27 instead of EU28. Projection for 2020 based on assessment of four approaches.					
2021	Projections are no longer an assessment of four approaches.	Official data included for a number of additional countries, new estimates for South Korea, added emissions from lime production in China.	ELUC estimate compared to the estimates adopted in national GHG inventories		Average of means of eight models and means of seven data-products. Current year prediction of SOCEAN using a feed-forward neural network method	Current year prediction of SLAND using a feed-forward neural network method	
Friedlingstein et al. (2022a) GCB2021							
2022			ELUC provided at country level. Revised components decomposition of ELUC fluxes. Revision of LUC	Use of nine atmospheric inversions	Average of means of ten models and means of seven data-products	Based on 16 models. Revision of LUC maps for Brazil.	
Friedlingstein et al. (2022) GCB2022							

Formatted Table

			maps for Brazil. New datasets for peat drainage.				
2023			Refined components decomposition of ELUC. Revision of LUC maps for Indonesia. Use of updated peat drainage estimates.	Use of 14 atmospheric inversions. Additional use of 4 Earth System Models to estimate current year CO2	Additional use of 4 Earth System Models and atmospheric oxygen method to assess SOCEAN. Regional distribution of river flux adjustment revised.	Based on 20 models. Additional use of 4 Earth System Models and atmospheric oxygen method to assess the net atmosphere-land flux.	Inclusion of an estimate of Carbon Dioxide Removal
2024			Fourth bookkeeping estimate (LUCE). Update in land-use data (HYDE3.4) including revision of LUC maps for China. Updated definition of forest (re-)growth fluxes (consistent with 2nd State of CDR Report).	Use of 14 atmospheric inversions models	Use of 10 GOBMs, 8 fCO2-products. Added evaluation for fCO2-products.	Use of 20 DGVMs	
	Inclusion of 2024 projections from Carbon Monitor	Inclusion of 2024 projections from Carbon Monitor for China, USA, EU27, India, and Rest of the World					
	This study						

Table 4. References for the process models, bookkeeping models, ocean data products, and atmospheric inversions. All models and products are updated with new data to the end of year 2023.

Model/data name	Reference	Change from Global Carbon Budget 2023 (Friedlingstein et al., 2023)
Bookkeeping models for land-use change emissions		
BLUE	Hansis et al. (2015)	No change to model, but simulations performed with LUH2-GCB2024 forcing. Update in added peat drainage emissions.
H&C2023	Houghton and Castanho (2023)	No change to model. Data for years after last modelled year (2020) extrapolated based on anomalies in deforestation fires from GFED. Update in added peat drainage emissions.
OSCAR	Gasser et al. (2020)	No change to model, but land-use forcing changed to LUH2-GCB2024 and FRA2020 extrapolated to 2023. Constraining based on GCB2023 data for SLAND over 1960-2022. Update in added peat drainage emissions.
LUCE	Qin et al. (2024)	New model in GCB2024.
Dynamic global vegetation models		
CABLE-POP	Haverd et al. (2018)	Bug fix applied to land use change calculations enabling variable crop and pasture fractions; corrections to the pre-industrial primary forest fraction in Europe; minor parameter changes
CLASSIC	Melton et al. (2020), Asaadi et al. (2018)	Permeable soil depth reduced to 4 m ; 15 soil layers in the top 4 m permeable soil and 5 bed rock layers from 4 m to 62 m; saturated hydraulic conductivity decreases with depth in the permeable soil layers; transpiration occurs from a partially-wet canopy leaves. These changes yield better runoff seasonality and a more realistic partitioning of precipitation into runoff and evapotranspiration.
CLM6.0	Lawrence et al. (2019)	Updates to surface datasets; improvement of roughness length calculation; updates to snow optical properties and snow thermal conductivity; improved excess ice; improved simulation of burial of vegetation by snow; urban updates, including transient urban, urban properties, and air conditioning; improvements to biomass heat storage; tillage and residue removal; crop phenology and planting dates; improvement to irrigation methods; PFT parameter update.

Formatted Table

DLEM	Tian et al. (2015), You et al. (2022)	Incorporate mechanistic representations of dynamic crop growth and development processes, such as crop-specific phenological development, carbon allocation, yield formation, and biological N fixation. Agricultural management practices such as N fertiliser use, irrigation, tillage, manure application, dynamic crop rotation, cover cropping, and genetic improvements are also included (You et al. 2022).
EDv3	Moorcroft et al. (2001), Ma et al. (2022)	Minor bug fixes, updated fire submodule
ELM	Yang et al.(2023), Burrows et al.(2020)	No change
IBIS	Xia et al., (2024)	Improved algorithm of leaf area index
iMAPLE	Yue et al. (2024)	The updated version of YIBs model with dynamic coupling between carbon and water cycles.
ISAM	Jain et al. (2013), Meiyappan et al. (2015), Shu et al. (2020)	Vertically resolved soil biogeochemistry (carbon and nitrogen) module, following Shu et al. (2020),
ISBA-CTRIP	Delire et al. (2020)	No change.
JSBACH	Mauritsen et al. (2019), Reick et al. (2021)	Minor bug fixes in post-processing
JULES-ES	Wiltshire et al. (2021), Sellar et al. (2019), Burton et al. (2019)	Minor bug fixes. (Using JULES v7.4)
LPJ-GUESS	Smith et al. (2014)	No change.
LPJml	Schaphoff et al., 2018, von Bloh et al., 2018, Lutz et al., 2019 (tillage), Heinke et al., 2023 (livestock grazing)	No change
LPJwsl	Poulter et al. (2011) (d)	Minor bug fixes, weighting of fire carbon by GFED to simulate annual cycle
LPX-Bern	Lienert and Joos (2018)	No change.
OCN	Zaehle and Friend (2010), Zaehle et al. (2011)	No change.
ORCHIDEEv3	Krinner et al. (2005), Zaehle and Friend (2010), Vuichard et al. (2019)	No change.
SDGVM	Woodward and Lomas (2004), Walker et al. (2017)	Parameter adjustment for reducing evaporation from vegetation that intercepted precipitation, as well as other adjustments to the calculation of evapotranspiration; bug fix in output of monthly NEP, NBP, soilr, and rh; bug fix on cLeaf monthly output; further development on gross land-use transitions, tracking of carbon from wood & crop harvest, and tracking of primary & secondary vegetation.
VISIT	Ito and Inatomi (2012), Kato et al. (2013)	No change.

Intermediate complexity land carbon cycle model		
CARDAMOM	Bloom et al. (2016), Smallman et al. (2021)	No change.
Global ocean biogeochemistry models		
NEMO-PlankTOM12	Wright et al. (2021)	Minor bug fixes, change to salinity restoring and restart file. New atmospheric CO2 input for simulations A and C.
NEMO4.2-PISCES (IPSL)	Aumont et al. (2015)	Switch to the new model version NEMO4.2-PISCES. Update following the new protocol (with 1750 preindustrial CO2 for spin-up). New atmospheric CO2 input for simulations A and C.
MICOM-HAMOCC (NorESM1-OCv1.2)	Schwinger et al. (2016)	No change in model set-up. New atmospheric CO2 file for simulations A and C. Corrected diagnostic output for pco2atm; diagnostic output for sfco2 and spco2 provided at the air-sea interface (not with respect to dry air at 1 atm).
MPIOM-HAMOCC6	Lacroix et al. Global Change Biology 2021	No change; only updated atmosphere CO2 input for A and C experiments and run 1948-2023.
NEMO3.6-PISCESv2-gas (CNRM)	Berthet et al. (2019) Séférian et al. (2019)	Updated simulations using 1750 preindustrial conditions instead of 1850. No change in model configuration. New atmospheric CO2 input for simulations A and C
FESOM2.1-REcoM3	Gürses et al. (2023)	Updated atmospheric CO2 for simulations A and C.
MOM6-COBALT (Princeton)	Liao et al. (2020)	No change.
CESM-ETHZ	Doney et al. (2009)	Compared to the 2023 submission, the spinup was extended to 1422 years before 1750. Also, starting at 1751 the new atmospheric CO2 concentrations provided by GCB have been used for simulations A and C.
MRI-ESM2-3	Tsujino et al. (2024), Sakamoto et al. (2023)	Iron circulation and its limitation on primary production are introduced. Updated atmospheric CO2 for simulations A and C
ACCESS (CSIRO)	Law et al. (2017)	No change in model set-up (since GCB2023). Updated atmospheric CO2 for simulations A and C.
fCO2-products		
VLIZ-SOMFFN (former MPI-SOM-FFN)	Landschützer et al. (2016)	Time period 1982-2023; The estimate now covers the full open ocean and coastal domain as well as the Arctic Ocean extension by merging 2 MLD proxies for year round full coverage. Additionally, in the SOM step, the Seaflux climatology is now used
Jena-MLS	Rödenbeck et al. (2014) updated to	Time period extended to 2023

	Rödenbeck et al (2022)	
CMEMS-LSCE-FFNNv2	Chau et al. (2022)	Time period now 1985-2023
UEXP-FNN-U (previously Watson et al.)	Watson et al. (2020) and Ford et al. (accepted)	Updated CCI-SST to v3 (Embury et al. 2024), with cool bias with respect to global drifter observations corrected following recommendations in Dong et al. (2022). Updated SOM-FFN implementation to Python.
NIES-ML3	Zeng et al. (2022)	Updated time period 1982-2023.
JMA-MLR	Iida et al. (2021)	Time period extended to 2023
OceanSODA-ETHZv2	Gregor et al. (2024)	Updated method following Gregor et al 2024 and time period extended to 2023
LDEO-HPD	Gloege et al. 2022 and Bennington et al. 2022	Timeperiod extended to 2023
CSIR-ML6	Gregor et al. (2019)	Time period 1982-2023.
Atmospheric inversions		
Jena CarboScope	Rödenbeck et al. (2018), Stephens et al. (2007)	Extension to end of year 2023. Slight change in station set. In the NBE-T inversion, removal of the relaxation term, instead, filtering out decadal variations from air temperature. Adding an additive correction to the result of the NBE-T inversion, to account for CO2 flux IAV not related to air temperature, based on 8 long atmospheric records available near-continuously since at least 1976. TM3 driven by ERA5 rather than NCEP.
CAMS	Chevallier et al. (2005), Remaud et al. (2018)	Extension to year 2023. Increase of the 3D resolution with hexagonal prisms rather than rectangular parallelepipeds (3 times more 3D cells than the previous submission). Update of the prior fluxes.
CarbonTracker Europe (CTE)	van der Laan-Luijkx et al. (2017)	Extension to 2023, update of prior fluxes.
NISMON-CO2	Niwa et al. (2022), Niwa et al. (2017).	Extension to 2023, update of prior fluxes.
CT-NOAA	Jacobson et al. (2023a), Jacobson et al. (2024), Byrne et al. (2023), Krol et al. (2005), Peiro et al. (2022)	Extended to 2023 using the CarbonTracker Near-Real Time release CT-NRT.v2024-1 (Jacobson et al. 2024).
CMS-Flux	Liu et al. (2021)	Extension to 2023, update of prior fluxes.
CAMS-Satellite	Chevallier et al. (2005), Remaud et al. (2018)	Extension to year 2023. Increase of the 3D resolution with hexagonal prisms rather than rectangular parallelepipeds (3 times more 3D cells than the previous submission). Update of the prior fluxes.

GONGGA	Jin et al. (2023), Nassar et al. (2010)	Extension to 2023, update of prior fluxes.
COLA	Liu et al. (2022)	Extension to 2023, update of prior fluxes.
GCASv2	Jiang et al. (2021) & Emmons et al. (2010)	Extension to 2023, update of prior fluxes.
UoE in-situ	Feng et al. (2016) & Palmer et al. (2019)	Extension to 2023, update of prior fluxes.
IAPCAS	Yang et al. (2021) & Feng et al. (2016)	Extension to 2023, update of prior fluxes.
MIROC4-ACTM	Chandra et al. (2022) & Patra et al. (2018)	Extension to 2023, update of prior fluxes using only CASA and not VISIT. Less observation sites used in the assimilation (46 instead of 50).
NTFVAR	Nayagam et al. (2024) & Maksyutov et al. (2021)	New this year
Earth System Models		
CanESM5	Swart et al. (2019), Sospedra-Alfonso et al. (2021)	Reconstructions are extended to 1960-2023, and predictions are extended to 2024.
EC-Earth3-CC	Döscher et al. (2021), Bilbao et al. (2021), Bernardello et al. (2024)	New this year.
IPSL-CM6A-CO2-LR	Boucher et al. (2020)	Reconstructions are extended to 1960-2023, and predictions are extended to 2024. No change to model, the CMIP6 CovidMIP CO2 emissions after 2015 are used.
MIROC-ES2L	Watanabe et al. (2020)	Reconstructions are extended to 1960-2023, and predictions are extended to 2024. No change to model, the simulations were rerun including a long spinup.
MPI-ESM1-2-LR	Mauritsen et al. (2019), Li et al. (2023)	Reconstructions are extended to 1960-2023, and predictions are extended to 2024.

Table 5. Comparison of results from the bookkeeping method and budget residuals with results from the DGVMs, as well as additional estimates from atmospheric oxygen, atmospheric inversions and Earth System Models (ESMs) for different periods, the last decade, and the last year available. All values are in GtCyr⁻¹. See Figure 7 for explanation of the bookkeeping component fluxes. The DGVM uncertainties represent ±1σ of the decadal or annual (for 2023) estimates from the individual DGVMs: for the inverse systems the mean and range of available results is given. All values are rounded to the nearest 0.1 GtC and therefore columns do not necessarily add to zero.

		Mean (GtC/yr)							
		1960s	1970s	1980s	1990s	2000s	2014-2023	2023	
Land-use change emissions (ELUC)	Bookkeeping (BK) Net flux (1a)	1.6±0.7	1.4±0.7	1.4±0.7	1.6±0.7	1.4±0.7	1.1±0.7	1±0.7	Formatted Table
	▼ BK - deforestation (total)	1.7 [1.3,2.2]	1.6 [1.2,2]	1.6 [1.3,1.9]	1.8 [1.6,2]	1.9 [1.6,2.2]	1.7 [1.4,2.3]	1.7 [1.3,2.3]	Deleted:
	▼ BK - forest regrowth (total)	-0.8 [- 1.1,0.6]	-0.9 [- 1.1,-0.7]	-0.9 [- 1,-0.7]	-0.9 [- 1.1,-0.8]	-1.1 [- 1.2,-0.9]	-1.2 [- 1.5,-0.9]	-1.2 [- 1.5,-0.9]	Deleted:
	▼ BK - other transitions	0.3 [0.3,0.4]	0.2 [0.2,0.3]	0.2 [0.1,0.3]	0.1 [0,0.2]	0.1 [0,0.1]	0.1 [0,0.1]	0 [0,0.1]	Deleted:
	▼ BK - peat drainage & peat fires	0.2 [0.1,0.2]	0.2 [0.1,0.2]	0.2 [0.2,0.2]	0.3 [0.2,0.3]	0.2 [0.2,0.3]	0.2 [0.2,0.3]	0.2 [0.2,0.3]	Deleted:
	▼ BK - wood harvest & forest management	0.2 [- 0.2,0.6]	0.3 [- 0.2,0.6]	0.3 [- 0.2,0.7]	0.3 [- 0.1,0.6]	0.3 [- 0.1,0.6]	0.3 [0,0.6]	0.3 [0,0.7]	Deleted:
	DGVMs-net flux (1b)	1.5±0.5	1.5±0.5	1.5±0.5	1.7±0.5	1.7±0.6	1.5±0.6	1.2±0.7	
Terrestrial sink (SLAND)	Residual sink from global budget (EFOS+ELUC(1a)-GATM-SOCEAN) (2a)	1.7±0.8	1.9±0.8	1.6±0.9	2.6±0.9	2.8±0.9	2.7±0.9	2.3±1	
	DGVMs (2b)	1.2±0.5	2±0.8	1.8±0.8	2.5±0.6	2.8±0.7	3.2±0.9	2.3±1	
Net land fluxes (SLAND-ELUC)	GCB2024 Budget (2b-1a)	- 0.4±0.9	0.5±1.1	0.4±1.1	0.9±0.9	1.4±1	2.1±1.1	1.3±1.2	
	Atmospheric O ₂	---	---	---	1.3±0.7	1±0.7	1±0.8	-	
	DGVMs-net (2b-1b)	- 0.3±0.5	0.5±0.7	0.3±0.6	0.8±0.4	1.1±0.4	1.7±0.6	1.1±0.8	
	Inversions*	- [-,-]	- [-,-]	0.3 [0.3,0.4] (2)	0.9 [0.6,1.1] (3)	1.2 [0.6,1.5] (4)	1.4 [0.3,2.2] (10)	0.9 [- 0.1-2.7] (14)	
	ESMs	0 [- 0.7,0.5]	1.5 [1.2,2]	1 [0.5,1.4]	1.7 [1.2,2.4]	1.8 [0.4,2.7]	2.2 [0.3,3.6]	1.8 [- 2.9-3.7]	

*Estimates are adjusted for the pre-industrial influence of river fluxes, for the cement carbonation sink, and adjusted to common EFOS (Sect. 2.7). The ranges given include varying numbers (in parentheses) of inversions in each decade (Table A4)

Deleted: Section Break (Next Page)

Table 6: Comparison of results for the ocean sink from the $f\text{CO}_2$ -products, from global ocean biogeochemistry models (GOBMs), the best estimate for GCB2024 as calculated from $f\text{CO}_2$ -products and GOBMs that is used in the budget Table 7, as well as additional estimates from atmospheric oxygen, atmospheric inversions and Earth System Models (ESMs) for different periods, the last decade, and the last year available. All values are in GtCyr^{-1} . Uncertainties represent $\pm 1\sigma$ of the estimates from the GOBMs ($N > 10$) and range of ensemble members is given for ensembles with $N < 10$ ($f\text{CO}_2$ -products, inversions, ESMs). The uncertainty of the GCB2024 budget estimate is based on expert judgement (Section 2 and Supplementary S1 to S4) and for oxygen it is the standard deviation of a Monte Carlo ensemble (Section 2.8).

Formatted: Font: Times New Roman, 10 pt, Not Italic

<i>Mean (GtC/yr)</i>							
Product	1960s	1970s	1980s	1990s	2000s	2014-2023	2023
$f\text{CO}_2$ -products	---	---	---	2.3 [1.9,2.9]	2.5 [2.3,2.7]	3.1 [2.9,3.7]	3 [2.3,4]
GOBMs	1±0.2	1.3±0.3	1.8±0.3	2±0.3	2.2±0.3	2.6±0.4	2.7±0.4
GCB2024 Budget	1.2±0.4	1.5±0.4	1.9±0.4	2.1±0.4	2.3±0.4	2.9±0.4	2.9±0.4
Atmospheric O ₂	---	---	---	2±0.5	2.8±0.4	3.4±0.5	-
Inversions	- [-,-]	- [-,-]	1.8 [1.8,1.9] (2)	2.3 [2.1,2.5] (3)	2.5 [2.3,3.1] (4)	3.1 [2.4,4.1] (10)	3 [1.8-4.1] (14)
ESMs	0.7 [0.1,1.1]	1 [0.4,1.4]	1.4 [0.7,1.7]	1.7 [1.1,2]	1.9 [1.5,2.2]	2.5 [2.2,2.8]	2.5 [2.2-3]

Formatted: Font: Cambria, 12 pt

Formatted: Normal, Line spacing: Multiple 1.15 li, No widow/orphan control

b.

Table 7: Decadal mean in the five components of the anthropogenic CO₂ budget for different periods, and last year available. All values are in GtC yr⁻¹, and uncertainties are reported as ±1σ. Fossil CO₂ emissions include cement carbonation. The table also shows the budget imbalance (B_M), which provides a measure of the discrepancies among the nearly independent estimates. A positive imbalance means the emissions are overestimated and/or the sinks are too small. All values are rounded to the nearest 0.1 GtC and therefore columns do not necessarily add to zero.

		<i>Mean (GtC/yr)</i>							
		1960s	1970s	1980s	1990s	2000s	2014-2023	2023	2024 (Projection)
Total emissions (EFOS + ELUC)	Fossil CO ₂ emissions (EFOS)	3±0.2	4.7±0.2	5.5±0.3	6.4±0.3	7.8±0.4	9.7±0.5	10.1±0.5	10.2±0.5
	Land-use change emissions (ELUC)	1.6±0.7	1.4±0.7	1.4±0.7	1.6±0.7	1.4±0.7	1.1±0.7	1±0.7	1.2±0.7
	Total emissions	4.6±0.7	6.1±0.7	6.9±0.8	7.9±0.8	9.2±0.8	10.8±0.9	11.1±0.9	11.4±0.9
	Growth rate in atmospheric CO ₂ (GATM)	1.7±0.07	2.8±0.07	3.4±0.02	3.1±0.02	4±0.02	5.2±0.02	5.9±0.2	6.0±0.3
Partitioning	Ocean sink (SOCEAN)	1.2±0.4	1.5±0.4	1.9±0.4	2.1±0.4	2.3±0.4	2.9±0.4	2.9±0.4	3±0.6
	Terrestrial sink (SLAND)	1.2±0.5	2±0.8	1.8±0.8	2.5±0.6	2.8±0.7	3.2±0.9	2.3±1	3.2±1.5
Budget Imbalance	BIM=E FOS+E LUC-(GATM +SOCE)	0.5	-0.1	-0.2	0.1	0	-0.4	0	-0.9

Formatted Table

Deleted: 1

Deleted: 3

Deleted: 5.9±

Deleted: .5

Deleted: 7

	1960s	1970s	1980s	1990s	2000s	2014-2023	2023	2024 (Projection)
AN+SL AND)								

Formatted Table

*Fossil emissions excluding the cement carbonation sink amount to 3 ± 0.2 GtC/yr, 4.7 ± 0.2 GtC/yr, 5.5 ± 0.3 GtC/yr, 6.4 ± 0.3 GtC/yr, 7.9 ± 0.4 GtC/yr, and 9.9 ± 0.5 GtC/yr for the decades 1960s to 2010s respectively and to 10.3 ± 0.5 GtC/yr for 2023, and 10.4 ± 0.5 GtC/yr for 2024.

Table 8. Cumulative CO₂ for different time periods in gigatonnes of carbon (GtC). Fossil CO₂ emissions include cement carbonation. The budget imbalance (B_{IM}) provides a measure of the discrepancies among the nearly independent estimates. All values are rounded to the nearest 5 GtC and therefore columns do not necessarily add to zero. Uncertainties are reported as follows: E_{FOS} is 5% of cumulative emissions; E_{LUC} prior to 1959 is 1σ spread from the DGVMs, E_{LUC} post-1959 is 0.7*number of years (where 0.7 GtC/yr is the uncertainty on the annual E_{LUC} flux estimate); G_{ATM} uncertainty is held constant at 5 GtC for all time periods; S_{OCEAN} uncertainty is 20% of the cumulative sink (20% relates to the annual uncertainty of 0.4 GtC/yr, which is ~20% of the current ocean sink); and S_{LAND} is the 1σ spread from the DGVMs estimates.

		1750-2023	1850-2014	1850-2023	1960-2023	1850-2024
Emissions	Fossil CO ₂ emissions (EFOS)	490±25	400±20	490±25	410±20	500±25
	Land-use change emissions (ELUC)	255±75	215±60	225±65	90±45	225±65
	Total emissions	745±80	615±65	710±70	500±50	725±70
Partitioning	Growth rate in atmos CO ₂ (G _{ATM})	305±5	235±5	285±5	220±5	290±5
	Ocean sink (S _{OCEAN})	195±40	160±30	185±35	130±25	185±35
	Terrestrial sink (S _{LAND})	245±65	190±55	220±60	150±40	225±60
Budget imbalance	B _{IM} =EFOS+ELUC-(G _{ATM} +S _{OCEAN} +S _{LAND})	0	30	25	0	20

Formatted Table

Table 9. Average annual growth rate in fossil CO₂ emissions over the most recent decade (2014-2023) and the previous decade (2004-2013). The data for the World include the cement carbonation sink. IAS are emissions from international aviation and shipping. Rest of the World is World minus China, USA, EU27, India and IAS.

	World	China	USA	EU27	India	OECD	Non-OECD	IAS	Rest of the World
2004-2013	2.4%	7.5%	-1.4%	-1.8%	6.4%	-0.9%	4.9%	2.6%	1.9%
2014-2023	0.6%	1.9%	-1.2%	-2.1%	3.6%	-1.4%	1.8%	-1.6%	0.4%

Deleted: .

Formatted Table

Deleted: Page Break

Table 10. Major known sources of uncertainties in each component of the Global Carbon Budget, defined as input data or processes that have a demonstrated effect of at least ±0.3 GtC yr⁻¹.

Source of uncertainty	Time scale (years)	Location	Evidence
Fossil CO₂ emissions (EFOS; Section 2.1)			
energy statistics	annual to decadal	global, but mainly China & major developing countries	(Korsbakken et al., 2016, Guan et al., 2012)
carbon content of coal	annual to decadal	global, but mainly China & major developing countries	(Liu et al., 2015)
system boundary	annual to decadal	all countries	(Andrew, 2020a)
Net land-use change flux (ELUC; section 2.2)			
land-cover and land-use change statistics	continuous	global; in particular tropics	(Houghton et al., 2012, Gasser et al., 2020, Ganzenmüller et al., 2022, Yu et al. 2022)
sub-grid-scale transitions	annual to decadal	global	(Wilkenskjeld et al., 2014, Bastos et al., 2021)
vegetation biomass	annual to decadal	global; in particular tropics	(Houghton et al., 2012, Bastos et al., 2021)
forest degradation (fire, selective logging)	annual to decadal	tropics; Amazon	(Aragão et al., 2018, Qin et al., 2021, Lapola et al., 2023)
wood and crop harvest	annual to decadal	global; SE Asia	(Arneth et al., 2017, Erb et al., 2018)
peat burning	multi-decadal trend	global	(van der Werf et al., 2010, 2017)
loss of additional sink capacity	multi-decadal trend	global	(Pongratz et al., 2014, Gasser et al., 2020; Obermeier et al., 2021; Dorgeist et al., 2024)

Formatted Table

environmental effects	multi-decadal trend	global	(Gasser et al. 2020, Dorgeist et al., 2024)
Atmospheric growth rate (GATM; section 2.4) no demonstrated uncertainties larger than ± 0.3 GtC yr ⁻¹ . The uncertainties in GATM have been estimated as ± 0.2 GtC yr ⁻¹ , although the conversion of the growth rate into a global annual flux assuming instantaneous mixing throughout the atmosphere introduces additional errors that have not yet been quantified.			
Ocean sink (SOCEAN; section 2.5)			
sparsity in surface fCO ₂ observations	mean, decadal variability and trend	global, in particular southern hemisphere	(Gloege et al., 2021, Denvil-Sommer et al., 2021, Hauck et al., 2023a; Dong et al., 2024b)
riverine carbon outgassing and its anthropogenic perturbation	annual to decadal	global, in particular partitioning between Tropics and South	(Aumont et al., 2001, Lacroix et al., 2020, Crisp et al., 2022)
Models underestimate interior ocean anthropogenic carbon storage	annual to decadal	global	(Friedlingstein et al., 2022a, this study, DeVries et al., 2023, Müller et al., 2023)
near-surface temperature and salinity gradients	mean on all time-scales	global	(Watson et al., 2020, Dong et al., 2022, Bellenger et al., 2023, Dong et al., 2024a)
Land sink (SLAND; section 2.6)			
strength of CO ₂ fertilisation	multi-decadal trend	global	(Wenzel et al., 2016; Walker et al., 2021)
response to variability in temperature and rainfall	annual to decadal	global; in particular tropics	(Cox et al., 2013; Jung et al., 2017; Humphrey et al., 2018; 2021)
nutrient limitation and supply	annual to decadal	global	(Zaehle et al., 2014)
carbon allocation and tissue turnover rates	annual to decadal	global	(De Kauwe et al., 2014; O'Sullivan et al., 2022)

tree mortality	annual	global in particular tropics	(Hubau et al., 2021; Brienen et al., 2020)
response to diffuse radiation	annual	global	(Mercado et al., 2009; O'Sullivan et al., 2021)
estimation under constant pre-industrial land cover	multi-decadal trend	global	(Gasser et al. 2020, Dorgeist et al., 2024)

Figures

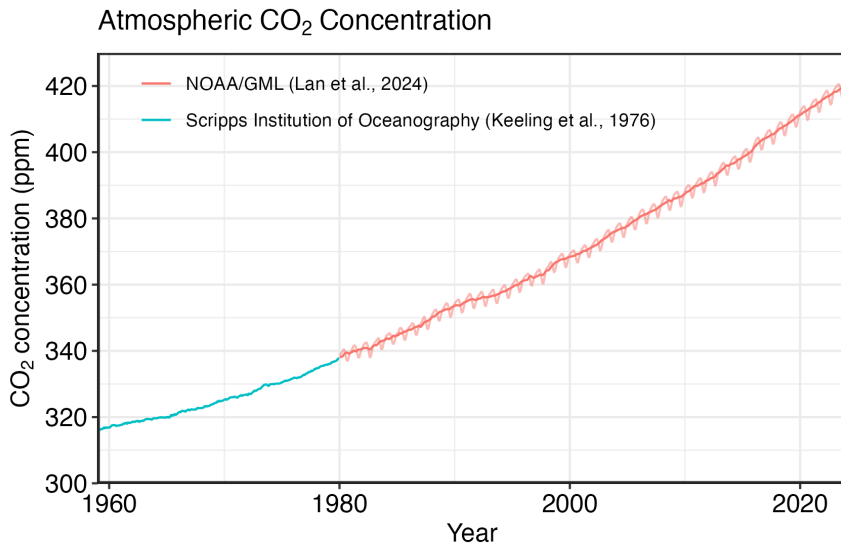
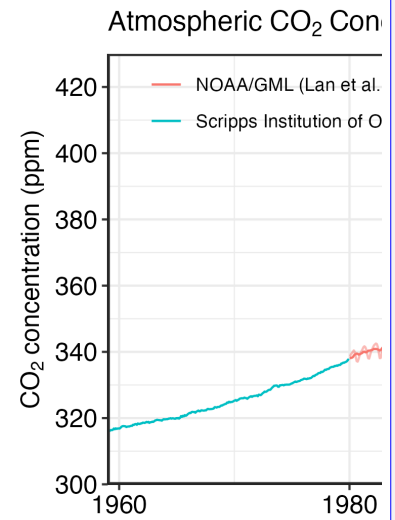


Figure 1. Surface average atmospheric CO₂ concentration (ppm). Since 1980, monthly data are from NOAA/GML (Lan et al., 2024a) and are based on an average of direct atmospheric CO₂ measurements from multiple stations in the marine boundary layer (Masarie and Tans, 1995). The 1958-1979 monthly data are from the Scripps Institution of Oceanography, based on an average of direct atmospheric CO₂ measurements from the Mauna Loa and South Pole stations (Keeling et al., 1976). To account for the difference of mean CO₂ and seasonality between the NOAA/GML and the Scripps station networks used here, the Scripps surface average (from two stations) was de-seasonalised and adjusted to match the NOAA/GML surface average (from multiple stations) by adding the mean difference of 0.667 ppm, calculated here from overlapping data during 1980-2012.

Deleted: and Captions

Formatted: French

Formatted: Indent: Left: 0.63 cm, Hanging: 0.63 cm



Deleted:

Formatted: Font: Not Bold

Formatted: Heading 2

Deleted: 2024

Formatted: Font: Not Bold

The global carbon cycle

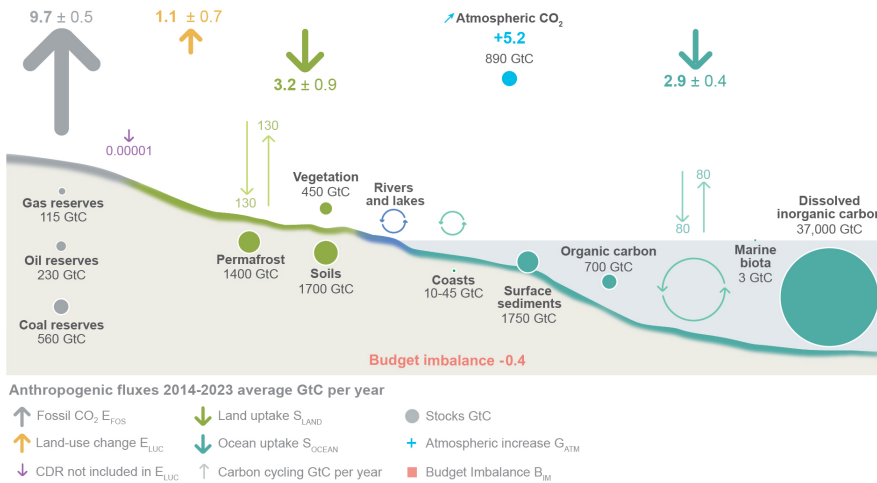
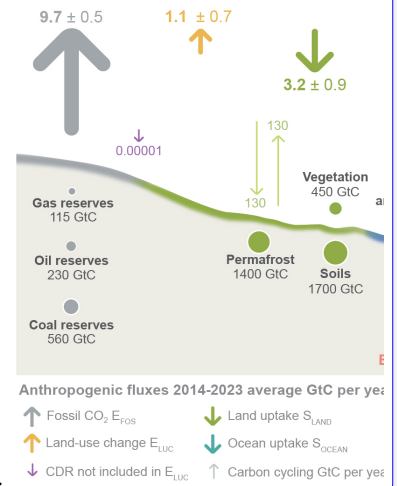


Figure 2. Schematic representation of the overall perturbation of the global carbon cycle caused by anthropogenic activities, averaged globally for the decade 2014-2023. See legends for the corresponding arrows. Fluxes estimates and their 1 standard deviation uncertainty are as reported in Table 7. The CDR estimate is for the year 2023 only. The uncertainty in the atmospheric CO₂ growth rate is very small (± 0.02 GtC yr⁻¹) and is neglected for the figure. The anthropogenic perturbation occurs on top of an active carbon cycle, with fluxes and stocks represented in the background and taken from Canadell et al. (2021) for all numbers, except for the carbon stocks in coasts which is from a literature review of coastal marine sediments (Price and Warren, 2016). Fluxes are in GtC yr⁻¹ and reservoirs in GtC.

The global carbon cycle



Deleted:

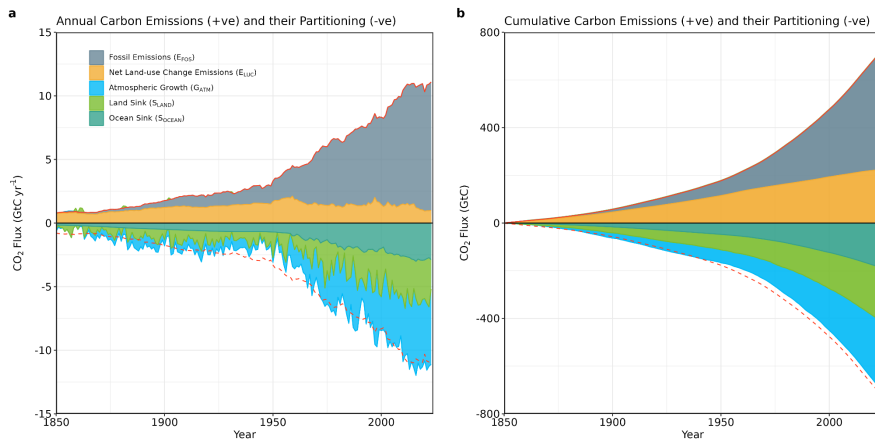
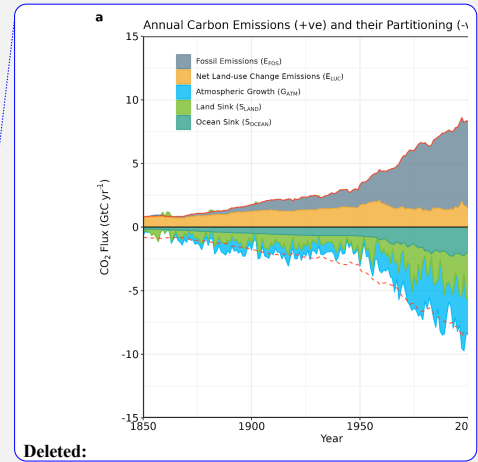


Figure 3. Combined components of the global carbon budget as a function of time, for fossil CO₂ emissions (E_{FOS} , including a small sink from cement carbonation; grey) and emissions from land-use change (E_{LUC} ; brown), as well as their partitioning among the atmosphere (G_{ATM} ; cyan), ocean (S_{OCEAN} ; blue), and land (S_{LAND} ; green). Panel (a) shows annual estimates of each flux (in $GtC\ yr^{-1}$) and panel (b) the cumulative flux (the sum of all prior annual fluxes, in GtC) since the year 1850. The partitioning is based on nearly independent estimates from observations (for G_{ATM}) and from process model ensembles constrained by data (for S_{OCEAN} and S_{LAND}) and does not exactly add up to the sum of the emissions, resulting in a budget imbalance (B_{IM}) which is represented by the difference between the bottom red line (mirroring total emissions) and the sum of carbon fluxes in the ocean, land, and atmosphere reservoirs. All data are in $GtC\ yr^{-1}$ (panel a) and GtC (panel b). The E_{FOS} estimate is based on a mosaic of different datasets, and has an uncertainty of $\pm 5\%$ ($\pm 1\sigma$). The E_{LUC} estimate is from four bookkeeping models (Table 4) with uncertainty of $\pm 0.7\ GtC\ yr^{-1}$. The G_{ATM} estimates prior to 1959 are from Joos and Spahni (2008) with uncertainties equivalent to about $\pm 0.1-0.15\ GtC\ yr^{-1}$ and from Lan et al. (2024a) since 1959 with uncertainties of about $\pm 0.07\ GtC\ yr^{-1}$ during 1959-1979 and $\pm 0.02\ GtC\ yr^{-1}$ since 1980. The S_{OCEAN} estimate is the average from Khatiwala et al. (2013) and DeVries (2014) with uncertainty of about $\pm 30\%$ prior to 1959, and the average of an ensemble of models and an ensemble of fCO_2 -products (Table 4) with uncertainties of about $\pm 0.4\ GtC\ yr^{-1}$ since 1959. The S_{LAND} estimate is the average of an ensemble of models (Table 4) with uncertainties of about $\pm 1\ GtC\ yr^{-1}$. See the text for more details of each component and their uncertainties.



Deleted:

Deleted: 2024

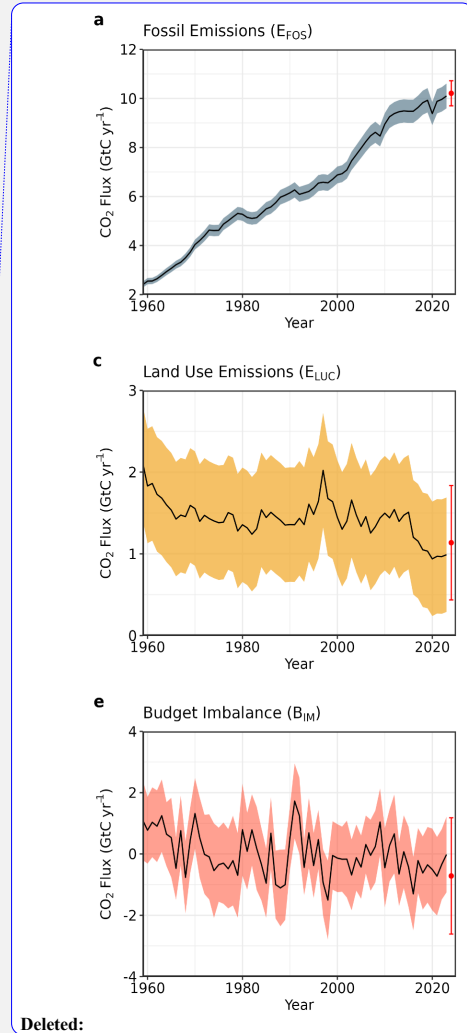
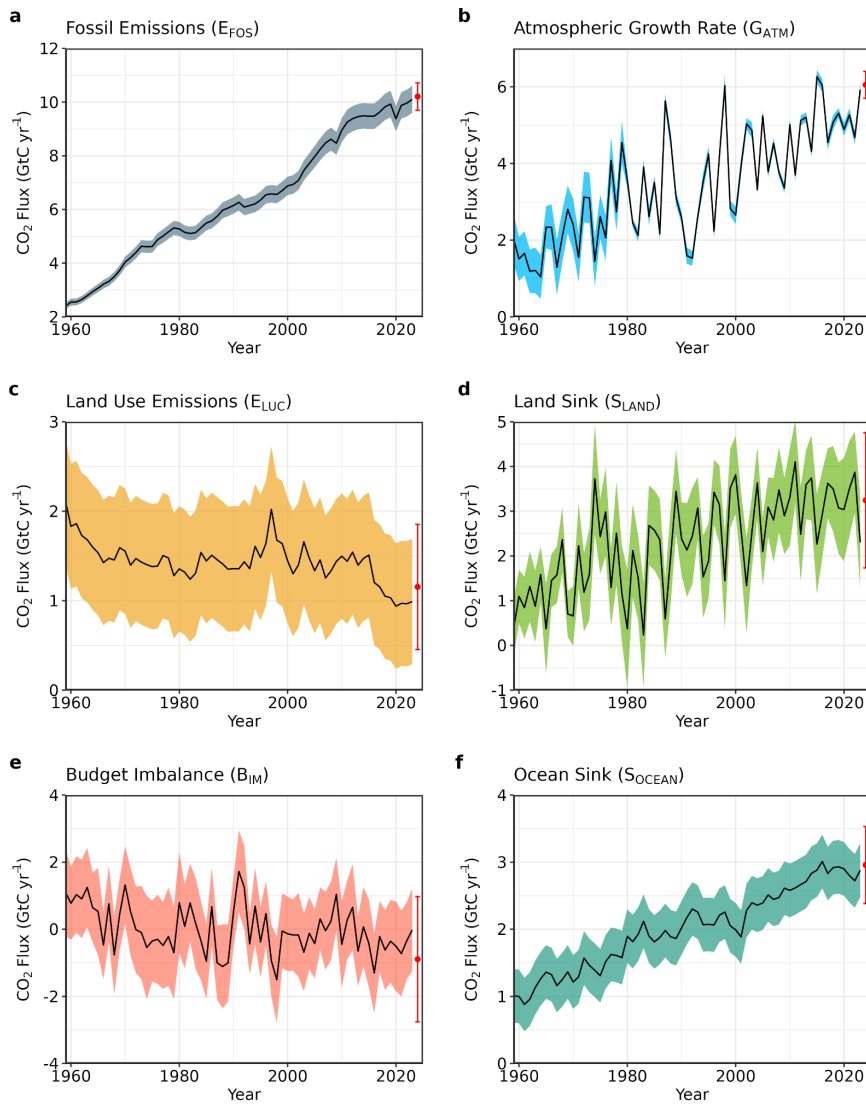


Figure 4. Components of the global carbon budget and their uncertainties as a function of time, presented individually for (a) fossil CO₂, including cement carbonation emissions (E_{FOS}), (b) growth rate in atmospheric CO₂ concentration (G_{ATM}), (c) emissions from land-use change (E_{LUC}), (d) the land CO₂ sink (S_{LAND}), (e) the ocean CO₂ sink (S_{OCEAN}), (f) the budget imbalance (B_{IM}) that is not accounted for by the other terms. Positive values of S_{LAND} and S_{OCEAN} represent a flux from the atmosphere to land or the ocean. All data are in $GtC\ yr^{-1}$

with the uncertainty bounds representing ± 1 standard deviation in shaded colour. Data sources are as in Figure 3. The red dots indicate our projections for the year 2024 and the red error bars the uncertainty in the 2024 projections (see methods).

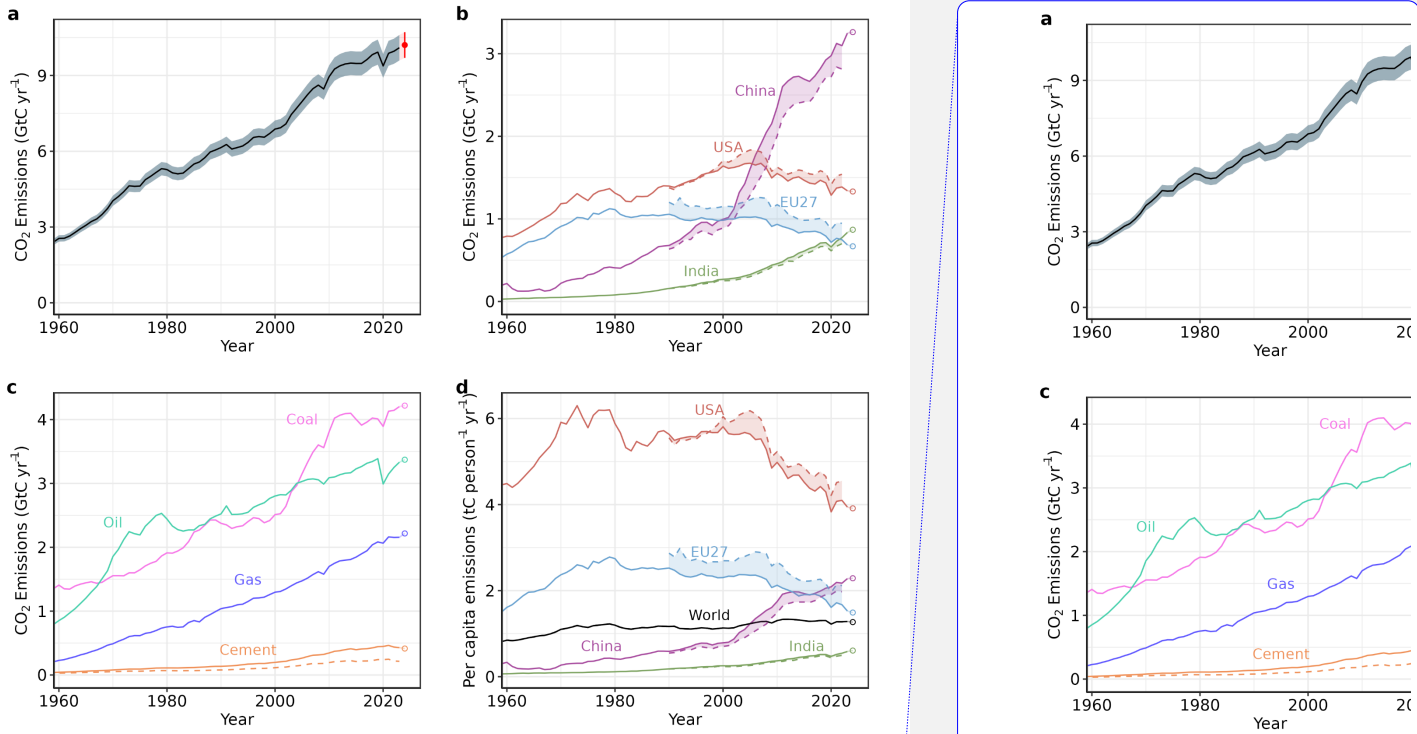


Figure 5. Fossil CO₂ emissions for (a) the globe, including an uncertainty of $\pm 5\%$ (grey shading) and a projection through the year 2024 (red dot and uncertainty range), (b) territorial (solid lines) and consumption (dashed lines) emissions for the top three country emitters (USA, China, India) and for the European Union (EU27), (c) global emissions by fuel type, including coal, oil, gas, and cement, and cement minus cement carbonation (dashed), and (d) per-capita emissions the world and for the large emitters as in panel (b). Territorial emissions are primarily from a draft update of Hefner and Marland (2023) except for national data for most Annex I countries for 1990-2022, which are reported to the UNFCCC as detailed in the text, as well as some improvements in individual countries, and extrapolated forward to 2023 using data from Energy Institute. Consumption-based emissions are updated from Peters et al. (2011a). See Section 2.1 and Supplement S.1 for details of the calculations and data sources.

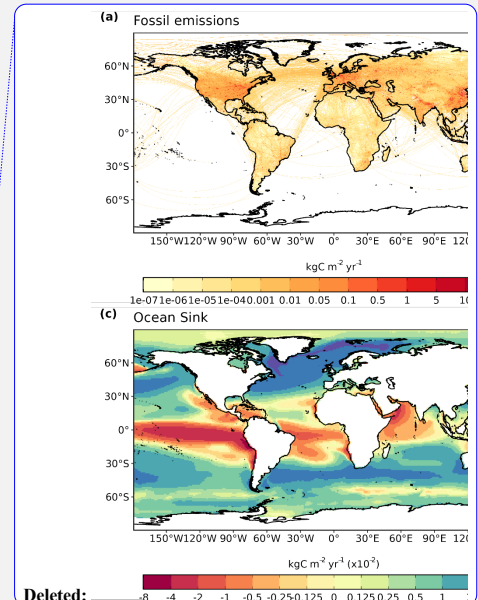
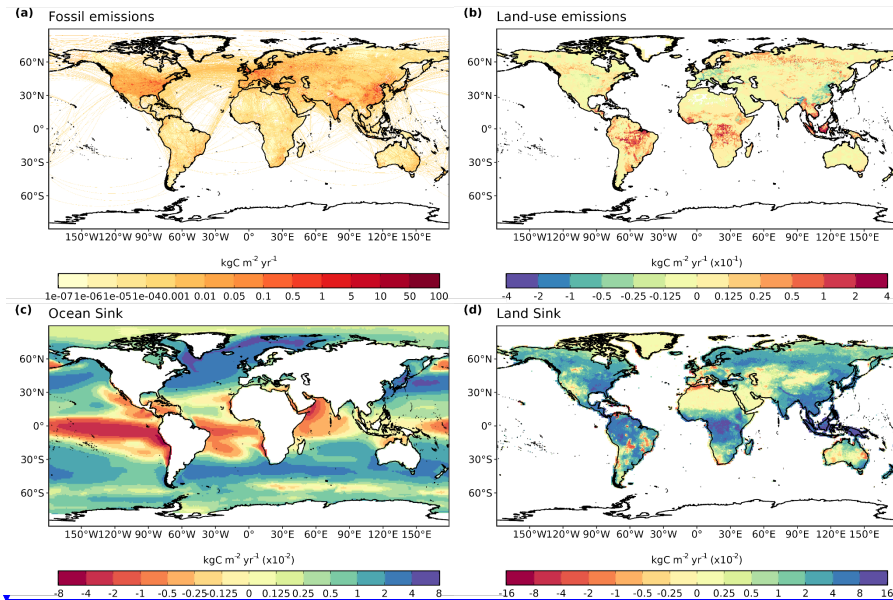


Figure 6. The 2014-2023 decadal mean components of the global carbon budget, presented for (a) fossil CO₂ emissions (E_{FOS}), (b) land-use change emissions (E_{LUC}), (c) the ocean CO₂ sink (S_{OCEAN}), and (d) the land CO₂ sink (S_{LAND}). Positive values for E_{FOS} and E_{LUC} represent a flux to the atmosphere, whereas positive values of S_{OCEAN} and S_{LAND} represent a flux from the atmosphere to the ocean or the land (carbon sink). In all panels, yellow/red colours represent a source (flux from the land/ocean to the atmosphere), green/blue colours represent a sink (flux from the atmosphere into the land/ocean). All units are in $\text{kgC m}^{-2} \text{yr}^{-1}$. Note the different scales in each panel. E_{FOS} data shown is from GCP-GridFEDv2024.0 and does not include cement carbonation. The E_{LUC} map shows the average E_{LUC} from the four bookkeeping models plus emissions from peat drainage and peat fires. BLUE and LUCE provide spatially explicit estimates at 0.25° resolution. Gridded E_{LUC} estimates for H&C2023 and OSCAR are derived by spatially distributing their national data based on the spatial patterns of BLUE gross fluxes in each country (see Schwingshackl et al., 2022, for more details about the methodology). S_{OCEAN} data shown is the average of GOBMs and f_{CO_2} -products means, using GOBMs simulation A, no adjustment for bias and drift applied to the gridded fields (see Section 2.5). S_{LAND} data shown is the average of the DGVMs for simulation S2 (see Section 2.6).

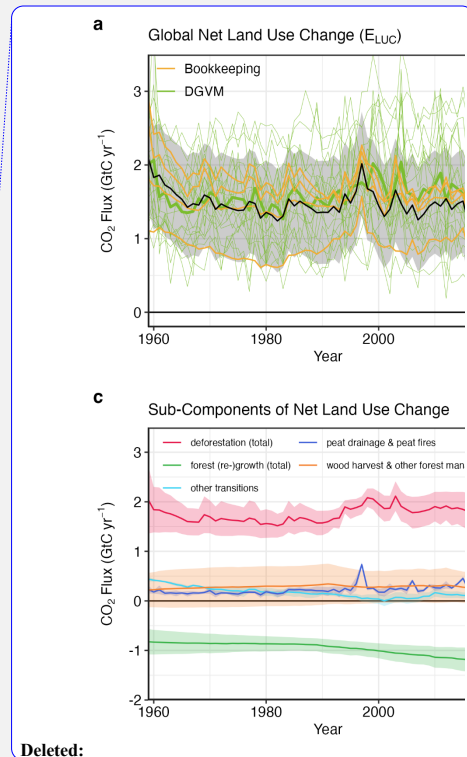
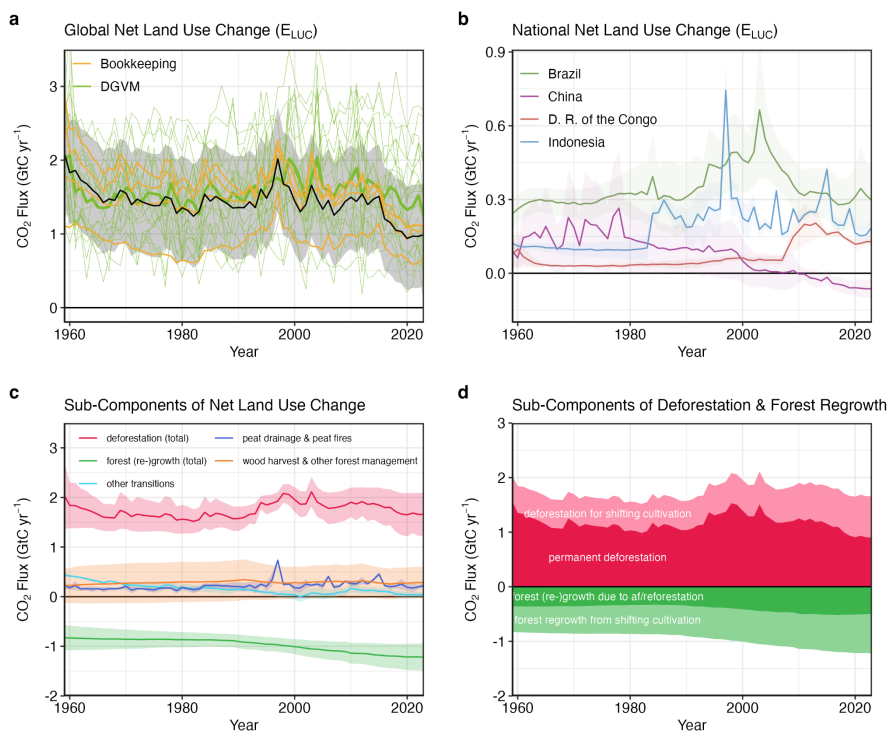
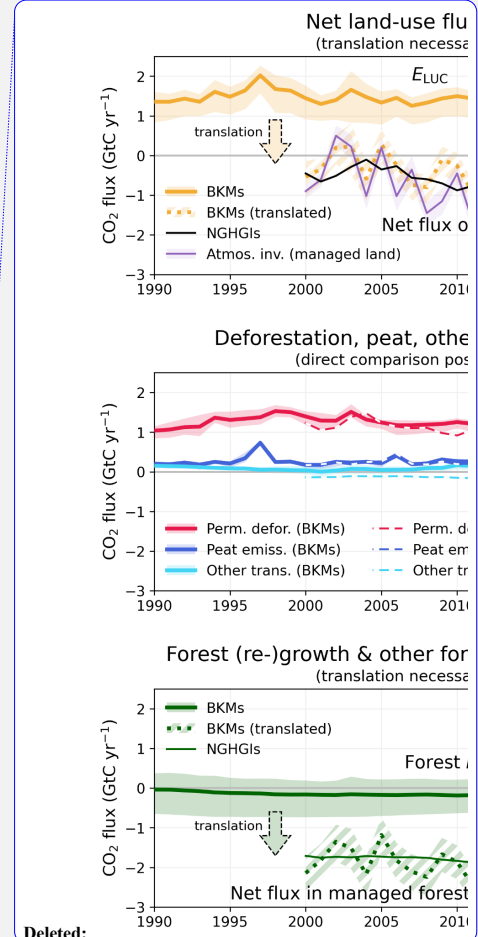
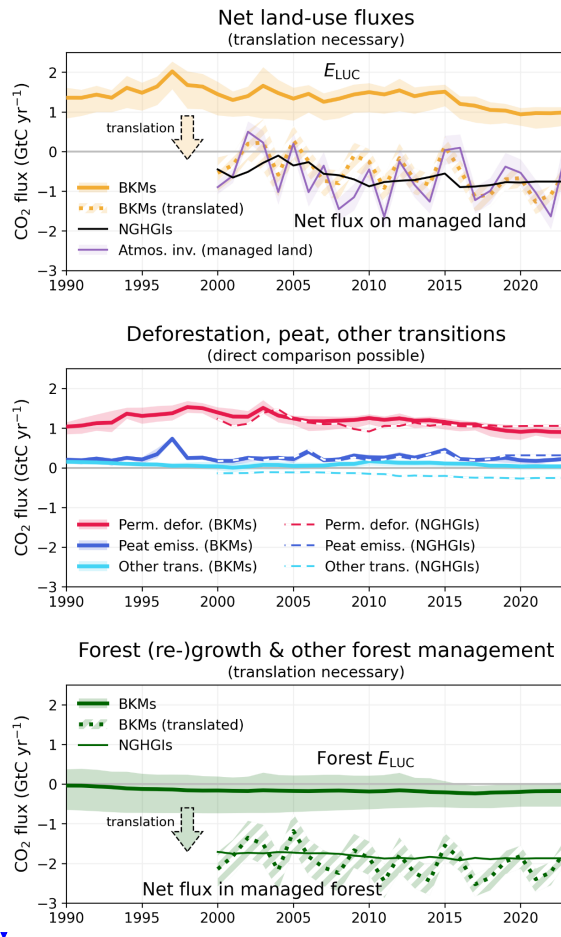


Figure 7. Net CO₂ exchanges between the atmosphere and the terrestrial biosphere related to land use change. (a) Net CO₂ emissions from land-use change (E_{LUC}) with estimates from the four bookkeeping models (yellow lines) and the budget estimate (black with $\pm 1\sigma$ uncertainty), which is the average of the four bookkeeping models. Estimates from individual DGVMs (narrow green lines) and the DGVM ensemble mean (thick green line) are also shown. (b) Net CO₂ emissions from land-use change from the four countries with largest cumulative emissions since 1959. Values shown are the average of the four bookkeeping models, with shaded regions as $\pm 1\sigma$ uncertainty. (c) Sub-components of E_{LUC} : (i) emissions from deforestation (including permanent deforestation and deforestation in shifting cultivation cycles), (ii) emissions from peat drainage & peat fires, (iii) removals from forest (re-)growth (including forest (re-)growth due to afforestation and reforestation and forest regrowth in shifting cultivation cycles), (iv) fluxes from wood harvest and other forest management (comprising slash and product decay following wood harvest, regrowth after wood harvest, and fire suppression), and (v) emissions and removals related to other land-use transitions. The sum of the five components is E_{LUC} shown in panel (a). (d) Sub-components of ‘deforestation (total)’ and of ‘forest (re-)growth (total)’: (i) deforestation in shifting cultivation cycles, (ii) permanent deforestation, (iii) forest (re-)growth due to afforestation and/or reforestation, and (iv) forest regrowth in shifting cultivation cycles.



Deleted:

Figure 8. Comparison of land-use flux estimates from bookkeeping models (BKMs; following the GCB definition of E_{LUC}), national GHG inventories (NGHGIs; following IPCC guidelines and thus including all carbon fluxes on managed land), and atmospheric inversion systems (considering fluxes on managed land only). To compare BKM results with NGHGIs, a translation is necessary for some subcomponents. (a) Net land-use fluxes, for which a translation of BKMs is necessary, (b) subcomponents permanent deforestation, peat drainage & peat fires, and other transitions, which can be directly compared and (c) subcomponent forest (re-)growth & other forest management, for which a translation is necessary. The lines represent the mean of 4 BKMs and 14 atmospheric inversion estimates, respectively; Shaded areas denote the full range across BKM estimates and the standard deviation for atmospheric inversions, respectively. The subcomponent forest (re-)growth & other forest management includes removals from forest (re-)growth (permanent), emissions and removals from wood

harvest & other forest management, and emissions and removals in shifting cultivation cycles. The translation of BKM estimates to NGHGI estimates in (a) and (c) is done by adding the natural land sink in managed forests to the BKM estimates (see also Table S10). The GCB definition of ELUC and the NGHGI definition of land-use fluxes are equally valid, each in its own context. For illustrative purposes we only show the translation of BKM estimates to the NGHGI definition.

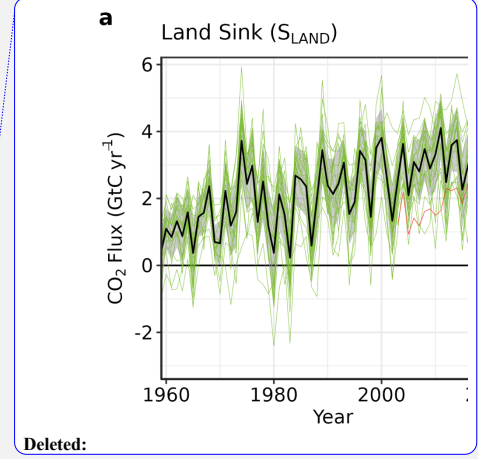
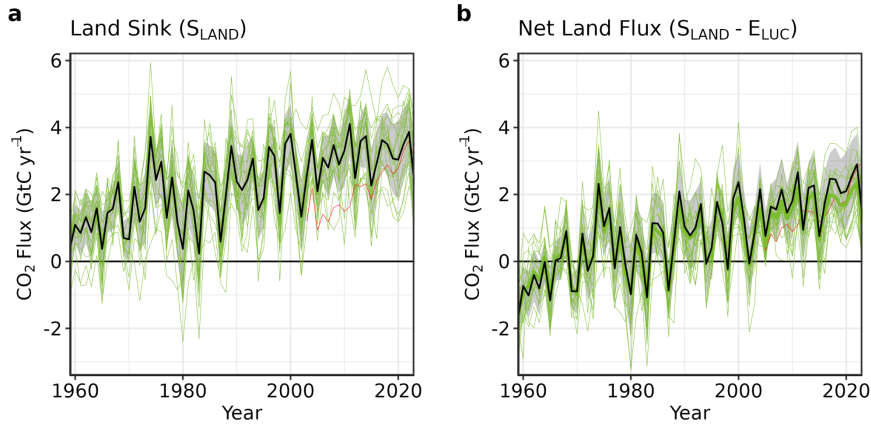


Figure 9. (a) The land CO₂ sink (S_{LAND}) estimated by individual DGVMs (green), and CARDAMOM (red), as well as the budget estimate (black with $\pm 1\sigma$ uncertainty), which is the average of all DGVMs. (b) Net atmosphere-land CO₂ fluxes ($S_{\text{LAND}} - E_{\text{LUC}}$). The budget estimate of the net land flux (black with $\pm 1\sigma$ uncertainty) combines the DGVM estimate of S_{LAND} from panel (a) with the bookkeeping estimate of E_{LUC} from Figure 7a. Uncertainties are similarly propagated in quadrature. DGVMs also provide estimates of E_{LUC} (see Figure 7a), which can be combined with their own estimates of the land sink. Hence panel (b) also includes an estimate for the net land flux for individual DGVMs (thin green lines) and their multi-model mean (thick green line).

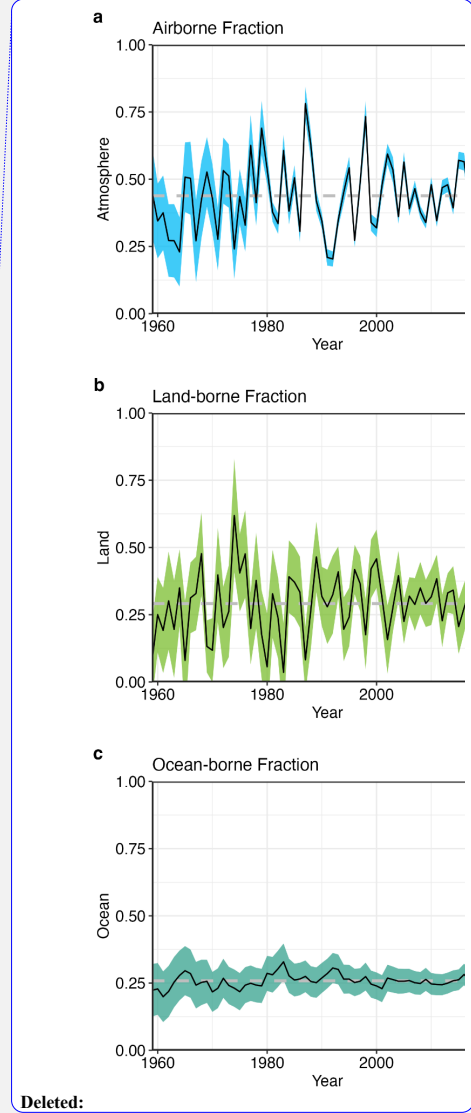
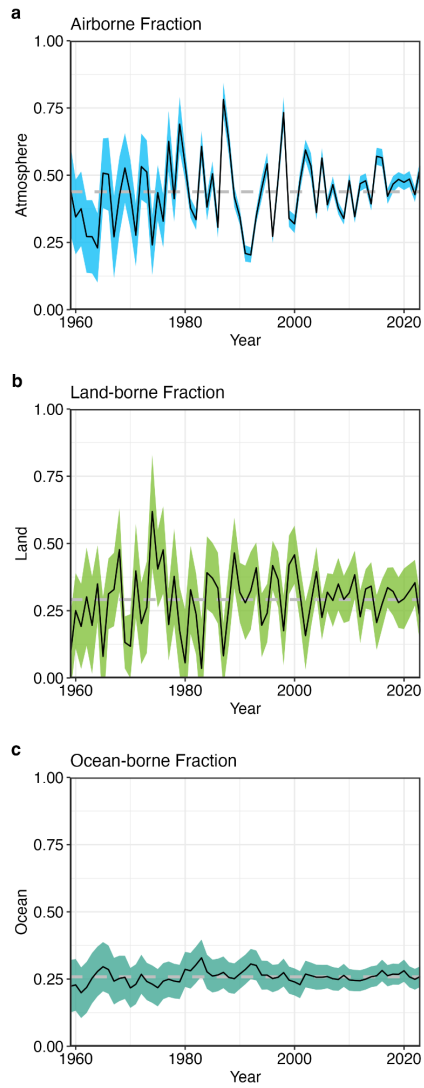


Figure 10. The partitioning of total anthropogenic CO₂ emissions ($E_{FOS} + E_{LUC}$) across (a) the atmosphere (airborne fraction), (b) land (land-borne fraction), and (c) ocean (ocean-borne fraction). Black lines represent the central estimate, and the coloured shading represents the uncertainty. The grey dashed lines represent the long-term average of the airborne (44%), land-borne (30%) and ocean-borne (25%) fractions during 1960-2023 (with a B_{IM} of 1%).

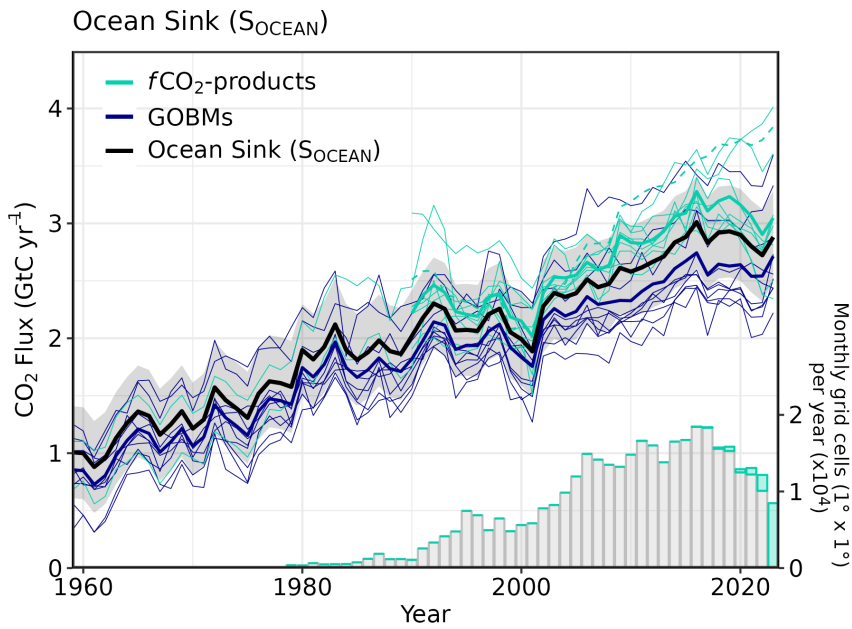
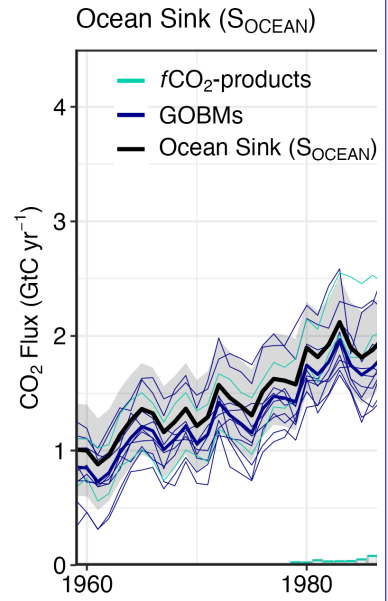
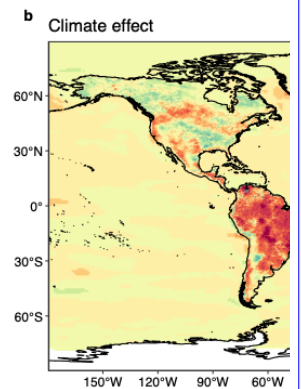
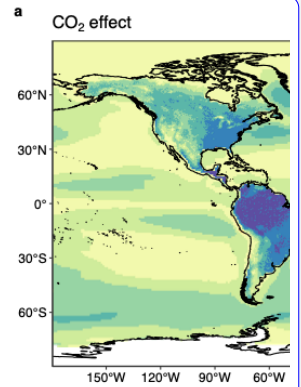


Figure 11. Comparison of the anthropogenic atmosphere-ocean CO₂ flux showing the budget values of S_{OCEAN} (black; with the uncertainty in grey shading), individual ocean models (royal blue), and the ocean $f\text{CO}_2$ -products (cyan; with UExp-FFN-U, previously Watson et al. (2020), in dashed line as not used for ensemble mean). Two $f\text{CO}_2$ -products (Jena-MLS, LDEO-HPD) extend back to 1959. The $f\text{CO}_2$ -products were adjusted for the pre-industrial ocean source of CO₂ from river input to the ocean, by subtracting a source of 0.65 GtC yr⁻¹ to make them comparable to S_{OCEAN} (see Section 2.5). Bar-plot in the lower right illustrates the number of monthly gridded values in the SOCAT v2024 database (Bakker et al., 2024). Grey bars indicate the number of grid cells in SOCAT v2023, and coloured bars indicate the newly added grid cells in v2024.



Deleted:



Deleted:

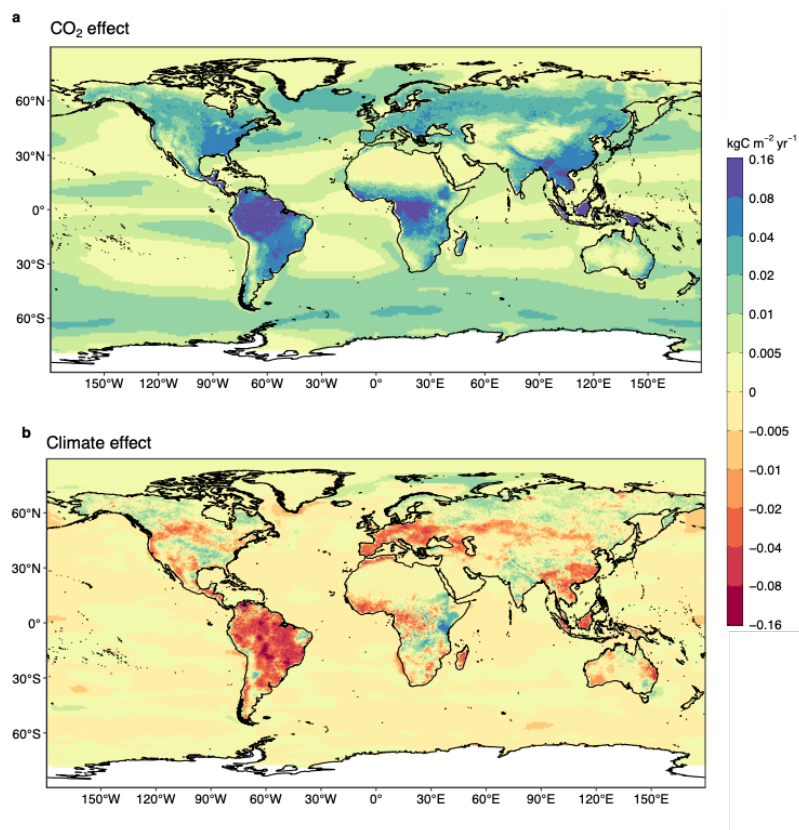
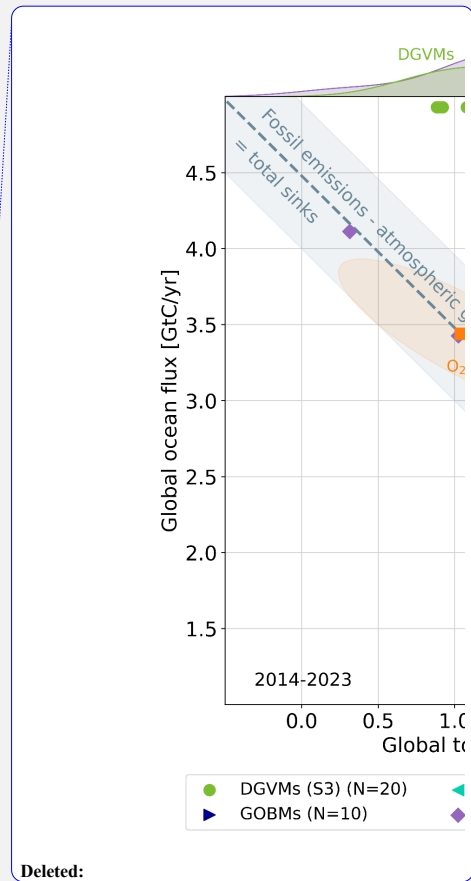
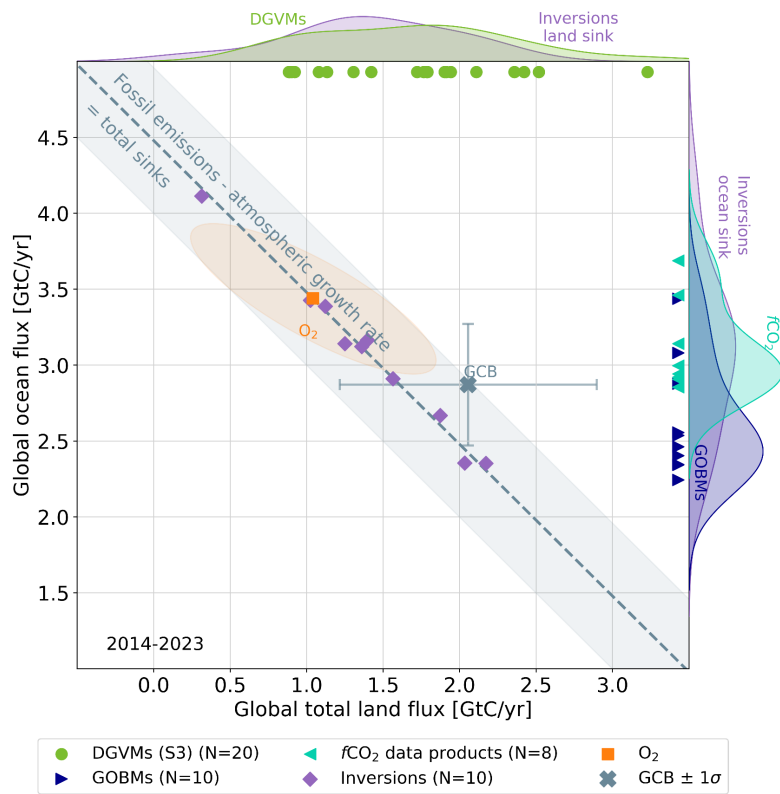


Figure 12. Attribution of the atmosphere-ocean (S_{OCEAN}) and atmosphere-land (S_{LAND}) CO₂ fluxes to (a) increasing atmospheric CO₂ concentrations and (b) changes in climate, averaged over the previous decade 2014-2023. All data shown is from the processed-based GOBMs and DGVMs. Note that the sum of ocean CO₂ and climate effects shown here will not equal the ocean sink shown in Figure 6, which includes the $f\text{CO}_2$ -products. See Supplement S.3.2 and S.4.1 for attribution methodology. Units are in kgC m⁻² yr⁻¹ (note the non-linear colour scale). Positive values (blue) are CO₂ sinks, negative values (red) are CO₂ sources.

Formatted: Font: Bold



Deleted:

Figure 13. The 2014-2023 decadal mean global net atmosphere-ocean and atmosphere-land fluxes derived from the ocean models and $f\text{CO}_2$ products (y-axis, right and left pointing blue triangles respectively), and from the DGVMs (x-axis, green symbols), and the same fluxes estimated from the atmospheric inversions (purple symbols). The shaded distributions show the densities of the ensembles of individual estimates. The grey central cross is the mean ($\pm 1\sigma$) of S_{OCEAN} and $(S_{\text{LAND}} - E_{\text{LUC}})$ as assessed in this budget. The grey diagonal line represents the constraint on the global land + ocean net flux, i.e. global fossil fuel emissions minus the atmospheric growth rate from this budget ($E_{\text{FOS}} - G_{\text{ATM}}$). The orange square represents the same global net atmosphere-ocean and atmosphere-land fluxes as estimated from the atmospheric O_2 constraint (the ellipse drawn around the central atmospheric O_2 estimate is a contour representing the 1σ uncertainty of the land and ocean fluxes as a joint probability distribution). Positive values are CO_2 sinks. Note that the inverse estimates have been scaled for a minor difference between E_{FOS} and GridFEDv2024.0 (Jones et al., 2024a).

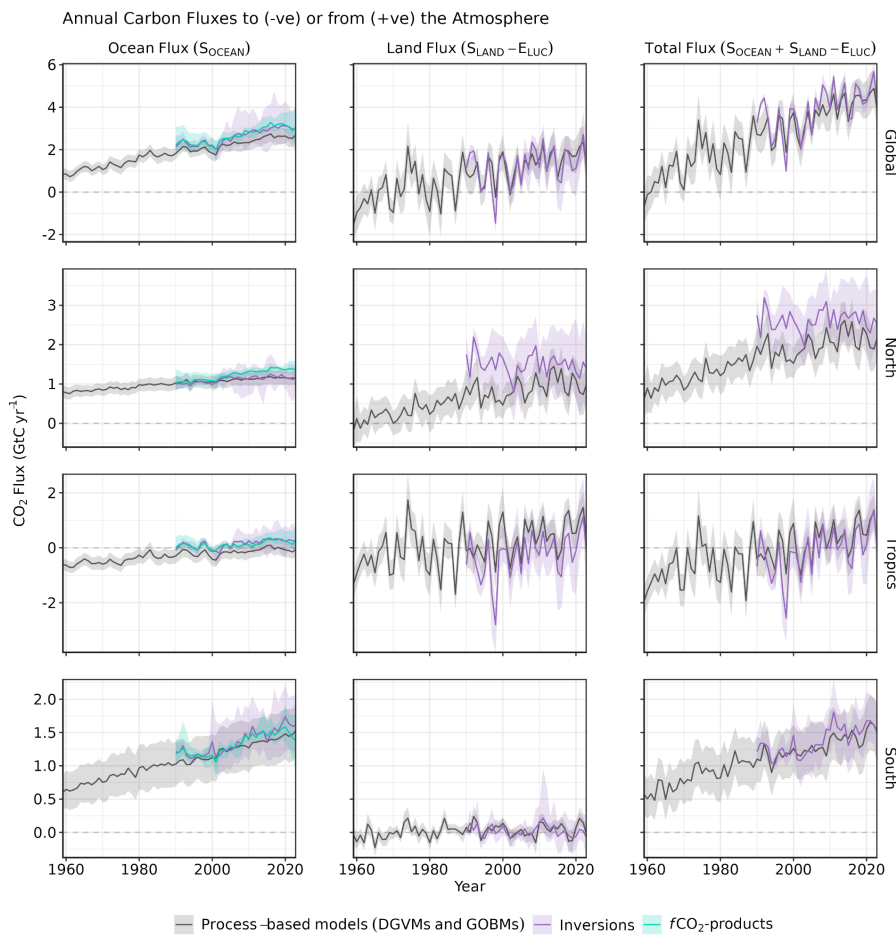
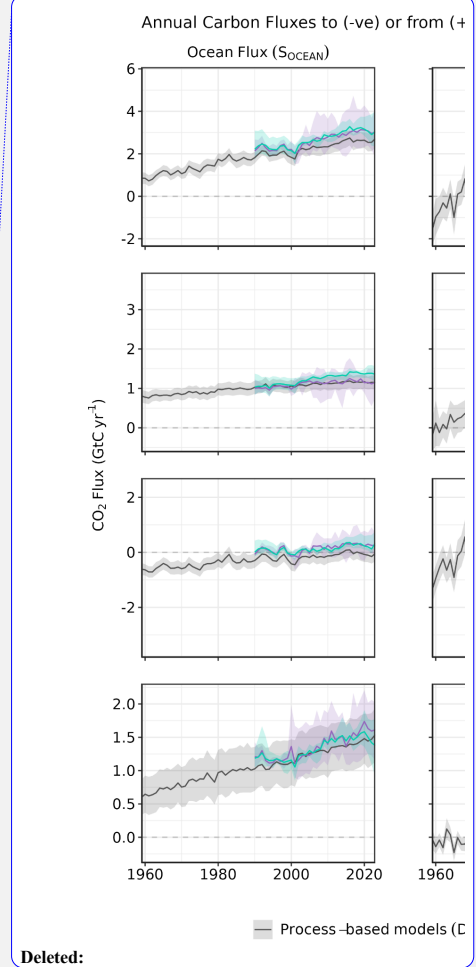
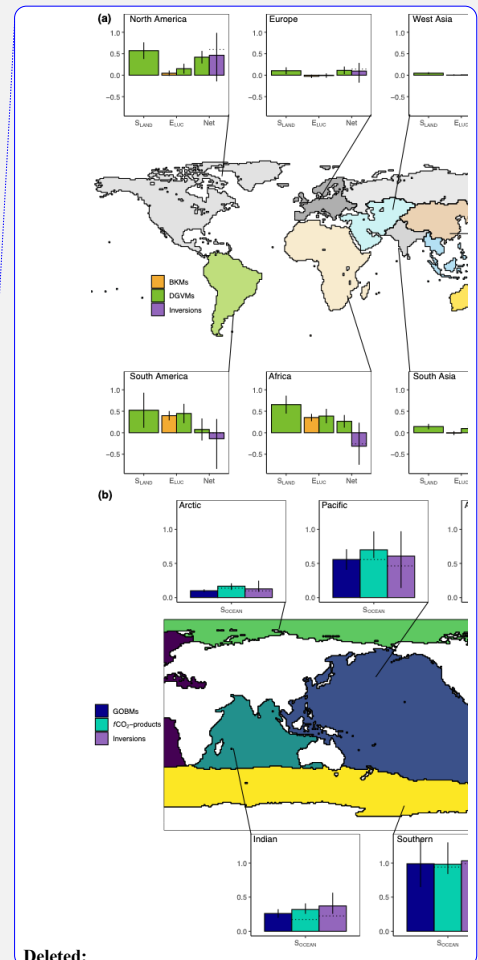
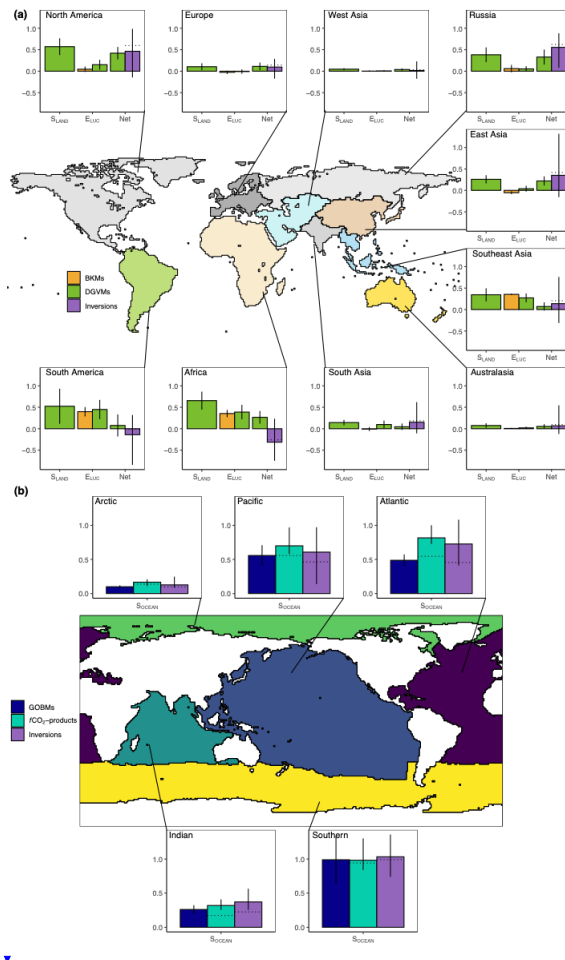


Figure 14. CO₂ fluxes between the atmosphere and the Earth's surface separated between land and oceans, globally and in three latitude bands. The ocean flux is S_{OCEAN} and the land flux is the net atmosphere-land fluxes from the DGVMs. The latitude bands are (top row) global, (2nd row) north (>30°N), (3rd row) tropics (30°S-30°N), and (bottom row) south (<30°S), and over ocean (left column), land (middle column), and total (right column). Estimates are shown for: process-based models (DGVMs for land, GOBMs for oceans); inversion systems (land and ocean); and $f\text{CO}_2$ -products (ocean only). Positive values are CO₂ sinks. Mean estimates from the combination of the process models for the land and oceans are shown (black line) with $\pm 1 \sigma$ of the model ensemble (grey shading). For the total uncertainty in the process-based estimate of the total sink, uncertainties are summed in quadrature. Mean estimates from the atmospheric inversions are shown (purple lines) with their full spread (purple shading). Mean estimates from the $f\text{CO}_2$ -products are shown for the ocean domain (light blue



Deleted:

lines) with full model spread (light blue shading). The global SOCEAN (upper left) and the sum of SOCEAN in all three regions represents the anthropogenic atmosphere-to-ocean flux based on the assumption that the preindustrial ocean sink was 0 GtC yr^{-1} when riverine fluxes are not considered. This assumption does not hold at the regional level, where preindustrial fluxes can be significantly different from zero. Hence, the regional panels for SOCEAN represent a combination of natural and anthropogenic fluxes. Bias-correction and area-weighting were only applied to global SOCEAN ; hence the sum of the regions is slightly different from the global estimate ($<0.07 \text{ GtC yr}^{-1}$).



Deleted:

Figure 15. Decadal mean (a) land and (b) ocean fluxes for RECCAP-2 regions over 2014-2023. For land fluxes, S_{LAND} is estimated by the DGVMs (green bars), with the error bar as $\pm 1\sigma$ spread among models. A positive S_{LAND} is a net transfer of carbon from the atmosphere to the land. E_{LUC} fluxes are shown for both DGVMs (green) and bookkeeping models (orange), again with the uncertainty calculated as the $\pm 1\sigma$ spread. Note, a positive E_{LUC} flux indicates a loss of carbon from the land. The net land flux is shown for both DGVMs (green) and atmospheric inversions (purple), including the full model spread for inversions. The net ocean sink (S_{OCEAN}) is estimated by GOBMs (royal blue), fCO_2 -products (cyan), and atmospheric inversions (purple). Uncertainty is estimated as the $\pm 1\sigma$ spread for GOBMs, and the full model spread for the other two datasets. The dotted lines show the fCO_2 -products and inversion results without river flux adjustment. Positive values are CO_2 sinks.

Anthropogenic carbon flows

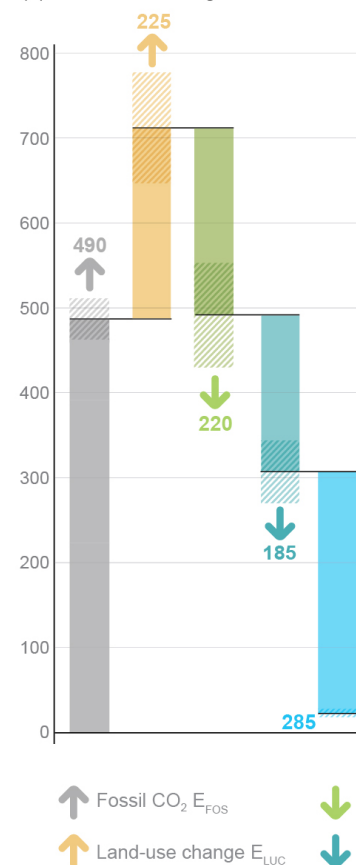
(a) Cumulative changes 1850-2023 GtC

(b) Mean fluxes 2014-2023 GtC per year



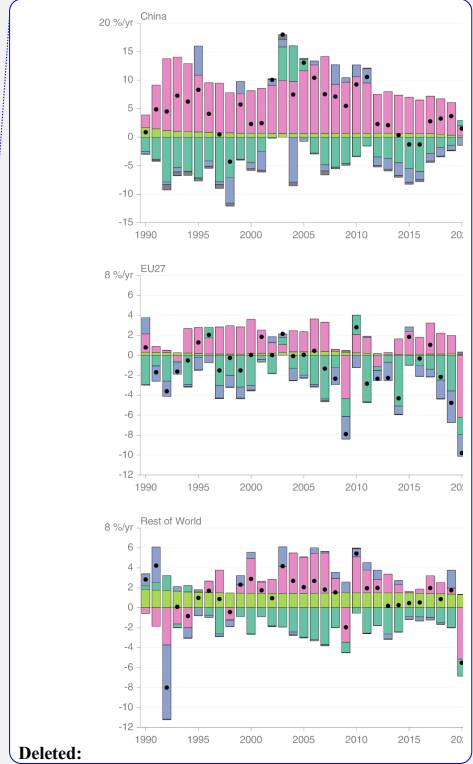
Anthropogenic carbon flows

(a) Cumulative changes 1850-2023 GtC



Deleted:

Figure 16. Cumulative changes over the 1850-2023 period (left) and average fluxes over the 2014-2023 period (right) for the anthropogenic perturbation of the global carbon cycle. See the caption of Figure 3 for key information and the methods in text for full details.



Deleted:

Figure 17. Kaya decomposition of the main drivers of fossil CO₂ emissions, considering population, GDP per person, Energy per GDP, and CO₂ emissions per energy, for China (top left), USA (top right), EU27 (middle left), India (middle right), Rest of the World (bottom left), and World (bottom right). Black dots are the annual fossil CO₂ emissions growth rate, coloured bars are the contributions from the different drivers to this growth rate. A general trend is that population and GDP growth put upward pressure on emissions (positive values), while energy per GDP and, more recently, CO₂ emissions per energy put downward pressure on emissions (negative values). Both the COVID-19 induced drop during 2020 and the recovery in 2021 led to a stark contrast to previous years, with different drivers in each region.

Page 1: [1] Deleted Friedlingstein, Pierre 24/01/2025 14:59:00

▼

Page 1: [1] Deleted Friedlingstein, Pierre 24/01/2025 14:59:00

▼

Page 1: [1] Deleted Friedlingstein, Pierre 24/01/2025 14:59:00

▼

Page 1: [1] Deleted Friedlingstein, Pierre 24/01/2025 14:59:00

▼

Page 1: [1] Deleted Friedlingstein, Pierre 24/01/2025 14:59:00

▼

Page 1: [1] Deleted Friedlingstein, Pierre 24/01/2025 14:59:00

▼

Page 1: [1] Deleted Friedlingstein, Pierre 24/01/2025 14:59:00

▼

Page 1: [1] Deleted Friedlingstein, Pierre 24/01/2025 14:59:00

▼

Page 1: [1] Deleted Friedlingstein, Pierre 24/01/2025 14:59:00

▼

Page 1: [1] Deleted Friedlingstein, Pierre 24/01/2025 14:59:00

▼

Page 1: [1] Deleted **Friedlingstein, Pierre** **24/01/2025 14:59:00**

▼

Page 1: [1] Deleted **Friedlingstein, Pierre** **24/01/2025 14:59:00**

▼

Page 1: [1] Deleted **Friedlingstein, Pierre** **24/01/2025 14:59:00**

▼

Page 1: [1] Deleted **Friedlingstein, Pierre** **24/01/2025 14:59:00**

▼

Page 1: [1] Deleted **Friedlingstein, Pierre** **24/01/2025 14:59:00**

▼

Page 1: [1] Deleted **Friedlingstein, Pierre** **24/01/2025 14:59:00**

▼

Page 1: [1] Deleted **Friedlingstein, Pierre** **24/01/2025 14:59:00**

▼

Page 1: [1] Deleted **Friedlingstein, Pierre** **24/01/2025 14:59:00**

▼

Page 1: [1] Deleted **Friedlingstein, Pierre** **24/01/2025 14:59:00**

▼

Page 1: [1] Deleted **Friedlingstein, Pierre** **24/01/2025 14:59:00**

▼

Page 1: [1] Deleted Friedlingstein, Pierre 24/01/2025 14:59:00

▼

Page 1: [1] Deleted Friedlingstein, Pierre 24/01/2025 14:59:00

▼

Page 1: [1] Deleted Friedlingstein, Pierre 24/01/2025 14:59:00

▼

Page 1: [1] Deleted Friedlingstein, Pierre 24/01/2025 14:59:00

▼

Page 1: [1] Deleted Friedlingstein, Pierre 24/01/2025 14:59:00

▼

Page 1: [1] Deleted Friedlingstein, Pierre 24/01/2025 14:59:00

▼

Page 1: [1] Deleted Friedlingstein, Pierre 24/01/2025 14:59:00

▼

Page 1: [1] Deleted Friedlingstein, Pierre 24/01/2025 14:59:00

▼

Page 1: [1] Deleted Friedlingstein, Pierre 24/01/2025 14:59:00

▼

Page 1: [1] Deleted Friedlingstein, Pierre 24/01/2025 14:59:00

▼

Page 1: [1] Deleted Friedlingstein, Pierre 24/01/2025 14:59:00

▼

Page 1: [1] Deleted Friedlingstein, Pierre 24/01/2025 14:59:00

▼

Page 1: [1] Deleted Friedlingstein, Pierre 24/01/2025 14:59:00

▼

Page 1: [1] Deleted Friedlingstein, Pierre 24/01/2025 14:59:00

▼

Page 1: [1] Deleted Friedlingstein, Pierre 24/01/2025 14:59:00

▼

Page 1: [1] Deleted Friedlingstein, Pierre 24/01/2025 14:59:00

▼

Page 1: [1] Deleted Friedlingstein, Pierre 24/01/2025 14:59:00

▼

Page 1: [1] Deleted Friedlingstein, Pierre 24/01/2025 14:59:00

▼

Page 25: [2] Deleted Friedlingstein, Pierre 24/01/2025 14:59:00

▼

Page 25: [2] Deleted Friedlingstein, Pierre 24/01/2025 14:59:00

▼

Page 25: [2] Deleted Friedlingstein, Pierre 24/01/2025 14:59:00

▼

Page 25: [3] Deleted Friedlingstein, Pierre 24/01/2025 14:59:00

▼

Page 25: [3] Deleted Friedlingstein, Pierre 24/01/2025 14:59:00

▼

Page 25: [3] Deleted Friedlingstein, Pierre 24/01/2025 14:59:00

▼

Page 25: [3] Deleted Friedlingstein, Pierre 24/01/2025 14:59:00

▼

Page 25: [3] Deleted Friedlingstein, Pierre 24/01/2025 14:59:00

▼

Page 25: [3] Deleted Friedlingstein, Pierre 24/01/2025 14:59:00

▼

Page 25: [3] Deleted Friedlingstein, Pierre 24/01/2025 14:59:00

▼

Page 25: [3] Deleted Friedlingstein, Pierre 24/01/2025 14:59:00

▼

Page 25: [3] Deleted Friedlingstein, Pierre 24/01/2025 14:59:00

▼

Page 25: [4] Deleted Friedlingstein, Pierre 24/01/2025 14:59:00

▼

Page 25: [4] Deleted Friedlingstein, Pierre 24/01/2025 14:59:00

▼

Page 25: [4] Deleted Friedlingstein, Pierre 24/01/2025 14:59:00

▼

Page 25: [4] Deleted Friedlingstein, Pierre 24/01/2025 14:59:00

▼

Page 25: [4] Deleted Friedlingstein, Pierre 24/01/2025 14:59:00

▼

Page 25: [4] Deleted Friedlingstein, Pierre 24/01/2025 14:59:00

▼

Page 25: [4] Deleted Friedlingstein, Pierre 24/01/2025 14:59:00

▼

Page 25: [4] Deleted Friedlingstein, Pierre 24/01/2025 14:59:00

▼

Page 25: [4] Deleted Friedlingstein, Pierre 24/01/2025 14:59:00

▼

Page 25: [4] Deleted Friedlingstein, Pierre 24/01/2025 14:59:00

▼

Page 25: [4] Deleted Friedlingstein, Pierre 24/01/2025 14:59:00

▼

Page 25: [5] Deleted Friedlingstein, Pierre 24/01/2025 14:59:00

▼

Page 25: [5] Deleted Friedlingstein, Pierre 24/01/2025 14:59:00

▼

Page 25: [5] Deleted Friedlingstein, Pierre 24/01/2025 14:59:00

▼

Page 25: [5] Deleted Friedlingstein, Pierre 24/01/2025 14:59:00

▼

Page 25: [5] Deleted Friedlingstein, Pierre 24/01/2025 14:59:00

▼

Page 25: [5] Deleted Friedlingstein, Pierre 24/01/2025 14:59:00

▼

Page 25: [5] Deleted Friedlingstein, Pierre 24/01/2025 14:59:00

▼

Page 25: [5] Deleted Friedlingstein, Pierre 24/01/2025 14:59:00

▼

Page 25: [5] Deleted Friedlingstein, Pierre 24/01/2025 14:59:00

▼

Page 25: [6] Deleted Friedlingstein, Pierre 24/01/2025 14:59:00

▼

Page 25: [6] Deleted Friedlingstein, Pierre 24/01/2025 14:59:00

▼

Page 25: [6] Deleted Friedlingstein, Pierre 24/01/2025 14:59:00

▼